General Disclaimer

One or more of the Following Statements may affect this Document

- This document has been reproduced from the best copy furnished by the organizational source. It is being released in the interest of making available as much information as possible.

- This document may contain data, which exceeds the sheet parameters. It was furnished in this condition by the organizational source and is the best copy available.

- This document may contain tone-on-tone or color graphs, charts and/or pictures, which have been reproduced in black and white.

- This document is paginated as submitted by the original source.

- Portions of this document are not fully legible due to the historical nature of some of the material. However, it is the best reproduction available from the original submission.

MR-6903
Project 6709

Nonlinear Combustion Instability in Liquid-Propellant Rocket Motors

by

Samuel Z. Burstein

Wallace Chinitz

Harold S. Schechter

Final Report

to

Jet Propulsion Laboratory

Contract No. 951946

December, 1970

MATHEMATICAL APPLICATIONS GROUP INC.
[illegible] Broadway, White Plains, New York 10605

MR-6903
Project 6709

Nonlinear Combustion Instability in Liquid-Propellant Rocket Motors

by

Samuel Z. Burstein

Wallace Chinitz

Harold S. Schechter

Final Report

to

Jet Propulsion Laboratory

Contract No. 951946

December, 1970

"This work was performed for the Jet Propulsion Laboratory, California Institute of Technology, as sponsored by the National Aeronautics and Space Administration under Contract NAS7-100."

"This report contains information prepared by Mathematical Applications Group, Inc. (MAGI) under JPL subcontract. Its content is not necessarily endorsed by the Jet Propulsion Laboratory, California Institute of Technology or the National Aeronautics and Space Administration."

TABLE OF CONTENTS

ABSTRACT

This report presents two mathematical models which describe, to a certain degree of approximation, the main physical processes that occur in liquid propellant rocket motors. A 'pancake' model describes some of the gas dynamic processes in the transverse (r-θ) plane of a cylindrical chamber. Several attempts were made to include the reacting drop combustion model in the pancake motor but were not successful. However, the annular model is able to describe gas dynamic and drop spray interaction processes in the cylindrical space described by θ-z coordinates. Both models are time dependent. However, the r-θ model seeks to describe the complicated nonlinear motion of gas dynamic waves in the spinning or sloshing mode near the injector face of the motor. The annular model seeks to describe the interaction of a reacting drop spray with finite amplitude waves which move both tangentially as well as axially. The annular model also includes the effects of a converging-diverging nozzle on the flow field. The combustion model, which is used in both the pancake and annular motors, is evaporation controlled and is similar to other combustion calculations which assume an evaporation controlled model.

I. INTRODUCTION

The phenomenon of combustion instability in the liquid propellant rocket system is characterized by cyclic variations of pressure in the feed system and combustion chamber, or, depending on the magnitude of the frequency, within the chamber alone. Generally speaking, frequencies greater than 1000 cps are confined to the combustion chamber, while oscillations in the low frequency range, say 400 cps, usually occur within the feedline and chamber. The fundamental characteristic of low frequency instability is the uniformity of the gas pressure throughout the combustion chamber at every instant, since oscillations occur, as a whole, about the mean or steady value of chamber pressure. On the other hand, the gas pressure inside the combustion chamber is not uniform at any instant under non-steady conditions when the frequency of gas oscillation in the combustion chamber is sufficiently high, i.e., when the wave length of the oscillation is of the same order as the length of the combustion chamber. Historically, the low-frequency class of instability was first recognized in Germany in about 1930. The high frequency mode of instability, on the other hand, was first observed in 1941 because the sophisticated experimental equipment required in high frequency instability was not available earlier. Today, low frequency instability is rather well understood and comparatively easy to cure. It is the high frequency form of combustion instability

that still concerns the designer. Under the conditions of high frequency instability, the combustion field experiences strong pressure and velocity waves which couple with the combustion process so as to make the entire interaction process self-sustaining. As a result, the heat transfer rates become extremely severe - so high that erosion of the injection plate and chamber walls result with associated loss of structural integrity.

There have really been two serious attempts to understand the instability process in the form of analysis. The model developed at NASA by Priem and Guentert (1), which has subsequently been extended and is reported in great detail in (2), is a numerical procedure which attempts to describe the interaction of propellant spray and combustion gas, considering mass, momentum and energy transport. A differential model is assumed with as few simplifying assumptions included as possible and it is then solved on a digital computer. This mechanistic procedure can be compared with the systems approach of Crocco and Cheng (3). This group at Princeton University used the concept of time lag which was originally used in stability methods in circuit analysis. The Princeton group modified the time lag theory by introducing a time-varying time lag which is dependent on the chamber pressure. This theory differs from the NASA work basically in that it is a linear theory, whereas the NASA model is nonlinear. A detailed discussion and comparison has been given by Priem (4) on the above models including a lengthy bibliography on the subject.

This report describes two mathematical models which use non-linear analysis and which further seek to define the relevant physical processes that occur in a liquid propellant rocket motor. The pancake model is used to describe the spinning or sloshing mode of nonlinear wave motion near the injector face of a rocket engine. However, this mode has certain limitations when coupling the axial flux to an orthogonal two space dimension gas dynamic calculation (i.e., the pancake model). Therefore, an annular model, which couples the predominantly axial spray flux to the gas dynamic field while omitting any radial effects, has been constructed. The annular model can handle time dependent mass and energy accumulations in the combustor flow field because of the inclusion of a converging-diverging nozzle. Hence, no a-priori assumption need be made as to the constancy of the mass or energy in the flow field (compare with Reference 1). Indeed, this model should demonstrate the need for local (time-like) accumulation of energy in order for the wave to build up from an initial perturbation. Once a finite amplitude oscillation has been sustained the assumption of constant energy in the motor may be valid.

Since the Priem-Guentert model cannot consider the questions of energy accumulation in wave formation and because it is one-dimensional it cannot consider interactions of tangential and radial waves and tangential and axial waves. On the other hand, the time lag theory of Crocco is linear and, therefore, cannot examine the question of the wave structure: when the amplitude

of the wave grows what limiting amplitude is reached for a particular initial disturbance in a given environment. These questions can be answered with the two models developed and reported on here.

Hence, the question of wave structure in the transverse plane is analyzed through the construction of the pancake model and the question of stability of a motor when combustion couples to the gas dynamic field, in the presence of a nozzle, is analyzed with the help of the annular model. A sequence of calculations which uses a more sophisticated version of the annular model has recently been completed, Reference 7, by the first and third authors for NASA. We suggest that the reader refer to this report for a more complete discussion of the capabilities of the annular model for use in stability analysis.

The numerical methods presented in this report are extensions of an earlier report, Reference 5, to the Jet Propulsion Laboratory. This report is divided into three general sections. The discussion centers first on the fluid dynamic and computational aspects of the pancake model including results. Secondly, the annular model theory is presented with some numerical results and finally the theory of the evaporation rate controlled droplet model is presented for 50/50 hydrazine/UDMH fuel mixture with nitrogen tetroxide as the oxidizer. The description of the computer programs are given in the Appendix.

II. FLUID DYNAMIC MODEL

A. General Nonlinear Differential Equations

The differential equations describing the motion of a compressible fluid in cylindrical coordinates can be written in vector form as

$$\frac{\partial W}{\partial t} + \frac{\partial F}{\partial r} + \frac{\partial G}{\partial \theta} + \frac{\partial H}{\partial z} + S = \dot{\psi} \tag{1}$$

We use the notation of a vector in the mathematical sense - not in the physical sense. This allows great convenience in allowing shorthand notation (associated with the use of vector notation) when describing the conservation equations of fluid dynamics. The source term, $\dot{\psi}$, has five components corresponding to the rate of production of mass, momentum and energy per unit volume due to combustion. In the section entitled 'Droplet Evaporation and Combustion Analysis', we show how to compute this vector. The vector W corresponds to the mass, momentum in the r, θ and z directions and total energy, all per unit volume. The vectors F, G, and H represent the flux of these quantities in the radial, tangential and axial directions respectively.

In order to compute the time dependent behavior of W, which has the components

$$W = r \begin{pmatrix} \rho \\ \rho u \\ \rho v \\ \rho w \\ \rho \left(e + \frac{1}{2}(u^2+v^2+w^2)\right) \end{pmatrix} \tag{2}$$

the fluxes

$$F = r\begin{pmatrix} \rho u \\ \rho u^2+p \\ \rho uv \\ \rho uw \\ (E+p)u \end{pmatrix} \qquad G = \begin{pmatrix} \rho v \\ \rho vu \\ \rho v^2+p \\ \rho vw \\ (E+p)v \end{pmatrix} \qquad H = r\begin{pmatrix} \rho w \\ \rho uw \\ \rho vw \\ \rho w^2+p \\ (E+p)w \end{pmatrix} \tag{3}$$

must be known. The pressure is p; the total energy is E (the fifth component of W). The velocity components in the radial, tangential and axial directions are u, v, and w, respectively. The vector S appears as a result of the transformation to cylindrical coordinates from cartesian coordinates. The components of S are given by

$$S = \begin{pmatrix} 0 \\ -(p+\rho v^2) \\ \rho uv \\ 0 \\ 0 \end{pmatrix} \tag{4}$$

The components of $\dot{\psi}$ which are considered in this paper are given schematically as

$$\dot{\psi} = r\begin{pmatrix} \dot{\psi}(\rho) \\ 0 \\ 0 \\ 0 \\ \dot{\psi}(E) \end{pmatrix} \tag{5}$$

The first and fifth terms correspond to the rate of generation of mass and energy per unit volume due to combustion. One observes that the sources of momentum generation have been set equal to zero under the assumption that they are small.

Once the source term $\dot{\psi}$ is computed, $\partial W/\partial t$ then can be obtained if the divergence of the flux can be computed. Since we are always going to be limiting the calculation to a prescribed space-plane and time (rather than include a true three-dimensional model by allowing an additional degree of freedom) the two models to be presented will be limiting cases of Equation (1).

The solution to our problem involves satisfying Equation (1) and the boundary condition specifying the vanishing of the normal velocity at the boundary of a non-porous wall. It is also assumed that the function form $\dot{\psi}=\dot{\psi}(W)$ is specified. Section III of the report gives the analysis used to derive the dependence of the source terms $\dot{\psi}$ on W and on the variables describing the behavior of an evaporating droplet.

Since Equation (1) is nonlinear, no general principle can be invoked to obtain a general solution satisfying this equation and the associated boundary conditions for the mixed initial boundary value problem. However, a substantial degree of success has been achieved in solving reduced forms of Equation (1) by using finite difference methods (see, for example, Reference 5). This involves the introduction of discrete coordinates overlaying the continuous domain of solution of Equation (1) and then writing down nonlinear

algebraic equations defined at these discrete coordinates. Such equations are called difference equations - approximations to the original differential equations. These approximations can have solutions which are arbitrarily close to the solution of the differential equation (1) if the difference equations are stable and are consistent with Equation (1). (Actually this statement has only been proved for linearized forms of Equation (1).) The difference between the solutions of the exact problem $W(t+\Delta t)$ and the numerical problem $\tilde{W}(t+\Delta t)$ is proportional to the truncation error or accuracy of the difference scheme. The difference equations that are used in the approximation to reduced forms of Equation (1) are of second order accuracy. They will be discussed in Subsections B and H where the pancake and annular motors are discussed. If W represents a vector solution of the numerical problem, then $\tilde{W}^n_{ijk}$ is defined on a lattice of net points in the four-dimensional space, the discrete points of which have the coordinate labels r_i, θ_j, z_k and t_n.

Because of the slowness of even the most recent computing machines, the solution of the four-dimensional problem, three space dimensions and time, can only be achieved, in reasonable economic limits, by first exploring suitable solution parameters in the two space and time domain. Hence, the finite difference solutions described in Subsections B and H can suggest the range of parameters to be used in the complete three-dimensional time-dependent problem. This preliminary investigation would insure that just a few computer runs would be sufficient to ascertain the gross behavior of the four-dimensional problem. This approach

seems to be a current limit for a solution to the complete problem using such a complicated model.

It is interesting to note that the form of the differential equations that are used to define the time-dependent problem, must be in the same form as the physical conservation law. When numerical integration is performed with the approximation to these differential equations, the result will yield the correct jump conditions across lines of discontinuities only when this condition is satisfied. In other words, across lines or surfaces of discontinuity the Rankine-Hugoniot conditions will automatically be satisfied. Other forms of the conservation laws, i.e., other forms of Equation (1), will, in general, not yield the proper jump conditions across lines or surfaces of discontinuity.

To amplify these last remarks, consider a model form of Equation (1),

$$u_t + (F(u))_r = 0 \qquad (6)$$

Let the flux vector F be given by

$$F(u) = \tfrac{1}{2}u^2,$$

Then Equation (6) is nonlinear and discontinuities will develop in a finite time even if the initial data $u(0,r)$, $|r|<\infty$ is smooth. Let $\{p\}$ signify the jump in the function p, then if there are lines of discontinuity in the solution of Equation (6), the jump

across such a discontinuity must satisfy

$$S\{u\} = -\tfrac{1}{2}\{u^2\} \tag{7}$$

The normal speed of propagation of the discontinuity is given the symbol S. Now, however, multiply Equation (6) by u. Noting the definition of F(u), the resulting conservation equation is given as

$$(\tfrac{1}{2}u^2)_t + (1/3u^3)_r = 0 \tag{8}$$

Hence, jumps in the solution across discontinuities arising in the solution of Equation (8), subject to the same initial data as Equation (6), must satisfy

$$S\{u^2\} = -\{\frac{2}{3}u^3\} \tag{9}$$

It is clear then, that the strength of the discontinuity, if measured by, say the speed of the discontinuity S will, in general, differ. This example shows that the value of the jump will be a function of the <u>form</u> of the differential equation used to generate the difference equations (integral equations). Another example can be obtained immediately from Equation (6), i.e., carry out the differentiation that is indicated in Equation (6) and divide by u to obtain

$$(\ln u)_t + u_r = 0$$

We have defined still another conservation law which obviously has an associated jump condition which differs from Equation (7) or Equation (9) and, therefore, is determined by the form of the equation rather than the conservation law it is intended to represent.

In the next subsection we consider a fluid dynamic model (obtained as a result of the reduction of the dimensionality of Equation (1)) in which the axial flow effects (z-motion) on the motion of the fluid in the cross plane described by coordinates r, θ, and t are neglected. This combustion chamber model is called the 'pancake' motor.

Actually, it is not quite correct to say that the z-motion is neglected. When rocket motors are built with nozzles having large contraction ratios, then the velocity as well as the gradient of the velocity in the combustion chamber will be small compared to motion in the transverse plane. Although this geometrical configuration is usually not used in large scale combustors, there is some experimental evidence available in the literature against which analytical data can be compared. If time-dependent z-motion exists, its behavior is prescribed by assumed mechanisms. This aspect is amplified in the next subsection.

B. Nonlinear Differential Equations For The Pancake Motor

If we assume that the contribution of the axial motion on processes occurring in the transverse plane can be decoupled, the differential equation describing such motion of a compressible fluid can be written in vector form as

$$\frac{\partial W}{\partial t} + \frac{\partial F}{\partial r} + \frac{\partial G}{\partial \theta} + S = \Psi \qquad (10)$$

Here, the source term, $\dot{\psi}$, has two non-zero components corresponding to the rate of production of mass and energy per unit volume; the momentum sources in the r and θ directions are ignored. The four vector, W, has components corresponding to the mass, momentum in the r and θ directions, and total energy, all per unit volume. The flux of these quantities in the radial and tangential direction is given by the vectors F and G, respectively. Since our model is defined in a thin slab of thickness Δz, we call our model the pancake model. This model, by definition, implies that only four components of W are necessary in the representation of the solution to the problem, i.e., the axial component of W (as given in Equation (1)) is ignored.

The time-dependent behavior of W can be computed once the divergence of the fluxes F(W) and G(W) are known. The pressure p, which appears in Equation (3), and the total energy E are related by

$$E = \rho(e+\tfrac{1}{2}(u^2+v^2)) \tag{11}$$

$$e = \frac{p}{\rho(\gamma-1)} \tag{12}$$

Using these relations in Equation (3) allows F and G to be given in terms of W only, i.e., F=F(W) and G=G(W).

Since there are replenishment (or source) terms in Equation (10) which are given by Equation (5), some provision must be made to allow this continual generation process to be balanced by a convective flux leaving the thin slab of thickness Δz. The solution vector, W, of the system, Equation (2), will decay if the total mass and energy generation in the r-θ cross plane is smaller than the axial flux or W can blow up if the generation $\dot{\psi}$ exceeds the axial flux H_z. A natural way to include such a description in the model, while retaining the desired reduction to a three-dimensional problem, is to associate this flux with either local or global behavior of W in the r-θ plane. We now describe in detail what we mean by this last statement.

Once the source term $\dot{\psi}$ and the divergence of the fluxes in the transverse plane is computed, $\partial W/\partial t$ can then be solved for if an approximation to the axial gradient can be computed. Since the calculation is limited to the transverse plane an additional relation must be introduced in place of the time-dependent axial momentum equation

$$(r\rho w)_t + (r\rho wu)_r + (\rho wv)_\theta + (r(p+\rho w^2))_z = 0 \qquad (13)$$

We emphasize this point because $\dot{\psi}(t)>0$ implies that $\partial W/\partial t$ will be positive. Hence, unless the axial (z) component of flux is included in the model, the solution vector W, or rather its integral over the plane, will continually increase. If the calculation is to be carried out to arbitrary time, this accumulation can become

arbitrarily large. It is certainly possible, in the complete three-dimensional problem, for local accumulation to exist. However, it would require a three-dimensional time-dependent calculation to ascertain the extent of this mass and energy accumulation. In the three-dimensional chamber the nozzle will be the mechanism for flow adjustment when accumulation occurs.

One can make some assumptions which might lead to an approximation of an adequate description of a two-dimensional pancake model with a coupled flux in the axial direction (see Reference (1)). In order to compute this flux, an additional relation is required. Equation (14) is one such relationship that will allow the computation of the divergence of the flux in the axial direction, i.e.,

$$\frac{\partial}{\partial t}\int\int W r dr d\theta = 0 \qquad (14)$$

The integration is over the plane z = constant. Equation (14) states that the associated conservation variables are conserved over the entire plane - not necessarily locally in time. The average axial flux which satisfies Equation (14) is, using Equation (1),

$$\overline{\frac{\partial H}{\partial z}} = -\int\int \{\frac{\partial F}{\partial r} + \frac{\partial G}{\partial \theta} - \dot{\psi}\}\, r dr d\theta / \int\int r dr d\theta \qquad (15)$$

The bar over the axial derivative of the flux indicates that it is an average value used throughout the chamber cross-section, i.e.,

$$\overline{\frac{\partial H}{\partial z}} = \bar{H}_z(t) \text{ only.} \tag{16}$$

The contribution of the inhomogeneous term S does not appear since Equation (15) applies only to the first and fourth components of H. Then Equation (10) may be modified so the net source term can be written as

$$\text{div } (W,F,G,S) = \dot{\psi} - \overline{\frac{\partial H}{\partial z}} \tag{17}$$

Here div is the generalized divergence operator in space-time and can be represented by

$$\text{div} = (\partial_t, \partial_r, \partial_\theta, 1) \tag{18}$$

The right member of Equation (17) is then considered to be specified through Equation (15). The integration indicated in Equation (15) can be simplified. Since G_θ is periodic in θ its contribution to the integral is zero. The value of $\bar{H}_z$, which changes in time, is just sufficient to allow the total mass and energy per unit volume, in the plane z = constant, to remain constant independent of time. Some remarks on this procedure are made in Section G where results for the pancake motor are given.

C. Linear Theory - Transverse Rotating Wave

By neglecting the right member of Equation (17) the resulting system

$$W_t + F_r + G_\theta + S = 0 \tag{19}$$

can be linearized so that an exact classical wave solution in the domain $\mathcal{D}$ (which we take as the unit disc) can be found. First, we write system (19) in its component form. The continuity equation is

$$\frac{D\rho}{Dt} + \rho \nabla . \underset{\sim}{q} = 0 \qquad (20a)$$

By subtracting the first component, i.e., the continuity equation, premultiplied by the $r(\theta)$ component of velocity from the $r(\theta)$ momentum equation, one obtains the two momentum equations in the form

$$\frac{D\underset{\sim}{q}}{Dt} = -\frac{1}{\rho} \text{ grad } p + \frac{1}{\rho r} \underset{\sim}{J} \qquad (20b)$$

The vectors $\underset{\sim}{J}$ and $\underset{\sim}{q}$ are given by

$$\underset{\sim}{q} = \begin{pmatrix} u \\ v \end{pmatrix} \qquad \underset{\sim}{J} = \begin{pmatrix} \rho v^2 \\ -\rho uv \end{pmatrix}$$

The Lagrangian operator

$$\frac{D}{Dt} \equiv (\ )_t + u(\ )_r + \frac{v}{r}(\ )_\theta$$

is the particle derivative in polar coordinates and

$$\nabla . \underset{\sim}{q} = \frac{1}{r} (ru)_r + \frac{1}{r} v_\theta$$

is the divergence operator in these coordinates.

In the absence of irreversible changes (heat conduction, viscous effects, etc.) the fluid undergoes a reversible, adiabatic change. The initial state of a fluid can be connected to its final state through

$$p\rho^{-\gamma} = \text{constant for a particle} \qquad (21)$$

If the fluid is initially uniform, the constant in Equation (21) is the same for each particle in the domain $\mathcal{D}$. It is then possible to replace $D\rho$ by $a^{-2}Dp$, where a is the sound speed. This replacement is made in system (20). Linearization of the flow field is now assumed so that a solution to the linearized form of Equations (20) can be obtained about the quiescent state $u_\infty = v_\infty = 0$. Let $\rho = \rho_\infty + \rho'$, $p = p_\infty + p'$ and $a_\infty^2 = \gamma p_\infty/\rho_\infty$. The perturbation pressure is p' while the perturbation density is ρ'. Then system (20) can be given in terms of the perturbation variables

$$q_t = -\frac{1}{\rho_\infty} \text{ grad } p'$$

$$p_t' = -\rho_\infty a_\infty^2 \text{ div } \underset{\sim}{q}$$

The total fluid velocity is, of course, the perturbation velocity. The vector $\underset{\sim}{J}$ in Equation (20), because it is quadratic in the perturbed velocity components, has been neglected. Now, it is clear that the vector $\underset{\sim}{q}$ is given as the gradient of a scalar function, in this case the perturbation pressure, p'. Because the entropy is constant $\nabla x \underset{\sim}{q} = 0$. Then the existence of a potential ϕ is implied such that $\underset{\sim}{q} = \text{grad}\phi$, i.e., the components of $\underset{\sim}{q}$ are given by

$$\underset{\sim}{q} = \begin{pmatrix} \phi_r \\ \frac{1}{r}\phi_\theta \end{pmatrix}$$

since the operator

$$\text{grad} = \frac{\partial}{\partial r} + \frac{1}{r}\frac{\partial}{\partial \theta}$$

Hence,

$$\phi_t = -\rho_\infty^{-1} p' \quad \text{or} \quad \phi_{tt} = -\rho_\infty^{-1} p_t' \tag{22a}$$

and

$$p_t' = -\rho_\infty a_\infty^2 \nabla^2 \phi \tag{22b}$$

The wave equation in the domain $\mathcal{D}$ can now be obtained from the above basic equations of acoustic theory. After substituting Equation (22b) into Equation (22a) the result is, of course, the familiar form

$$\phi_{tt} = a_\infty^2 \nabla^2 \phi \tag{23}$$

In acoustic theory one usually expresses the solution of Equation (23) as a series; each term of which corresponds to a particular Fourier component of the wave motion. This is equivalent to expressing a general solution in wave number space as a superposition of Fourier harmonics. One can also represent the solution of Equation (23) as a sum of two waves, g_1 and g_2

$$\phi(x,t) = g_1 (\alpha \cdot x - a_\infty t) + g_2 (\alpha \cdot x + a_\infty t) \tag{24}$$

Equation (24) states that the solution can be given in terms of a family of steady progressing incoming and outgoing waves traveling at normal speed a_∞ in the α direction in the space of $\mathcal{D}$ (x).

It has been shown (6) that in the case of fluid dynamic problems,with the severe restriction of constant pressure but still retaining nonlinear terms in velocity, exact solutions can be obtained by using the functions g_1 and g_2. More important, in this reference, a class of difference methods are generated based on the above functions. Since Equation (23) is linear, the solution can be built up by a superposition of these waves in which the amplitude and phase may vary.

Solutions to Equation (23) can be easily obtained by separation of variables. We write Equation (23), using the definition of ∇^2 as

$$\phi_{tt} = a_\infty^2 \left(\phi_{rr}+\frac{1}{r}\phi_r+\frac{1}{r^2}\phi_{\theta\theta}\right) \qquad (25)$$

and the associated homogeneous boundary condition

$$\phi_r(1,\theta,t) = 0 \qquad (26)$$

which expresses the fact that the normal velocity is zero on the boundary where r=1. Since we consider $\mathcal{D}$ to be the unit disc, normalization will be required when the radial component of the solution is generated. Since Equation (25) is second order, the function as well as its first derivative must be specified as initial conditions. They are

$$\phi(r,\theta,0) = \phi_0(r,\theta) \qquad (27a)$$

and

$$\phi_t(r,\theta,t)\Big|_{t=0} = -\rho_\infty^{-1} p'(r,\theta,0) \tag{27b}$$

We assume that the solution to Equation (25) has the product form

$$\phi = R(r)\ H(\theta)\ e^{\pm iKa_\infty t} \tag{28}$$

By substituting Equation (28) into Equation (25) the two resulting ordinary differential equations which the functions R and H must satisfy are:

$$\frac{d^2R}{dr^2} + \frac{1}{r}\frac{dR}{dr} + \left(K^2 - \frac{n^2}{r^2}\right) R = 0 \tag{29}$$

$$\frac{d^2H}{d_\theta^2} + n^2H = 0 \tag{30}$$

To obtain the periodicity of ϕ, that is $\phi(\theta+2\pi) = \phi(\theta)$, we restrict the numbers which n can take on to be integers. Hence, H satisfies Equation (30) if

$$H(\theta) = e^{\pm in\theta} \tag{31}$$

We require solutions which are finite at r=0 so that we restrict solutions to Equation (29) to be

$$R = J_n(Kr)$$

where $J_n(Kr)$ denotes the Bessel function of the first kind of order n and argument Kr. Solutions of Equation (25) can be built up from a series which has, as a general term, the form

$$J_n(Kr)\ e^{\pm in\theta \pm iKa_\infty t}$$

To satisfy the boundary condition given by Equation (26), we set

$$\frac{d}{dr}J_n(Kr) = 0 \text{ at } r = 1$$

The relation defines a transendental equation defining the numbers K. For n=1 K=1.84118 ...

We take the imaginary component of the θ-component of the solution given by Equation (31). This corresponds to the previous traveling wave solutions. With n=1, we then have the fundamental tangential mode

$$\phi = \frac{a_\infty}{K}\ \varepsilon J_1(Kr)\ \sin\ (Ka_\infty t+\theta) \qquad (32a)$$

$$p' = -\gamma p_\infty\ \varepsilon J_1(Kr)\ \cos\ (Ka_\infty t+\theta) \qquad (32b)$$

It is clear that the above result is of the same form as given by Equation (24). The density is computed using Equation (21) and ε is a dimensionless measure of the wave amplitude; it is defined below.

The solution we seek to Equation (25), i.e., Equation (32), will satisfy the boundary condition of zero normal velocity at r=1. In addition, the solution will also satisfy the initial

conditions given by Equation (27) if we take for the initial value of the potential, ϕ_o, the particular form

$$\phi_o = \frac{a_\infty}{K} \varepsilon J_n(Kr) \sin(n\theta) \qquad (32c)$$

and for the initial value of the first derivative $\phi_t|_{t=0}$ the form

$$\partial\phi/\partial t = \varepsilon a_\infty^2 J_n(Kr) \cos(n\theta), \; n=1 \qquad (32d)$$

Finally, one observation: The solution is completely specified by satisfying only one boundary condition, i.e., $u(1,t)=\phi_r|_{r=1}=0$. The specification that the normal velocity at the boundary must vanish is carried over to the nonlinear problem.

Since the solution represented by system (32) is physically the deviation from the uniform state, we can define a dimensionless parameter, ε, which, in effect, measures the maximum of this deviation denoted by $p'_{max}=p^*$, i.e.,

$$\varepsilon = \frac{(p_\infty+p^*)-p_\infty}{\gamma p_\infty J_1(K)} = p^*/(p_\infty \gamma J_1(K)), \; K=1.841 \ldots$$

It is clear that ε is determined by specifying the deviation from the uniform pressure state at the point $(r,\theta,t) = (1,\pi,0)$. The solution can be written in terms of ε if the pressure is normalized by the quiescent pressure, p_∞, i.e., the pressure at any point on the disc $\mathcal{D}$ is given by

$$p(r,\theta,t)/p_\infty = 1+\varepsilon\gamma J_1(Kr)\cos(Ka_\infty t+\theta) \qquad (33a)$$

If Equation (32a) is differentiated with respect to r, the radial velocity is obtained:

$$\frac{u}{a_\infty} = \varepsilon J_1'(Kr)\ \sin(Ka_\infty t+\theta), \quad J_1' \equiv \frac{1}{2}\ (J_0-J_2) \qquad (33b)$$

The tangential velocity is obtained by differentiating Equation (32a) with respect to θ and dividing by r, i.e.,

$$\frac{v}{a_\infty} = \frac{\varepsilon J_1(Kr)}{Kr}\ \cos(Ka_\infty t+\theta) \qquad (33c)$$

The singularity at r = 0 offers no difficulty since the identity

$$\frac{J_n(x)}{x} = \frac{1}{2n}\ \left(J_{n-1}(x) + J_{n+1}(x) \right)$$

shows that v/a_∞ is well behaved as $x \to 0$.

The solution for the pressure field of this transverse rotating wave, corresponding to the initial state at t=0, is given in Figure (1), with $p^*=300.001$. For $t>0$ the contour lines (isobars) undergo a uniform rotation with rotational frequency $f=2\pi/Ka_\infty$ corresponding to the first spinning mode, i.e., n=1. The plot of the density field (by Equation 21) is similar. Figure (2) corresponds to the initial velocity field computed from the orthogonal components defined by Equations (33b) and (33c). The magnitude of the vectors are proportional to the drawn length.

The next two figures, Figure (3) and Figure (4), show the pressure field and velocity field given by the system (33) at time t=.825 milliseconds. This time corresponds to the total

integration time used for the finite difference calculation which is described in the next section. Here we will compare the results of a numerical calculation which indicates the convergence of the numerical procedure used to integrate Equation (10) subject to the initial conditions given by Equations (27a) and (27b). The solution to this linearized problem will be characterized by uniform rotation of the pressure and velocity field.

D. Difference Equations, Boundary Conditions and Some Numerical Results for the Pancake Motor

We seek a solution to Equation (10) by the method of finite differences. Equation (10) is a conservation law including production terms. The difference approximation to this equation will be in conservation form and the accuracy will be second order. The solution we seek will lie on the periodic space $\mathcal{D}$ defined by $t \geq 0$, $0 \leq \theta \leq 2\pi$ and $0 \leq r \leq 1$. We introduce an orthogonal mesh which has as points of intersection the coordinates

$$r_i = i\Delta r, \quad \theta_j = j\Delta\theta, \quad t_n = n\Delta t, \quad i,j,n = 0,1,2,\ldots$$

This set of net points, called $\mathcal{D}_h$, is defined by the set

$$\mathcal{D}_h = \{r_i, \theta_j, t_n \mid i=0,1,\ldots; \quad j=0,1,\ldots; \quad n=0,1,\ldots\}$$

The approximation to $W(r,\theta,t)$, defined on the space $\mathcal{D}$, is represented by $V(r_i,\theta_j,t_n)=V_{ij}^n$ defined on $\mathcal{D}_h$. The approximate solution of Equation (10), V_{ij}^n, is written as a two step difference

equation. (The reader should refer to Reference (5) for an earlier discussion on the difference equations.) Then, we have as the predictor step,

Step 1:

$$\tilde{V}(r_{i+\frac{1}{2}},\theta_{j+\frac{1}{2}},t+\Delta t) = \frac{1}{4}(V_{i+1,j}+V_{i,j+1}+V_{i+1,j+1}+V_{i,j})$$

$$- \frac{\Delta t}{2\Delta r} \{F(V_{i+1,j})-F(V_{i,j})+F(V_{i+1,j+1})$$

$$-F(V_{i,j+1})\} \quad -\frac{\Delta t}{2\Delta \theta} \{G(V_{i+1,j+1})-G(V_{i+1,j})$$

$$+G(V_{i,j+1})-G(V_{i,j})\} \quad -\frac{\Delta t}{4} \{B(V_{i+1,j})$$

$$+B(V_{i,j+1})+B(V_{i+1,j+1})+B(V_{i,j})\} \qquad (34a)$$

which leads to the final or corrector step,

Step 2:

$$V(r_i,\theta_j,t+\Delta t) = V(r_i,\theta_j,t) - \frac{\Delta t}{4\Delta r}\{F(V_{i+1,j}) - F(V_{i-1,j})$$

$$+F(\tilde{V}_{i+\frac{1}{2},j+\frac{1}{2}}) - F(\tilde{V}_{i-\frac{1}{2},j+\frac{1}{2}}) + F(\tilde{V}_{i+\frac{1}{2},j-\frac{1}{2}})$$

$$-F(\tilde{V}_{i-\frac{1}{2},j-\frac{1}{2}})\} \quad - \frac{\Delta t}{4\Delta\theta} \{G(V_{i,j+1}) - G(V_{i,j-1})$$

$$+G(\tilde{V}_{i+\frac{1}{2},j+\frac{1}{2}}) \quad -G(\tilde{V}_{i+\frac{1}{2},j-\frac{1}{2}})$$

$$+G(\tilde{V}_{i-\frac{1}{2},j+\frac{1}{2}}) \quad -G(\tilde{V}_{i-\frac{1}{2},j-\frac{1}{2}})\}$$

$$-\frac{\Delta t}{2}\{\frac{1}{4}\ (B(\tilde{V}_{i+\frac{1}{2},j-\frac{1}{2}}) + B(\tilde{V}_{i+\frac{1}{2},j+\frac{1}{2}})$$

$$+B(\tilde{V}_{i-\frac{1}{2},j+\frac{1}{2}}) + B(\tilde{V}_{i-\frac{1}{2},j-\frac{1}{2}}))$$

$$+\tfrac{1}{2}(S(V_{i+1,j}) + S(V_{i-1,j})) - \dot{\psi}(V_{i,j})\} \qquad (34b)$$

Here we have used the notation $\tilde{V}_{i,j} = \tilde{V}^{n+1}_{i,j}$ and $V_{i,j} = V^{n}_{i,j}$ and have set $B=S-\dot{\psi}$. The system (34) differs from the corresponding difference equations given in Reference (5) by the inhomogeneous terms B and S. This is so because we now include a combustion model with source $\dot{\psi}$ and because in the cited reference the inhomogeneous term S was inadvertently omitted.

Except for the inhomogeneous term the difference approximations, Equations (34a) and (34b), are accurate to $O(\Delta t^3)$. The intermediate solution, $\tilde{V}$, computed from Equation (34a) satisfies

$$|\tilde{V}-W| = O(\Delta t^2)$$

while V, computed from Equation (34b), satisifes

$$|V-W| = O(\Delta t^3)$$

Furthermore, system (34) is stable in the sense of linear stability theory if the time step satisfies the inequality

$$\frac{\Delta t}{\Delta} < \frac{1}{\sqrt{2}} \frac{1}{|u|+c}$$

The local sound speed is c and the particle velocity is u while Δ is the space step. This result was first obtained by Richtmyer and has been born out in practical calculations.

The difference equations used (to approximate Equation (10)) are, from consistency requirements, the analogue of the physical conservation laws. Numerical integration carried out with the above difference equations will result in a solution which, if discontinuities appear, will automatically satisfy the Rankine-Hugoniot conditions. As we discussed in Section A, other difference equations will not yield the proper jump conditions across a finite zone of rapid variation - which is the difference approximation to the physical discontinuity.

The boundary condition of zero normal velocity is satisfied by using the reflection rules at the cylindrical wall. If the subscript + denotes image points and the subscript - denotes corresponding interior points then the reflection rules are given by

$$
\begin{aligned}
(\rho r)_+ &= (\rho r)_- \\
u_+ &= -u_- \\
(\rho v)_+ &= (\rho v)_- \\
p_+ &= p_- + 2\Delta r \left(\frac{\rho v^2}{r}\right)_-
\end{aligned}
\tag{35}
$$

These conditions will yield a zero value of normal velocity. In addition, we satisfy the condition that the pressure gradient in the radial direction is balanced by the centrifugal force $\rho v^2/r$ which is due to fluid motion in the tangential direction. In cartesian coordinates, when the radius of curvature becomes infinite, the above conditions reduce to the familiar forms

$\rho_+ = \rho_-$, $u_+ = -u_-$, $v_+ = v_-$ and $p_+ = p_-$.

Since there is a singularity in Equation (10) at r=0, which is due to the coordinate system chosen, the calculation at the center is carried out in a local cartesian coordinate system. The generalized divergence of the flow field at r=0 is given in cartesian coordinates via the differential conservation law

$$
\frac{\partial W}{\partial t} + \frac{\partial F}{\partial x} + \frac{\partial G}{\partial y} = \dot{\psi} \tag{36}
$$

in which the x-y components of momentum are related to the r-θ components of momentum by

$$\text{x-component:} \quad \rho u = \rho(u\cos\theta - v\sin\theta)$$

$$\text{y-component:} \quad \rho v = \rho(u\sin\theta + v\cos\theta)$$

We transform $f(r,\theta)\rightarrow f(x,y)$ and $g(r,\theta)\rightarrow g(x,y)$ using the above momentum transformations. The density and pressure are not affected by the coordinate transformations.

We now wish to compute the divergence of the flux of mass, momentum and energy at r=0, i.e.,

$$\left(\frac{\partial F}{\partial x} + \frac{\partial G}{\partial y}\right)\Bigg|_{r=0}$$

If we consider a region R with boundary ∂R in the x-y plane then, if $\partial F/\partial x$, and $\partial G/\partial y$ exist, we have, at some point in R,

$$\frac{\partial F}{\partial x} = \oint_{\partial R} F\,dy \Big/ \oint_{\partial R} x\,dy$$

$$\frac{\partial G}{\partial y} = -\oint_{\partial R} G\,dx \Big/ \oint_{\partial R} x\,dy$$

where all the contour integrals are taken counterclockwise. For this calculation ∂R is a circle of radius Δr and the contour integrals are approximated by the sums

$$\widehat{\frac{\partial F}{\partial x}} \approx \sum_{j=1}^{N} (F_{j+1}+F_j)\,(y_{j+1}-y_j) \Big/ \sum_{j=1}^{N} (x_{j+1}+x_j)\,(y_{j+1}-y_j)$$

$$\frac{\partial \hat{G}}{\partial y} \approx \sum_{j=1}^{N} (G_{j+1}+G_j)\ (x_{j+1}-x_j) \Big/ \sum_{j=1}^{N} (x_{j+1}+x_j)\ (y_{j+1}-y_j) \qquad (37)$$

Then, if we evaluate $\dot{\psi}$ at the origin, the solution can be advanced by the equation

$$V(0,t+\Delta t) = V(0,t) - \Delta t \left(\frac{\partial \hat{F}}{\partial x} + \frac{\partial \hat{G}}{\partial y} - \dot{\psi} \right) \qquad (38)$$

Equation (38) will be second order accurate if the fluxes are time averaged, i.e.,

$$F = \tfrac{1}{2}(F(t+\Delta t)+F(t)) \text{ and } G = \tfrac{1}{2}(G(t+\Delta t)+G(t))$$

These are exactly the fluxes used in Equation (37). Hence, Equation (38) is second order accurate, consistent with the accuracy attained at regular mesh points in the interior of the combustion chamber.

At r=0, the density, energy, magnitude and direction of the velocity vector is known. The local radial and tangential velocity components, in any direction θ, are obtained by projecting the cartesian velocity vector at the origin onto and perpendicular to each ray θ = constant. These values and those on the first row are used to obtain the values of V at half mesh points, i.e., $V(\Delta r/2,\theta,t)$. The values of $V(3\Delta r/2,\theta,t)$ are obtained by averaging the function V at Δr and $2\Delta r$. Using the given data at $(\Delta r,\theta,t)$ new values of $V=V(\Delta r,\theta,t+\Delta t)$ are obtained by using the two step difference equations over the interval $\Delta r/2<r<\frac{3\Delta r}{2}$, $0<\theta<2\pi$.

A test problem was run using the pancake motor code (called COMB). It consisted of the initial conditions given by Equations (32c) and (32d) and boundary conditions given by Equation (35) for the case where $\varepsilon = 3^{-1} \cdot 10^{-5}$ and $\dot{\psi}=0$. The solution produced by the numerical procedure described above yielded a solution which conserves the original distribution but rotates it uniformly in time - exactly what is predicted from linear theory. Figures (5) and (6) show the numerical solution for the pressure and velocity field at time t=.825. During this time the wave has undergone 1.8 revolutions - the period is 460 millisec. If the numerical pressure field is superimposed over the linearized pressure field, Figure (3), the contour lines are virtually coincident indicating good accuracy for the numerical method.

E. Convergence of the Difference Equations

It is to be expected, from approximation theory, that as the mesh, on which the solution vector V is defined, gets finer and finer, the solution vector will converge to the exact solution of the differential equation, W. The truncation error for the approximation used in this calculation is second order everywhere (except for the evaluation of the interpolated data for the first row calculation). We have carried out a finite difference calculation to the exact linear solution on two meshes, the finer one (all the results presented in this paper have been computed using this mesh) containing 11 points in r and 36 points in θ, and the coarse mesh containing 6 points in r and 18 points in θ. Figures (7) and (8) give the distribution of the pressure field

and velocity field at a time of 0.825 for the coarse mesh. These results may be compared to the fine mesh solution at approximately the same physical time in Figures (5) and (6). It is clear that some accuracy in the solution is absent using the coarse mesh. The two calculations can be compared to the exact calculation, given in Figures (1) and (2), to estimate the rate of convergence of the numerical solution. We also include Figures (9) through (11) to assist in estimating convergence of the difference method. Here, the linear theory, coarse mesh and fine mesh pressure distributions at the boundary of the chamber are shown. The shape of this distribution may be compared to nonlinear solutions in the next section. The pressure distributions at r=0, R/2 and R for $0 \leq t \leq 0.825$ for the coarse and fine meshes are shown in Figures (12) and (13). The linear nature of the solution is shown by the undistorted sinusoidal pressure distribution.

In this section we also show, in Figures (14) through (17) the ability of the difference equations to approximate the exact linear solution for the second tangential mode. The pressure and velocity distribution at t=0, obtained by first solving for the second root, K_2, in the transcendental equation $\partial J(Kr)/\partial r = 0$ at r=R and then using Equations (33a), (33b) and (33c), is shown in the first two plots of this series. The linear solution is characterized by noting that since $K_2 > K_1$ the rotation speed of the second tangential mode is higher than the first tangential mode,

and since there is no wave coalescence,because nonlinear effects are neglected,the initial distribution undergoes uniform rotation. By comparing the initial pressure and velocity distribution with that obtained after six hundred integration steps, the conservation of the initial distributions is demonstrated. We also show the pressure distribution on the boundary as a function of theta, Figure (18), and the pressure distribution at r=0, R/2 and R for $0 \leq t \leq 0.825$, Figure (19). The latter figure again substantiates the nonexistence of nonlinear gas motion since the sinusoidal distribution is undistorted.

F. Finite Amplitude Calculation of the First Tangential Mode

In order to carry out a finite amplitude analysis, only one parameter need be changed from the previous calculation. That parameter is the maximum initial pressure which, in this calculation, is 450 psia while the minimum initial pressure is 150 psia (or pressure ratio of 1.8). The velocity field at t=0 corresponding to this pressure is given in Figure (20). Figures (21) through (26) show in detail, the motion of the velocity field up to 600 cycles of computation after every 100 steps of integration. The final time corresponds to a value of time of 0.615 milliseconds. From Figures (27) to (29) a plot of the velocity field each 600 subsequent cycles of computation is shown. It is clear that

a) the velocity field does not remain symmetric (see Figure (28));

b) an induced flow is generated behind the compression wave;

c) the flow field is fully developed in about one period of rotation.

Figures (30) to (39) show the contours of the pressure field for this calculation every 100 integration steps up to 600 and then every 600 steps. Figure (30) is the initial field at $t=0$. It is clear, by scanning through these figures, that one observes that

a) the pressure field steepens in the leading edge of the compression pulse and spreads in the region of the trailing edge;

b) this steepening is most pronounced in the first half to three quarters of the first period, but the solution appears to remain continuous for all time,

c) a periodic ($\omega t+2\pi$) continuous wave solution seems to be the asymptotic ($t\to\infty$) solution. A total of about 5 3/4 rotations were computed and are shown in this sequence of figures. The pressure pulse has an almost constant amplitude.

These observed effects are clearly nonlinear in nature. This is substantiated by Figure (40) which shows the pressure distribution as a function of time at $r=0$, $R/2$ and R.

Figure (41) shows the tangential pressure distribution at the chamber wall shortly after the start of the calculation. Figure (42) shows the wave shape after steepening has occurred because of nonlinearities. The wave has undergone almost one

rotation. Figure (43) shows a streakline plot of a test particle with initial coordinates of r=4.95 inches and $\theta=0^{o}$. A streakline is the path traced out by an imaginary particle which is moving as a function of time. The cross lines indicate the four quadrants of the motor. Even though the path appears elliptical, the line does not close on itself and is moving in the direction of rotation. The motion of a particle in the linear case, is a closed elliptical path so that the net motion is zero.

In a second calculation, in which $\dot{\psi}=0=\bar{H}_Z$, the maximum initial pressure was raised to 590 psia while the corresponding minimum pressure was 10 psia (a pressure ratio of 59). The base pressure p=300 psia with $\gamma=1.2$. Figures (44) and (54) show the initial states of the pressure (and hence, density) field and velocity field for this calculation. As this series of plots shows, Figures (44) through (63), the calculated history of those fields differ quite markedly from the previous calculation because

a) a curved shock forms at the boundary. It is strongest at the wall while decreasing in strength as it curves inward towards the center of the chamber (sss Figure (46)).

b) The shock propagates circumferentially so that it is normal to the boundary.

c) Since there is no energy source the shock decays quickly because of reflection at the curved boundary (see Figure (47)).

The swirls seen behind the shock wave are due to numerical oscillations which occur when high order accuracy difference methods (accuracy greater than one) are used. The strong discontinuous behavior of the velocity field, in the neighborhood of this wave, is clearly seen and may be used to help locate the numerically smeared discontinuity (see Figure (56)).

It appears that if the pressure ratio (the maximum to minimum pressure) in the chamber is above a critical value, the asymptotic solution is reached, from the initial data, by first passing through a portion of the solution which is discontinuous. If the initial pressure ratio is below this value, the asymptotic solution is reached through a sequence of states which exhibit continuous states. We know that this critical pressure ratio lies between the two values used for the finite amplitude calculations shown here.

The reason a critical pressure ratio is required to achieve a shock is due to the presence of a curved wall. In one-dimensional flow, a shock wave evolves from an initial state which contains a continuous compression wave of arbitrary amplitude. However, when this normal shock propagates down a tube and strikes an inclined wall reflection occurs so that the shock which travels normal to the inclined wall is weaker than the original incident shock. The curved wall can be considered to be a continuous sequence of inclined walls continuously weakening the progressing shock. If the initial strength of the wave is such that nonlinear coalescence (which causes steepening of the wave) cannot dominate the continuous reflection process, the wave will remain continuous even though it is a compression wave.

Figures (64) through (68) show the pressure distribution at the chamber wall for successive instants in time. The gradual steepening of the initial wave (which is sinusoidal) is clearly shown. Figure (69) shows the pressure versus time at $\theta=0$ and for r=0, R/2 and R. The amplitude of the pressure pulse as it arrives at the reference line $\theta=0$ is seen to be a strong function of the radius with maximum amplitudes occurring at the chamber wall. The pressure level of these pulses are about 1100-1500 psia while at r=0, the pressure oscillates closely about the base chamber pressure of 300 psia.

Figure (70) shows a streakline for a particle starting at the point r=4.95 inches and $\theta=0^{\circ}$. The motion is complicated but, on the average, the particle traverses the chamber in a circular path. The particle has rotated through one quarter of the chamber while the wave has made five rotations.

G. Energy Release with Finite Amplitude Waves: Simple Energy Source

This calculation consists of adding an energy source term to the energy equation. There is no associated mass source term in the continuity equation. The energy term is dependent on the local pressure through the prescription

$$\dot{E} = \text{const}\ (p-1)^{\nu}, \quad \nu = \tfrac{1}{2} \text{ if } 0<p<1, \quad \nu = 1 \text{ otherwise} \qquad (39)$$

For this calculation we turn on the energy source slowly, i.e., the actual term used in the difference equation is $\omega\dot{E}$ where ω is a monitonically increasing function of time t in the closed interval $0<\omega<1$. We take ω to be the fraction of the first rotation completed at time t during the first rotation of the wave and is taken as unity for all subsequent rotations of the wave.

The sample calculation presented here starts with initial data corresponding to a maximum pressure equal to 590 psia, i.e., as shown in Figure (44) with velocity field given in Figure (54). Figures (71) through (73) show the development of the pressure wave until .625 millisecs. There is no axial flux calculation included for this case so that the energy and pressure will accumulate. It is clear that the pressure structure which develops is similar to the non-reactive case except that a peak pressure of 12900 psia is generated by the introduction of energy. The velocity field, Figures (74) through (76), is also similar to the non-reactive case. The maximum velocity for this calculation occurs behind the wave and is approximately 7000 ft/sec. Of course, as the calculation proceeds, the pressure amplitude continues to grow reaching a value approximately forty times the reference pressure while the maximum velocity reaches a value six times the reference sound speed after just six hundred more cycles of calculation. The constant in Equation (39) is proportional to the internal energy in the transverse plane at t=0.

Figure (77) shows the passage of the pressure pulse followed by a rapid rise in the pressure for all values of r. Note the large values of pressure represented on the scale.

Using Equation (39) a second calculation was completed in which the axial flux was included (Run 3). It is clear from the last section (Run 5) that unless energy is allowed to leave the system convectively, the pressure (as well as the specific internal energy) will continue to increase monotonically. Program COMB was modified to include, in an approximate way, a value for the axial flux of energy.

Several approximations were tried. The first method, and perhaps the most obvious, involved the computation of the total energy (and mass) contained in the r-θ plane for each cycle of computation.

Consider Integrals I of the form

$$I\{W\}=\int_0^R\int_0^{2\pi} W d\theta r dr \tag{40}$$

where W is a vector valued function $W=W(r,\theta)$. It is clear that the domain of integration is defined for r and θ over the closed interval $0\leq\theta\leq 2\pi$ and $0\leq r\leq R$.

Introduce for the function W a function of the single variable r via

$$\beta(W;r) = \int_0^{2\pi} W(r,\theta)d\theta \tag{41}$$

Then the double integral (40) becomes

$$I\{W\}=J\{\beta\} =\int_0^R \beta(W;r)rdr \tag{42}$$

Since the interval [0,R] will, in general, have N+1 net points that may be even, use of Simpson's rule cannot be considered since the number of points for that algorithm must be odd. For the case when an even number of net points is required to define the integrals, the following procedure may be used. Let h be the step size. Then split the integral into two parts so that

$$\int_0^R = \int_0^{3h} + \int_{3h}^R \tag{43}$$

where

$$\int_0^{3h} \beta(W;r)\,r\,dr = \frac{3h}{8}\left[3\beta'(W;h)+3\beta'(W;2h)+\beta'(W;0)\right.$$

$$\left.+\beta'(W;3h)\right] \quad +e_1, \quad \beta'=r\beta$$

We have included the error term e_1 which is defined by

$$e_1 = -\frac{3h^5}{80}\,\beta^{(IV)}(\xi) \quad 0<\xi<3h$$

and the second integral is obtained by applying Simpson's rule, i.e.,

$$\int_{3h}^{R} \beta(W;r)\,r\,dr = \frac{h}{3}\left[\beta'(W;3h)+\beta'(W;R)+2\sum_{j=1}^{m-1}\beta(W;3h+2jh)\right.$$

$$\left.+\,4\sum_{j=1}^{m-1}\beta(W;3h+(2j-1)h)\right] \quad +e_2$$

with error term e_2 defined by

$$e_2 = \frac{R}{180}\,h^4\beta^{(IV)}(\xi) \qquad 3h<\xi<R$$

It remains for us to evaluate $\beta(W;r)$. A condition of periodicity exists on W, i.e.,

$$W(\theta+2\pi) = W(\theta)$$

The Euler-Maclaurin summation formula with $h=h_\theta$ yields

$$\sum_{j=0}^{p-1} W(\theta+jh)=\frac{1}{h}\int_{\theta}^{\theta+ph} W(\tau)d\tau -\frac{1}{2}\left[W(\theta+ph)-W(\theta)\right]$$

$$+\frac{h}{12}\left[W'(\theta+ph)-W'(\theta)\right] -\frac{h^3}{120}\left[W'''(\theta+ph)-W'''(\theta)\right]$$

$$+\frac{h^5}{30240}\left[W^{V}(\theta+ph)-W^{V}(\theta)\right] -...$$

Setting p=1 and $\theta=0$ we obtain

$$\int_0^h W(\tau)d\tau = hW(0) + \frac{h}{2}\left[W(h)-W(0)\right]-\frac{(h)^2}{12}\left[W'(h)-W'(0)\right] +...$$

Due to periodicity the terms in the brackets cancel to zero if the above formula is used over the entire θ domain defined in terms of the contiguous intervals (θ_j,θ_{j+1}) $0<j<N-1$.

We can now write for β

$$\beta(W;r) = \int_0^{2\pi} W(r;\theta)d\theta = \frac{2\pi}{N}\sum_{j=0}^{N-1} W(r,\theta_j)+e \qquad (44)$$

with error e defined by

$$e = h^{2m+2}\ 2\pi C_m\ W^{(2m+2)}\ (\xi) \quad \underline{0}<\xi\leq 2\pi$$

where the function W is assumed to have 2m+2 bounded derivatives in the closed interval $[0,2\pi]$ and is 2π periodic. The above

formulae for $\beta(W;r)$ is used in the integration routine in COMB when computing the total mass and energy in the r-θ plane. We just apply Equation (44) to approximate Equation (41) which gives the integrand of Equation (42). Applying the approximations given for Equation (43) using this integrand, we can complete the appoximation to the original integral I, Equation (40). Then, to compute the divergence of the axial flux, $\partial H/\partial Z$, we compute I at some time t and require

$$\frac{d}{dt} I(t) = 0 \qquad (45)$$

or, equivalently, $I(t+\tau)-I(t)=0$, $\tau>0$. If $\tau=\Delta t$, the value of $I(t+\tau)$ is computed from the approximations to Equation (40) and is compared with I(t). The axial divergence at any of the q mesh points in $\mathcal{D}$ is just

$$H_Z = \frac{1}{q}(I\ (t+\tau)-I(t))$$

It is seen then that the excess due to accumulation of mass and energy is parceled equally so that, at each mesh point, there exists a contribution to outflow which will exceed the inflow by just the amount that is accumulated. It was found that this formulation worked for small amplitude pressure waves where small spatial variations in the energy release exist. However, for finite amplitude waves which initiate locally large influxes of energy (due to the increased velocity field) this formulation

fails to work. The reason is due to the fact that some regions of the flow field have little reaction occurring. Yet, according to this procedure, a relatively large axial outflow of energy is required. If this occurs for a sufficient number of time steps, the flow pressure (or density) gets quite small and can even become negative locally. Indeed, this has been our observation. It is clear that a weighting of the outflow according to the inflow or a retardation of the outflow would be more desirable.

A retardation procedure was carried out for the simple energy release model given by Equation (39). The results are given in the following table. The energy that was input due to the simulated combustion model was allowed to reside in the r,θ plane for one time step. It was then considered to contribute to the axial flux. Each calculation started with a maximum pressure of 590 psia and minimum pressure of 10 psia. In Table I, the first column is an inert calculation with no energy term, the second with the simple energy model including a retarded energy flux term approximating the divergence in the axial direction. Finally the third calculation is with the simple energy model but no convective flux in the x or axial direction.

Table I - Maximum Wave Amplitude (psia)

Cycle	Inert Case	With Axial Flux	Trapped Case
0	590	590	590
600	1151	1120	4289
1000		1150	7922
1200	884	1134	12872

The final row of data corresponds to approximately 3.27 rotations of the wave and it is clear that by including the axial flux, the rapid growth of the wave is controlled even while the energy source supplies energy to the wave as seen by the excess pressure over the inert case. Figure (78) shows the pressure history for this case.

It was found, however, that for values of ten times the constant in the energy law in Equation (39), the solution could not be continued beyond 300 cycles. This value is consistent with a physically real energy release near the injector. It is clear that the evaluation of the axial flux is quite critical. To adequately couple the axial dimension requires either a third dimension or an annular model so as to mathematically pose the calculation correctly.

A final sample calculation utilizing the pancake model with energy addition as well as mass addition, incorporates the simplified/modified Godsave analysis given in Section II of this report. This calculation includes the interaction process between a tangential pressure wave and a system of droplets (mean diameter=75μ) which evaporate and burn according to the simplified Godsave model of droplet combustion. For this calculation there is both an energy source for the energy equation as well as a mass source included in the continuity equation. However, the axial flux calculation is not included.

The calculation is initiated by specifying the flow field at t=0. For illustrative purposes we have chosen the one given in Figures (44) and (54) with the maximum (minimum) pressure being

590 psia (10 psia). The calculation proceeds without energy addition for as long as it takes the wave to make one complete rotation. Then the calculation incorporates Equations (34) through (41) developed in Section II of this report for the evaporation and combustion of the droplets. The energy and mass source is turned on completely just as the wave is starting its second period of rotation. Figures (79) through (86) give the fluid dynamic field for the entire run (number 6). The pressure and velocity distribution at t=.525 ms. is shown just after the energy is switched on in Figures (79) and (83). The large transient is clearly evident and the wave is moving clockwise.

The next two figures, Figures (80) and (84), show the pressure and velocity field after the energy and mass source terms have been turned on and the wave has made two rotations. The mass and energy addition, as the remainder of Figures (81) and (82) and Figures (85) and (86) show, are smearing out the gradients in the flow field. The solution is tending towards the linear theory distribution shown earlier since the maximum pressure ratio, as determined from Figure (82) is approximately 1.28, not a strong perturbation from unity. In Figure (87) we show the complete pressure time history at the radial positions r=0, R/2 and R. The pressure levels are rising continually due to accumulation of mass and energy.

In the next subsection we describe the annular combustion instability model which couples the energy release model to the gas dynamic field without a-priori outflow assumptions.

H. Nonlinear Differential and Difference Equations for the Annular Motor

The differential equations describing the motion of a compressible fluid in a cylindrical shell of fixed radius r with coordinates θ-z-t can be given, in vector notation, by the differential equation

$$\frac{\partial W}{\partial t} + \frac{1}{r}\frac{\partial G}{\partial \theta} + \frac{\partial H}{\partial z} + H^* \frac{\partial \mathrm{Ln}A}{\partial z} = \dot{\psi} \qquad (46)$$

As in the pancake motor, the vector W is a four vector, the components of which are as defined before except that the radial momentum is replaced by the axial momentum component. The vectors G and H represent the tangential and axial flux of the conservation quantities defining the vector W while the source term $\dot{\psi}$ has already been described in the pancake model.

The term containing the logarithmic derivative of the area variation, A(z), corresponds to an approximate way of treating small radial variations in the annular geometry. It is analogous to the treatment of one-dimensional time-dependent flows which include area variations. This term can also be considered as a source term of flux proportional to the derivative of the logarithmic variation of the area, A=A(z), the proportionality constant being the flux

$$H^* = H - p\delta_{i2} - pu\delta_{i4}$$

where

$$\delta_{i2} = \begin{cases} 1 \text{ for } i=2 \\ 0 \text{ for } i=1,3,4 \end{cases} \qquad \delta_{i4} = \begin{cases} 1 \text{ for } i=4 \\ 0 \text{ for } i=1,2,3 \end{cases}$$

This term allows us to treat, in a simple way, an annular subsonic-supersonic nozzle which has, by definition, a radial area variation. The reason for the introduction of such a term will be discussed at greater length in the section on boundary conditions but it is clear that converging-diverging nozzles exist on real annular motors and should be included in the approximation.

We may differentiate G and H with respect to W and write Equation (46) in the standard form for quasilinear partial differential equations, i.e.,

$$\sum_{i=0}^{n-1} A_i W_{x_i} + B = 0 \qquad (47)$$

We associate the matricies I, $\partial G/\partial W$ and $\partial H/\partial W$ with A_0, A_1 and A_2 respectively. In this notation our variables become $x_0=t$, $x_1=\theta$ and $x_2=z$ while the inhomogeneous term is a specified function of W, i.e.,

$$B = H^* \frac{\partial \text{Ln} A}{\partial z} - \dot{\psi} \qquad (48)$$

In order to test the annular model without the complication of the droplet field, we first studied, numerically, a computational scheme for a gas annular motor. In this first step toward construction of the complete annular model we must specify the flow

rate at the injector face in terms of a nonzero value of the axial gas velocity. Equation (47) will be the starting point for the construction of a stable difference approximation of the subsonic inflow boundary condition at the injector face. We must also consider the boundary condition required at the exit plane of the nozzle. This will be discussed in the following sections on boundary conditions. Once the techniques developed in the gas combustor are proven, the condition that u=0 on the injector face will be used while the complete droplet model is added.

We seek a solution to Equation (46) by the method of finite difference approximations. Equation (46) is a conservation law and the difference approximation to Equation (46) will also be in conservation form. The accuracy of the approximation will be second order. The method will be essentially the same as that adopted for the pancake motor.

On the periodic space $\mathcal{D}$ defined by $t>0$, $0\leq\theta\leq 2\pi$, $0\leq z\leq L$, we introduce a uniformly spaced mesh or net which consists of the points

$$\theta_i = i\Delta\theta,\ z_j = j\Delta z,\ t_n = n\Delta t,\ i,j,n = 0,1,2$$

The set of net points $\mathcal{D}_h$ is defined by

$$\mathcal{D}_h = \{\theta_i, z_j, t_n \mid i=0,1,\ldots;\quad j=0,1,\ldots;\quad n=0,1,\ldots\}$$

The approximation to $W(\theta_i, z_j, t_n)$ defined on the space $\mathcal{D}$ is represented by $V(\theta_i, z_j, t_n) = V^n_{ij}$ defined on $\mathcal{D}_h$. The approximation that is used is most easily written in two steps:

Let $\tilde{V}^{n}_{ij}$ be the first predicted value. It is given by

$$\tilde{V}^{n}_{i+\frac{1}{2},j+\frac{1}{2}} = \tfrac{1}{4}\left[V^{n-1}_{i+1,j+1} + V^{n-1}_{i,j+1} + V^{n-1}_{i+1,j} + V^{n-1}_{i,j}\right] \qquad (49a)$$

$$- \frac{\Delta t}{2\Delta\theta}\left[G(V^{n-1}_{i+1,j}) - G(V^{n-1}_{i,j}) + G(V^{n-1}_{i+1,j+1}) - G(V^{n-1}_{i,j+1})\right]$$

$$- \frac{\Delta t}{2\Delta Z}\left[H(V^{n-1}_{i+1,j+1}) - H(V^{n-1}_{i+1,j}) + H(V^{n-1}_{i,j+1}) - H(V^{n-1}_{i,j})\right]$$

$$- \frac{\Delta t}{4}\left[B(V^{n-1}_{i+1,j}) + B(V^{n-1}_{i,j+1}) + B(V^{n-1}_{i+1,j+1}) + B(V^{n-1}_{i,j})\right]$$

The final value is obtained from

$$V^{n}_{i,j} = V^{n-1}_{i,j} - \frac{\Delta t}{4\Delta\theta}\left[G(V^{n-1}_{i+1,j}) - G(V^{n-1}_{i-1,j}) + G(\tilde{V}^{n}_{i+\frac{1}{2},j+\frac{1}{2}})\right.$$

$$\left. - G(\tilde{V}^{n}_{i-\frac{1}{2},j+\frac{1}{2}}) + G(\tilde{V}^{n}_{i+\frac{1}{2},j-\frac{1}{2}}) - G(\tilde{V}^{n}_{i-\frac{1}{2},j-\frac{1}{2}})\right] \qquad (49b)$$

$$- \frac{\Delta t}{4\Delta Z}\left[H(V^{n-1}_{i,j+1}) - H(V^{n-1}_{i,j-1}) + H(\tilde{V}^{n}_{i+\frac{1}{2},j+\frac{1}{2}}) - H(\tilde{V}^{n}_{i+\frac{1}{2},j-\frac{1}{2}})\right.$$

$$\left. + H(\tilde{V}^{n}_{i-\frac{1}{2},j+\frac{1}{2}}) - H(\tilde{V}^{n}_{i-\frac{1}{2},j-\frac{1}{2}})\right]$$

$$- \frac{\Delta t}{2}\left[\tfrac{1}{4}(B(\tilde{V}^{n}_{i+\frac{1}{2},j-\frac{1}{2}}) + B(\tilde{V}^{n}_{i+\frac{1}{2},j+\frac{1}{2}}) + B(\tilde{V}^{n}_{i-\frac{1}{2},j+\frac{1}{2}})\right.$$

$$\left. + B(\tilde{V}^{n}_{i-\frac{1}{2},j-\frac{1}{2}})) + \frac{1}{2}\frac{\partial \mathrm{Ln}A_{i,j}}{\partial z}(H^{*}(V_{i,j+1}) + H^{*}(V_{i,j-1})) - \dot{\psi}(V_{i,j})\right]$$

The system of Equations (49) constitute the difference approximation to Equation (46). One may verify that the System (49) is indeed a second order accurate approximation to Equation (46) by allowing $\delta G = A_1 \delta V$ and $\delta H = A_2 \delta V$. Here δ corresponds to a spatial difference operator in θ or z and A_1, A_2, which were previously defined, are taken to be constant matrices. Then substituting Equation (49a) in Equation (49b) after using the definitions for the spatial differences in G and H, the following result is obtained

$$V_{i,j}^{n} = V_{i,j}^{n-1} + \Delta t(A_1+A_2)\delta V_{i,j}^{n-1} + \frac{\Delta t^2}{2}(A_1+A_2)^2\delta^2 V_{i,j}^{n-1} + \mathcal{O}(\Delta t^2)$$

$$+ \text{terms } \mathcal{O}(\Delta t \cdot B)$$

This expression is the Taylor expansion for V about $t=n\Delta t$ in terms of first and second order space operators δ and δ^2. This shows that the difference approximation to the exact solution W is second order accurate except for the inhomogeneous terms.

The periodicity condition in θ on the solution V, i.e.,

$$V(\theta,z,t) = V(\theta+2\pi,z,t)$$

reduces the specification of the problem to finding boundary conditions for the inflow and outflow conditions at z=0 and z=L. The theory is presented in the next section.

I. Boundary Conditions, Injector Face (Z=0)

If we were to seek a solution in some domain, $\mathcal{D}$, where $|z|<\infty$ (rather than the finite interval $0\leq z\leq L$) boundary conditions would not be required. For $|z|<\infty$, the differential problem is called an initial value problem. However, since the range of z is finite for the annular model, boundary conditions must be prescribed at the endpoints, z=0 and z=L. The natural conditions at the injector, z=0, are that the momenta $m=\rho w$ and $n=\rho v$ be prescribed

$$m(\theta,0,t) = m_o$$

$$n(\theta,0,t) = n_o \qquad (50a)$$

as well as energy

$$\frac{\frac{1}{2}(m_o^2+n_o^2)}{\rho^2(\theta,0,t)} + e(\theta,0,t) + p(\theta,0,t)\rho^{-1}(\theta,0,t) = L_o \qquad (50b)$$

The constant L_o is usually identified as the stagnation enthalpy.

The boundary conditions defined from Equations (50a) and (50b) are used to simulate the boundary values that one would impose on a gas injected rocket motor. Axial injection implies $n_o=0$ and we will only consider axial injection. Since we are prescribing subsonic inflow, one variable cannot be arbitrarily prescribed on the boundary. This is most easily seen by writing Equation (47) in characteristic form, i.e.,

$$W_t + A_1 W_\theta + A_2 W_z + B = 0 \qquad (51)$$

Let P be a matrix whose eigenvectors are that of A_2. Define V so that W=PV and substitute for W in Equation (51) to obtain

$$(PV)_t + A_1(PV)_\theta + A_2(PV)_z + B = 0 \qquad (52)$$

By carrying out the indicated differentiation one obtains an equation for V_t:

$$V_t + P^{-1}A_2PV_z = -P^{-1}\left[B + P_tV + A_2P_zV + A_1(PV)_\theta\right] \qquad (53)$$

which is in the simple characteristic form. We obtained this result by premultiplication of P^{-1} after the differentiation is carried out. Now $P^{-1}A\,P=\Lambda$ is a diagonal matrix with β_i the elements on the diagonal. This allows us to observe that differentiation on the left hand side of Equation (53) is in the characteristic direction

$$\frac{dz}{dt} = \beta_i \qquad (54)$$

i.e., the total differential of V itself is the left member of Equation (53):

$$V_t + \Lambda V_z = dV/dt$$

The elements β_i are the eigenvalues of A_2 which are linear combinations of the particle speed w in the z direction and sound speed c, i.e., w, w+c, and w-c. The direction w-c is left running for w<c; hence this characteristic runs to the boundary z=0 from the interior z>0. The vector V has the components

$$V = \begin{vmatrix} p + v - \rho c^2 \\ p + \rho cw \\ p - \rho cw \\ p - v - \rho c^2 \end{vmatrix}$$

Hence the data $p-\rho cw$ appears as a total differentiated quantity in the direction w-c. In the direction w-c the differential equation is given by

$$(p-\rho cw)_t + (w-c)\ (p-\rho cw)_z = -v(p-\rho cw)_\theta - \rho c^2 v_\theta - w(\rho c)_t -$$

$$-(w-c)(\rho c)_z - v(\rho c)_\theta \qquad (55)$$

The information $p-\rho cw$, on the boundary $z=0$, is then determined by integrating Equation (55) using conditions in the interior of the chamber. By solving Equation (55), the behavior of this characteristic variable coupled with the other boundary conditions will determine the complete time-dependent behavior at the injector boundary.

One simple numerical approximation to Equation (55) is obtained by allowing

$$\overline{\rho c} = \tfrac{1}{2}\left[(\rho c)^{n-1}_{i,0} + (\rho c)^{n}_{i,1}\right]$$

$$\overline{v} = \tfrac{1}{2}\left[v^{n-1}_{i,0} + v^{n}_{i,1}\right]$$

$$\overline{w} = \tfrac{1}{2}\left[w^{n-1}_{i,0} + w^{n}_{i,1}\right]$$

We solve for the pressure by using forward differences for the time and centered axial differences (θ differences can be centered) in Equation (55) via

$$p^{n}_{i,0} = p^{n-1}_{i,0} + \overline{\rho c}\,(w^{n}_{i,1}-w^{n-1}_{i,1}) + \frac{\Delta t}{\Delta z}\,(\bar{w}-\bar{c})\left[p^{n-1}_{i,0}-p^{n-1}_{i,1}\right.$$

$$\left. - \overline{\rho c}\,(w^{n-1}_{i,0}-w^{n-1}_{i,1})\right] - \bar{v}\,\frac{\Delta t}{4\Delta\theta}\left[p^{n-1}_{i+1,0}-p^{n-1}_{i-1,0}+p^{n}_{i+1,1}-p^{n}_{i-1,1}\right]$$

$$+ \overline{\rho c}\,\bar{v}\,\frac{\Delta t}{4\Delta\theta}\left[w^{n-1}_{i+1,0}-w^{n-1}_{i-1,0}+w^{n}_{i+1,1}-w^{n}_{i-1,1}\right] \qquad (56)$$

$$- \overline{\rho c}^{2}\,\frac{\Delta t}{4\Delta\theta}\left[v^{n-1}_{i+1,0}-v^{n-1}_{i-1,0}+v^{n}_{i+1,1}-v^{n}_{i-1,1}\right]$$

Now that the pressure is known at the advance time $n\Delta t$ on the injector face, $z=0$, we may then solve for the density ρ from Equation (50a), (50b) and the equation of state, Equation (12). Following this procedure we obtain for the positive root of the resulting quadratic equation for the density,

$$\rho = \frac{\gamma p}{2(\gamma-1)L_o}\left\{1 + \left[1+2L_o\,\left(\frac{(\gamma-1)}{\gamma p}\right)^2\,(m_o^2+n_o^2)\right]^{\frac{1}{2}}\right\} \qquad (57)$$

An iterative procedure could now be used by redefining the barred quantities $\bar{\rho}$ and $\bar{c}$ in terms of the latest estimate of the density, which is given above. Now that the density is known, as well as the pressure, all the data required to advance the solution to the next time level is known. The next section considers the boundary condition at the plane of outflow where $z=L$.

J. Nozzle Exit Plane (z=L)

The simplest and perhaps the fastest way to compute a supersonic outflow condition is to impose the following condition on all the outgoing characteristics facing the boundary (we assume, without loss of generality, a positive slope (all $\beta_i > 0$) when the flow velocity is $w > c$): that the total variation along the characteristic, of the function V, is zero. This means that if at the boundary z=L of $\mathcal{D}$, the flow is supersonic, then all three characteristics with slope w, w±c will intersect the boundary when the characteristics originate from the interior of $\mathcal{D}$. Then our prescription is equivalent to the statement that the boundary data are completely specified by the interior flow field data. Conversely, information specified at the boundary because of the geometry of the characteristics can have an effect only on the field to the right, or outside of $\mathcal{D}$.

We insure that the condition at the boundary of $\mathcal{D}$ will be supersonic by specifying a schedule of area variation in the axial direction, $\delta \mathrm{Ln}A/\delta z$. At some arbitrary point, say $z=\ell$ the chamber length, the area decreases simulating a converging nozzle section. At a section further downstrean, $\ell < z_t < L$ the area then increases up to the point z=L. The throat of our motor occurs at $z = z_t$ and the diverging section, of length $L - z_t$, produces a sufficiently strong supersonic outflow condition. The only conditions imposed on how to choose an area variation A(z) is the requirement on the steady state flow rate for the steady state operation of the rocket

motor. Hence, the ratio of the chamber area $A(z<\ell)$ to the throat area $A(z_t)$ is determined by allowing the Mach number at the throat section to be unity for the desired rate of flow specified at the injector. The area at the exit plane of the motor, $A(z=L)$, is chosen large enough so as to produce a Mach number on the flow sufficiently greater than one. Even under transient conditions the outflow must remain supersonic so that some experimentation on how large an area on the boundary of $\mathcal{D}$ to choose may be required. The "nozzle shape" chosen for this calculation is the parabola

$$\frac{A}{A_\ell} = 1-\alpha(z-z_\ell)+\beta(z-z_\ell)^2, \quad \alpha=1$$

The constant β was chosen so that the minimum area is reached at $1/3(z_L-z_\ell)$.

Then the boundary condition specified at $z=L$ is just

$$W(\theta,L,t) = W(\theta,L-\Delta z,t).$$

This corresponds to zero order extrapolation of the original function and is sufficient to produce smooth results. Any errors that result in specifying W rather than V will decay rapidly in the direction normal to the boundary of $\mathcal{D}$.

This completes the discussion of the boundary conditions. The next section presents some results of a calculation using these boundary conditions in the annular motor.

K. Results of a Test Case - Gas Annular Motor

The previously described theory was programmed and a test case was run. We wanted to evaluate the rate of convergence to the steady state solution starting from somewhat arbitrary initial data. The initial data prescribed is

$$\left.\begin{aligned} p &= 1/\gamma \\ \rho &= 1. \\ w &= 0.4 \\ v &= 0 \end{aligned}\right\} \quad 0 \leq z < \ell$$

$$\left.\begin{aligned} p &= p(z) \\ \rho &= \rho(z) \\ w &= w(z) \\ v &= 0 \end{aligned}\right\} \quad \ell \leq z \leq L$$

The exit Mach number was approximately two for the area variation chosen. The exact dependence of the density, pressure and velocity in the second interval was linear in z, the endpoint values $p(L)$, $\rho(L)$ and $w(L)$ being obtained from one-dimensional reversible flow tables at $\gamma=1.2$. Table II shows the convergence of the solution at the exit plane of the combustor, $z=z_\ell$.

Table II - Gas Annular Motor Convergence Test

Pressure at $z=z_\ell$	Iteration Cycle Number
$1./\gamma$	0
0.57281	200
0.52067	400
0.51894	600
0.52048	800
0.52018	1000

L. Results of a Test Case - Annular Motor and Complete Droplet Model

The previous model descriptions in Section H and Section J are used in this calculation. The previous treatment of the injector boundary is not required for this calculation. Here, a very much simpler condition is used, namely $w(0,\theta,t)=0$. To achieve this condition, a set of virtual points $z=-\Delta z$, $0\leqslant\theta\leqslant 2\pi$, which is parallel to the injector plane, take on the reflected quantities

$$\begin{aligned} \rho(-\Delta z,\theta,t) &= \rho(\Delta z,\theta,t) \\ w(-\Delta z,\theta,t) &= -w(\Delta z,\theta,t) \\ v(-\Delta z,\theta,t) &= v(\Delta z,\theta,t) \\ E(-\Delta z,\theta,t) &= E(\Delta z,\theta,t) \end{aligned} \qquad (58)$$

A test calculation without droplet evaporation and combustion was carried out with the above injector boundary conditions. The initial conditions imposed were the final results of the test case in Section K. As one would suppose, the combustion chamber merely evacuated since there was no source term while there was outflow through the converging-diverging nozzle. The calculation was terminated as the pressure dropped to 10^{-5} times its initial value at the injector. The solution remained stable and smooth throughout the complete calculation.

Next, the droplet spray program was coupled to the annular model. The equations used to describe the droplet motion are the conservation of mass and the momentum equations in the z and θ direction:

$$\frac{dm_\ell}{dt} = -\dot{m}_F$$

$$\frac{dv_1}{dt} = \frac{3}{8} C_D \frac{\rho}{\rho_\ell} \frac{(u_1-v_1)|u_1-v_1|}{r} \qquad (59)$$

$$\frac{dv_2}{dt} = \frac{3}{8} C_D \frac{\rho}{\rho_\ell} \frac{(u_2-v_2)|u_2-v_2|}{r}$$

where $m_\ell = \frac{4}{3} \pi \rho_\ell r^3$ is the mass of the drop, ρ_ℓ is the drop density, r is the drop radius, and ρ is the gas density. The axial and tangential components of drop velocity are v_1 and v_2; the corresponding components in the gas are u_1 and u_2. A simple drag coefficient correlation is used and it is dependent on the Reynolds number through

$$C_D = 27 Re^{-0.84}$$

Equation (33) in Section III-C defines $\dot{m}_F$ in terms of the local Reynolds and Prandtl numbers.

The computational procedure is as follows. Each mesh point is initially assigned a droplet of arbitrary radius and velocity. In practice this is accomplished by letting the drop radius decrease linearly to one-tenth its initial value and the drop velocity increase linearly from its injector value to the fluid velocity.

For each time step the above kinematic equations, Equation (59), are integrated using the initial droplet and gas dynamic

data. New drops are introduced at the injector (the droplet injection velocity is taken as a fixed constant). The computed drop velocities are then used to obtain the new drop positions. In general, the drops in the field $\mathcal{D}$ will no longer be defined at mesh points. However, the values of droplet mass, radius and velocity are redefined at the mesh points by two-dimensional linear interpolation. These values may then be used to compute a new value of the source term $\dot{\psi}$ in Equation (49b). In the event that the mass of the drop has decreased to .001 times its initial injected value, $\dot{\psi}$ at that point is set to zero. The next two tables give the initial distribution and the final converged distribution values for a complete solution of the gas dynamic equations coupled to the droplet model. The distributions shown in Table IV are independent of time and represent a self-consistent steady state solution to the coupled gas and droplet equations.

Initial Data in Combustor

Table III - Complete Model of Annular Motor

time = 0

	Density	Pressure	Velocity (axial)	Mach Number
Injector	1.50000E+00	1.25000E+00	0.	0.
	1.50000E+00	1.25000E+00	9.52381E-03	9.52381E-03
	1.00000E+00	8.33333E-01	2.85714E-02	2.85714E-02
	1.00000E+00	8.33333E-01	4.28571E-02	4.28571E-02
	1.00000E+00	8.33333E-01	5.71429E-02	5.71429E-02
	1.00000E+00	8.33333E-01	7.14286E-02	7.14286E-02
	1.00000E+00	8.33333E-01	8.57143E-02	8.57143E-02
	1.00000E+00	8.33333E-01	1.00000E-01	1.00000E-01
	1.00000E+00	8.33333E-01	1.14286E-01	1.14286E-01
	1.00000E+00	8.33333E-01	1.28571E-01	1.28571E-01
	1.00000E+00	8.33333E-01	1.42857E-01	1.42857E-01
	1.00000E+00	8.33333E-01	1.57143E-01	1.57143E-01
	1.00000E+00	8.33333E-01	1.71429E-01	1.71429E-01
	1.00000E+00	8.33333E-01	1.85714E-01	1.85714E-01
	1.00000E+00	8.33333E-01	2.00000E-01	2.00000E-01
	1.00000E+00	8.33333E-01	2.14286E-01	2.14286E-01
	1.00000E+00	8.33333E-01	2.28571E-01	2.28571E-01
	1.00000E+00	8.33333E-01	2.42857E-01	2.42857E-01
	1.00000E+00	8.33333E-01	2.57143E-01	2.57143E-01
	1.00000E+00	8.33333E-01	2.71429E-01	2.71429E-01
	1.00000E+00	8.33333E-01	2.85714E-01	2.85714E-01
	1.00000E+00	8.33333E-01	3.00000E-01	3.00000E-01
	1.00000E+00	8.33333E-01	3.14286E-01	3.14286E-01
	1.00000E+00	8.33333E-01	3.28571E-01	3.28571E-01
	1.00000E+00	8.33333E-01	3.42857E-01	3.42857E-01
	1.00000E+00	8.33333E-01	3.57143E-01	3.57143E-01
	1.00000E+00	8.33333E-01	3.71429E-01	3.71429E-01
	1.00000E+00	8.33333E-01	3.85714E-01	3.85714E-01
	1.00000E+00	8.33333E-01	4.00000E-01	4.00000E-01
Nozzle	9.29605E-01	7.63444E-01	5.52204E-01	5.56250E-01
	8.47546E-01	6.83305E-01	6.96713E-01	7.08333E-01
	7.60028E-01	5.99535E-01	8.33074E-01	8.56250E-01
	6.72210E-01	5.17398E-01	9.61060E-01	1.00000E+00
Throat	5.87944E-01	4.40577E-01	1.08064E+00	1.13958E+00
	5.09785E-01	3.71264E-01	1.19192E+00	1.27500E+00
	4.39168E-01	3.10438E-01	1.29517E+00	1.40625E+00
	3.76650E-01	2.58193E-01	1.39069E+00	1.53333E+00
	3.22168E-01	2.14051E-01	1.47888E+00	1.65625E+00
	2.75256E-01	1.77216E-01	1.56017E+00	1.77500E+00
	2.35226E-01	1.46758E-01	1.63499E+00	1.88958E+00
	2.01293E-01	1.21734E-01	1.70378E+00	2.00000E+00

Table IV - Complete Model of Annular Motor

time = 18.37 (1000 cycles)

	Density	Pressure	Velocity (Axial)	Mach Number
Injector	9.28150E-01	7.89215E-01	0.	0.
	9.13538E-01	7.73810E-01	6.41201E-02	6.35989E-02
	9.12505E-01	7.75075E-01	1.09623E-01	1.08582E-01
	8.89369E-01	7.51797E-01	1.83289E-01	1.81986E-01
	8.63476E-01	7.30310E-01	2.49047E-01	2.47208E-01
	8.27442E-01	6.95029E-01	3.25172E-01	3.23884E-01
	7.83244E-01	6.57257E-01	4.01881E-01	4.00486E-01
	7.32131E-01	6.07199E-01	4.88423E-01	4.89592E-01
	6.67104E-01	5.51421E-01	5.94258E-01	5.96678E-01
	5.81310E-01	4.67778E-01	7.31957E-01	7.44868E-01
	6.59025E-01	5.43878E-01	6.07480E-01	6.10439E-01
	5.94234E-01	4.80373E-01	7.09843E-01	7.20712E-01
	6.49877E-01	5.34865E-01	6.21127E-01	6.25006E-01
	6.03343E-01	4.89272E-01	6.94590E-01	7.04118E-01
	6.43187E-01	5.28278E-01	6.31268E-01	6.35859E-01
	6.09430E-01	4.95240E-01	6.84519E-01	6.93185E-01
	6.38178E-01	5.23340E-01	6.38961E-01	6.44114E-01
	6.13856E-01	4.99604E-01	6.77233E-01	6.85280E-01
	6.34552E-01	5.19748E-01	6.44605E-01	6.50190E-01
	6.16850E-01	5.02598E-01	6.72266E-01	6.79876E-01
	6.31935E-01	5.17111E-01	6.48774E-01	6.54707E-01
	6.18905E-01	5.04728E-01	6.68736E-01	6.76001E-01
	6.30185E-01	5.15256E-01	6.51774E-01	6.57975E-01
	6.20278E-01	5.06288E-01	6.66095E-01	6.73039E-01
	6.29106E-01	5.13916E-01	6.54036E-01	6.60582E-01
	6.20872E-01	5.07275E-01	6.64070E-01	6.70660E-01
	6.28991E-01	5.13251E-01	6.56029E-01	6.62963E-01
	6.20202E-01	5.07392E-01	6.61601E-01	6.67729E-01
	6.31056E-01	5.14208E-01	6.59789E-01	6.67236E-01
Nozzle	5.97427E-01	4.79087E-01	7.27485E-01	7.41598E-01
	5.91646E-01	4.67889E-01	7.66437E-01	7.86765E-01
	5.23376E-01	4.02085E-01	8.98350E-01	9.35627E-01
	5.24841E-01	4.02182E-01	9.03470E-01	9.42162E-01
Throat	4.53790E-01	3.38652E-01	1.03487E+00	1.09357E+00
	4.03407E-01	2.95989E-01	1.12696E+00	1.20102E+00
	3.57834E-01	2.58922E-01	1.20921E+00	1.29768E+00
	3.11213E-01	2.21971E-01	1.29833E+00	1.40339E+00
	2.71992E-01	1.91872E-01	1.37392E+00	1.49328E+00
	2.33512E-01	1.62681E-01	1.45834E+00	1.59497E+00
	2.03801E-01	1.40907E-01	1.52101E+00	1.66985E+00
	1.74090E-01	1.18918E-01	1.60507E+00	1.77282E+00

The oscillatory nature of the above steady solution is due to the fact that the difference scheme is not dissipative. For the shortest component of the solution, wavelength of $2\Delta z$, the amplification matrix has its largest eigenvalue lying on the unit circle (see Reference (8)). This defect has been remedied by the addition of an artificial viscosity (see Reference (7)).

The values in Table IV are changing by about 1 part in 1000 per 50 integration steps indicating that the solution has just about converged. It is to be noted that this computation started with a value of tangential velocity equal to zero. If it were non-zero, i.e., an initial disturbance characterizing spinning were present, then a steady state would take much longer to achieve. Indeed, depending on the energy value of the spin, there may be no steady state such as that presented in Table IV (see Reference (7)).

In the next section a complete theory of a burning droplet is presented and, as a result of numerical calculations using this model, the model is simplified as shown in Section E.

We have arbitrarily continued the number sequence from the gas dynamic analysis into the droplet analysis for the results given in tables and figures and references but have restarted the number sequence for equations.

III. DROPLET EVAPORATION AND COMBUSTION ANALYSES

A. The "Complete" Model

The propellant system considered will be hydrazine (N_2H_4)/ nitrogen tetroxide (N_2O_4). The oxidation behavior of this system has been the subject of intensive investigation for a number of years (References (9) through (18)). Recent evidence (Reference (18)) suggests that at moderate pressures, hydrazine decomposition occurs very close to the droplet surface, with the combustible decomposition products (NH_3 and H_2) partially oxidizing first with NO, followed by complete oxidation with O_2. The two distinct oxidation regimes result in the two-flame appearance characteristic of N_2H_4/N_2O_4 droplet combustion.

Since the rate-controlling chemical kinetic reactions were believed likely to change under very low or very high pressure conditions (the former is characteristic of high-altitude ignition, and the latter of high pressure rocket motor operation), a complete model of hydrazine droplet combustion would be one which includes a detailed description of the chemical kinetics. If it is assumed initially that the droplet undergoes spherically-symmetric, quasi-steady-state burning at constant pressure in quiescent oxidizer surroundings, and if it is further assumed that no viscous or body forces are present, and that thermal radiation can be neglected, the three-dimensional, time-dependent spherical conservation equations can be shown to reduce to:

1. Overall Continuity

$$\frac{d}{dr}(\rho r^2 v) = 0 \tag{1}$$

which if integrated between the droplet surface and any arbitrary radial location becomes

$$\rho v r^2 = \rho_s v_s r_D^2 \tag{2}$$

here v refers to the velocity of the droplet.

2. Species Continuity

$$\frac{1}{r^2}\left(a r_D \frac{dY_i}{dr} - \frac{d}{dr}\left(r^2 \frac{dY_i}{dr}\right)\right) = \frac{Sc}{\mu} R_i \tag{3}$$

where 'a' is a dimensionless mass burning rate:

$$a \equiv \frac{\rho_s v_s r_D}{\rho D} \tag{4}$$

Y_i = mass fraction of species i,

Sc = dimensionless Schmidt number ($\mu/\rho D$),

R_i = rate of generation or disappearance of i,

D = the diffusion coefficient

The boundary conditions for equation (3) are that (a) the net mass flux of all species (excepting the fuel, N_2H_4) at the droplet surface must equal zero:

$$\text{at } r = r_D: \quad \frac{a}{r_D} Y_i = \frac{dY_i}{dr}; \quad i \neq N_2H_4$$

$$\frac{a}{r_D}(Y_i - 1) = \frac{dY_i}{dr}; \quad i = N_2H_4 \tag{3a}$$

and (b) as $r \to \infty$, the gas environment consists only of N_2O_4 and its decomposition products (NO_2, NO, and O_2):

$$\text{at } r \to \infty: \quad Y_i = 0, \; i = 1,2,3,4 \qquad (3b)$$

$$Y_i = Y_{i,\infty}; \quad i = 5,6,7,8$$

The species numbering system is indicated in Table V. If the N_2O_4 and its products are assumed to be in chemical equilibrium, the $Y_{i,\infty}$ values are readily calculated.

TABLE V

Species		Molecular Weight	Heat of Formation (kcal/mole)
1)	N_2H_4	32	22.750
2)	NH_3	17	-11.040
3)	H_2	2	0
4)	N_2	28	0
5)	N_2O_4	92	2.170
6)	NO_2	46	7.910
7)	NO	30	21.580
8)	O_2	32	0
9)	H_2O	18	-57.798

3. Energy Conservation

$$\frac{1}{r^2}\left(ar_D c_p \frac{dT}{dr} - \frac{1}{Le}\cdot\frac{d}{dr}\left(r^2 c_p \frac{dT}{dr}\right)\right) =$$

$$\frac{dT}{dr}\left(\sum_i c_{p_i}\frac{dY_i}{dr}\right) - \frac{Sc}{\mu}\sum_i H_i R_i \qquad (5)$$

where Le = Lewis number ($\rho D c_p/k$)

k = thermal conductivity

c_p = mixture specific heat $\sum_i Y_i c_{p_i}$

H_i = enthalpy of species i

The appropriate boundary conditions are that (a) when the temperature of the droplet is taken to be uniform and constant, the heat conducted to the droplet must equal the heat required to vaporize the fuel leaving the droplet:

$$\text{at } r = r_D: \qquad \frac{1}{Le}\left(c_p\frac{dT}{dr}\right) = \frac{a}{r_D} L \qquad (5a)$$

and (b) as $r\to\infty$, the temperature approaches the rocket environmental temperature:

$$\text{as } r\to\infty: \quad T\to T_\infty \qquad (5b)$$

A series of species generation equations are required (the R_i terms). The actual chemical kinetic mechanism for N_2H_4/N_2O_4 is known to be enormously complicated, involving tens of species and probably well over one hundred elementary chemical reactions (Reference (19)). As an initial approximation to the actual chemical kinetic mechanism, the sequence of ten overall (global) irreversible reactions shown in Table VI may be taken to represent the

kinetic mechanism. Sawyer (Reference (14)) has investigated each of these reactions, and his values for the individual reaction rate constants are given in Table VI. (It should be noted that Sawyer observed no reaction between NH_3 and NO, and between H_2 and NO, which reduces this kinetic mechanism to 8 overall, irreversible reactions.) Based on this kinetic mechanism, the R_i terms may be written in terms of the reaction rate constants (k_m), the gas density, and the species mass fractions and molecular weights as shown in Table VII.

Assuming all gases to be ideal, the equation of state may be written

$$\rho = \frac{P}{R_o T \, \Sigma_i \frac{Y_i}{M_i}} \qquad (6)$$

Given the required thermochemical data (c_{p_i}, H_i, etc.), Equations (1), (3), (5), (6) and the R_i equations (Table VII), with the associated boundary conditions lead to a system of equations in which a number of functions must take on particular values; that is, this formulation leads to a multiple eigenvalue problem. The physical necessity for multiple eigenvalues is a subject of current research and debate (References (20) and (24)). Wehner (Reference (24)) argues that the second eigenvalue may be a kinetic parameter to which the flammability limits are related. (The first eigenvalue is the flame velocity in the theory of laminar, one-dimensional, premixed flames, and is the surface mass flux,

$\rho_s v_s$, in the droplet flame problem.) Williams (Reference (23)) refutes Wehner's arguments for the existence of more than one physical eigenvalue. In any event, the work of Campbell (References (20) through (22)) indicates the current inability to obtain solutions to systems of equations of this type without a number of additional simplifying assumptions. In the next section we simplify the model of the flame surface so as to be able to compute the evaporation rate while still retaining some aspect of the chemical kinetic effects.

TABLE VI

	REACTION	ORDER	REACTION RATE CONSTANT
1)	$N_2H_4 \rightarrow NH_3 + \frac{1}{2}H_2 + \frac{1}{2}N_2$	1	$10^{10.33} \exp - \frac{36,170}{RT}$
2)	$N_2H_4 + 4NO_2 \rightarrow 6NO + 2H_2O$	2	$10^{15.83} \exp - \frac{26,700}{RT}$
3)	$N_2H_4 + 2NO \rightarrow 2H_2O + 2N_2$	1	$10^{10.17} \exp - \frac{39,600}{RT}$
4)	$N_2H_4 + O_2 \rightarrow 2H_2O + N_2$	1	$10^{9.91} \exp - \frac{37,200}{RT}$
5)	$NH_3 + \frac{5}{2}NO_2 \rightarrow \frac{7}{2}NO + \frac{3}{2}H_2O$	2	$10^{15.85} \exp - \frac{33,800}{RT}$
6)	$NH_3 + \frac{3}{2}NO \rightarrow \frac{5}{4}N_2 + \frac{3}{2}H_2O$	-	No reaction
7)	$NH_3 + \frac{3}{4}O_2 \rightarrow \frac{1}{2}N_2 + \frac{3}{2}H_2O$	2	$10^{14.61} \exp - \frac{38,700}{RT}$
8)	$H_2 + NO_2 \rightarrow NO + H_2O$	2	$10^{21.5} \exp - \frac{58,000}{RT}$
9)	$H_2 + NO \rightarrow H_2O + \frac{1}{2}N_2$	-	No reaction
10)	$H_2 + \frac{1}{2}O_2 \rightarrow H_2O$	1	$10^{10.96} \exp - \frac{38,200}{RT}$

TABLE VII

SPECIES GENERATION EQUATIONS

(a) $$R_1 = -\rho Y_1 \left(k_1+k_2 \left(\frac{\rho Y_6}{M_6}\right) + k_3+k_4\right)$$

(b) $$R_2 = k_1 \rho Y_1 \frac{M_2}{M_1} - \rho Y_2 \left(k_5 \frac{\rho Y_6}{M_6} + k_7 \frac{\rho Y_8}{M_8}\right)$$

(c) $$R_3 = \tfrac{1}{2}k_1 \rho Y_1 \frac{M_3}{M_1} - \rho Y_3 \left(k_8 \frac{\rho Y_6}{M_6} + k_{10}\right)$$

(d) $$R_6 = -\rho Y_6 \left(4k_2 \frac{\rho Y_1}{M_1} + \frac{5}{2} k_5 \frac{\rho Y_2}{M_2} + k_8 \frac{\rho Y_3}{M_3}\right)$$

(e) $$R_7 = \frac{\rho Y_6 M_7}{M_6} \left(6k_2 \frac{\rho Y_1}{M_1} + \frac{7}{2} k_5 \frac{\rho Y_2}{M_2} + k_8 \frac{\rho Y_3}{M_3} - 2k_3 \rho Y_1 \frac{M_7}{M_1}\right)$$

(f) $$R_8 = -\left(k_4 \rho Y_1 \frac{M_8}{M_1} + \frac{3}{4} k_7 \rho^2 \frac{Y_2 Y_8}{M_2} + \tfrac{1}{2}k_{10} \rho Y_3 \frac{M_8}{M_3}\right)$$

(g) $$R_9 = 2 \rho Y_1 \frac{M_9}{M_1} \left(k_2 \frac{\rho Y_6}{M_6} + k_3+k_4\right) + \frac{3}{2} \rho Y_2 \frac{M_9}{M_2} \left(k_5 \frac{\rho Y_6}{M_6} + k_7 \frac{\rho Y_8}{M_8}\right) + \rho Y_3 \frac{M_9}{M_3} \left(k_8 \frac{\rho Y_6}{M_6} + k_{10}\right)$$

(h) $$R_4 = \rho Y_1 \frac{M_4}{M_1} \left(\tfrac{1}{2}k_1+2k_3+k_4\right) + \tfrac{1}{2}k_7 \rho^2 Y_2 Y_8 \frac{M_4}{M_2 M_8}$$

B. The Modified Flame Surface Analysis

1. Details of the Analysis

Recently, Peskin (References (25) and (26) has obtained solutions to the problem of a fuel droplet burning steadily in an oxidizing atmosphere by assuming, in addition to the assumptions noted in the previous section, that (a) the reaction mechanism could be adequately represented by a one-step, irreversible reaction of the type:

$$\nu_F F + \nu_o O \xrightarrow{k_f} \nu_P P \qquad (7)$$

where the ν_i represent the stoichiometric coefficients, F is the fuel, O the oxidizer, and P the product; (b) assuming the Lewis number to be unity; (c) taking constant averaged values for the specific heats, density, and heats of vaporation and combustion; (d) assuming transport parameters independent of temperature and chemical composition; (e) neglecting the energy transport due to species diffusion (i.e., the term $\frac{dT}{dr}\left(\sum_i c_{p_i} \frac{dY_i}{dr}\right)$ in equation (5)); and (f) by employing the modified flame surface approximation discussed below.

Although the analysis employs a number of assumptions, it has the advantage of retaining some aspect of the chemical kinetics. As a result, the feature of droplet extinction and re-ignition is retained; a feature which is of potential consequence in an unstable rocket system wherein the droplets may encounter regions of expansion and compression. Since droplet combustion analyses which

assume diffusional processes to be rate-controlling neglect the chemical kinetics entirely, the extinction-ignition feature is absent. Such an approximation is discussed in Section C.

Employing the additional assumptions discussed above, the species continuity equation

$$\frac{1}{r^2}\left(ar_D\frac{dY_i}{dr} - \frac{d}{dr}\left(r^2\frac{dY_i}{dr}\right)\right) = \frac{R_i}{\rho D}$$

may be written

$$a\frac{dY_i}{d\eta} - \frac{d}{d\eta}\left(\eta 2\frac{dY_i}{d\eta}\right) = i_i\eta^2 b\left(\frac{M_F^{(1-N_F)}}{M_O^{N_O}}\right)\left[Y_F\right]^{N_F}\left[Y_O\right]^{N_O} \qquad (8)$$

where $\eta \equiv \frac{r}{r_D}$, $b \equiv \frac{r_D^2 B}{D}$, $B \equiv \rho A(T)e^{-E/R_oT}$, and N_F and N_O represent the reaction orders with respect to fuel and oxidizer. The i_i term arises from the fact that

$$R_{ox} = \frac{\nu_O M_O}{\nu_F M_F} R_F \text{ and } R_p = \frac{-\nu_P M_P}{\nu_F M_F} R_F.$$

Thus, for the assumed one-step, irreversible reaction

$$N_2H_4 + NO_2 \rightarrow 2H_2O + \frac{3}{2}N_2 \qquad (9)$$

$i_1 = -1$, $i_2 = -(23/16)$, $i_3 = (9/8)$, and $i_4 = (21/16)$.

The simplified form of the energy equation (Equation 5) is

$$\frac{1}{r^2}\left(ar_D\frac{d}{dt}(c_pT) - \frac{d}{dr}\left(r^2\frac{d}{dr}(c_pT)\right)\right) = \frac{-1}{\rho D}\sum_i H_iR_i \qquad (10)$$

Introducing the notation $t \equiv (T-T_\infty)/(Q/c_p)$, and $Q = H_1+i_2H_2+i_3H_3+i_4H_4$, Equation (10) becomes:

$$a\frac{dt}{d\eta} - \frac{d}{d\eta}\left(\eta^2\frac{dt}{d\eta}\right) = \eta^2 b\left(\frac{M_F^{(1-N_F)}}{M_O^{N_O}}\right)\left[Y_F\right]^{N_F}\left[Y_O\right]^{N_O} \qquad (11)$$

Writing Equation (9) for the fuel, multiplying the resulting expression by i_2, then subtracting from it Equation (9) written for the oxidizer, leads to:

$$a\frac{d}{d\eta}\left(i_2Y_F-Y_O\right) - \frac{d}{d\eta}\left(\eta^2\frac{d}{d\eta}\left(i_2Y_F-Y_O\right)\right) = 0 \qquad (12)$$

which can be integrated to yield:

$$i_2Y_F-Y_O = c_1+c_2\exp(-a/\eta) \qquad (13)$$

Subtracting Equation (9) for the fuel from Equation (11) leads to

$$a\frac{d}{d\eta}(t+Y_F) - \frac{d}{d\eta}\left(\eta^2\frac{d}{d}(t+Y_F)\right) = 0 \qquad (14)$$

which, when integrated, becomes:

$$Y_F+t = c_3+c_4\exp(-a/\eta) \qquad (15)$$

The boundary conditions, Equations (3a), (3b), (5a) and (5b), reduce to:

$$\text{at } \eta=1: \quad \frac{d}{d\eta}Y_k\Big|_{\eta=1} = aY_k\Big|_{\eta=1}; \qquad k = O,P$$

$$\frac{d}{d\eta}Y_F\Big|_{\eta=1} = aY_F\Big|_{\eta=1} - a \qquad (12a)$$

as $\eta\to\infty$: $Y_F\Big|_{\eta\to\infty}=0$

$Y_k\Big|_{\eta\to\infty}=Y_{k,\infty}$ $k=O,P$ (12b)

at $\eta=1$: $\left.\frac{dt}{d\eta}\right|_{\eta=1} = \left(\frac{L}{Q}\right)a$ (14a)

as $\eta\to\infty$: $t\Big|_{\eta\to\infty} = 0$

Insertion of the appropriate boundary conditions into Equation (15), and after algebraic manipulation, an expression can be derived for the dimensionless mass burning rate:

$$a = \ln\left(\frac{1+t_s-\frac{L}{Q}}{1-Y_{F,s}-\frac{L}{Q}}\right) \qquad (16)$$

where $t_s = t\Big|_{\eta=1}$ and $Y_{F,s} = Y_F\Big|_{\eta=1}$

We now introduce the additional assumption that the flame zone of finite thickness can be replaced by an infinitessimal one represented by a Dirac-delta function located such that the fuel and oxidant react stoichiometrically. As a consequence, the right-hand sides of Equation (8) (written for the fuel) and (11) become:

$$\eta^2 b\, Y_F^* \cdot \delta(\eta-\eta^*)$$

where the asterisk refer to the values at the hypothetical flame surface, and δ is the delta function. (Note that the fact that

N_o=0 has been used in writing this term. The justification for this is detailed in the next section.)

Peskin (Reference (25)) shows that a solution to Equation (8) with this right-hand side is given by generalized function theory as

$$Y_F = \frac{b^*}{a} Y_F^* \eta^{*2} e^{-a/\eta} \left\{ \begin{array}{l} 1-e^{a/\eta} \text{ for } \eta>\eta^* \\ 1-e^{a/\eta^*} \text{ for } \eta<\eta^* \end{array} \right\} + 1-e^{-a/\eta} \qquad (17)$$

Therefore, for $\eta=\eta^*$ and $Y_F=Y_F^*$, Equation (17) becomes:

$$Y_F^* = \frac{(1-e^{-a/\eta^*})}{1+\frac{b^*}{a} \eta^{*2} (1-e^{-a/\eta^*})} \qquad (18)$$

Now when Equation (17) is solved at η=1 where $Y_F=Y_{F,s}$, and Equation (18) is used, the result is

$$Y_{F,s} = \frac{\frac{b^*}{a} \eta^{*2} (e^{-a}) (1-e^{a/\eta^*}) (1-e^{-a/\eta^*})}{1+\frac{b^*}{a} \eta^{*2} (1-e^{-a/\eta^*})} + 1-e^{-a} \qquad (19)$$

From the difference between Equation (8) written for the fuel and the oxidizer, and using the appropriate boundary conditions, the following expression is obtained for η^*

$$\eta^* = \frac{a}{\ln\left(\frac{i_o Y_{F,s}+Y_o(\infty)}{Y_o(\infty)e^{-a}+i_o Y_{F,s}}\right)} \qquad (20)$$

From the sum of Equation (8) (written for the fuel) and (11), again subject to the appropriate boundary conditions, the following expression can be derived for t*:

$$t^* = \frac{(Y_{F,s}+t_s)(e^{-a/\eta^*}-1)}{e^{-a}-1} - \frac{(1-e^{-a/\eta^*})}{1+\frac{b^*}{a}\eta^{*2}(1-e^{-a/\eta^*})} \qquad (21)$$

in which Equation (18) was also used.

Finally, using the result of the next section, b* can be written:

$$b^* = \frac{r_D^2}{D}\left[1.2 \times 10^{10} \cdot \exp(-26{,}800/RT^*)\right] \qquad (22)$$

Equations (16), (19), (20), (21) and (22) constitute five equations in the five unknowns a, $Y_{F,s}$, η^*, T*, and b*. (Unlike Peskin (Reference (25) and (26)), we are not interested here in species and temperature profiles surrounding the droplet, but in the mass burning rate, a; as a consequence, the equations developed above are particularly suited to this purpose.)

2. The Rate of the N_2H_4/N_2O_4 Reaction

In order to apply the previous modified flame surface analysis, realistic estimates must be obtained for the reaction rate constant, $k=A(T)\exp(-E/RT)$, and the reaction orders, N_F and N_O, corresponding to the N_2H_4/N_2O_4 reaction. These can be obtained from a one-dimensional, finite-rate analysis of the oxidation process, using the simplified chemical kinetic mechanism deduced from Sawyer (Reference (14)). This method is formulated in the following manner.

As mentioned above, the flow equations are written for one-dimensional, constant pressure, inviscid flow along streamtubes, with the following additional assumptions:

a. Negligible diffusion normal to the flow direction, leading to a uniform mixture of (gaseous) species at any streamwise point. Therefore, the oxidation is taken to be 'reaction-controlled'.

b. The flow is steady and adiabatic.

c. The initial concentrations of the oxidizing species are obtained in accordance with the following reaction equation and with the assumption of chemical equilibrium:

$$N_2O_4 \rightarrow a\ N_2O_4 + b\ NO_2 + c\ NO + d\ O_2 \qquad (23)$$

With these assumptions, the relevant equations are:

Energy Conservation

$$\frac{dh}{dt} = 0; \quad h = \text{constant} \qquad (24)$$

where h includes sensible and chemical enthalpy.

Species Conservation

$$\rho \frac{dY_i}{dt} = r_i \qquad (25)$$

Equation of State

$$\rho = \frac{pM}{RT} \qquad (26)$$

Auxiliary Equations

$$h = \sum_i Y_i h_i \tag{27}$$

$$M = \left(\sum_i \frac{Y_i}{M_i} \right)^{-1} \tag{28}$$

The enthalpy terms are taken to be linear in form:

$$h_i = \Delta_i + \bar{c}_{p_i} (T - T_{REF}) \tag{29}$$

where the reference temperature was chosen to be 1000°K. Values for Δ_i and $\bar{c}_{p_i}$ were obtained from the data of Reference (27).

It should be emphasized that this premixed, homogeneous gas-phase analysis is designed to supply an appropriate representation of the overall (global) oxidation reaction rate, for use in Equations (8) and (11). It is not, of course, a representation of the processes occurring around the fuel drop, where a counter-flow diffusion flame exists, as described by Equations (8) and (11).

Results are presented in Figure (88). Defining the ignition delay time (t_{ID}) qualitatively as the time required for the principal oxidation reactions to occur, Figure (88) yields the anticipated result that t_{ID} is a strong function of the initial mixture temperature. On the other hand, these results indicate that in the range examined, t_{ID} is nearly independent of the pressure. As can be seen, at the higher pressures, the second-order reactions (which become more significant at higher pressures)

produce an initial partial oxidation which results in a slight temperature increase. However, a leveling-off period is seen to subsequently occur, followed by the principal, first-order oxidation processes which drive the reaction to completion.

As a result, the reaction may be said to be first-order, with ignition delay times (taken from Figure (88)) as shown in Figure (89). In this latter figure, T_i is the initial mixture temperature. The approximate straight line behavior of ln t_{ID} when plotted against reciprocal initial temperature is in accordance with elementary chemical kinetic theory which predicts a function of the form

$$t_{ID} = \alpha \cdot \exp(E/RT_i)$$

where α is a constant and E is an overall activation energy. From Figure (89) E was determined to be about 26,800 calories/mole.

As an initial estimate, the pre-exponential factor in the overall reaction rate constant was chosen to be the average of the pre-exponential factors for the N_2H_4 oxidation reactions as deduced by Sawyer (Table VI). From this and the result obtained above, the initial estimate of the overall reaction rate constant was

$$k_f = 1.2 \times 10^{10} \exp(-26{,}800/RT) \qquad (30)$$

To check this estimate, results using Equation (30) were checked against results obtained using the complete streamtube analysis. The comparison was made at high pressure (20 atm), where the first-order approximation and Equation (30) would be least accurate. The results are shown in Figure (90), with the streamtube result labeled 'exact'. The global model does not, of course, predict the initial reactions or the leveling off period after the initial second-order reactions have occurred, but the general behavior and the delay time appear to be reasonable. Although the result for this particular case could have been improved by adjustment of the pre-exponential factor in Equation (30), this was felt to be unwarranted, and Equation (30) was selected as a suitably accurate overall reaction rate constant for inclusion in the modified flame surface analysis. This result is reflected in that analysis through Equation (22), and the fact that N_o was taken equal to zero.

C. The Diffusion-Controlled Flame Analysis

For the purpose of comparison with the previous analysis, a diffusion flame model was developed. Introducing the rate of disappearance of the fuel

$$\dot{m}_f^o \equiv \rho_s v_s (4\pi r_D^2) \tag{31}$$

Setting $Q=Q_T$, where Q_T is the heat of reaction per unit mass of fuel and oxidizer consumed, while using the definition of t_s ($t_s=c_p(T_S-T)/Q$), and the fact that Le=1, and noting that $Y_{F,s}=1$ for this elementary diffusion flame model, Equation (16) reduces to

$$\dot{m}_F^o = \frac{4\pi r_D k}{c_p} \ln\left(1+\frac{c_p(T_\infty-T_s)+Y_{O,\infty}\ \phi f_s \Delta H_R}{L}\right) \tag{32}$$

where $Q_T=(Y_{O,\infty}\phi f_s \Delta H_R)$, $Y_{O,\infty}$ is the mass fraction of oxidizer in the chamber gases, ϕ is the fuel-oxidant equivalence ratio, f_s is the stoichiometric fuel-oxidant ratio, ΔH_R is the heat of reaction per unit mass of fuel, and the superscript zero on the $\dot{m}_f^o$ term indicates that this is the fuel mass flux in a <u>stationary</u> environment; that is, in the absence of forced convection effects. Written in a slightly modified form, Equation (32) is frequently referred to as the Godsave equation.

In order to extend this equation to account for the fact that there will, in general, be a difference in velocity between the droplet and its surroundings, it will be assumed that the mass flux dependence can be represented by the expression of Agoston, Wise, and Rosser (Reference (28)):

$$\frac{\dot{m}_F}{\dot{m}_F^o} = 1+0.276(\mathrm{Re})^{\frac{1}{2}}(\mathrm{Pr})^{1/3} \tag{33}$$

where $\mathrm{Re} = (2\rho_\infty r_D)|u-v|/\mu_\infty$ and $\mathrm{Pr} = c_{p\infty}\mu_\infty/k_\infty$.

In this manner, the components of the $\dot{\psi}$-vector of the hydrodynamics code can be written (assuming no drag force interactions for the pancake or annular model):

$$\dot{\psi} = N \begin{vmatrix} \dot{m}_F & (1+\frac{1}{\phi f_s}) \\ & 0 \\ & 0 \\ \dot{m}_F & (\Delta H_R - L - \frac{L_o}{\phi f_s}) \end{vmatrix} \tag{34}$$

where L_o is the latent heat of the oxidizer and N is the number density of the drop field, i.e., number of drops per unit volume.

D. Results

Results using these analyses have been obtained for the following values of the parameters:

$Y_o(\infty) = 0.25 \qquad \phi = 1$

$D = 10^{-4} \ \frac{ft^2}{sec}$

$i_o = \frac{23}{16}$ (see Equation (1))

Q was calculated from the enthalpies obtained from Equation (29); L was obtained from the Clausius-Clapeyron equation using the vapor pressure data in Reference (29); in going from a to $\dot{m}_F^o$, k was obtained from Reference (29) and c_p from Reference (30).

Results are shown in Figures (91), (92), and (93). In Figure (91), the results are compared with the previous results obtained from the Godsave analysis (Equation (32)) and the experimental results of Reference (31). As can be seen, the current analysis yields results which are about 80% higher over most of the range of r_D than the corresponding Godsave value. This is due, at least in part, to the values chosen for $Y_O(\infty)$ and D, as well as the differences inherent in the two approaches. It is interesting to note, however, that the line corresponding to $T=1035^oK$, p=300 psia (Curve B) passes right through the experimental points of Reference (31). Unfortunately, Reference (31) does not indicate the level of pressure at which these experiments were conducted, leaving this possible correlation unresolved. However, the linear dependence of the burning rate on droplet diameter is retained by the modified flame surface analysis, in accordance with the experimental results.

Figure (92) contrasts the ambient temperature dependence of this analysis and the Godsave analysis for the particular conditions noted. It can be seen in Figure (92), that the Godsave analysis yields a very weak, almost linear ambient temperature dependence.

Most experimental work indicates a stronger, nonlinear dependence. The modified flame surface analysis does yield this latter type of dependence. It may be justifiably said, however, that the difference between the two analyses at these particular conditions are not sufficiently great to warrant using the current analysis in the pancake or annular computer program. In particular, no evidence of extinction can be seen down to ambient temperatures near the boiling point of the fuel. If this same result is discovered at other values of the ambient pressure as well, this will constitute ample justification for the use of the simpler Godsave analysis.

The effect of ambient temperature on the values of $Y_{F,s}$, η^* and T^* are shown in Figure (93). The value of $Y_{F,s} \to 1$, as T_∞ increases, in accordance with the assumption of the Godsave diffusion-flame approximation ($Y_{F,s}=1$). The hypothetical flame surface moves away from the droplet as T_∞ increases; this stems from the fact that in order to sustain a stoichiometric combustion process, the flame location must move away from the flame surface where a larger quantity of fuel vapor ($Y_{F,s}$) is being produced. Finally, T^* exhibits a linear dependence on T_∞.

E. The Reduced Godsave Analysis

Preliminary runs which coupled the complete Godsave analysis to the fluid dynamics program indicated that the running times were excessively long. (Roughly, five times slower than with the elementary energy term previously used.) As a consequence, the results obtained from the Godsave analysis were used to formulate the following simplified version of this analysis:

The weak, almost linear, temperature dependence of the dimensionless mass burning rate can be approximately expressed as

$$a_{300} = (3.73 \times 10^{-5})(T_\infty) + 1.855 \qquad (35)$$

where a_{300} is the dimensionless burning rate at a chamber pressure of 300 psia. The pressure dependence of the mass burning rate, a_p, is approximately given by

$$\frac{a_p}{a_{300}} = \left(\frac{p_\infty}{300}\right)^{0.0108} \qquad (36)$$

Once a_p is computed, the burning rate in stationary surroundings is obtained from

$$\dot{m}_F^o = \frac{2\pi k}{c_p} \; d_L a_p \qquad (37)$$

where d_L is the drop diameter, and the thermal conductivity and specific heat are functions of the liquid drop temperature.

The drop temperature, T_L, which is the boiling temperature at the chamber pressure, can be obtained to a good approximation from the integrated Clausius-Clapeyron equation

$$\ln \frac{p}{2131} = (8.7 \times 10^3) \left(\frac{1}{1176} - \frac{1}{T_L} \right) \tag{38}$$

where p is in psia, T_L is in $^{\circ}R$, and the critical point conditions are 2131 psia, $1176^{\circ}R$.

Knowing T_L, k is obtained from a linear curve fit of the data in Reference (14):

$$k = \frac{1}{3600} \left[(-8.33 \times 10^{-5}) (T_L - 460) + 0.2107 \right] \tag{39}$$

and c_p is obtained from Reference (15):

$$c_p = 0.138 + 0.527 \times 10^{-3} T_L - 0.120 \times 10^{-6} T_L^2 \tag{40}$$

From $\dot{m}_F^o$, the burning rate in the convective environment is then obtained from Equation (33):

$$\frac{\dot{m}_F}{\dot{m}_F^o} = 1 + 0.276 (Re)^{\frac{1}{2}} (Pr)^{1/3} \tag{41}$$

Under the engine conditions of interest, the following constant values are reasonable:

$$Pr^{1/3} = 0.6$$

$$L_F = 540 \frac{Btu}{lbm}$$

$$L_o = 178.2 \frac{Btu}{lbm}$$

$$Q = 12,400 \frac{Btu}{lbm}$$

where L_F is the latent heat of the fuel, L_O is the latent heat of the oxidizer, and Q is the heat of reaction. The appropriate terms in the ψ-vector of the fluid dynamics program may now be obtained (Equation 34).

IV. CONCLUSIONS AND RECOMMENDATIONS

The conclusions reached from the computations carried out thus far are that a stable convergent numerical method has been constructed which can analyze nonlinear liquid propellant rocket stability. The pancake model and the annular model are two distinct codes which can analyze nonlinear wave motion in r-θ-t space and θ-z-t space respectively. In the pancake model we have observed:

1. Linear tangential waves do not coalesce while maintaining a constant rotational period. These results are, of course, not new but can be predicted from the nonlinear computer program.
2. Nonlinear tangential waves having an amplitude of approximately 1100 psia on a base pressure of 300 psia have a completely different structure from linear waves and, indeed, may even become shock-like depending on the initial pressure ratio. Interestingly, the period of wave rotation for the nonlinear problem is close to the period for the linear problem.
3. Large induced velocity fields are generated by the nonlinear compression spike and appear behind the wave front.

4. When energy is coupled to the perturbing wave, the wave amplitude is larger than the nonenergy case.
5. Only when outflow is constructed does there appear to be any hope of achieving asymptotically, $t \to \infty$, a finite wave amplitude rather than a solution which blows up.
6. The ability to construct outflow conditions for the pancake model simulating the effect of a converging-diverging nozzle, in steady flow, along the lines which are described in the Priem-Guentert instability model were not successful for finite waves. The method, modified for two space dimensions, seemed to work for limited integration time only with infinitesimal finite amplitude waves; the solution eventually became unbounded.
7. The annular model, however, can compute the complete flow field, including a dilute droplet spray approximation, for a subsonic combustor and transonic-supersonic nozzle. A fuel shut-off calculation was used as one test for the code.

8. Steady one-dimensional flows have been obtained with the annular model as asymptotic, $t \to \infty$, solutions. The complete gas dynamic and droplet evaporation model was solved as a coupled system. No additional calculations were performed with this model.

In conclusion, we feel that the pancake model can be used to describe, with good accuracy, the transverse motion of finite amplitude waves in rocket motors but without coupling with a combustion model. A-priori assumptions on energy and mass accumulations necessary to solve the problem fail to yield physically realistic solutions.

The annular model can be used to yield stable solutions without the introduction of such assumptions. The annular model program can, therefore, compute time-dependent coupled gas dynamic and droplet combustion problems for a two-dimensional rocket motor.

As a result, the annular model should be further developed to be used with baffles and, in conjunction with the pancake model, slots and ports. The stability of a rocket engine should be amenable to evaluation and study using the models described in this report.

REFERENCES

1. Priem, R.J. and Guentert, D.C., Combustion Instability Limits Determined by a Non-Linear Theory and a One-Dimensional Model, NASA TN-D-1409, October 1962.

2. Campbell, D.T. and Chadwick, W.D., Combustion Instability Analysis at High Chamber Pressure - Final Report, AFRPL-TR-68-179, Edwards Air Force Base, California, August 1968.

3. Crocco, L. and Cheng, S.I., Theory of Combustion Instability in Liquid Propellant Rocket Motors, ARGARDograph, No. 8, Butterworths Scientific Publications Ltd., London 1956.

4. Priem, R.J., Theoretical and Experimental Models for Unstable Rocket Combustor, 9th International Symposium on Combustion, The Williams and Wilkins and Co., Baltimore, p.982.

5. Burstein, S.Z., Nonlinear Combustion Instability in Liquid Propellant Rocket Engines, JPL TR 32-1111, September 1967.

6. Protter, M.H., Nonlinear Partial Differential Equations, edited by W.F. Ames, Academic Press, 1967.

7. Burstein, S.Z. and Schechter, H.S., A Study of High Frequency Nonlinear Combustion Instability in Baffled Annular Liquid Propellant Rocket Motors, Vols. I-II, MAGI Final Report to NASA, Contract NAS7-752, August 1970.

8. Richtmyer, R.D. and Morton, K.W., Difference Methods for Initial Value Problems, Interscience 1967.

9. Eberstein, I.J. and Glassman, I., Progress in Astronautics and Rocketry, Vol 2: "Liquid Rockets and Propellants, Academic Press, Inc., New York, 1960; p.s. 351-366.

10. Eberstein, I.J. and Glassman, I., Tenth Symposium (International) on Combustion, The Comb. Inst., 1965; pp. 365-374.

11. McHale, E.T. et al, Tenth Symposium (International on Combustion), The Comb. Inst. 1965; pp. 341-351.

12. Christos, T., et al, Third ICRPG Combustion Conference; pp. 475-476.

13. Lawver, B.R., AIAA Journal, 4, 659-662 (1966).

14. Sawyer, R.F., "The Homogeneous Gas Phase Kinetics of Reactions in the N_2H_4-N_2O_4 Propellant System", Ph.D. Thesis, Univ. Microfilms, Inc., Ann Arbor, Michigan, Order No. 66-9638, 1966.

15. Sawyer, R.F., Third ICRPG Comb. Conf; pp. 481-495.

16. Sawyer, R.F. and Glassman, I., Eleventh Symposium (International) on Combustion, The Comb. Inst., 1967; pp 861-869.

17. Breen, B.P. and Beltran, M.R., Paper WSCI 65-21, 1965 Fall Meeting of the Western States Section/The Comb. Inst., Oct. 25, 1965.

18. Hersh, S., et al, Paper WSCI-67-24, 1967 Spring Meeting of the Western States Section/The Comb. Inst., March 20, 1967.

19. Chinitz, W. and Baurer, T., "Nonequilibrium Aspects of the Combustion and Freezing of the Liquid Rocket Propellants Aerozine-50 and N_2O_4", GASL TR 587, January 1966.

20. Campbell, E.S., Sixth Symposium (International) on Combustion, Reinhold, New York, 1957; p. 213 et seq.

21. Campbell, E.S., et al, Seventh Symposium (International) on Combustion, Butterworths, London, 1959; p. 332 et seq.

22. Campbell, E.S., et al, Ninth Symposium (International) on Combustion, Academic Press, New York, 1963; p. 72 et seq.

23. Williams, F.A., Combustion and Flame, 8, p. 165 (1964).

24. Wehner, J.F., Ibid, p. 166.

25. Peskin, R.L. and Wise, H., AIAA Journal, 4, p. 1646 (1966).

26. Polymeropoulos, E.C. and Peskin, R.L., Paper WSCI 67-5, 1967 Spring Meeting of the Western States Section/The Comb. Inst., April 24-25, 1967.

27. Dow Chemical Company, JANAF Thermochemical Tables.

28. Agoston, G., et al, Sixth Symposium (International) on Combustion, Reinhold, New York, 1957.

29. Aerojet-General Corp. Report on Properties of Propellants.

30. Haws, J.L. and Harden, D.G., J. Spacecraft and Rockets, 2, 972 (1965).

31. Dynamic Science Report No. SN-95-4, Monthly Progress Report under Contract No. NAS7-567, 1967.

PANCAKE MOTOR COMPUTER RUN CONDITIONS

Run	Base Pressure (psia)	Maximum Initial Pressure (psia)	Energy Model	Mesh Size
1	300	300.0001	None	11 x 36
2	300	450	None	11 x 36
3	300	590	Simple Model with Axial Flux	11 x 36
4	300	590	None	11 x 36
5	300	590	Simple Model without Axial Flux	11 x 36
6	300	590	Godsave Model without Axial Flux	11 x 36
7	300 (second tangential mode)	300.0001	None	11 x 36
8	300	300.0001	None	6 x 18

One of the above run numbers appear on each figure heading of the figures associated with Section II of this report. This helps to identify, in each figure, the conditions that characterize the data shown in the figure.

LIST OF FIGURES

PANCAKE MOTOR-1

PRESSURE ISOBARS

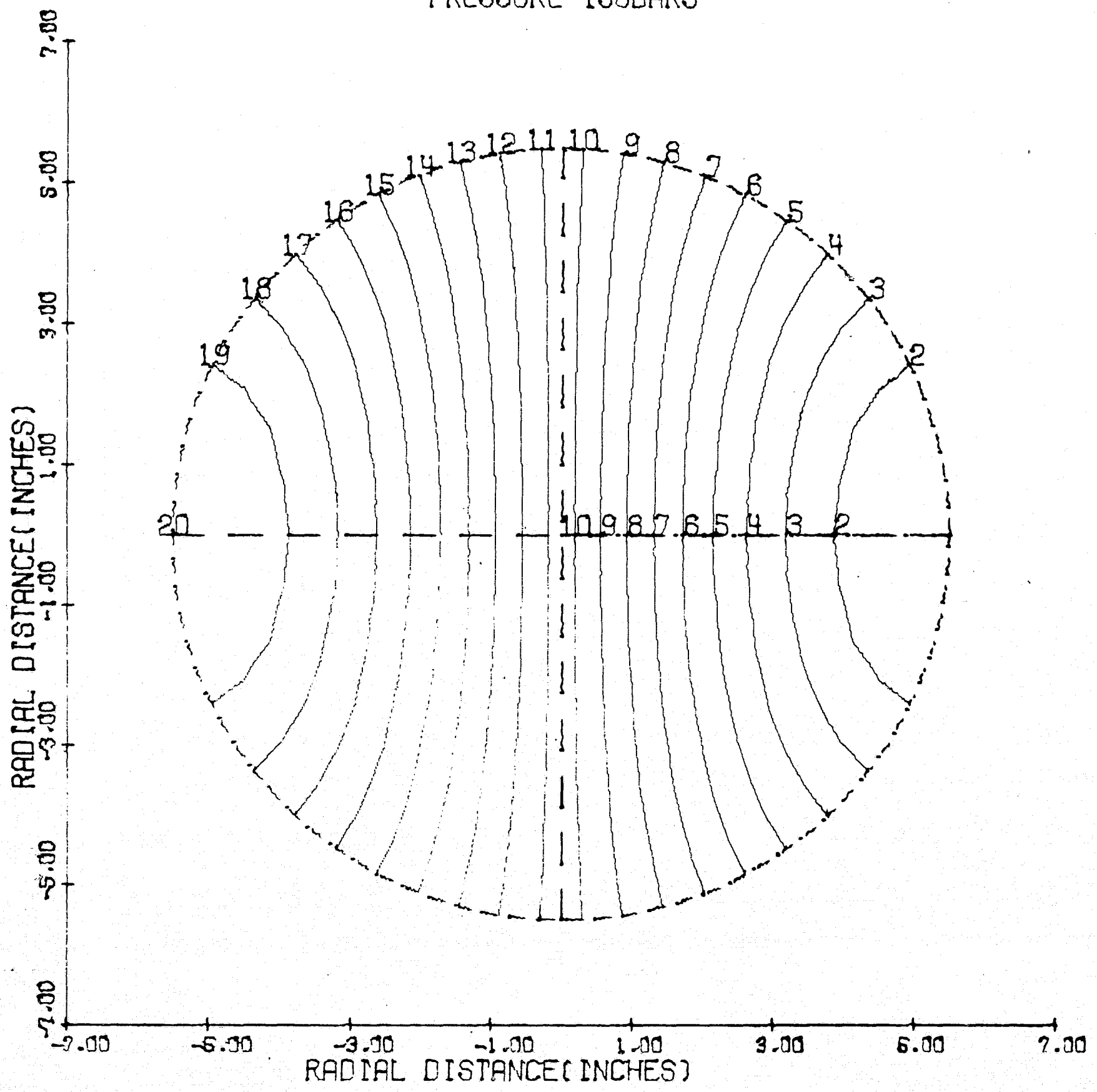

T= 0.000 MILLISECONDS

Figure 1

PANCAKE MOTOR-1

T= 0.000 MILLISECONDS

ISOBAR	PRESSURE(PSI)
1	299.999
2	299.999
3	299.999
4	299.999
5	299.999
6	300.000
7	300.000
8	300.000
9	300.000
10	300.000
11	300.000
12	300.000
13	300.000
14	300.000
15	300.000
16	300.001
17	300.001
18	300.001
19	300.001
20	300.001

PANCAKE MOTOR-1

PREF=REFERENCE PRESSURE = 300.00 PSI
AREF=REFERENCE SOUND SPEED= 3498.5 FT/SEC
R =CHAMBER RADIUS = .45830 FEET
TREF=REFERENCE TIME=R/AREF=.0001310 SEC

T/TREF= 0.00000

ISOBAR	PRESSURE/PREF
1	1.000
2	1.000
3	1.000
4	1.000
5	1.000
6	1.000
7	1.000
8	1.000
9	1.000
10	1.000
11	1.000
12	1.000
13	1.000
14	1.000
15	1.000
16	1.000
17	1.000
18	1.000
19	1.000
20	1.000

PANCAKE MOTOR-1

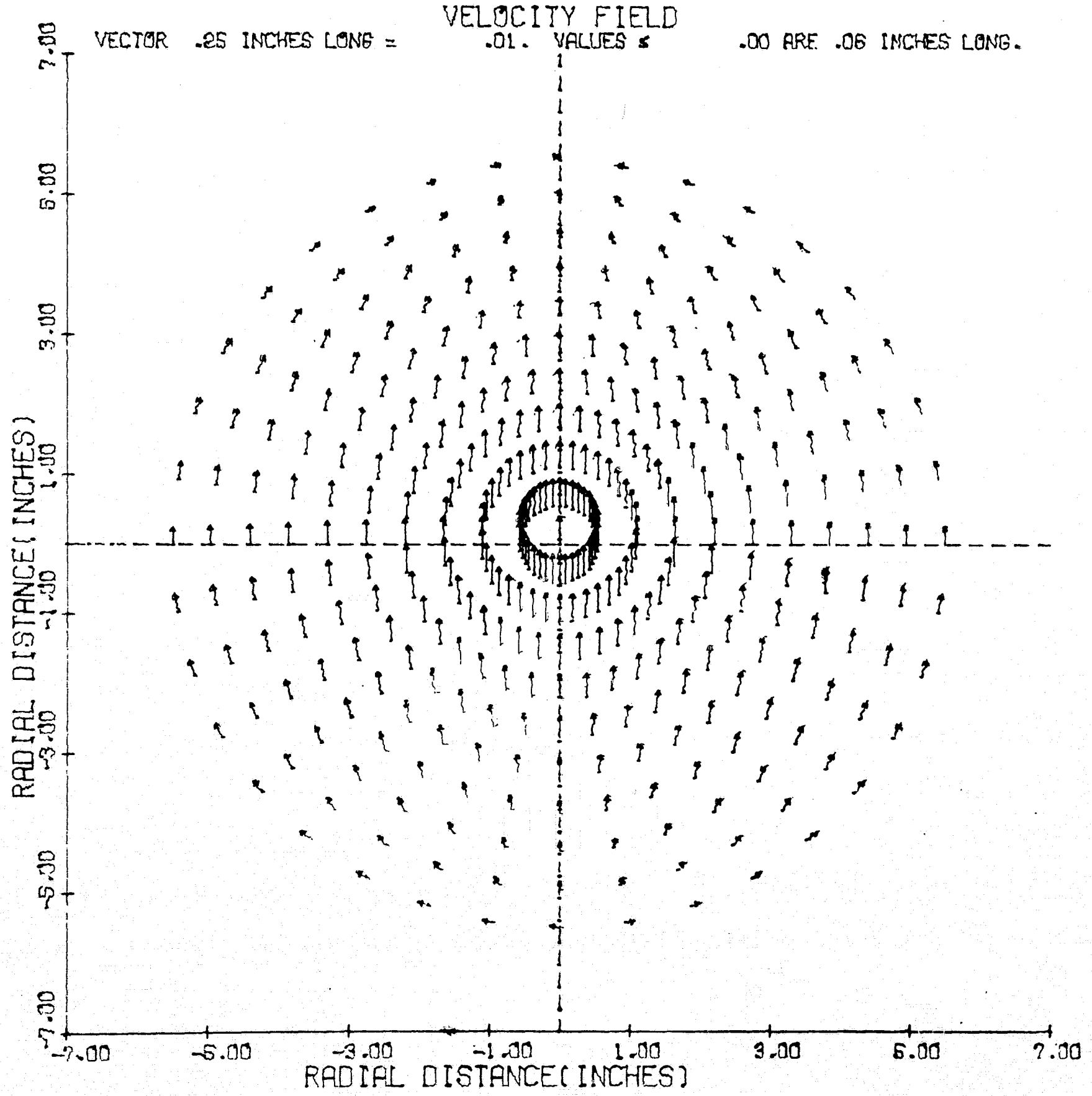

T= 0.000 MILLISECONDS

Figure 2

PANCAKE MOTOR-1 LINEAR

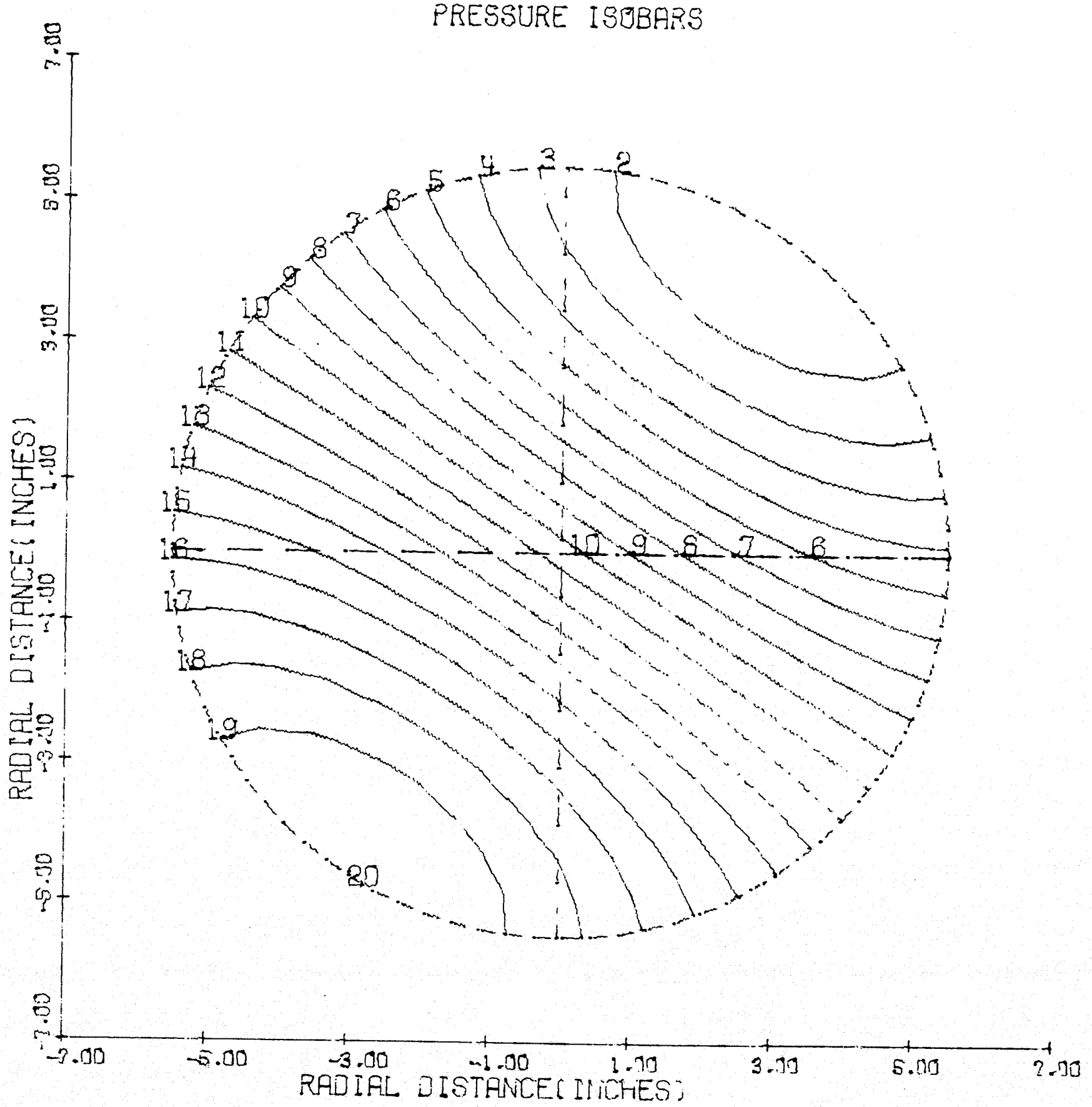

T= .825 MILLISECONDS

Figure 3

PANCAKE MOTOR-1 LINEAR

T= .825 MILLISECONDS

ISOBAR	PRESSURE(PSI)
1	299.999
2	299.999
3	299.999
4	299.999
5	299.999
6	300.000
7	300.000
8	300.000
9	300.000
10	300.000
11	300.000
12	300.000
13	300.000
14	300.000
15	300.000
16	300.001
17	300.001
18	300.001
19	300.001
20	300.001

PANCAKE MOTOR-1 LINEAR

PREF=REFERENCE PRESSURE = 300.00 PSI
AREF=REFERENCE SOUND SPEED= 3498.5 FT/SEC
R =CHAMBER RADIUS = .45830 FEET
TREF=REFERENCE TIME=R/AREF=.0001310 SEC

T/TREF= 6.29407

ISOBAR	PRESSURE/PREF
1	1.000
2	1.000
3	1.000
4	1.000
5	1.000
6	1.000
7	1.000
8	1.000
9	1.000
10	1.000
11	1.000
12	1.000
13	1.000
14	1.000
15	1.000
16	1.000
17	1.000
18	1.000
19	1.000
20	1.000

PANCAKE MOTOR-1

LINEAR

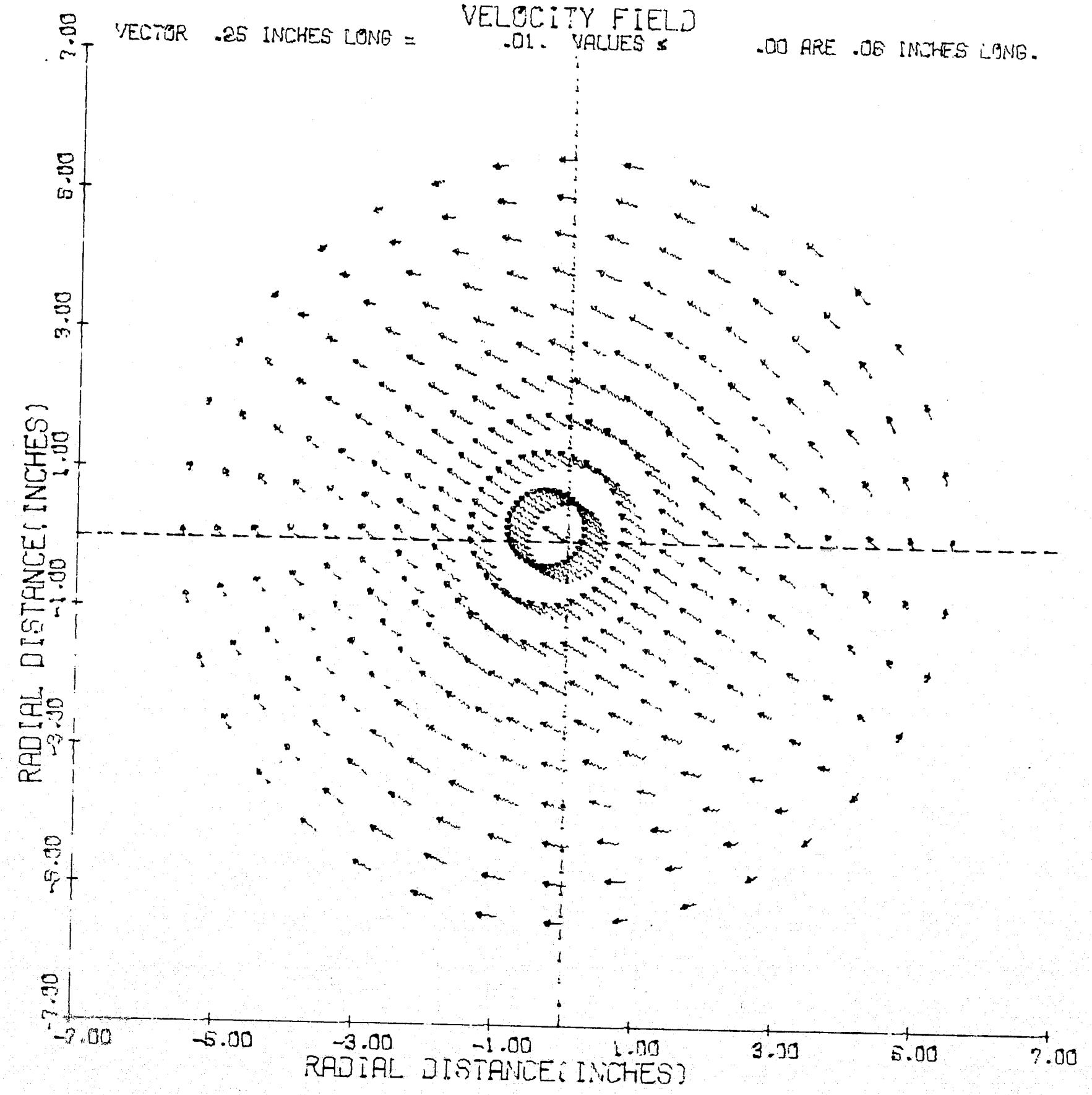

T= .825 MILLISECONDS

Figure 4

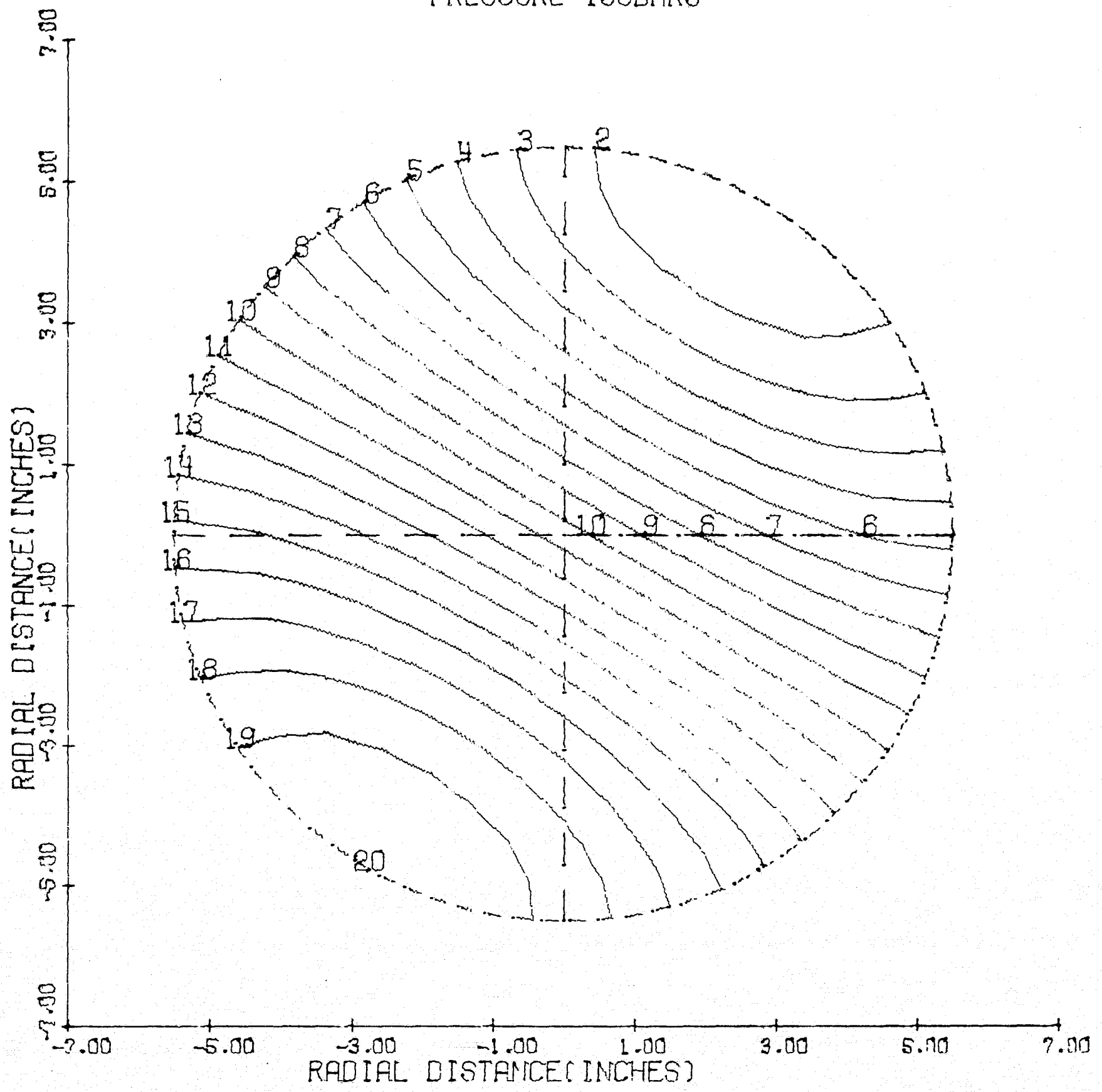
PANCAKE MOTOR-1
PRESSURE ISOBARS
RADIAL DISTANCE(INCHES)
7.00
5.00
3.00
1.00
-1.00
-3.00
-5.00
-7.00
1
2
3
4
5
6
7
8
9
10
11
12
13
14
15
16
17
18
19
20
10
9
8
7
6
-7.00
-5.00
-3.00
-1.00
1.00
3.00
5.00
7.00
RADIAL DISTANCE(INCHES)
T= .825 MILLISECONDS

Figure 5

PANCAKE MOTOR-1

T= .825 MILLISECONDS

ISOBAR	PRESSURE(PSI)
1	299.999
2	299.999
3	299.999
4	299.999
5	299.999
6	300.000
7	300.000
8	300.000
9	300.000
10	300.000
11	300.000
12	300.000
13	300.000
14	300.000
15	300.000
16	300.001
17	300.001
18	300.001
19	300.001
20	300.001

PANCAKE MOTOR-1

PREF=REFERENCE PRESSURE = 300.00 PSI
AREF=REFERENCE SOUND SPEED= 3498.5 FT/SEC
R =CHAMBER RADIUS = .45830 FEET
TREF=REFERENCE TIME=R/AREF=.0001310 SEC

T/TREF= 6.29407

ISOBAR	PRESSURE/PREF
1	1.000
2	1.000
3	1.000
4	1.000
5	1.000
6	1.000
7	1.000
8	1.000
9	1.000
10	1.000
11	1.000
12	1.000
13	1.000
14	1.000
15	1.000
16	1.000
17	1.000
18	1.000
19	1.000
20	1.000

PANCAKE MOTOR-1

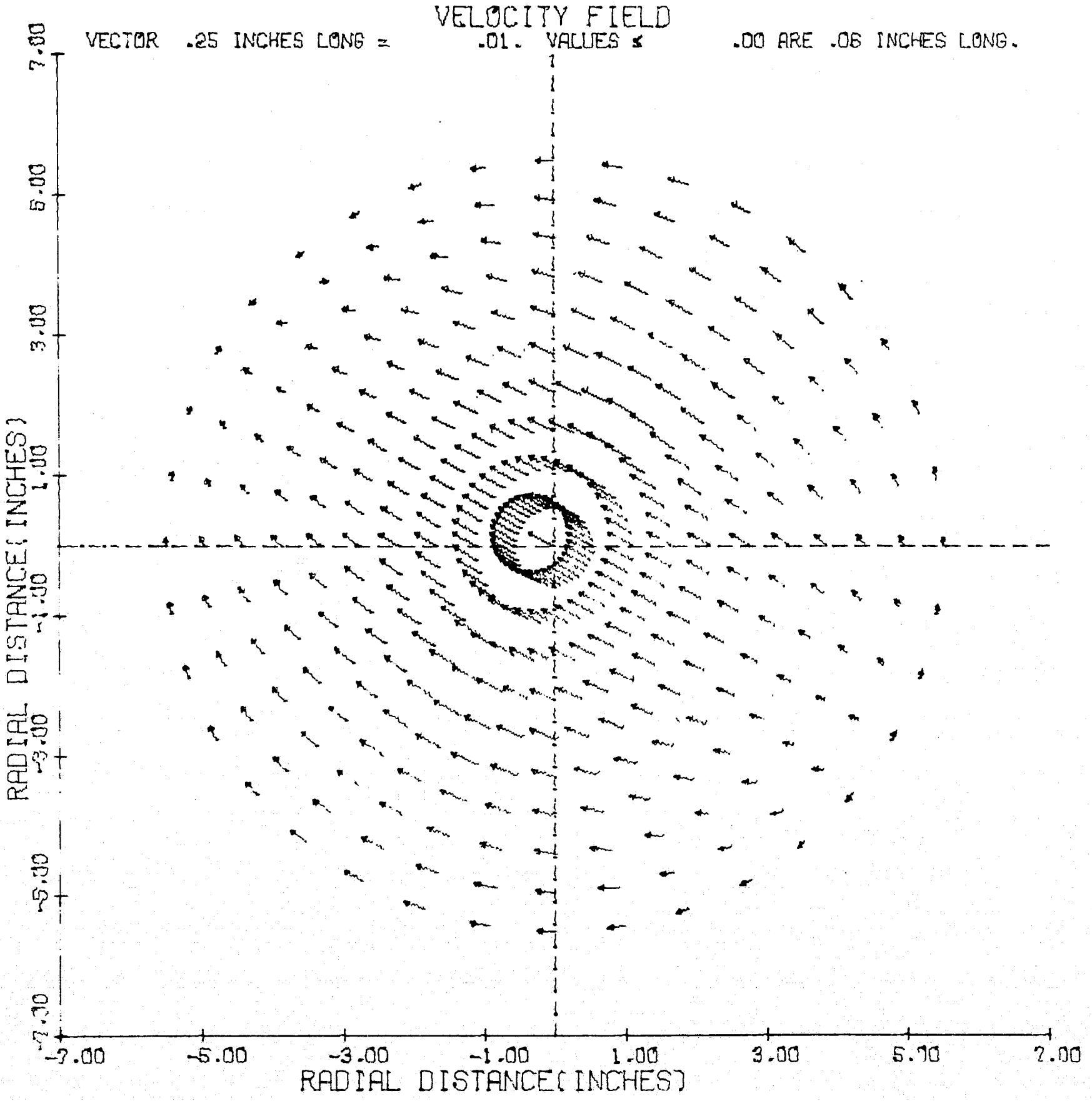

T= .825 MILLISECONDS

Figure 6

PANCAKE MOTOR-8

PRESSURE ISOBARS

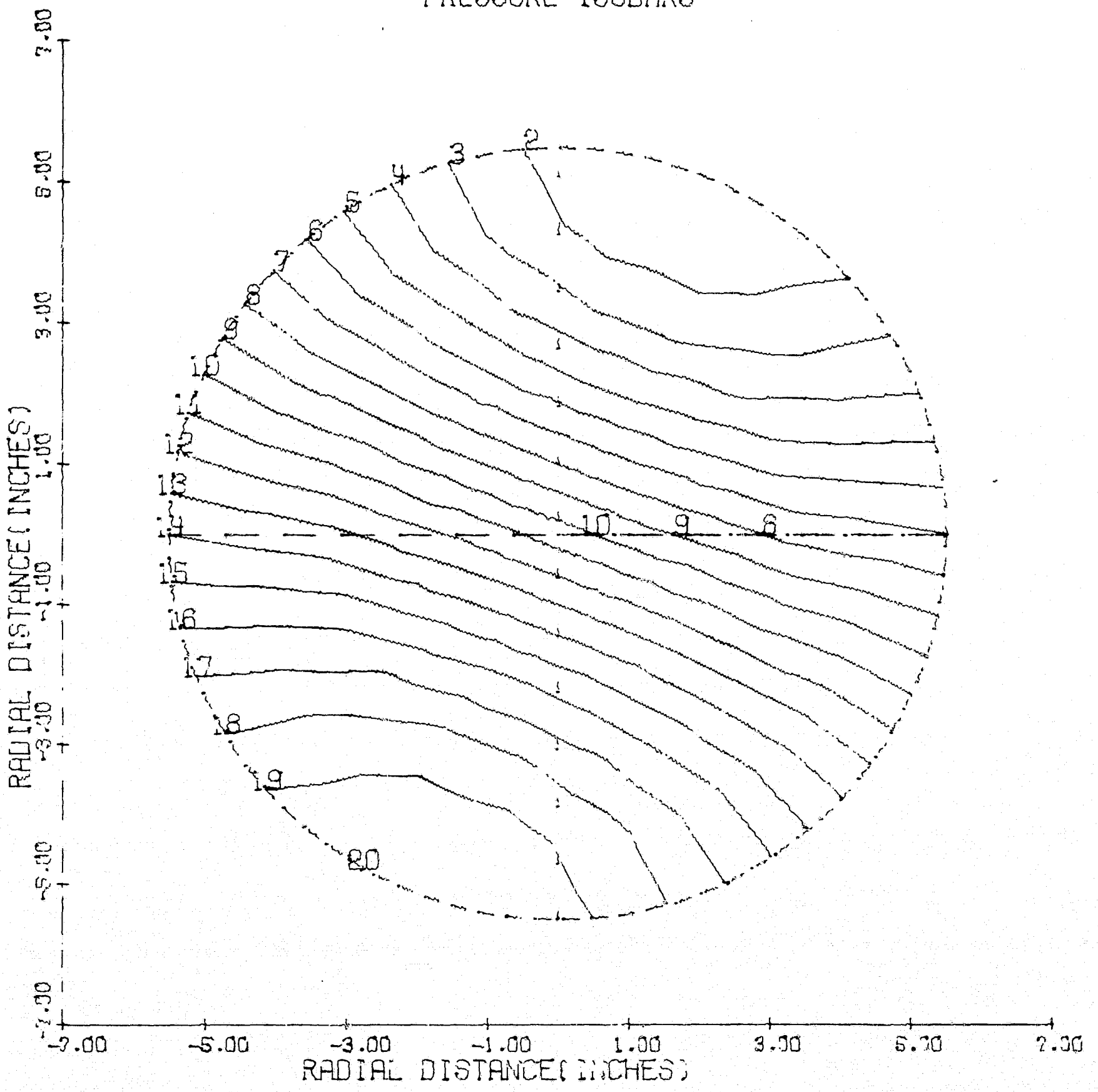

T= .825 MILLISECONDS

Figure 7

PANCAKE MOTOR-8

T= .825 MILLISECONDS

ISOBAR	PRESSURE(PSI)
1	299.999
2	299.999
3	299.999
4	299.999
5	299.999
6	300.000
7	300.000
8	300.000
9	300.000
10	300.000
11	300.000
12	300.000
13	300.000
14	300.000
15	300.000
16	300.001
17	300.001
18	300.001
19	300.001
20	300.001

PANCAKE MOTOR-8

PREF=REFERENCE PRESSURE = 300.00 PSI
AREF=REFERENCE SOUND SPEED= 3498.5 FT/SEC
R =CHAMBER RADIUS = .45830 FEET
TREF=REFERENCE TIME=R/AREF=.0001310 SEC

T/TREF= 6.29407

ISOBAR	PRESSURE/PREF
1	1.000
2	1.000
3	1.000
4	1.000
5	1.000
6	1.000
7	1.000
8	1.000
9	1.000
10	1.000
11	1.000
12	1.000
13	1.000
14	1.000
15	1.000
16	1.000
17	1.000
18	1.000
19	1.000
20	1.000

PANCAKE MOTOR-8

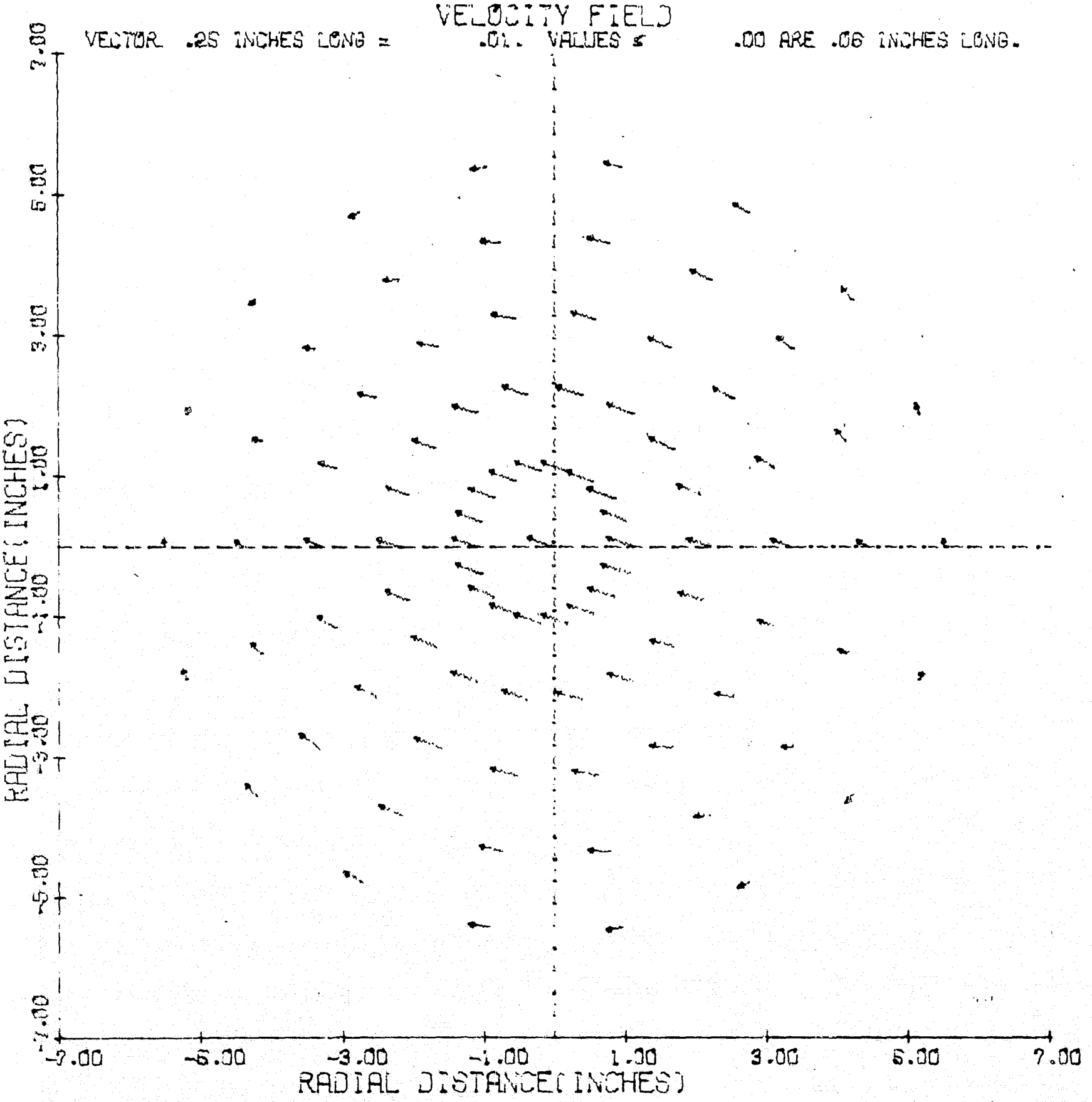

T= .825 MILLISECONDS

Figure 8

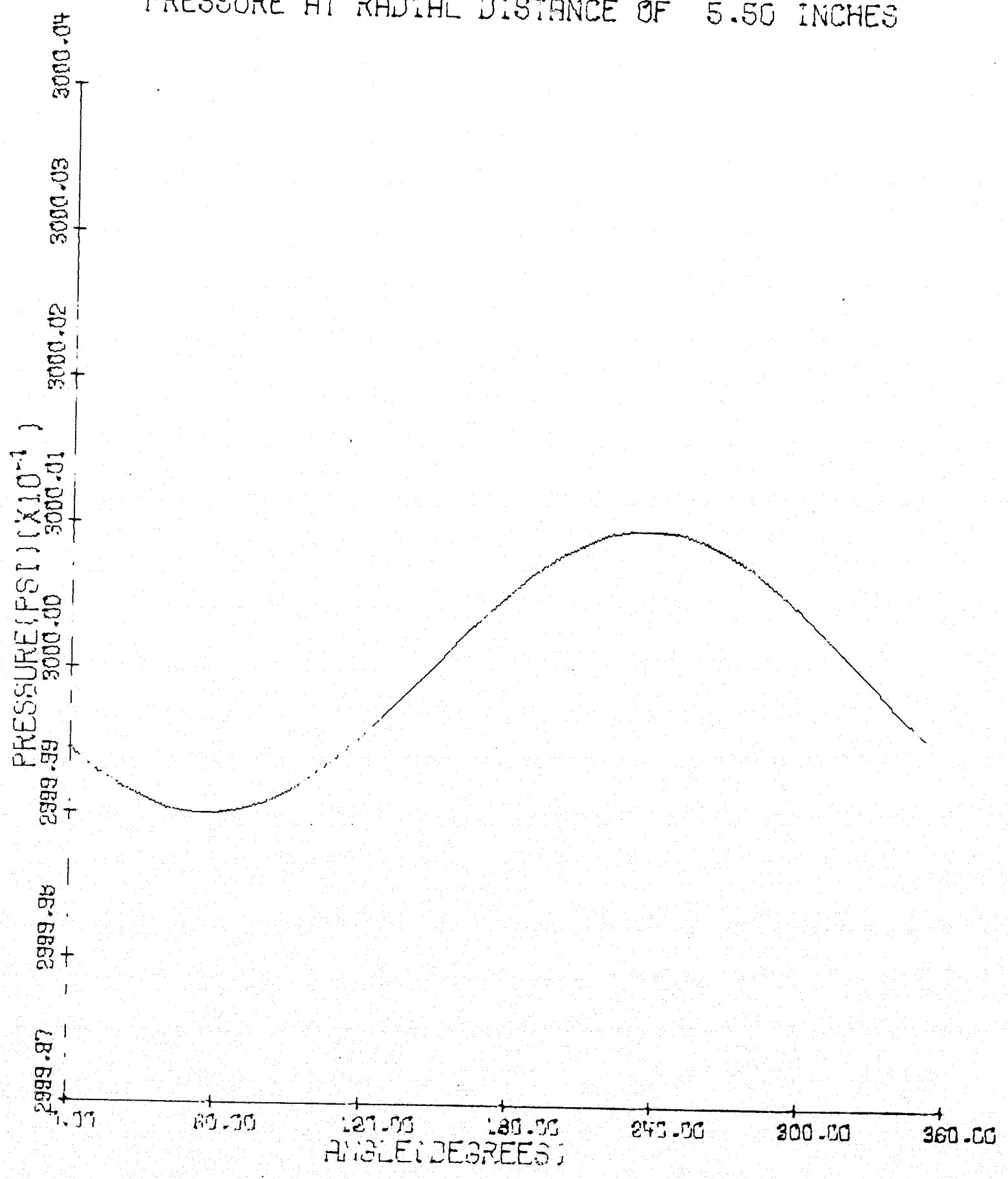
PANCAKE MOTOR-1
LINEAR
PRESSURE AT RADIAL DISTANCE OF 5.50 INCHES
PRESSURE(PSI)(X10^-1)
3000.04
3000.03
3000.02
3000.01
3000.00
2999.99
2999.98
2999.97
.00
60.00
120.00
180.00
240.00
300.00
360.00
ANGLE(DEGREES)
T= .825 MILLISECONDS

Figure 9

PANCAKE MOTOR-8

PRESSURE AT RADIAL DISTANCE OF 5.50 INCHES

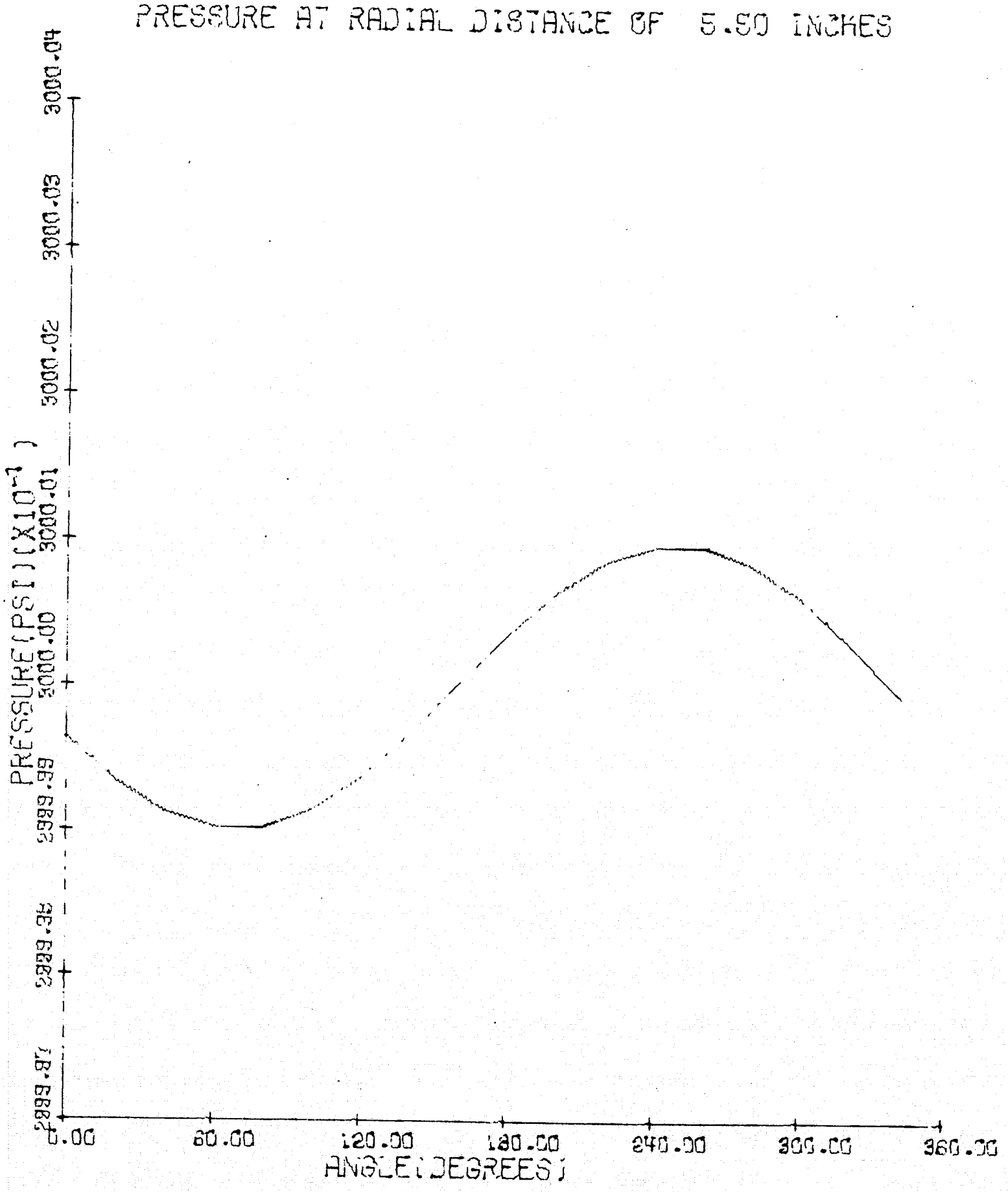

T= .825 MILLISECONDS

Figure 10

PANCAKE MOTOR-1

PRESSURE AT RADIAL DISTANCE OF 5.50 INCHES

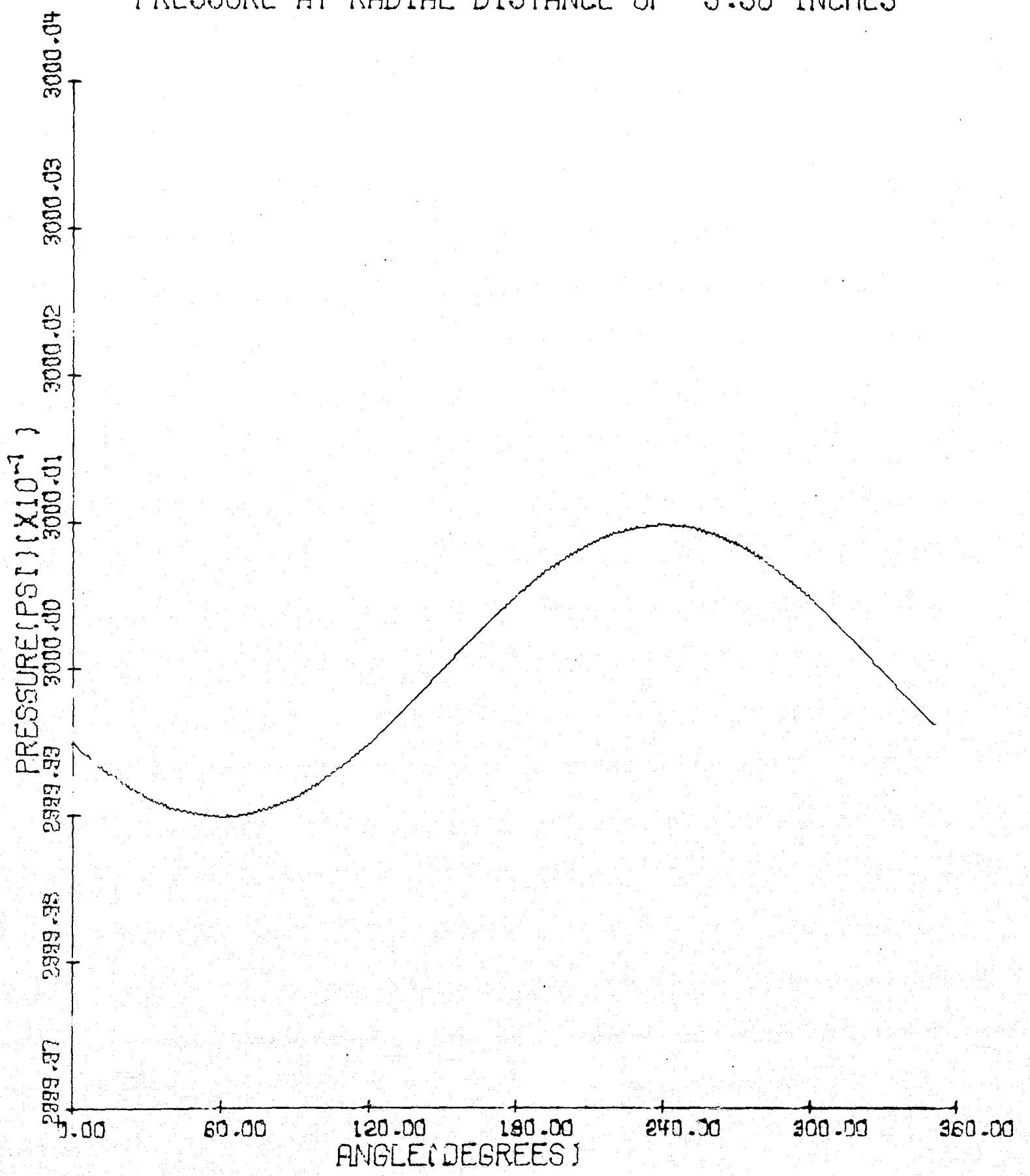

T= .825 MILLISECONDS

Figure 11

PANCAKE MOTOR-8

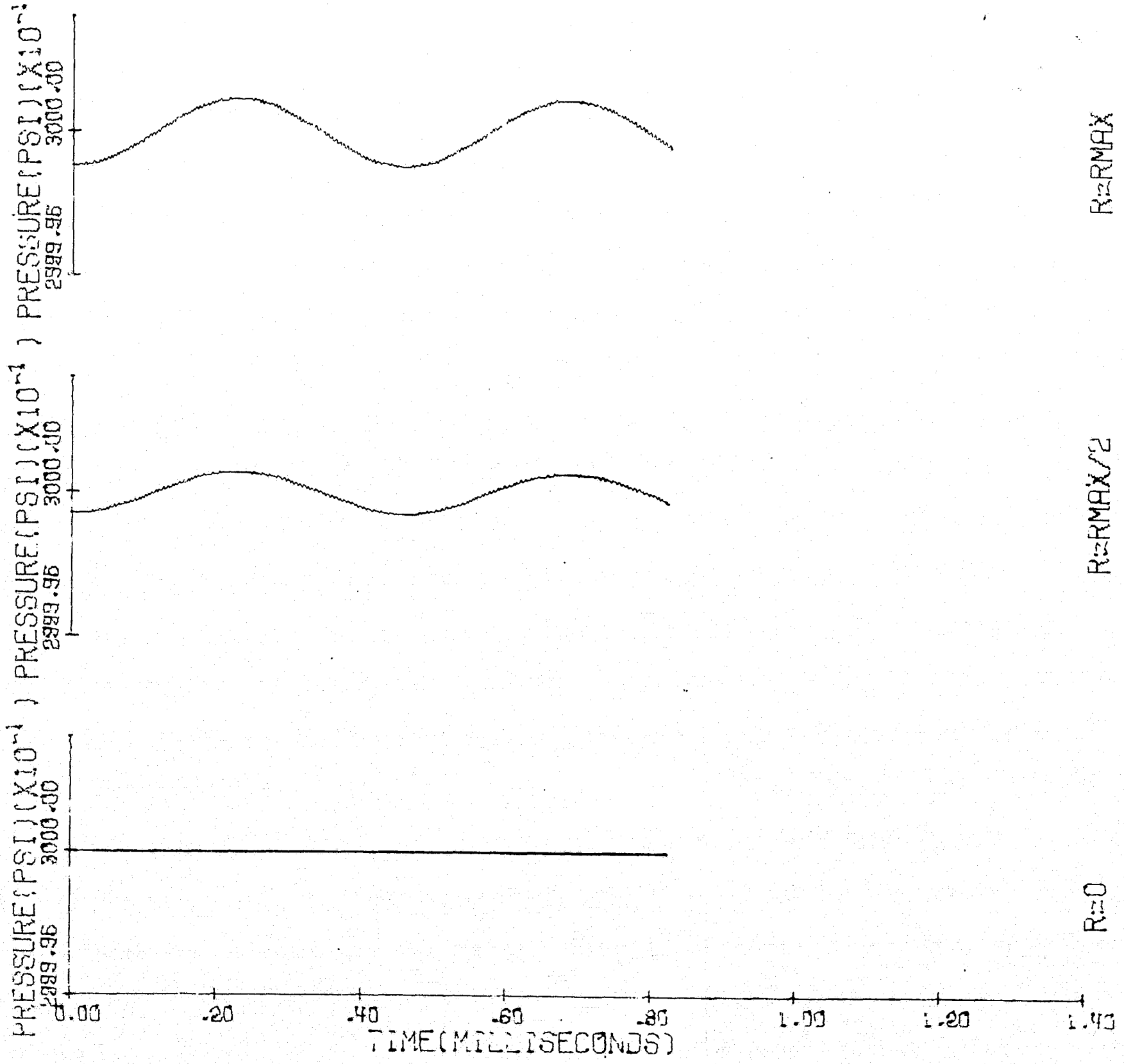

Figure 12

PANCAKE MOTOR-1

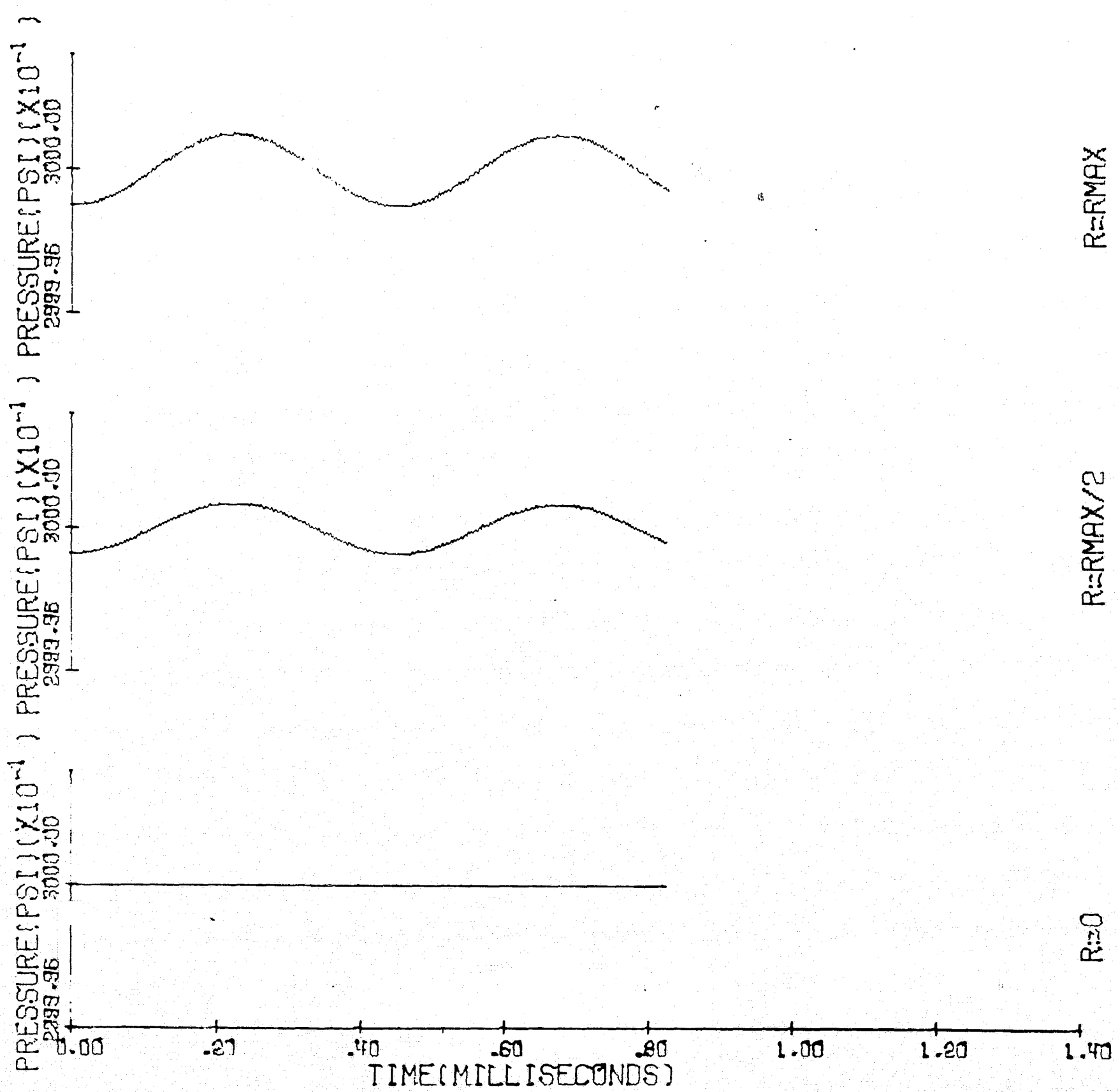

Figure 13

PANCAKE MOTOR-7

PRESSURE ISOBARS

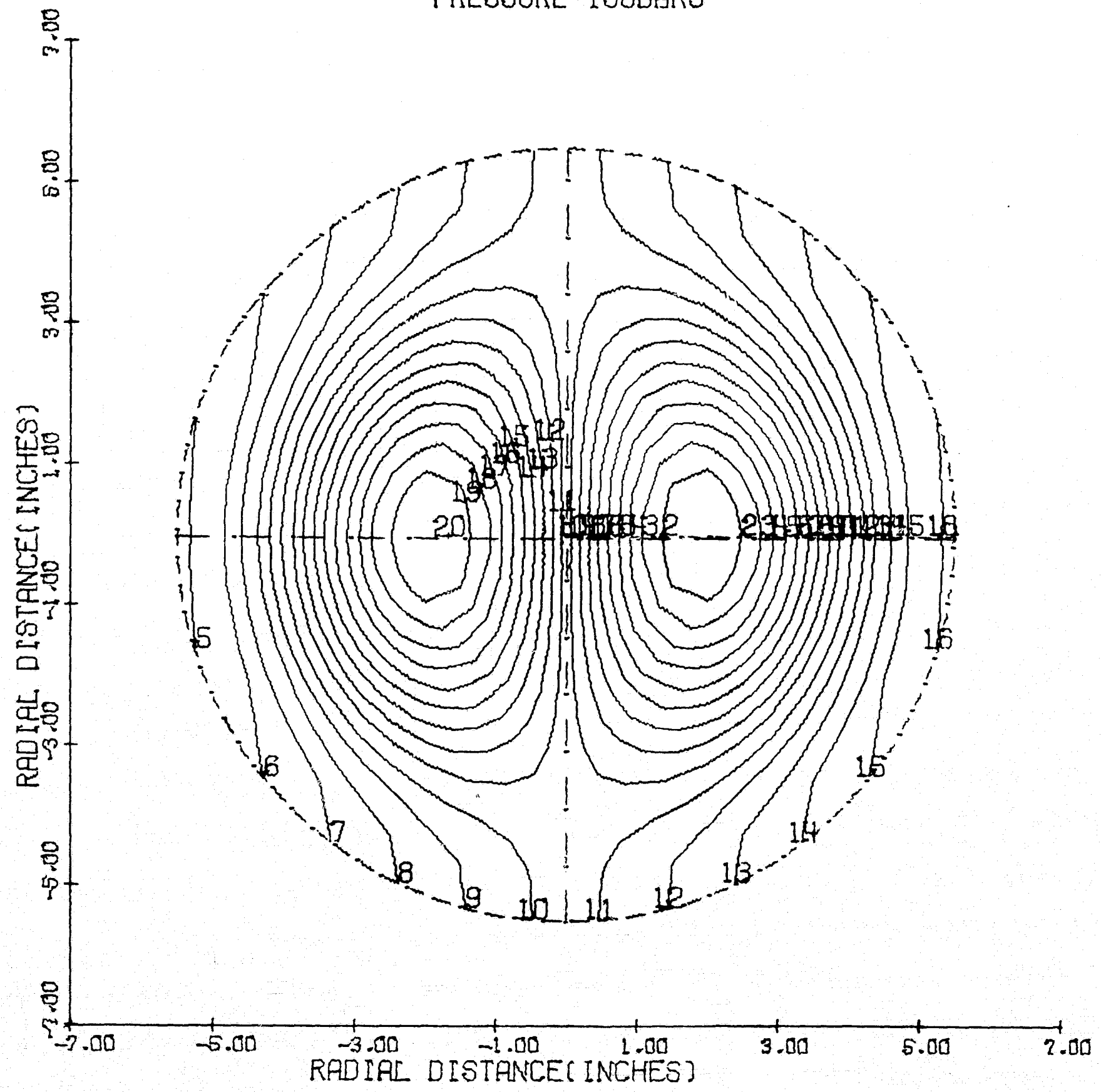

T= 0.000 MILLISECONDS

Figure 14

PANCAKE MOTOR-7

T= 0,000 MILLISECONDS

ISOBAR	PRESSURE(PSI)
1	299,999
2	299,999
3	299,999
4	299,999
5	299,999
6	300,000
7	300,000
8	300,000
9	300,000
10	300,000
11	300,000
12	300,000
13	300,000
14	300,000
15	300,000
16	300,001
17	300,001
18	300,001
19	300,001
20	300,001

PANCAKE MOTOR-7

PREF=REFERENCE PRESSURE = 300,00 PSI
AREF=REFERENCE SOUND SPEED= 3498,5 FT/SEC
R =CHAMBER RADIUS = ,45830 FEET
TREF=REFERENCE TIME=R/AREF=,0001310 SEC

T/TREF= 0,00000

ISOBAR	PRESSURE/PREF
1	1,000
2	1,000
3	1,000
4	1,000
5	1,000
6	1,000
7	1,000
8	1,000
9	1,000
10	1,000
11	1,000
12	1,000
13	1,000
14	1,000
15	1,000
16	1,000
17	1,000
18	1,000
19	1,000
20	1,000

PANCAKE MOTOR-7

PRESSURE ISOBARS

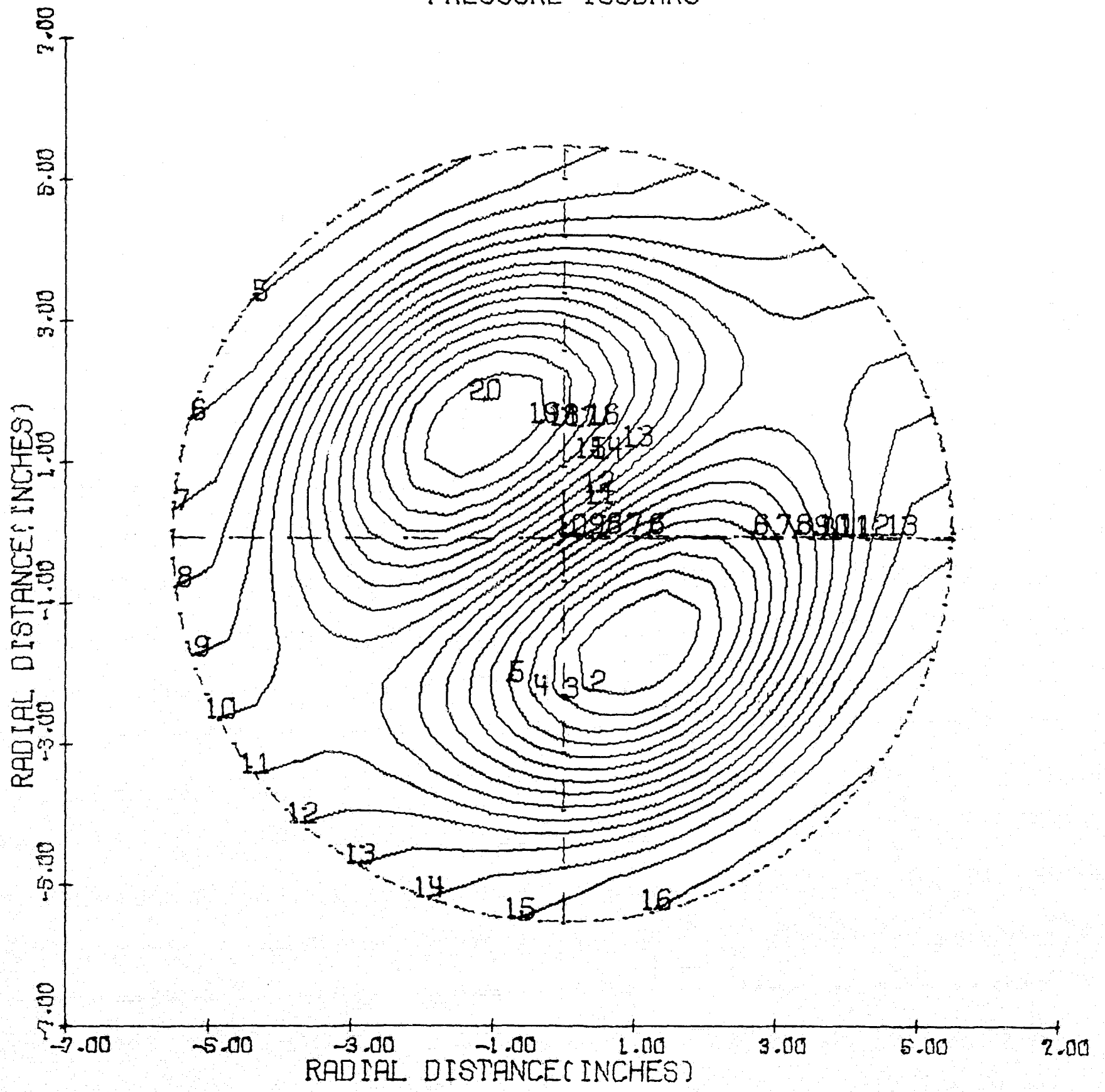

T= .825 MILLISECONDS

Figure 15

PANCAKE MOTOR-7

T= .825 MILLISECONDS

ISOBAR	PRESSURE(PSI)
1	299,999
2	299,999
3	299,999
4	299,999
5	299,999
6	300,000
7	300,000
8	300,000
9	300,000
10	300,000
11	300,000
12	300,000
13	300,000
14	300,000
15	300,000
16	300,001
17	300,001
18	300,001
19	300,001
20	300,001

PANCAKE MOTOR-7

PREF=REFERENCE PRESSURE = 300.00 PSI
AREF=REFERENCE SOUND SPEED= 3498.5 FT/SEC
R =CHAMBER RADIUS = .45830 FEET
TREF=REFERENCE TIME=R/AREF=.0001310 SEC

T/TREF= 6.29407

ISOBAR	PRESSURE/PREF
1	1,000
2	1,000
3	1,000
4	1,000
5	1,000
6	1,000
7	1,000
8	1,000
9	1,000
10	1,000
11	1,000
12	1,000
13	1,000
14	1,000
15	1,000
16	1,000
17	1,000
18	1,000
19	1,000
20	1,000

PANCAKE MOTOR-7

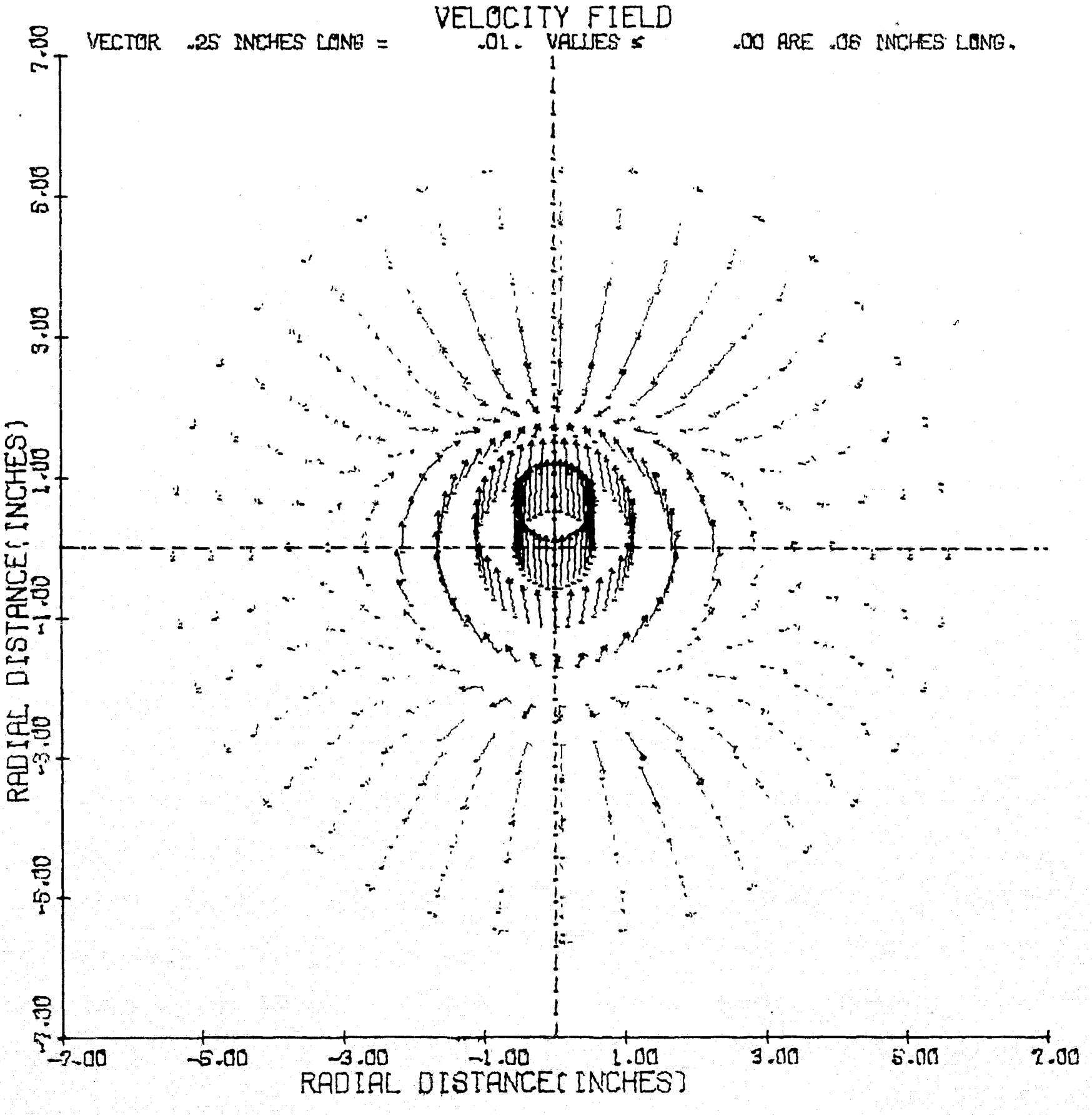

T= 0.000 MILLISECONDS

Figure 16

PANCAKE MOTOR-7

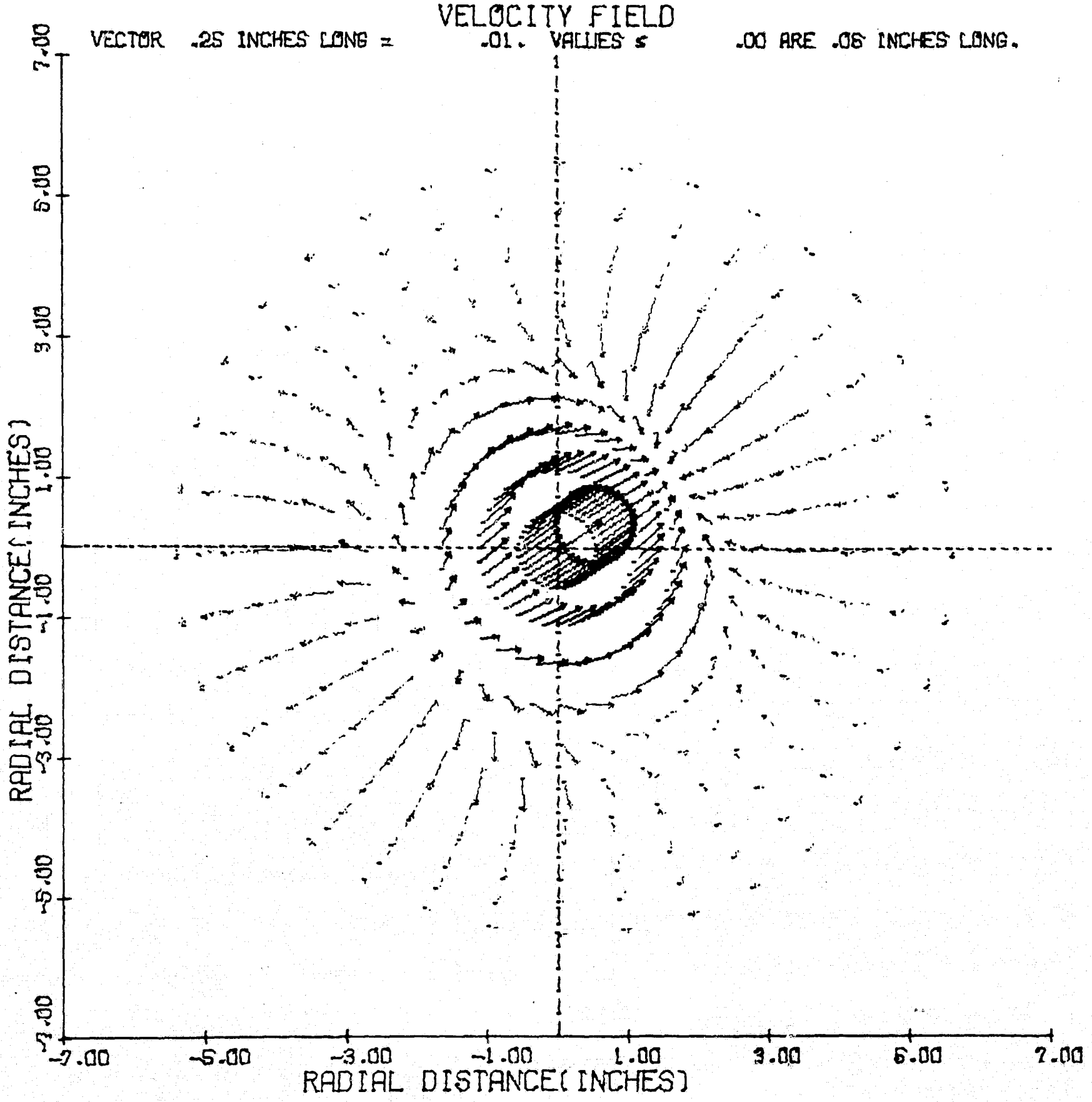

T= .825 MILLISECONDS

Figure 17

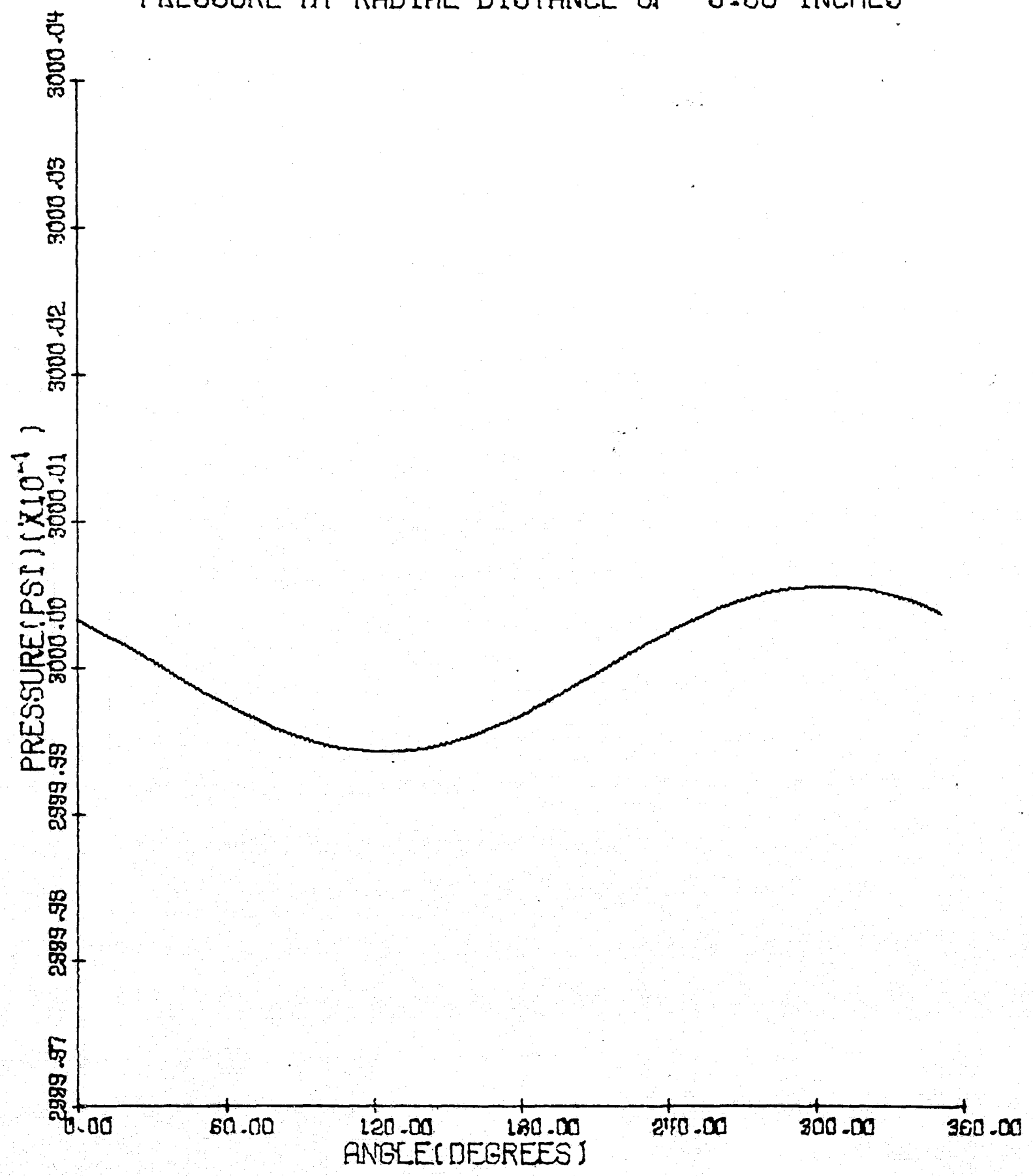
PANCAKE MOTOR-7
PRESSURE AT RADIAL DISTANCE OF 5.50 INCHES
PRESSURE(PSI)(X10^-1)
3000.04
3000.03
3000.02
3000.01
3000.00
2999.99
2999.98
2999.97
0.00
60.00
120.00
180.00
240.00
300.00
360.00
ANGLE(DEGREES)
T= .825 MILLISECONDS

Figure 18

PANCAKE MOTOR-7

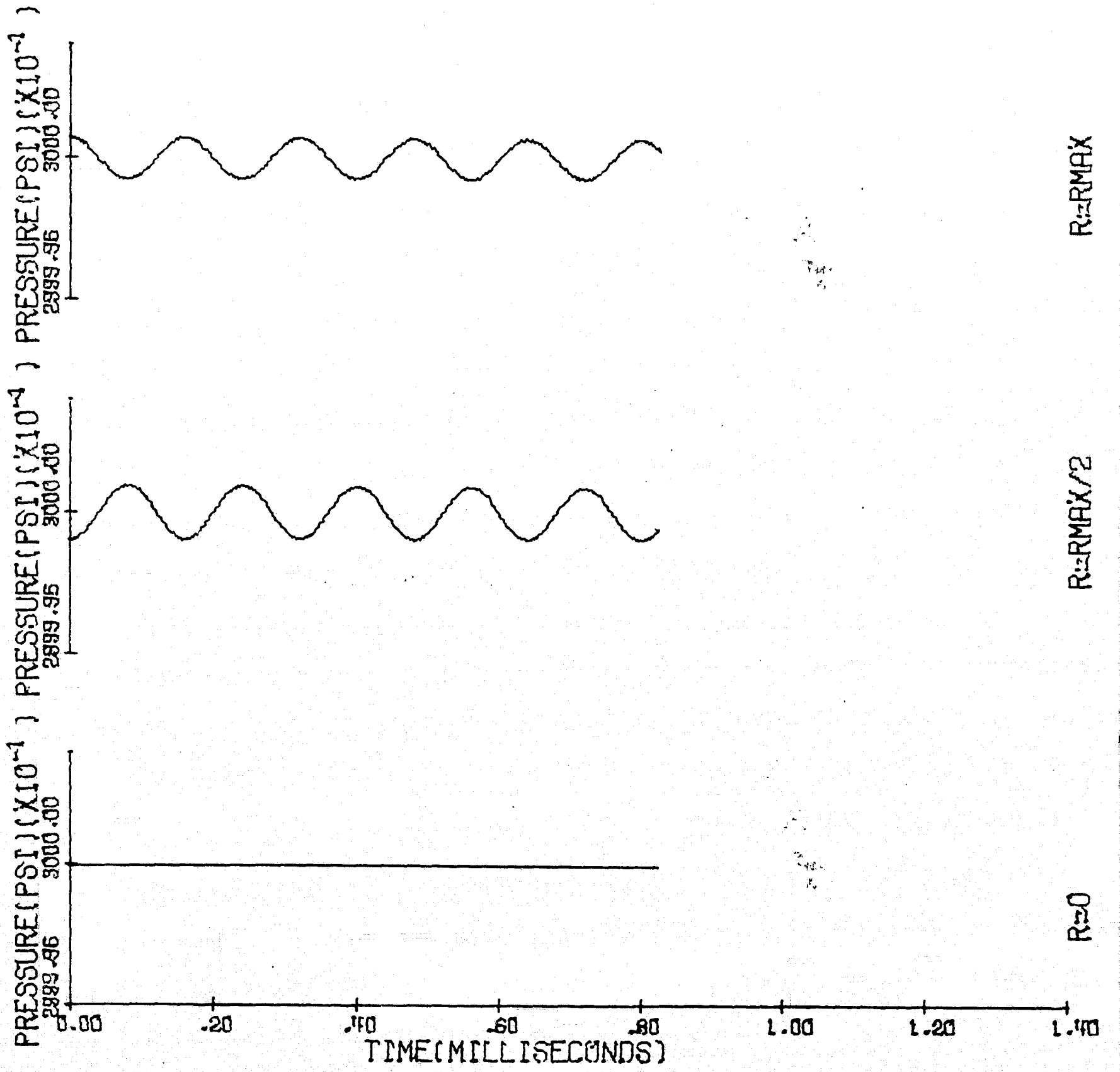

Figure 19

PANCAKE MOTOR-2

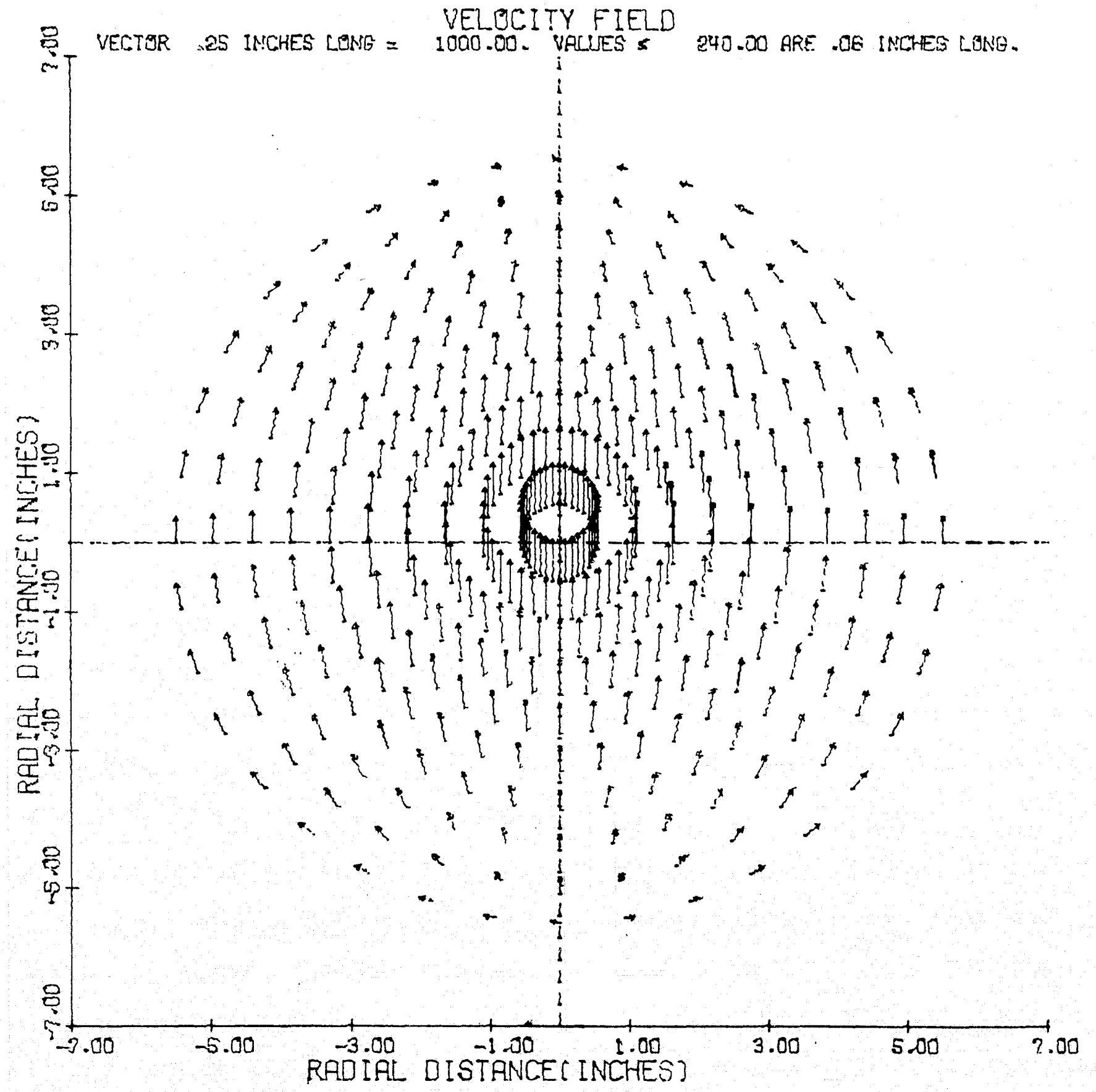

T= 0.000 MILLISECONDS

Figure 20

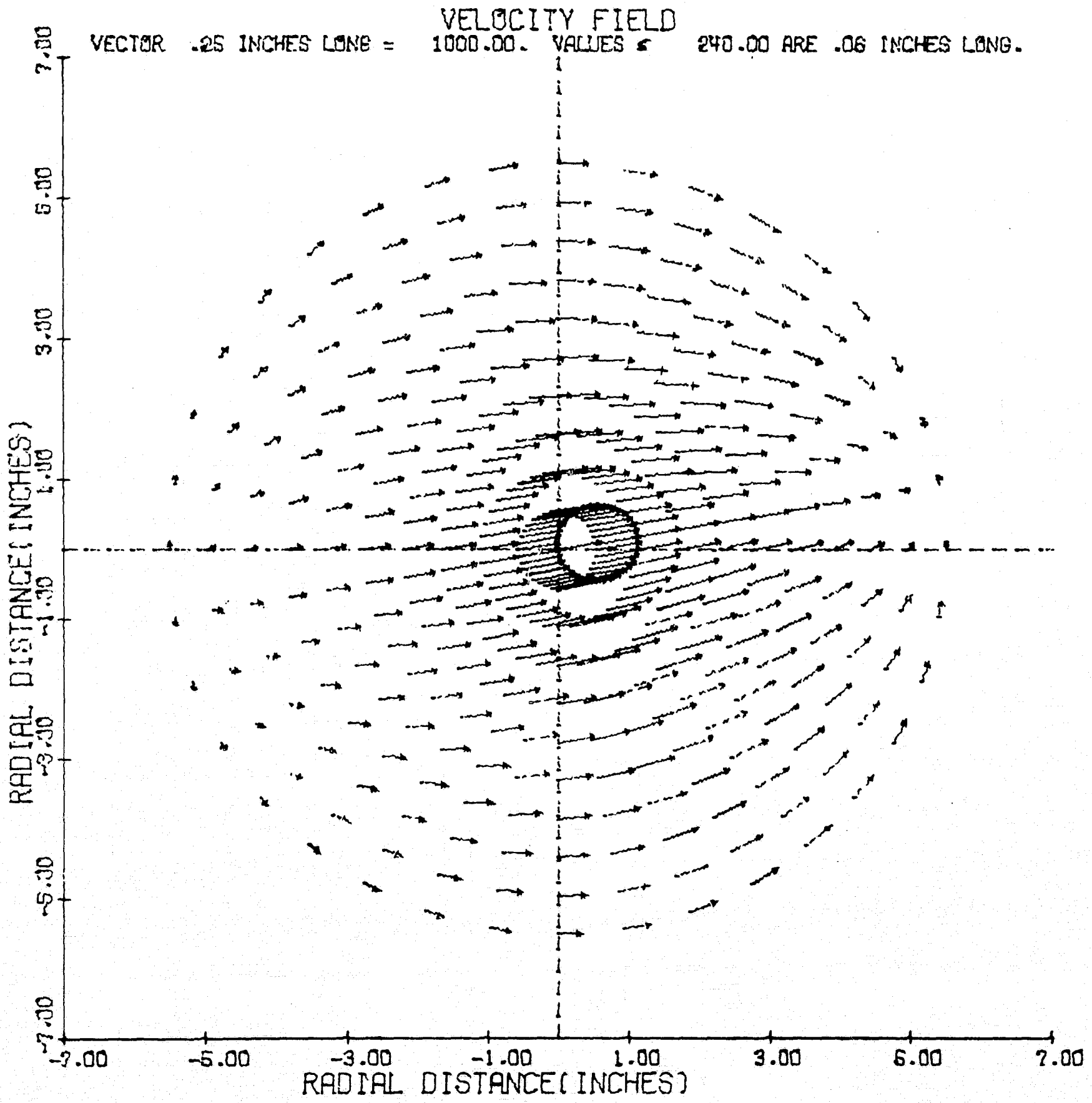
PANCAKE MOTOR-2
VELOCITY FIELD
VECTOR .25 INCHES LONG = 1000.00. VALUES < 240.00 ARE .06 INCHES LONG.
RADIAL DISTANCE(INCHES)
7.00
5.00
3.00
1.00
-1.00
-3.00
-5.00
-7.00
-7.00
-5.00
-3.00
-1.00
1.00
3.00
6.00
7.00
RADIAL DISTANCE(INCHES)
T= .101 MILLISECONDS

Figure 21

PANCAKE MOTOR-2

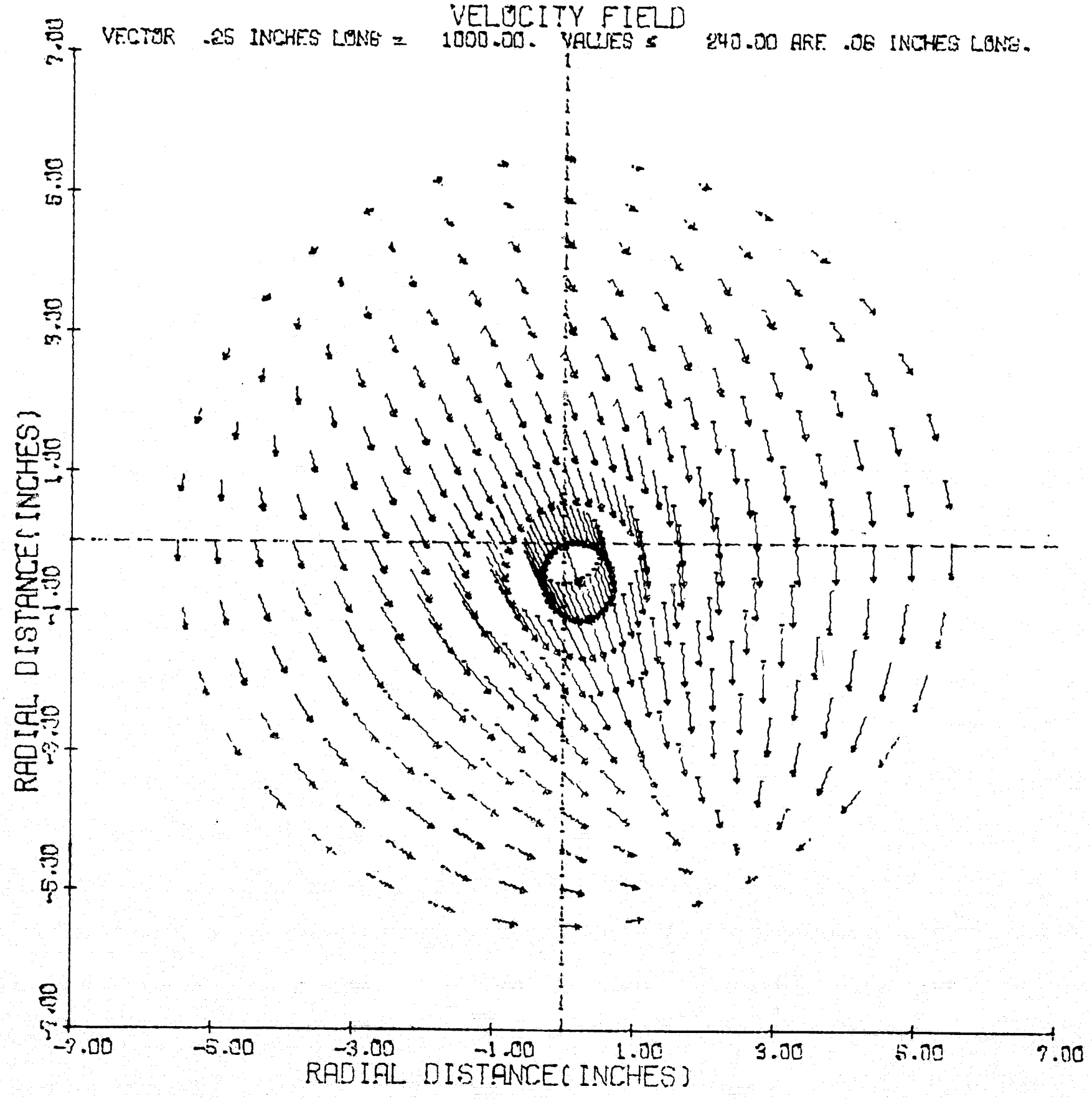

T= .201 MILLISECONDS

Figure 22

PANCAKE MOTOR-2

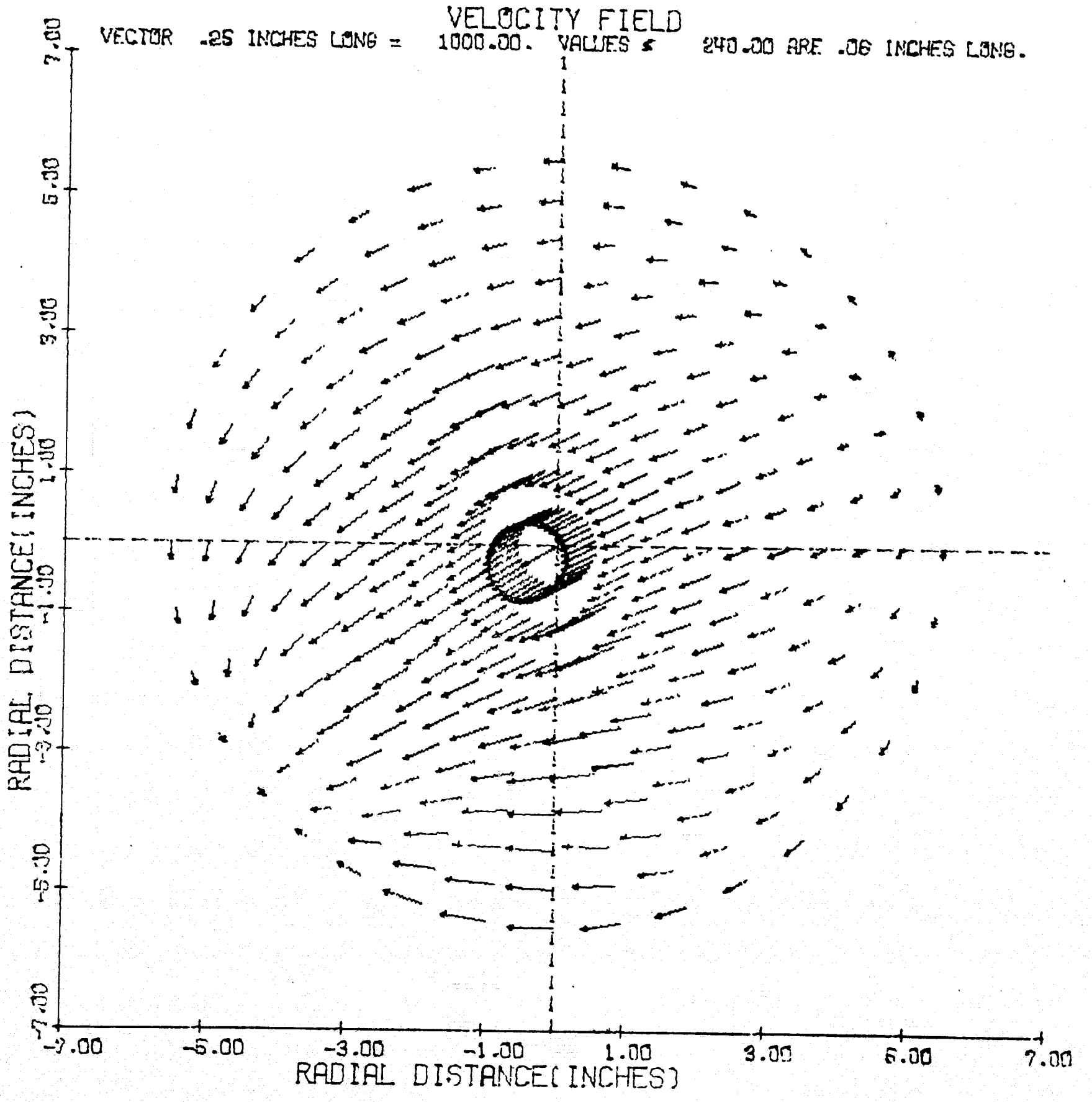

T= .304 MILLISECONDS

Figure 23

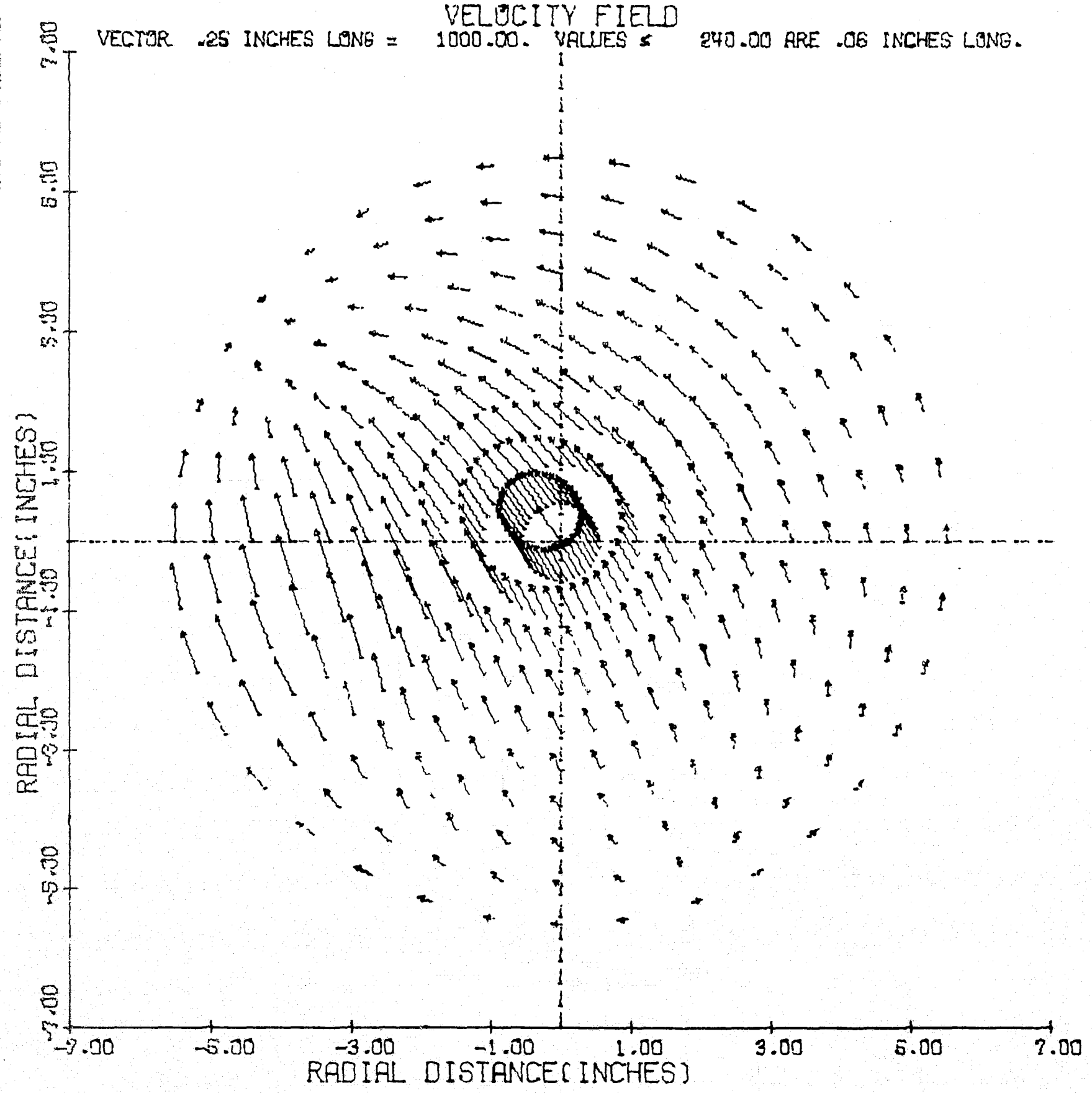
PANCAKE MOTOR-2
VELOCITY FIELD
VECTOR .25 INCHES LONG = 1000.00. VALUES ≤ 240.00 ARE .06 INCHES LONG.
RADIAL DISTANCE(INCHES)
7.00
5.00
3.30
1.30
-3.30
-5.30
-7.00
-7.00
-5.00
-3.00
-1.00
1.00
3.00
5.00
7.00
RADIAL DISTANCE(INCHES)
T= .406 MILLISECONDS

Figure 24

PANCAKE MOTOR-2

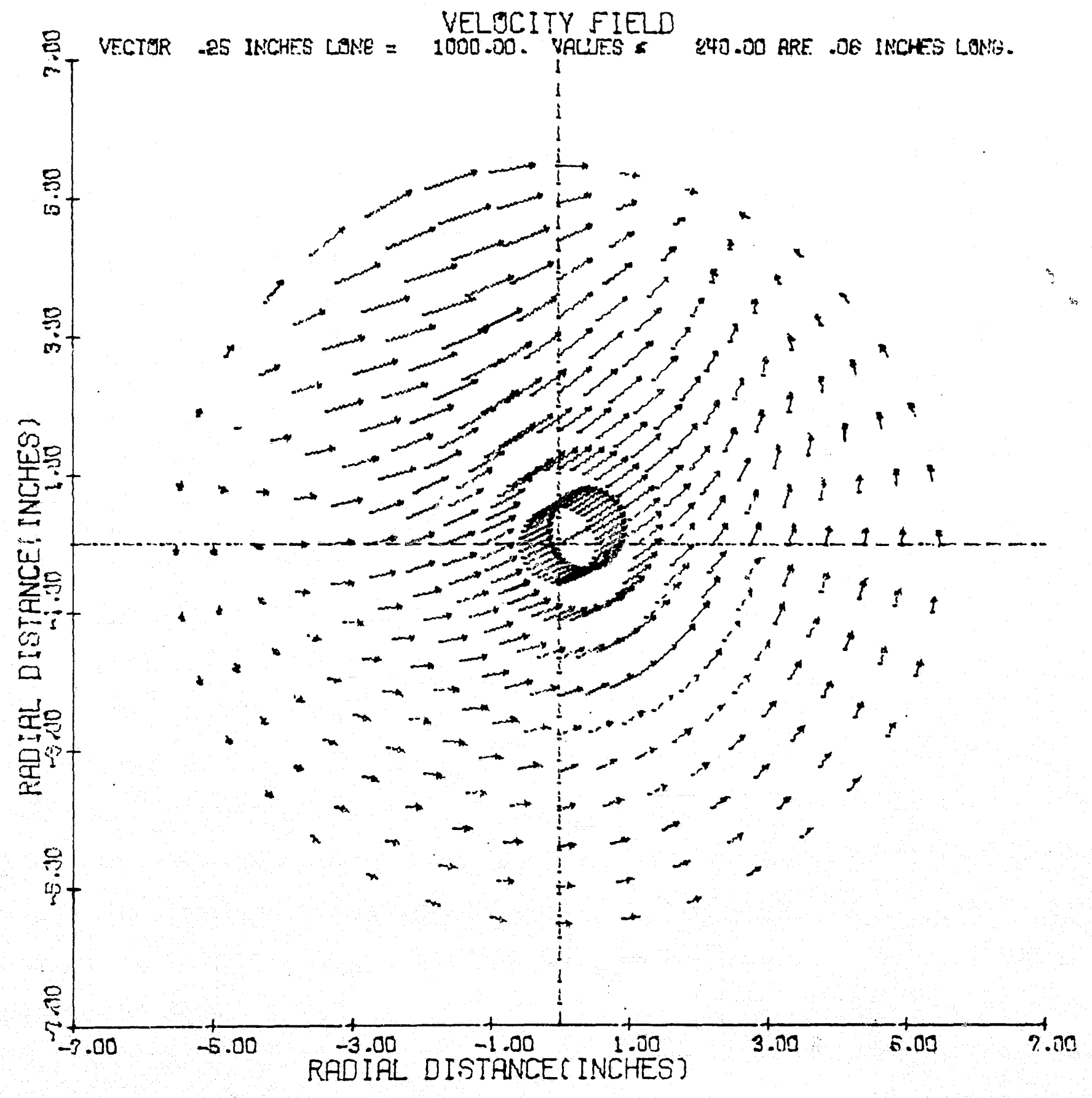

T= .511 MILLISECONDS

Figure 25

PANCAKE MOTOR-2

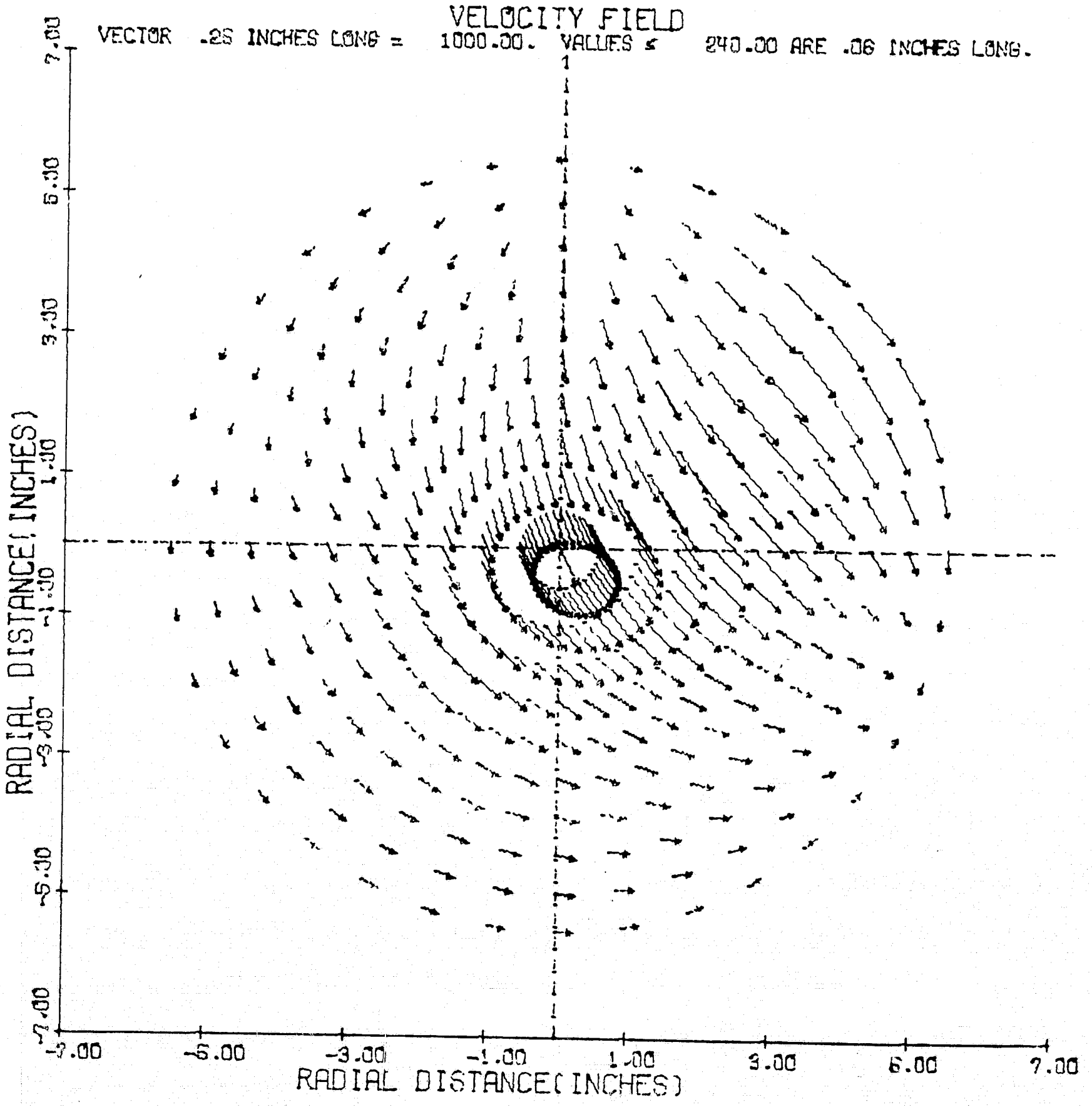

T= .615 MILLISECONDS

Figure 26

PANCAKE MOTOR-2

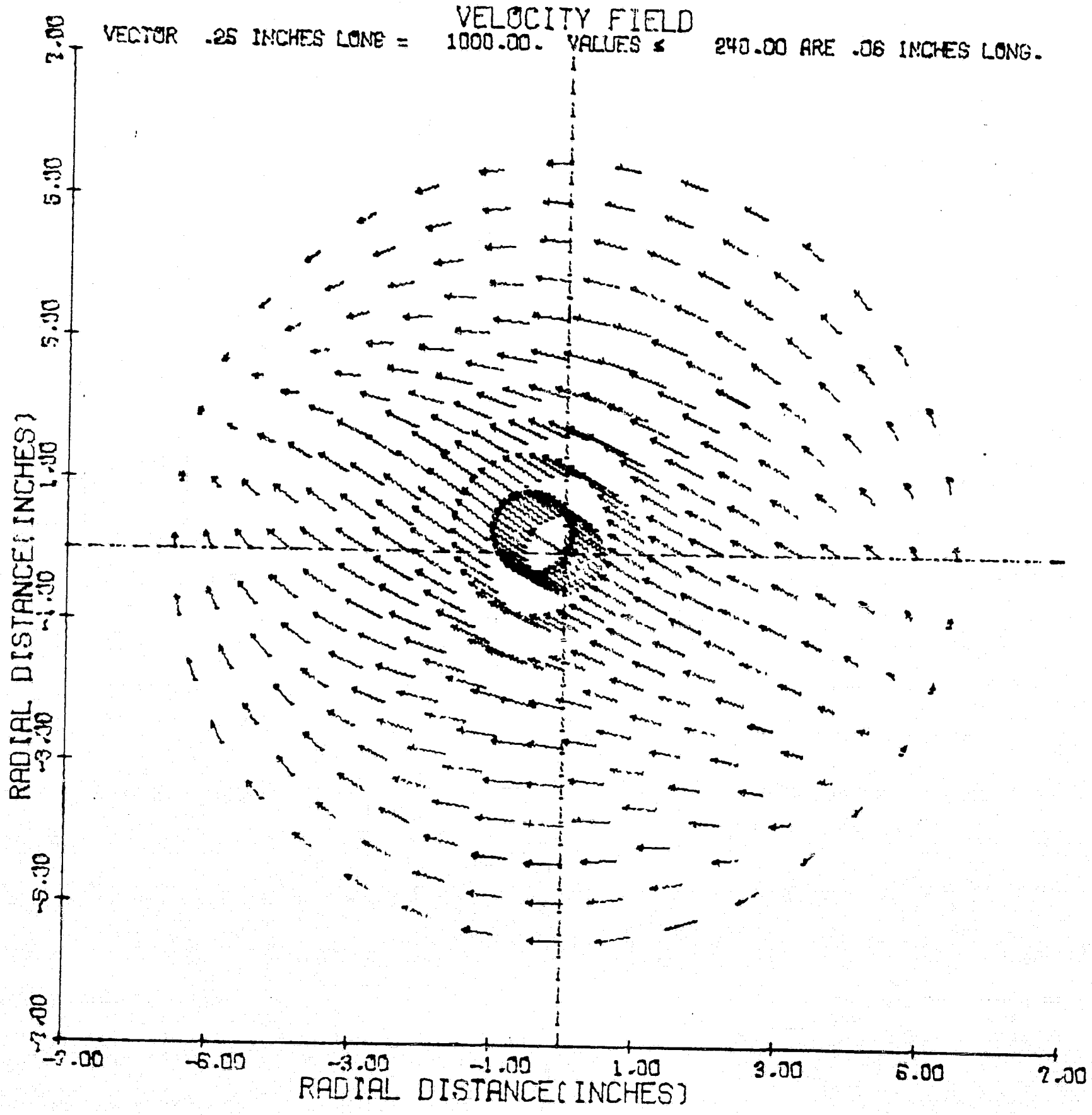

T= 1.232 MILLISECONDS

Figure 27

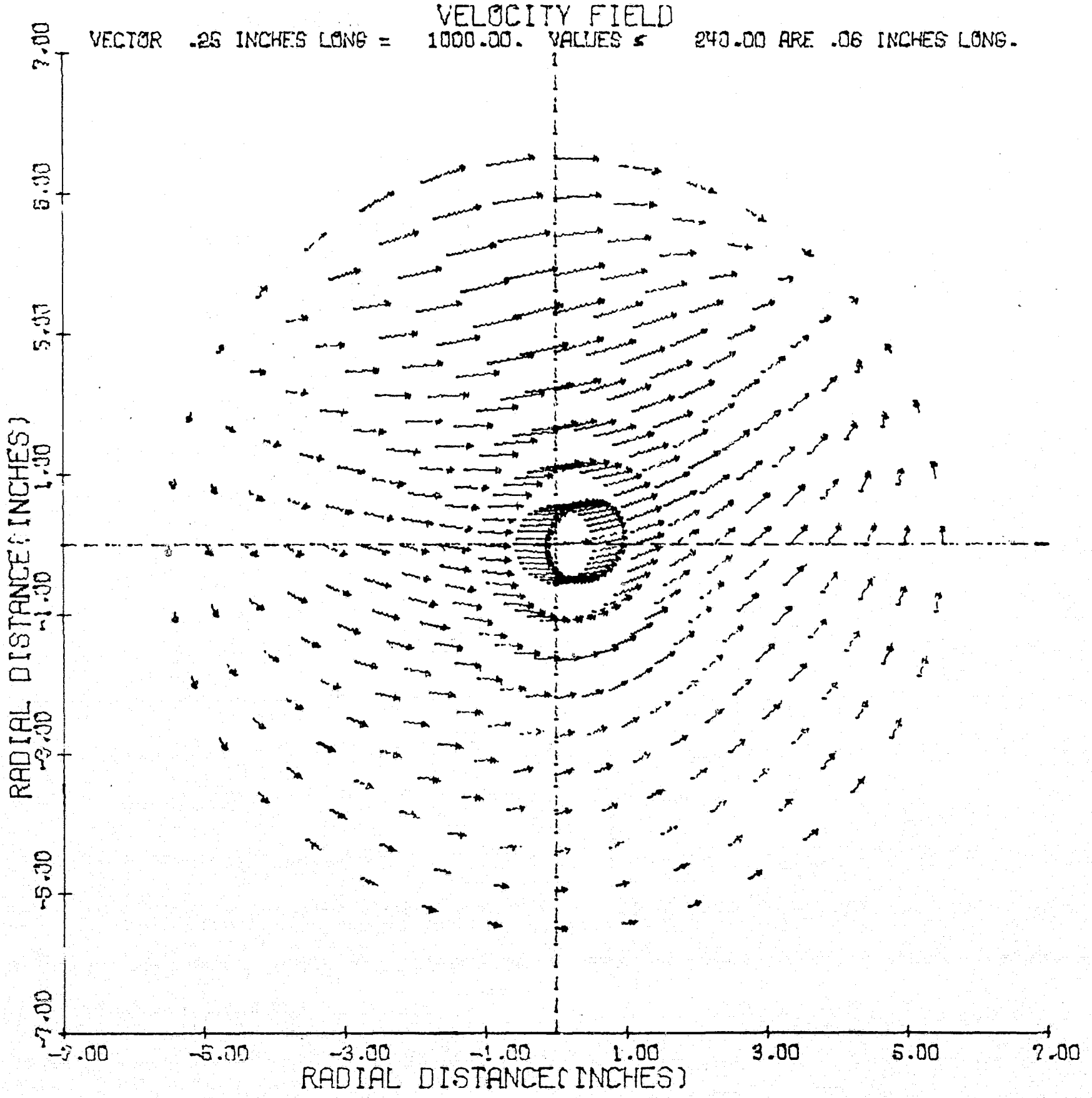
PANCAKE MOTOR-2
VELOCITY FIELD
VECTOR .25 INCHES LONG = 1000.00. VALUES ≤ 240.00 ARE .06 INCHES LONG.
RADIAL DISTANCE(INCHES)
7.00
5.00
3.00
1.00
-1.00
-3.00
-5.00
-7.00
-7.00
-5.00
-3.00
-1.00
1.00
3.00
5.00
7.00
RADIAL DISTANCE(INCHES)
T= 1.847 MILLISECONDS

Figure 28

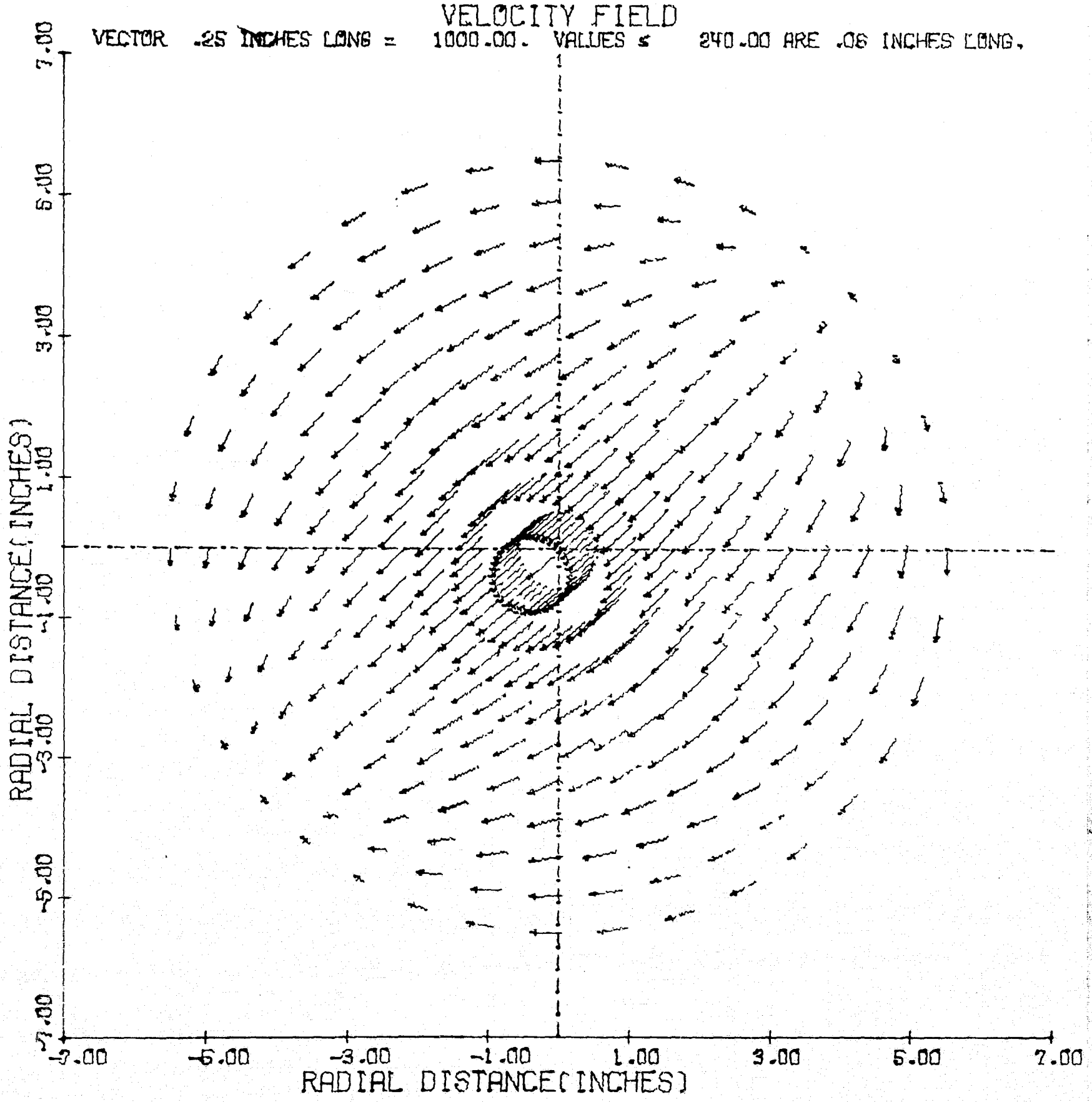
PANCAKE MOTOR-2
VELOCITY FIELD
VECTOR .25 INCHES LONG = 1000.00. VALUES ≤ 240.00 ARE .06 INCHES LONG.
RADIAL DISTANCE(INCHES)
7.00
5.00
3.00
1.00
-1.00
-3.00
-5.00
-7.00
-7.00
-5.00
-3.00
-1.00
1.00
3.00
5.00
7.00
RADIAL DISTANCE(INCHES)
T= 2.467 MILLISECONDS

Figure 29

PANCAKE MOTOR-2

PRESSURE ISOBARS

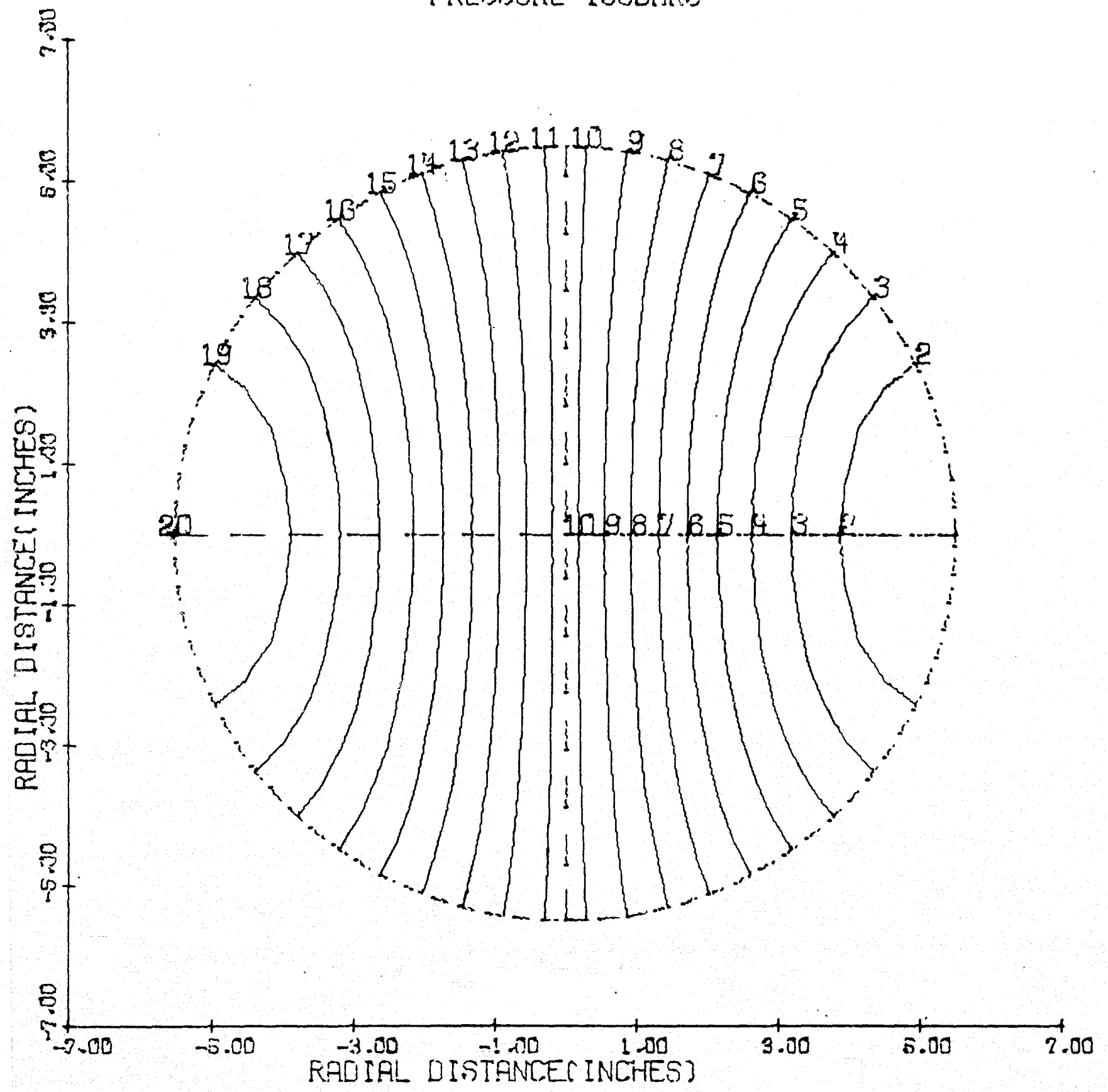

T= 0.000 MILLISECONDS

Figure 30

PANCAKE MOTOR-2

T= 0,000 MILLISECONDS

ISOBAR	PRESSURE(PSI)
1	150,000
2	165,789
3	181,579
4	197,368
5	213,158
6	228,947
7	244,737
8	260,526
9	276,316
10	292,105
11	307,895
12	323,684
13	339,474
14	355,263
15	371,053
16	386,842
17	402,632
18	418,421
19	434,211
20	450,000

PANCAKE MOTOR-2

PREF=REFERENCE PRESSURE = 300,00 PSI
AREF=REFERENCE SOUND SPEED= 3498,5 FT/SEC
R =CHAMBER RADIUS = ,45630 FEET
TREF=REFERENCE TIME=R/AREF=,0001310 SEC

T/TREF= 0,00000

ISOBAR	PRESSURE/PREF
1	,500
2	,553
3	,605
4	,658
5	,711
6	,763
7	,816
8	,868
9	,921
10	,974
11	1,026
12	1,079
13	1,132
14	1,184
15	1,237
16	1,289
17	1,342
18	1,395
19	1,447
20	1,500

PANCAKE MOTOR-2

PRESSURE ISOBARS

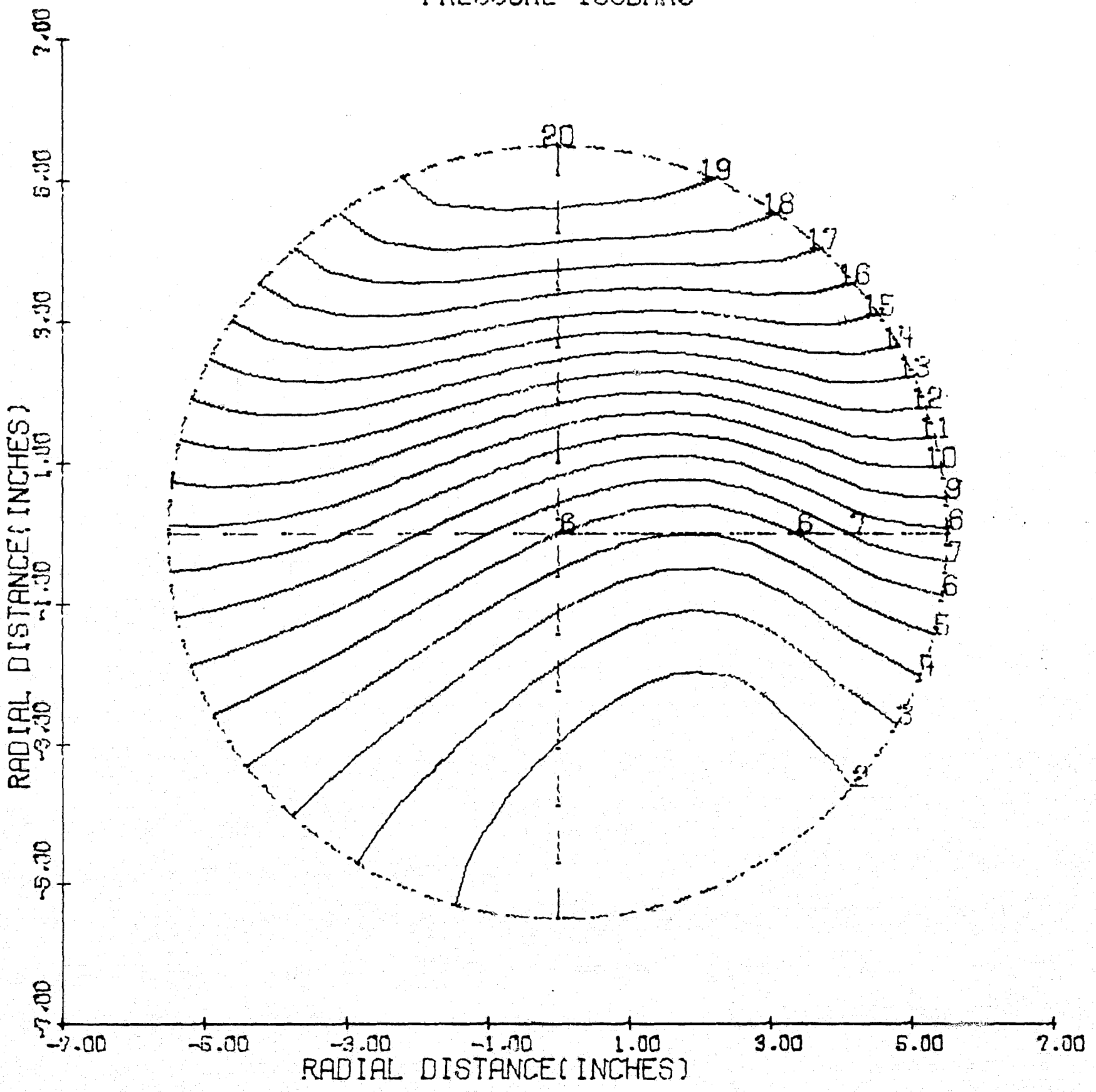

T= .101 MILLISECONDS

Figure 31

PANCAKE MOTOR-2

T= .101 MILLISECONDS

ISOBAR	PRESSURE(PSI)
1	180.376
2	196.358
3	212.340
4	228.321
5	244.303
6	260.285
7	276.266
8	292.248
9	308.230
10	324.212
11	340.193
12	356.175
13	372.157
14	388.138
15	404.120
16	420.102
17	436.083
18	452.065
19	468.047
20	484.029

PANCAKE MOTOR-2

PREF=REFERENCE PRESSURE = 300.00 PSI
AREF=REFERENCE SOUND SPEED= 3498.5 FT/SEC
R =CHAMBER RADIUS = .45830 FEET
TREF=REFERENCE TIME=R/AREF=.0001310 SEC

T/TREF= .7358

ISOBAR	PRESSURE/PREF
1	.601
2	.655
3	.708
4	.761
5	.814
6	.868
7	.921
8	.974
9	1.027
10	1.081
11	1.134
12	1.187
13	1.241
14	1.294
15	1.347
16	1.400
17	1.454
18	1.507
19	1.560
20	1.613

PANCAKE MOTOR-2

PRESSURE ISOBARS

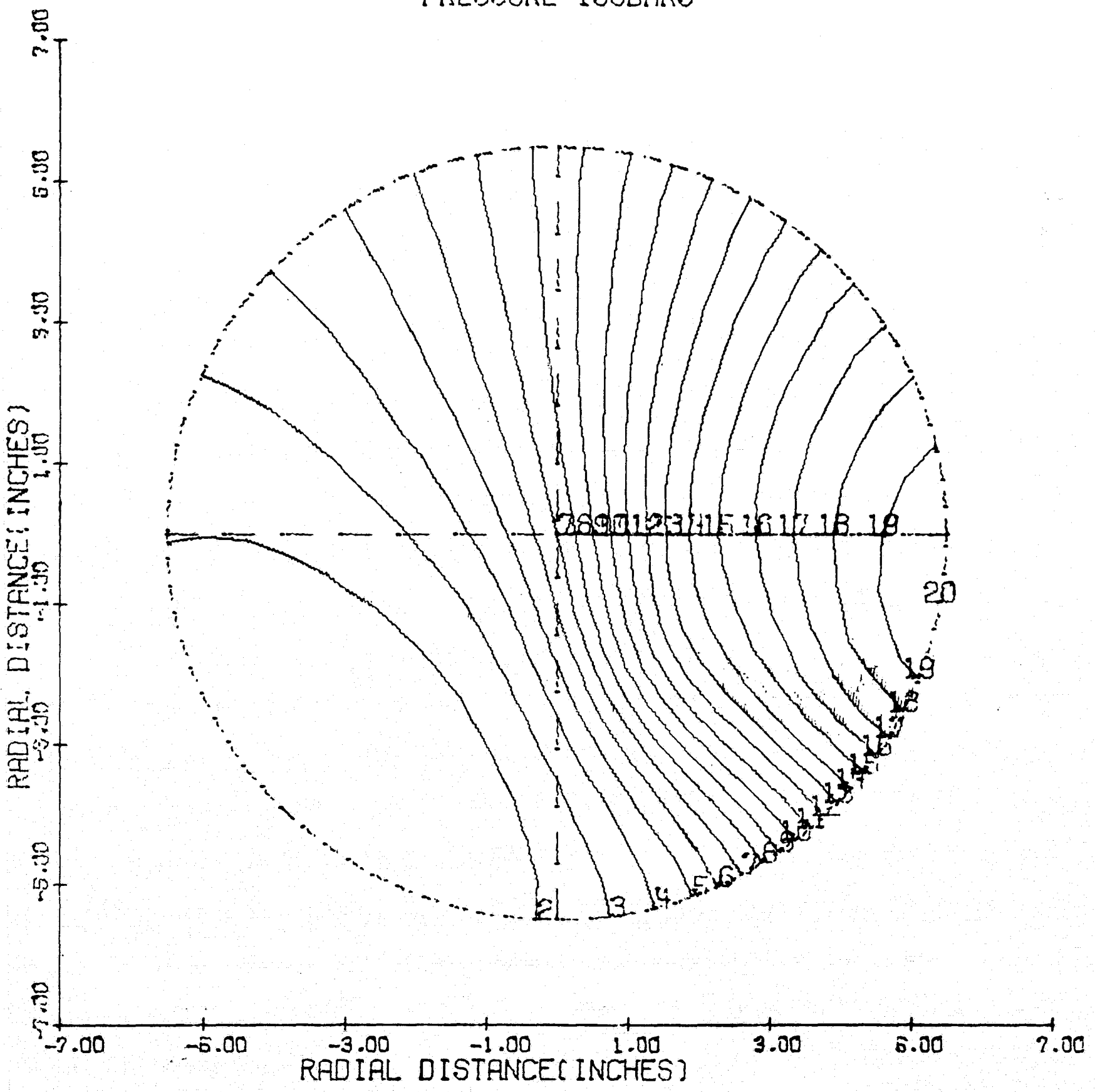

T= .201 MILLISECONDS

Figure 32

PANCAKE MOTOR-2

T= ,201 MILLISECONDS

ISOBAR	PRESSURE(PSI)
1	191,352
2	206,997
3	222,643
4	238,289
5	253,934
6	269,580
7	285,226
8	300,871
9	316,517
10	332,163
11	347,808
12	363,454
13	379,100
14	394,745
15	410,391
16	426,037
17	441,682
18	457,328
19	472,974
20	488,619

PANCAKE MOTOR-2

PREF=REFERENCE PRESSURE = 300,00 PSI
AREF=REFERENCE SOUND SPEED= 3498,5 FT/SEC
R =CHAMBER RADIUS = ,45830 FEET
TREF=REFERENCE TIME=R/AREF=,0001310 SEC

T/TREF= 1,53543

ISOBAR	PRESSURE/PREF
1	,638
2	,690
3	,742
4	,794
5	,846
6	,899
7	,951
8	1,003
9	1,055
10	1,107
11	1,159
12	1,212
13	1,264
14	1,316
15	1,368
16	1,420
17	1,472
18	1,524
19	1,577
20	1,629

PANCAKE MOTOR-2

PRESSURE ISOBARS

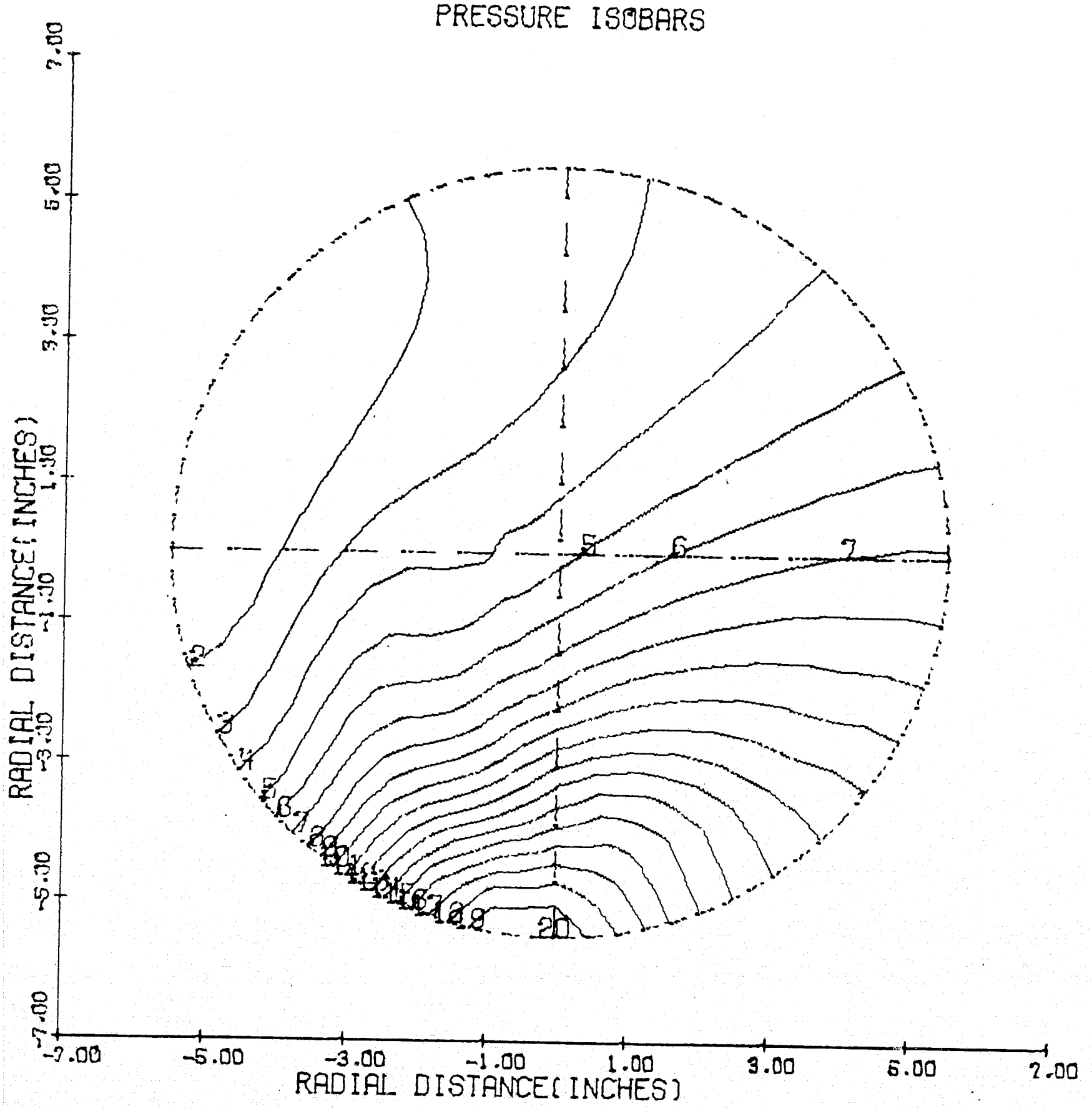

T= .304 MILLISECONDS

Figure 33

PANCAKE MOTOR-2

T= .304 MILLISECONDS

ISOBAR	PRESSURE(PSI)
1	186,244
2	208,282
3	230,320
4	252,359
5	274,397
6	296,435
7	318,473
8	340,512
9	362,550
10	384,588
11	406,626
12	428,665
13	450,703
14	472,741
15	494,780
16	516,818
17	538,856
18	560,894
19	582,933
20	604,971

PANCAKE MOTOR-2

PREF=REFERENCE PRESSURE = 300,00 PSI
AREF=REFERENCE SOUND SPEED= 3498,5 FT/SEC
R =CHAMBER RADIUS = ,45830 FEET
TREF=REFERENCE TIME=R/AREF=,0001310 SEC

T/TREF= 2,32008

ISOBAR	PRESSURE/PREF
1	,621
2	,694
3	,768
4	,841
5	,915
6	,988
7	1,062
8	1,135
9	1,208
10	1,282
11	1,355
12	1,429
13	1,502
14	1,576
15	1,649
16	1,723
17	1,796
18	1,870
19	1,943
20	2,017

PANCAKE MOTOR-2

PRESSURE ISOBARS

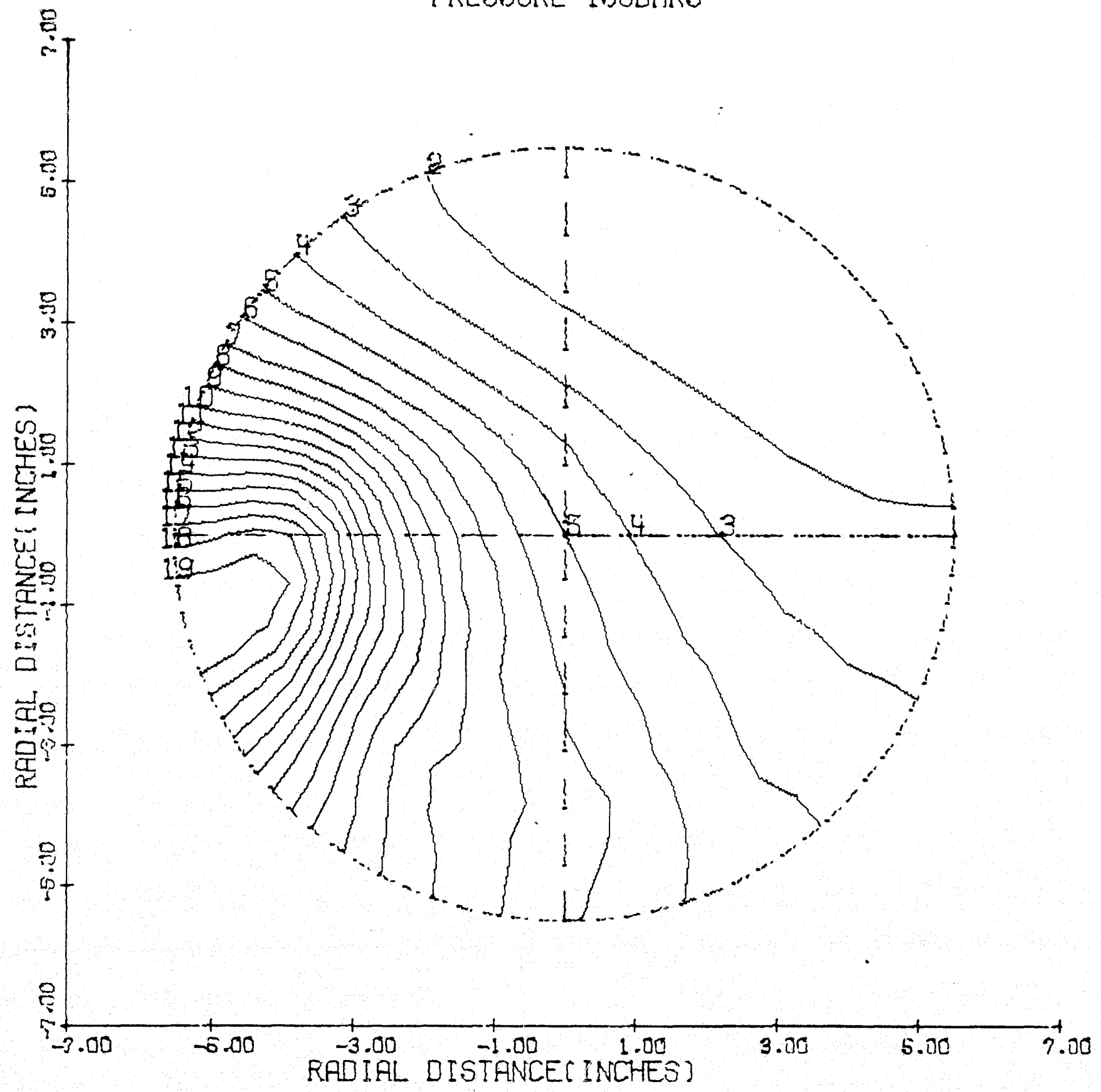

T= .406 MILLISECONDS

Figure 34

PANCAKE MOTOR-2

T= ,406 MILLISECONDS

ISOBAR	PRESSURE(PSI)
1	203,801
2	223,864
3	243,927
4	263,990
5	284,053
6	304,116
7	324,179
8	344,242
9	364,304
10	384,367
11	404,430
12	424,493
13	444,556
14	464,619
15	484,682
16	504,745
17	524,808
18	544,870
19	564,933
20	584,996

PANCAKE MOTOR-2

PREF=REFERENCE PRESSURE = 300,00 PSI
AREF=REFERENCE SOUND SPEED= 3498,5 FT/SEC
R =CHAMBER RADIUS = ,45830 FEET
TREF=REFERENCE TIME=R/AREF=,0001310 SEC

T/TREF= 3,10147

ISOBAR	PRESSURE/PREF
1	,679
2	,746
3	,813
4	,880
5	,947
6	1,014
7	1,081
8	1,147
9	1,214
10	1,281
11	1,348
12	1,415
13	1,482
14	1,549
15	1,616
16	1,682
17	1,749
18	1,816
19	1,883
20	1,950

PANCAKE MOTOR-2

PRESSURE ISOBARS

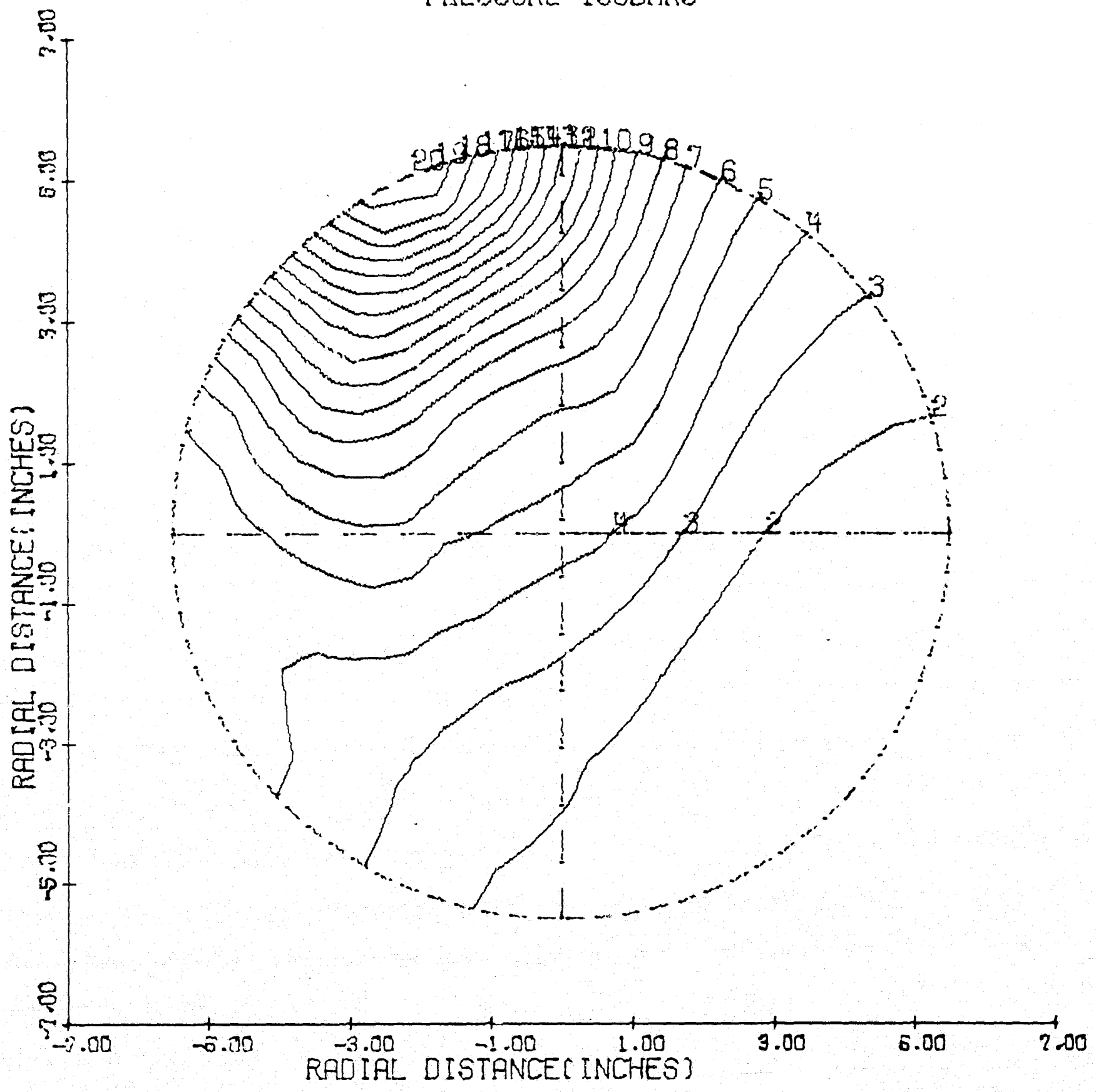

T= .511 MILLISECONDS

Figure 35

PANCAKE MOTOR-2

T= ,511 MILLISECONDS

ISOBAR	PRESSURE(PSI)
1	203,963
2	228,874
3	253,785
4	278,696
5	303,607
6	328,518
7	353,428
8	378,339
9	403,250
10	428,161
11	453,072
12	477,983
13	502,894
14	527,805
15	552,716
16	577,627
17	602,538
18	627,449
19	652,359
20	677,270

PANCAKE MOTOR-2

PREF=REFERENCE PRESSURE = 300,00 PSI
AREF=REFERENCE SOUND SPEED= 3498,5 FT/SEC
R =CHAMBER RADIUS = ,45830 FEET
TREF=REFERENCE TIME=R/AREF=,0001310 SEC

T/TREF= 3,89977

ISOBAR	PRESSURE/PREF
1	,680
2	,763
3	,846
4	,929
5	1,012
6	1,095
7	1,178
8	1,261
9	1,344
10	1,427
11	1,510
12	1,593
13	1,676
14	1,759
15	1,842
16	1,925
17	2,008
18	2,091
19	2,175
20	2,258

PANCAKE MOTOR-2

PRESSURE ISOBARS

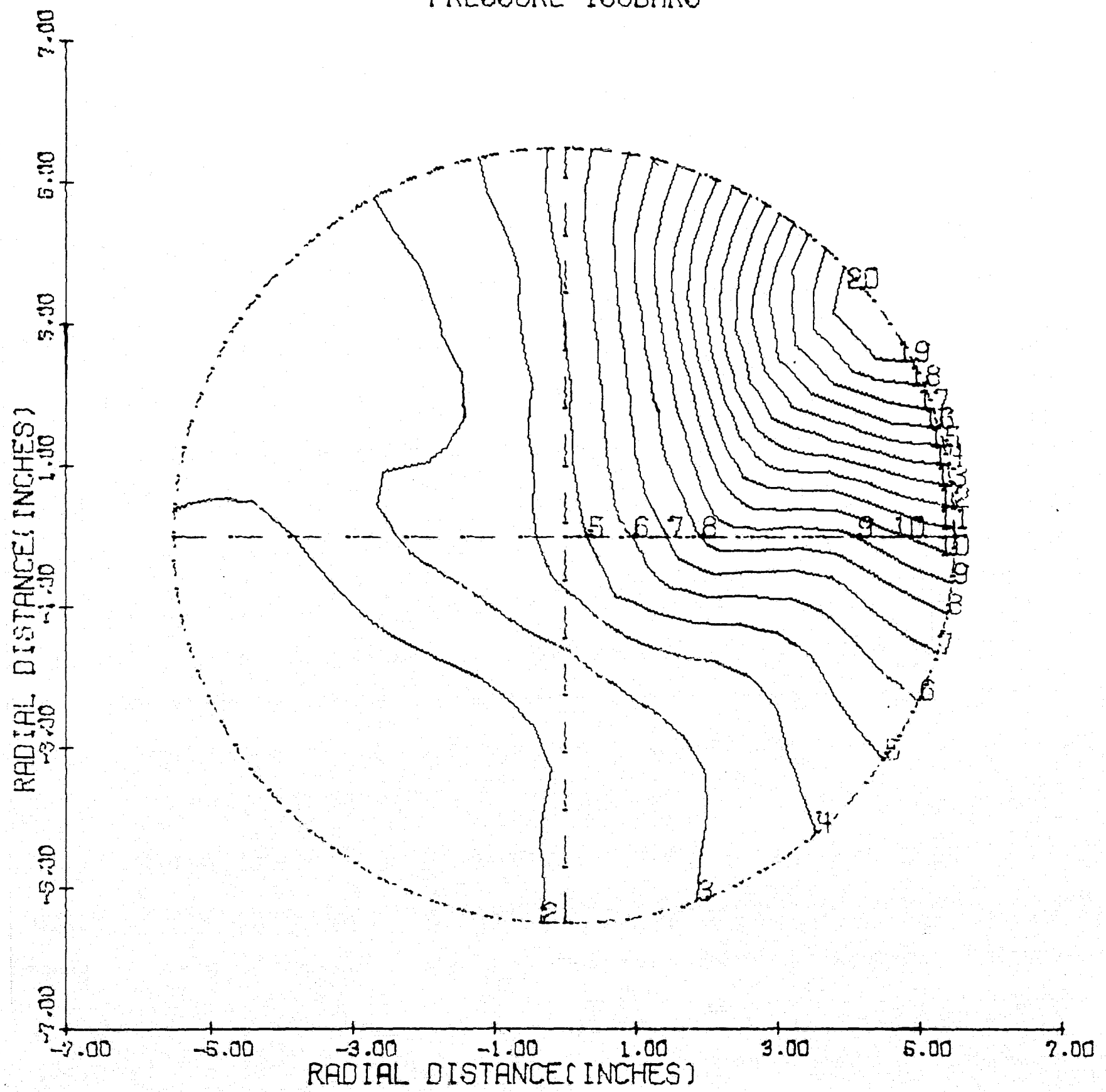

T= .615 MILLISECONDS

Figure 36

PANCAKE MOTOR-2

T= ,615 MILLISECONDS

ISOBAR	PRESSURE(PSI)
1	212,923
2	233,970
3	255,018
4	276,066
5	297,113
6	318,161
7	339,209
8	360,256
9	381,304
10	402,352
11	423,399
12	444,447
13	465,495
14	486,542
15	507,590
16	528,637
17	549,685
18	570,733
19	591,780
20	612,828

PANCAKE MOTOR-2

PREF=REFERENCE PRESSURE = 300,00 PSI
AREF=REFERENCE SOUND SPEED= 3498,5 FT/SEC
R =CHAMBER RADIUS = ,45830 FEET
TREF=REFERENCE TIME=R/AREF=,0001310 SEC

T/TREF= 4,69291

ISOBAR	PRESSURE/PREF
1	,710
2	,780
3	,850
4	,920
5	,990
6	1,061
7	1,131
8	1,201
9	1,271
10	1,341
11	1,411
12	1,481
13	1,552
14	1,622
15	1,692
16	1,762
17	1,832
18	1,902
19	1,973
20	2,043

PANCAKE MOTOR-2

PRESSURE ISOBARS

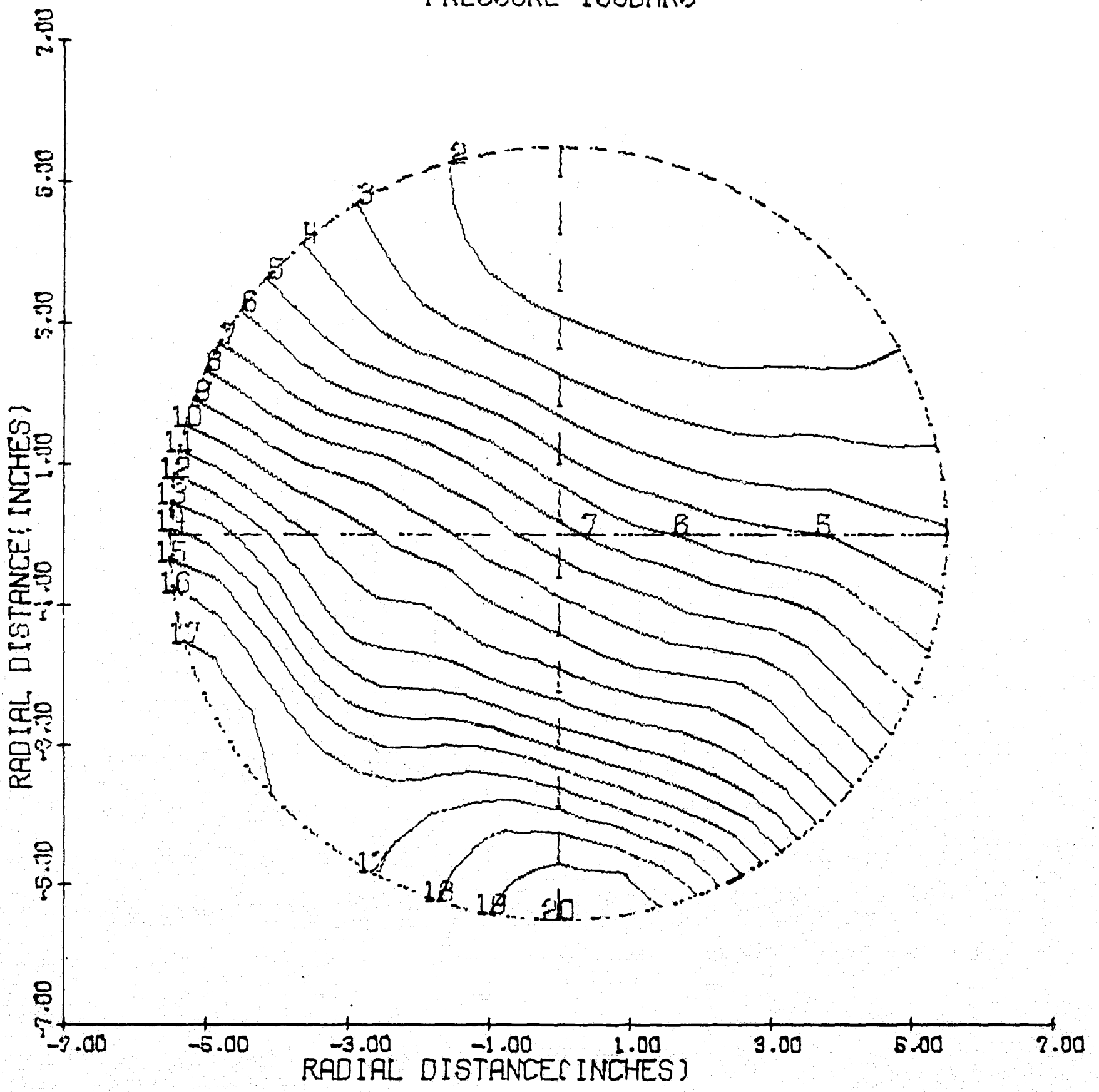

T= 1.232 MILLISECONDS

Figure 37

PANCAKE MOTOR-2

T= 1,232 MILLISECONDS

ISOBAR	PRESSURE(PSI)
1	178,783
2	195,488
3	212,192
4	228,896
5	245,601
6	262,305
7	279,009
8	295,714
9	312,418
10	329,122
11	345,826
12	362,531
13	379,235
14	395,939
15	412,644
16	429,348
17	446,052
18	462,757
19	479,461
20	496,165

PANCAKE MOTOR-2

PREF=REFERENCE PRESSURE = 300,00 PSI
AREF=REFERENCE SOUND SPEED= 3498,5 FT/SEC
R =CHAMBER RADIUS = ,45830 FEET
TREF=REFERENCE TIME=R/AREF=,0001310 SEC

T/TREF= 9,40473

ISOBAR	PRESSURE/PREF
1	,596
2	,652
3	,707
4	,763
5	,819
6	,874
7	,930
8	,986
9	1,041
10	1,097
11	1,153
12	1,208
13	1,264
14	1,320
15	1,375
16	1,431
17	1,487
18	1,543
19	1,598
20	1,654

PANCAKE MOTOR-2

PRESSURE ISOBARS

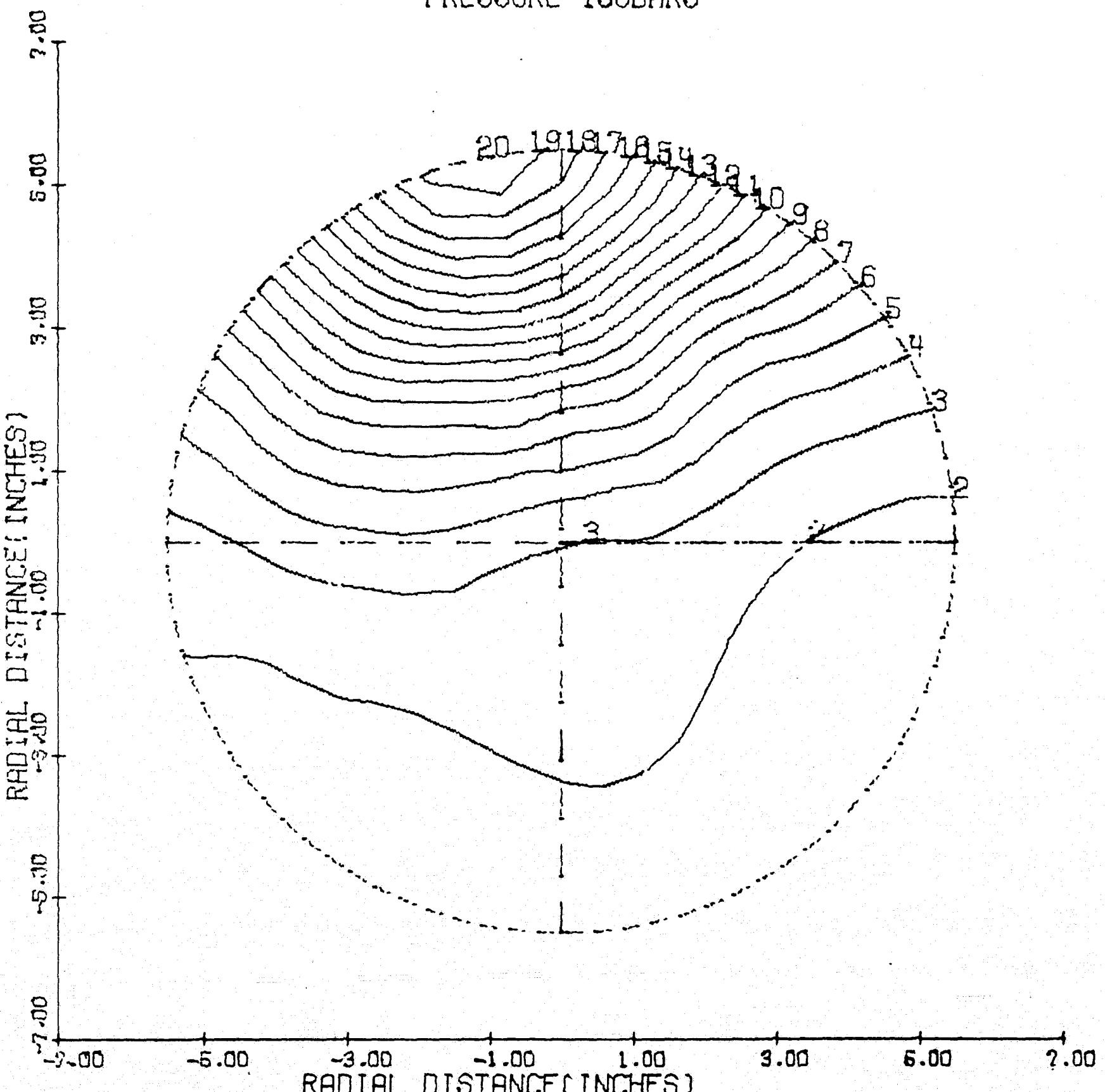

T= 1.847 MILLISECONDS

Figure 38

PANCAKE MOTOR-2

T= 1,847 MILLISECONDS

ISOBAR	PRESSURE(PSI)
1	215,942
2	237,481
3	259,020
4	280,558
5	302,097
6	323,636
7	345,174
8	366,713
9	388,252
10	409,790
11	431,329
12	452,868
13	474,406
14	495,945
15	517,484
16	539,022
17	560,561
18	582,100
19	603,638
20	625,177

PANCAKE MOTOR-2

PREF=REFERENCE PRESSURE = 300,00 PSI
AREF=REFERENCE SOUND SPEED= 3498,5 FT/SEC
R =CHAMBER RADIUS = ,45830 FEET
TREF=REFERENCE TIME=R/AREF=,0001310 SEC

T/TREF= 14,10001

ISOBAR	PRESSURE/PREF
1	,720
2	,792
3	,863
4	,935
5	1,007
6	1,079
7	1,151
8	1,222
9	1,294
10	1,366
11	1,438
12	1,510
13	1,581
14	1,653
15	1,725
16	1,797
17	1,869
18	1,940
19	2,012
20	2,084

PANCAKE MOTOR-2

PRESSURE ISOBARS

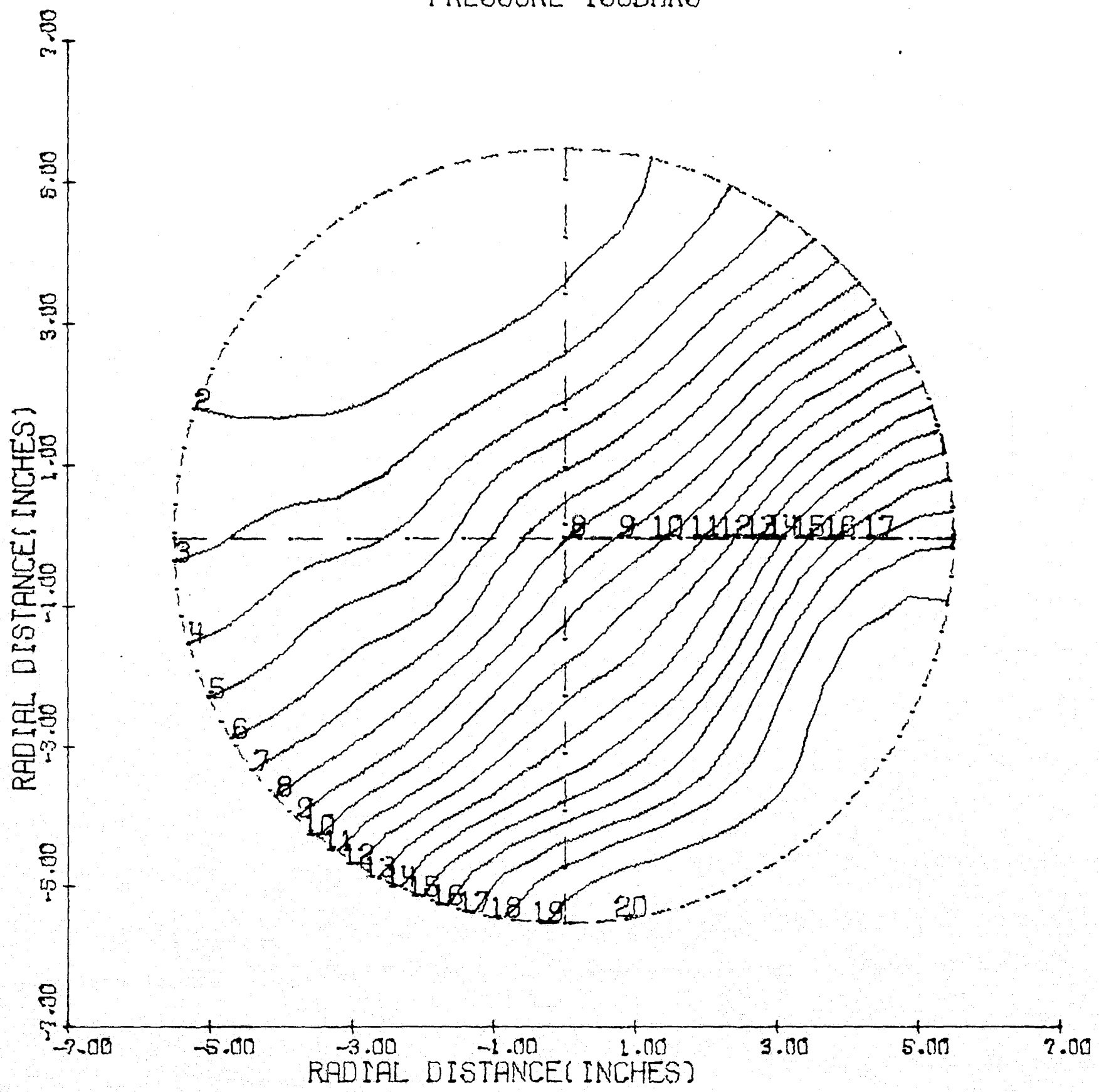

T= 2.467 MILLISECONDS

Figure 39

PANCAKE MOTOR-2

T= 2.467 MILLISECONDS

ISOBAR	PRESSURE(PSI)
1	185.283
2	200.258
3	215.232
4	230.207
5	245.181
6	260.155
7	275.130
8	290.104
9	305.079
10	320.053
11	335.027
12	350.002
13	364.976
14	379.951
15	394.925
16	409.899
17	424.874
18	439.848
19	454.823
20	469.797

PANCAKE MOTOR-2

PREF=REFERENCE PRESSURE = 300.00 PSI
AREF=REFERENCE SOUND SPEED= 3498.5 FT/SEC
R =CHAMBER RADIUS = .45830 FEET
TREF=REFERENCE TIME=R/AREF=.0001310 SEC

T/TREF= 18.83099

ISOBAR	PRESSURE/PREF
1	.618
2	.668
3	.717
4	.767
5	.817
6	.867
7	.917
8	.967
9	1.017
10	1.067
11	1.117
12	1.167
13	1.217
14	1.267
15	1.316
16	1.366
17	1.416
18	1.466
19	1.516
20	1.566

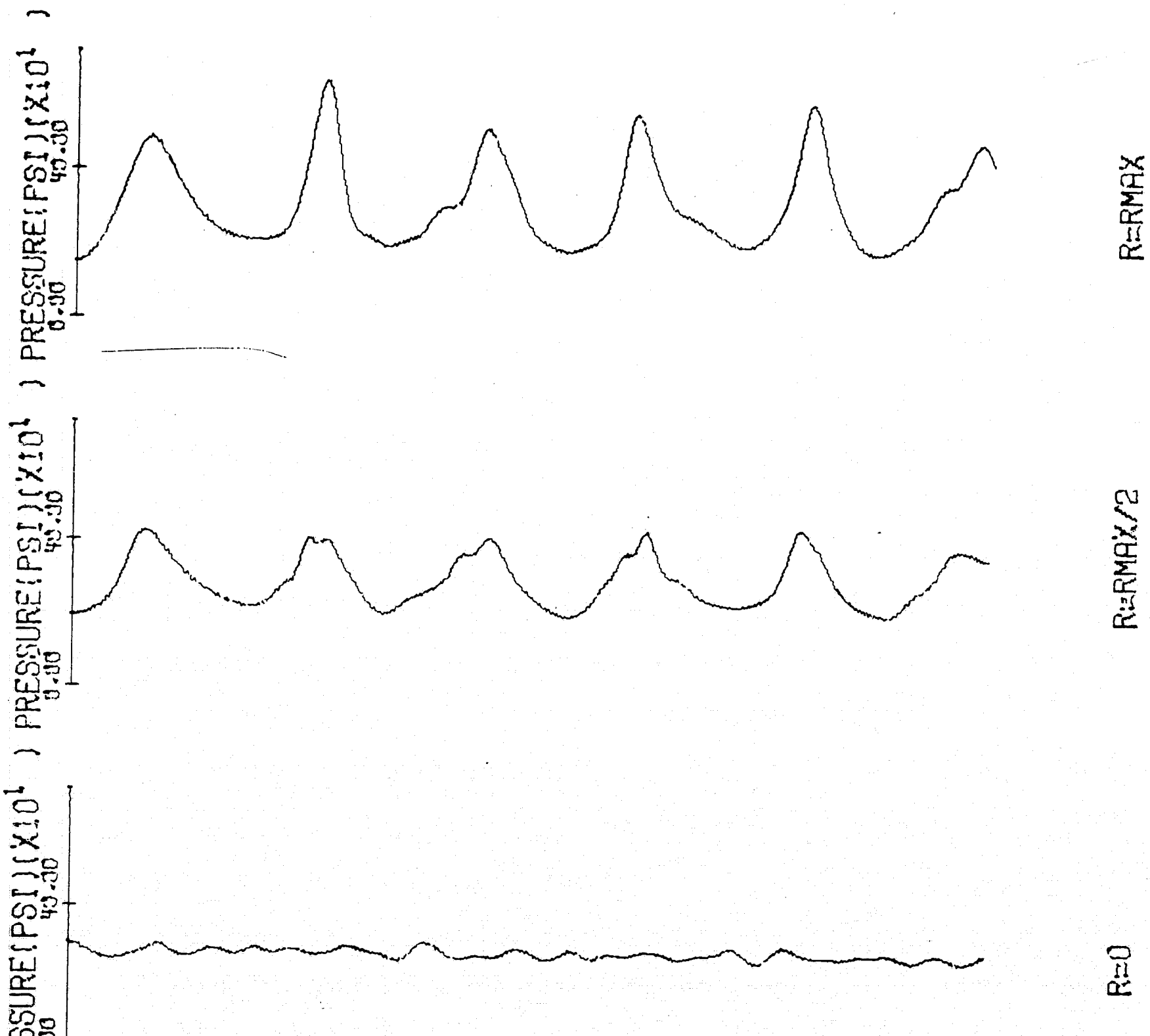
PANCAKE MOTOR-2
PRESSURE(PSI)(X10¹)
49.30
0.00
R=RMAX
R=RMAX/2
R=0
0.00
.40
.80
1.20
1.60
2.00
2.40
2.80
TIME(MILLISECONDS)

Figure 40

PANCAKE MOTOR-2

PRESSURE AT RADIAL DISTANCE OF 5.50 INCHES

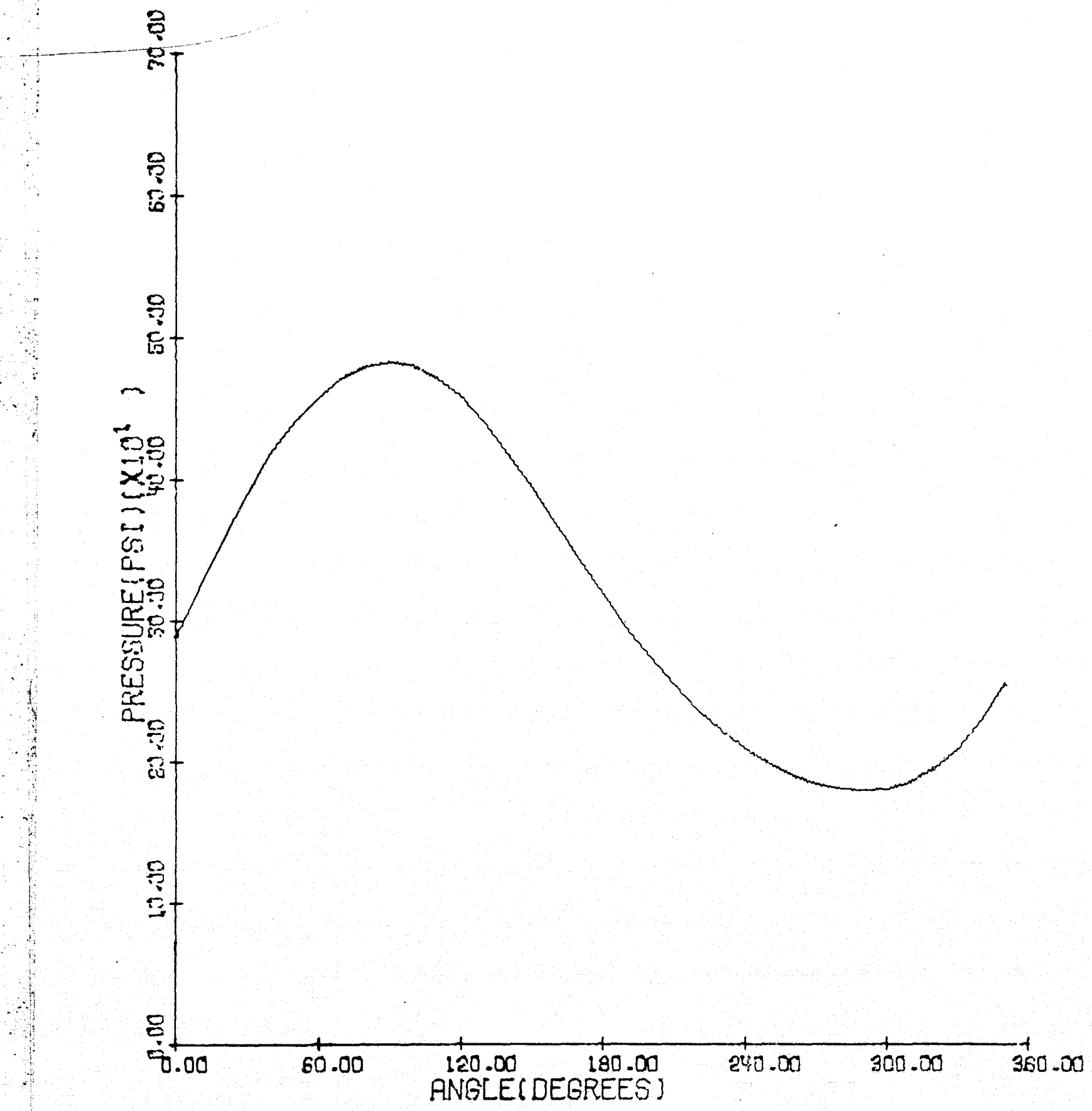

T= .101 MILLISECONDS

Figure 41

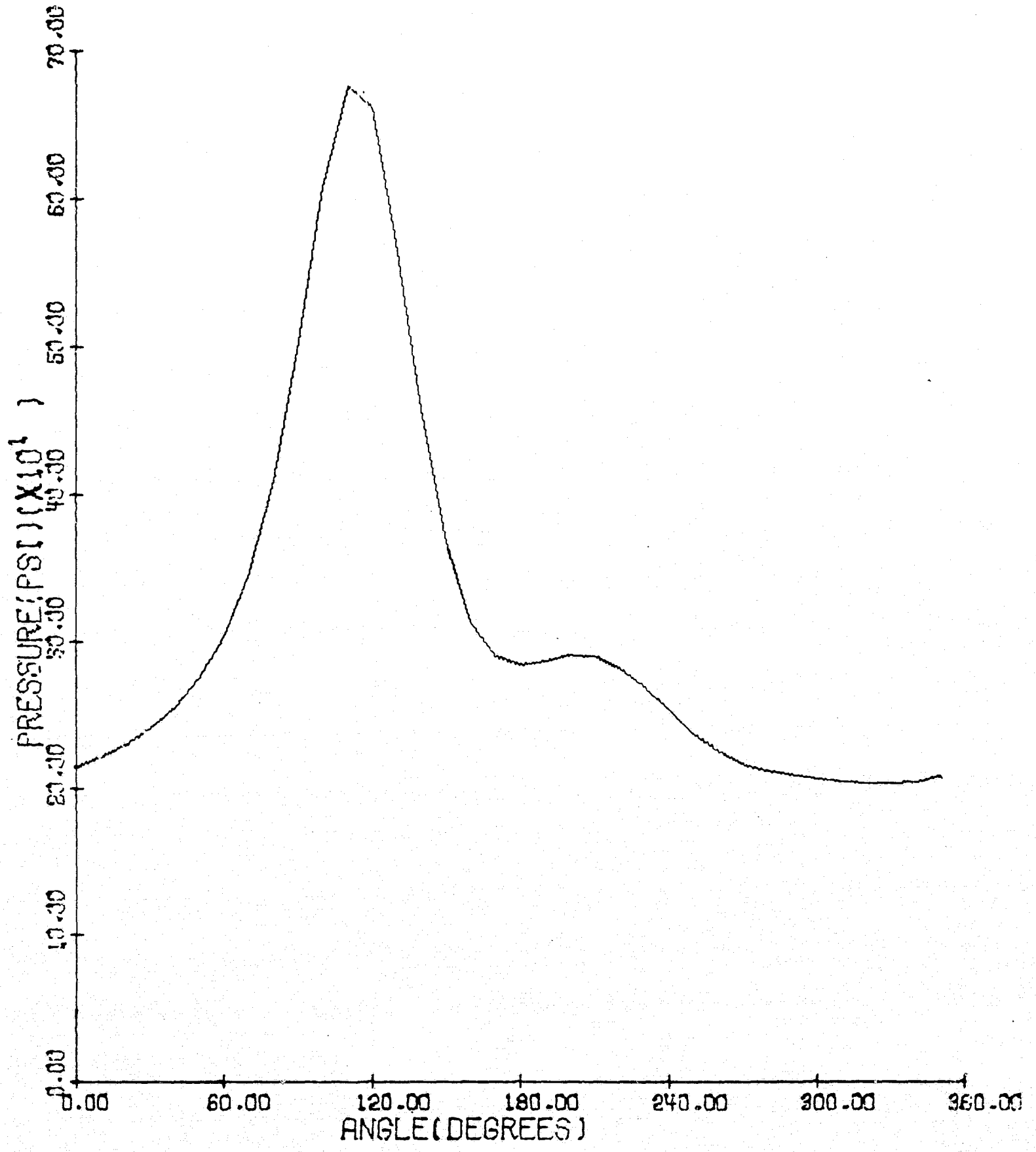
PANCAKE MOTOR-2
PRESSURE AT RADIAL DISTANCE OF 5.50 INCHES
PRESSURE(PSI)(X10¹)
0.00
10.30
20.30
30.30
40.30
50.00
60.00
70.00
0.00
60.00
120.00
180.00
240.00
300.00
360.00
ANGLE(DEGREES)
T= .511 MILLISECONDS

Figure 42

PANCAKE MOTOR-2

STREAKLINE

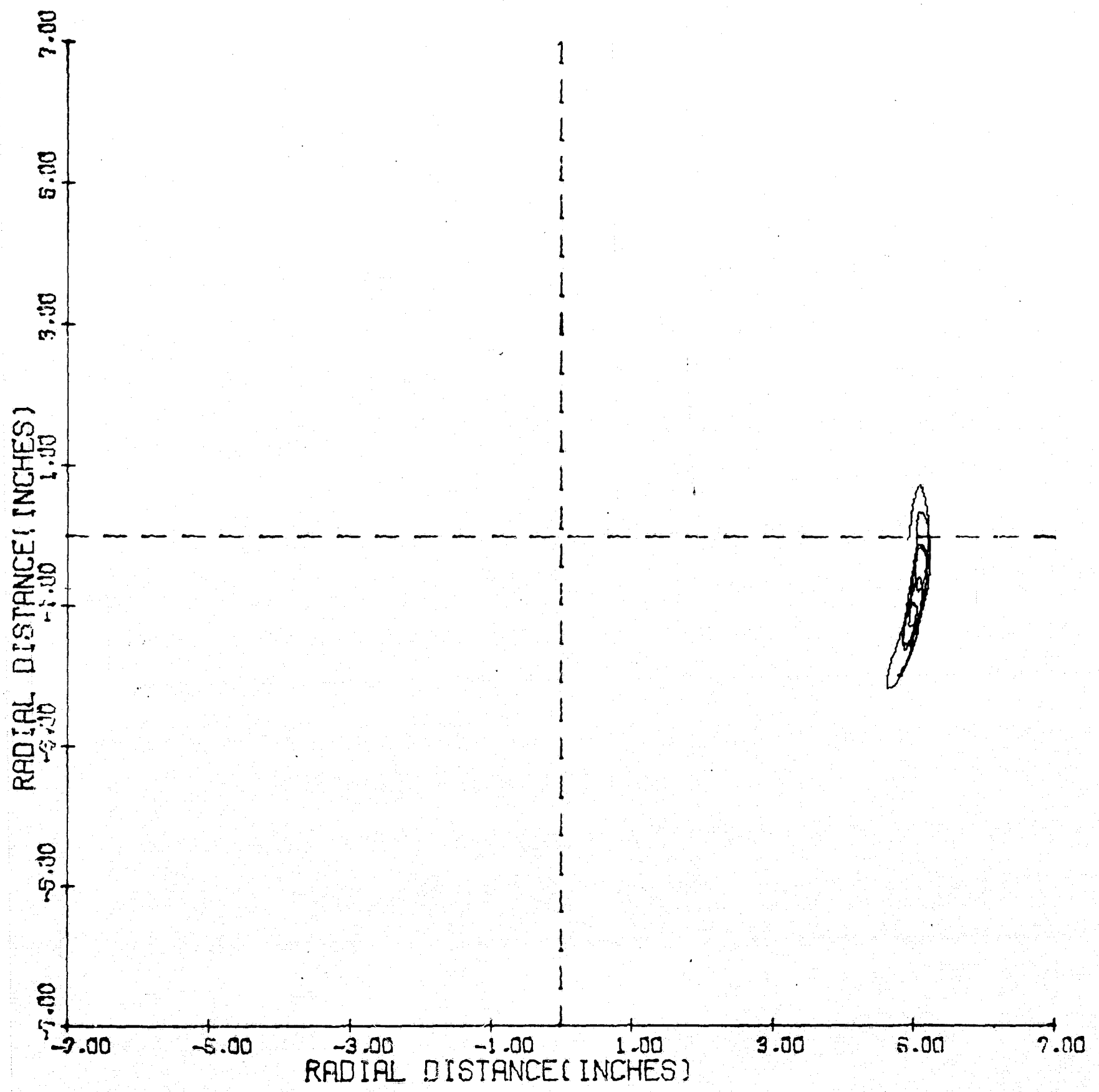

T= 2.467 MILLISECONDS

Figure 43

PANCAKE MOTOR-4

PRESSURE ISOBARS

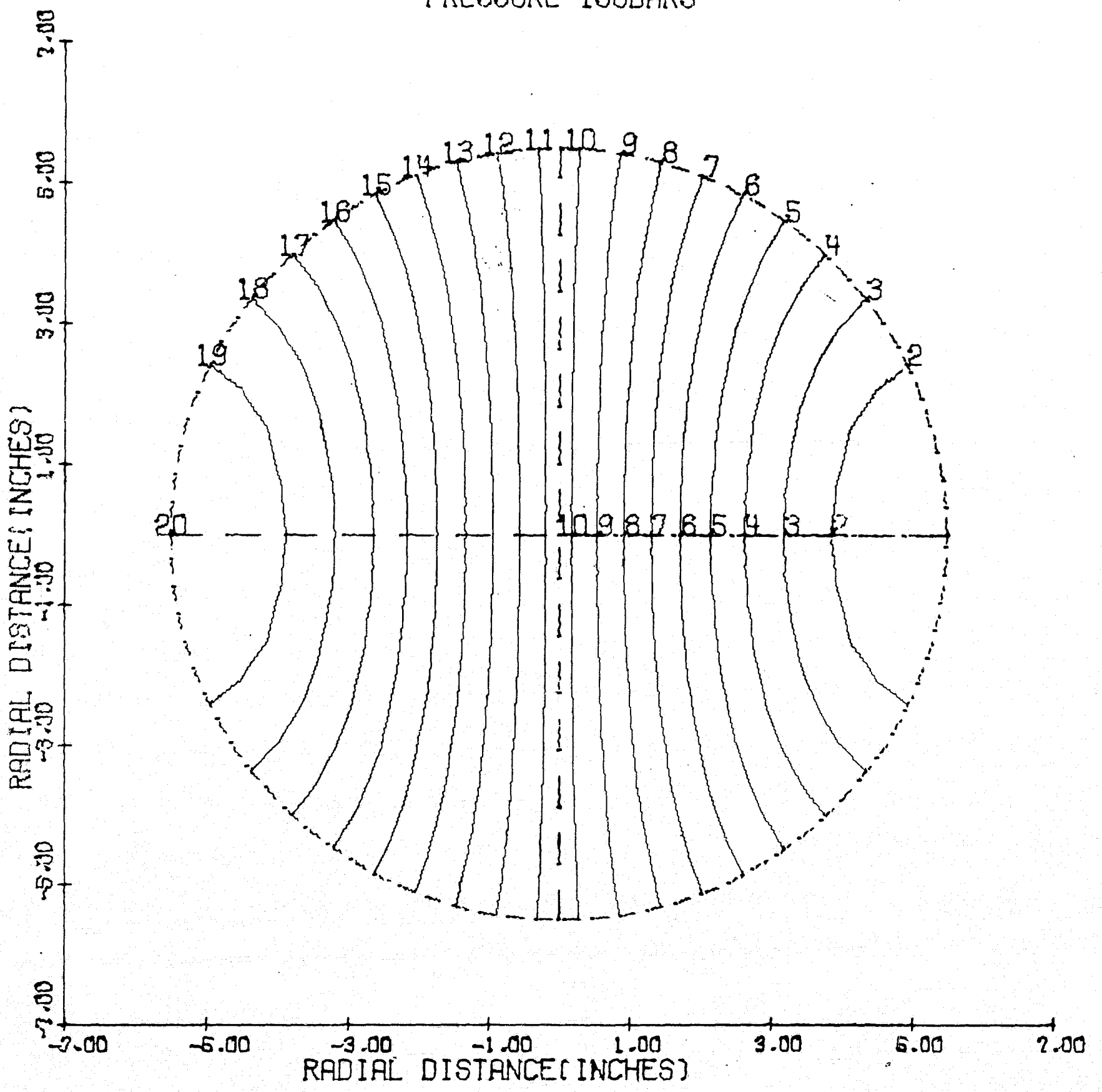

T= 0.000 MILLISECONDS

Figure 44

PANCAKE MOTOR-4

T= 0,000 MILLISECONDS

ISOBAR	PRESSURE(PSI)
1	10,000
2	40,526
3	71,053
4	101,579
5	132,105
6	162,632
7	193,158
8	223,684
9	254,211
10	284,737
11	315,263
12	345,789
13	376,316
14	406,842
15	437,368
16	467,895
17	498,421
18	528,947
19	559,474
20	590,000

PANCAKE MOTOR-4

PREF=REFERENCE PRESSURE = 300,00 PSI
AREF=REFERENCE SOUND SPEED= 3498,5 FT/SEC
R =CHAMBER RADIUS = ,45830 FEET
TREF=REFERENCE TIME=R/AREF=,0001310 SEC

T/TREF= 0,00000

ISOBAR	PRESSURE/PREF
1	,033
2	,135
3	,237
4	,339
5	,440
6	,542
7	,644
8	,746
9	,847
10	,949
11	1,051
12	1,153
13	1,254
14	1,356
15	1,458
16	1,560
17	1,661
18	1,763
19	1,865
20	1,967

PANCAKE MOTOR-4

PRESSURE ISOBARS

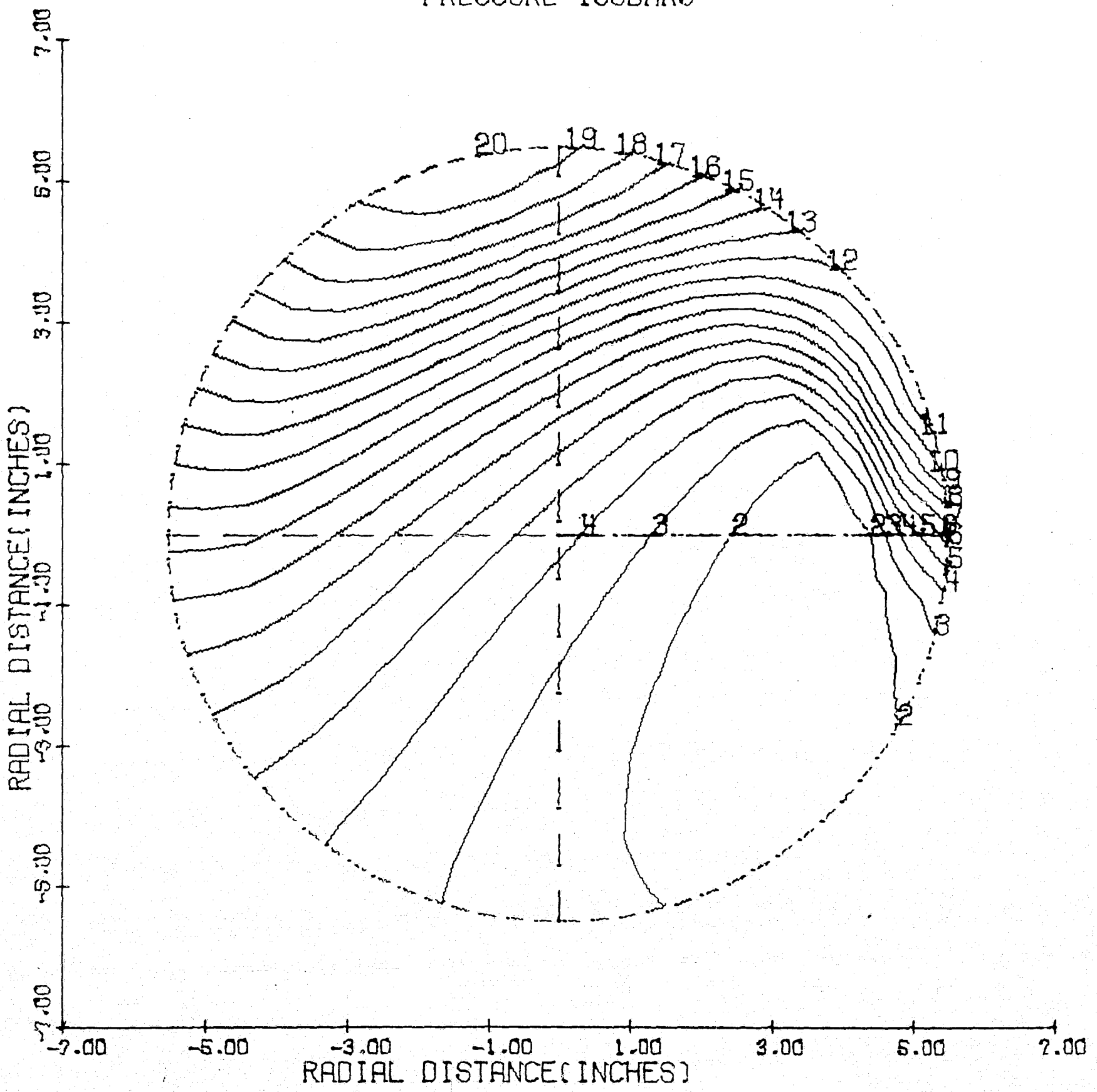

T= .082 MILLISECONDS

Figure 45

PANCAKE MOTOR-4

T= ,082 MILLISECONDS

ISOBAR	PRESSURE(PSI)
1	88,935
2	124,831
3	160,728
4	196,625
5	232,521
6	268,418
7	304,314
8	340,211
9	376,107
10	412,004
11	447,900
12	483,797
13	519,693
14	555,590
15	591,486
16	627,383
17	663,279
18	699,176
19	735,072
20	770,969

PANCAKE MOTOR-4

PREF=REFERENCE PRESSURE = 300,00 PSI
AREF=REFERENCE SOUND SPEED= 3498,5 FT/SEC
R =CHAMBER RADIUS = ,45830 FEET
TREF=REFERENCE TIME=R/AREF=,0001310 SEC

T/TREF= ,62629

ISOBAR	PRESSURE/PREF
1	,296
2	,416
3	,536
4	,655
5	,775
6	,895
7	1,014
8	1,134
9	1,254
10	1,373
11	1,493
12	1,613
13	1,732
14	1,852
15	1,972
16	2,091
17	2,211
18	2,331
19	2,450
20	2,570

PANCAKE MOTOR-4

PRESSURE ISOBARS

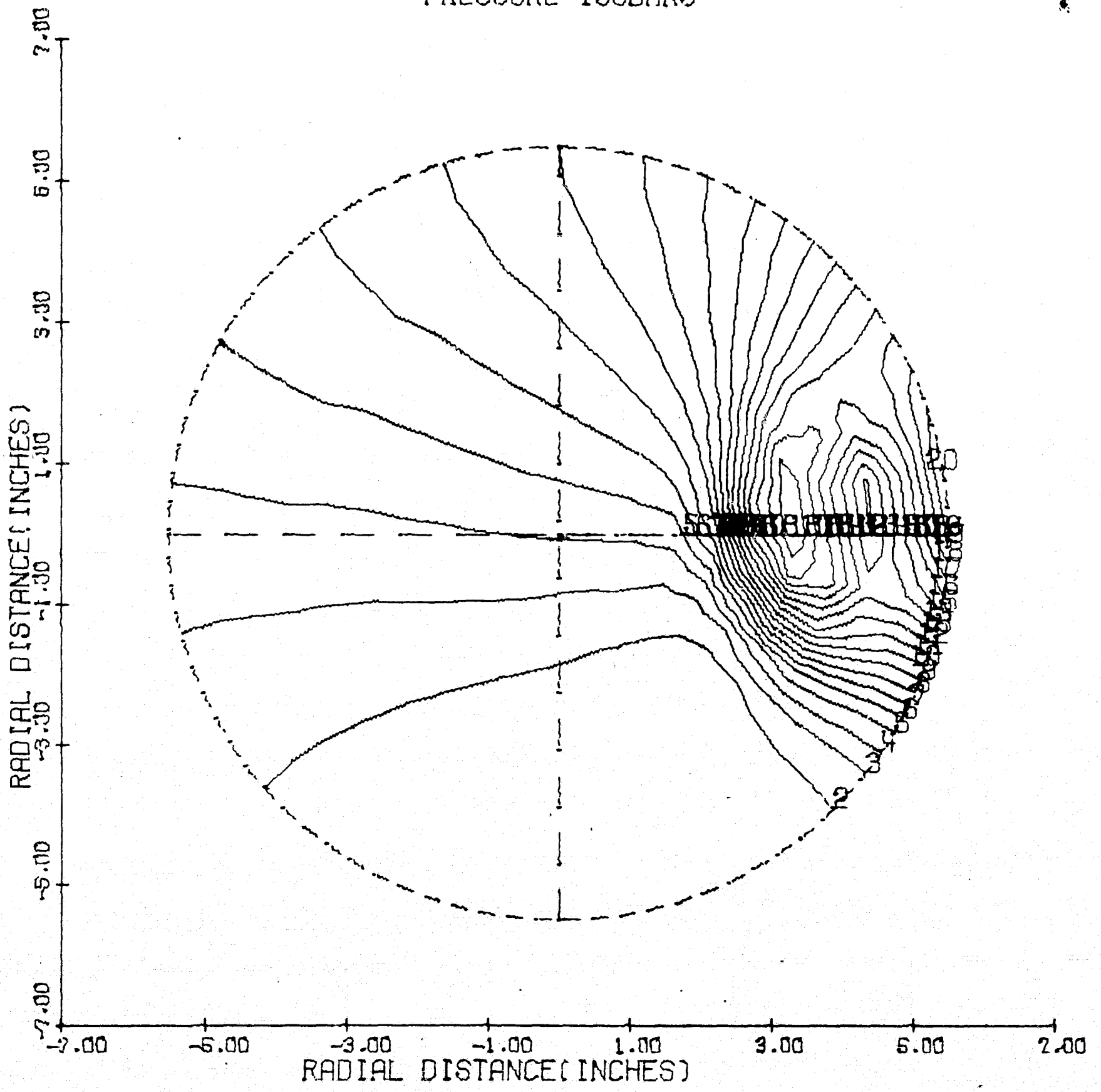

T= .163 MILLISECONDS

Figure 46

PANCAKE MOTOR-4

T= .163 MILLISECONDS

ISOBAR	PRESSURE(PSI)
1	114.541
2	152.611
3	190.680
4	228.750
5	266.819
6	304.889
7	342.958
8	381.028
9	419.097
10	457.167
11	495.236
12	533.306
13	571.375
14	609.445
15	647.514
16	685.584
17	723.653
18	761.723
19	799.792
20	837.862

PANCAKE MOTOR-4

PREF=REFERENCE PRESSURE = 300.00 PSI
AREF=REFERENCE SOUND SPEED= 3498.5 FT/SEC
R =CHAMBER RADIUS = .45830 FEET
TREF=REFERENCE TIME=R/AREF=.0001310 SEC

T/TREF= 1.24509

ISOBAR	PRESSURE/PREF
1	.382
2	.509
3	.636
4	.762
5	.889
6	1.016
7	1.143
8	1.270
9	1.397
10	1.524
11	1.651
12	1.778
13	1.905
14	2.031
15	2.158
16	2.285
17	2.412
18	2.539
19	2.666
20	2.793

PANCAKE MOTOR-4

PRESSURE ISOBARS

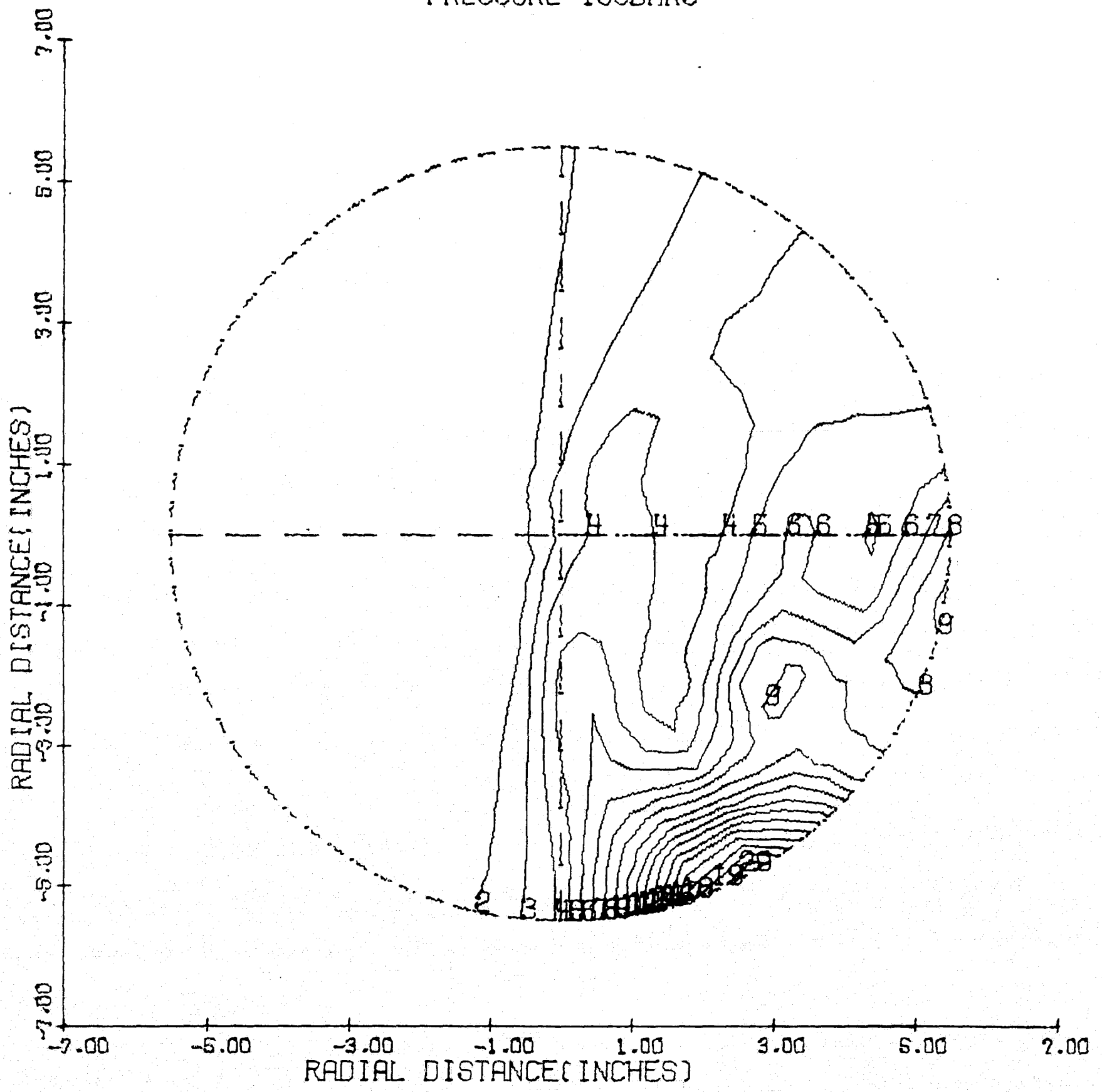

T= .245 MILLISECONDS

Figure 47

PANCAKE MOTOR-4

T= ,245 MILLISECONDS

ISOBAR	PRESSURE(PSI)
1	140,707
2	203,986
3	267,265
4	330,543
5	393,822
6	457,101
7	520,379
8	583,658
9	646,937
10	710,215
11	773,494
12	836,773
13	900,051
14	963,330
15	1026,609
16	1089,887
17	1153,166
18	1216,445
19	1279,724
20	1343,002

PANCAKE MOTOR-4

PREF=REFERENCE PRESSURE = 300,00 PSI
AREF=REFERENCE SOUND SPEED= 3498,5 FT/SEC
R =CHAMBER RADIUS = ,45830 FEET
TREF=REFERENCE TIME=R/AREF=,0001310 SEC

T/TREF= 1,86735

ISOBAR	PRESSURE/PREF
1	,469
2	,680
3	,891
4	1,102
5	1,313
6	1,524
7	1,735
8	1,946
9	2,156
10	2,367
11	2,578
12	2,789
13	3,000
14	3,211
15	3,422
16	3,633
17	3,844
18	4,055
19	4,266
20	4,477

PANCAKE MOTOR-4

PRESSURE ISOBARS

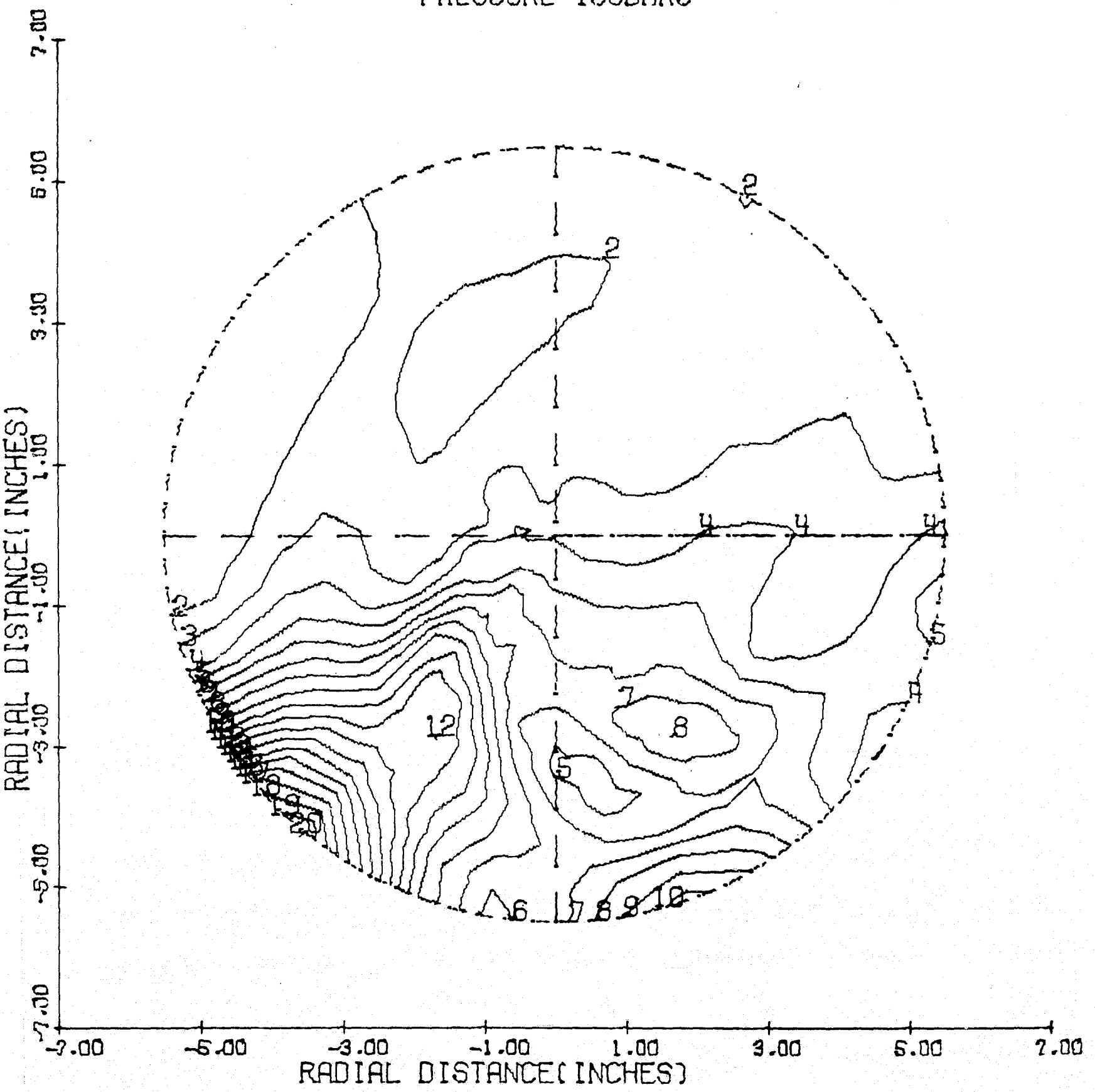

T= .334 MILLISECONDS

Figure 48

PANCAKE MOTOR-4

T= ,334 MILLISECONDS

ISOBAR	PRESSURE(PSI)
1	115,851
2	168,970
3	222,089
4	275,209
5	328,328
6	381,447
7	434,567
8	487,686
9	540,805
10	593,924
11	647,044
12	700,163
13	753,282
14	806,402
15	859,521
16	912,640
17	965,760
18	1018,879
19	1071,998
20	1125,117

PANCAKE MOTOR-4

PREF=REFERENCE PRESSURE = 300,00 PSI
AREF=REFERENCE SOUND SPEED= 3498,5 FT/SEC
R =CHAMBER RADIUS = ,45830 FEET
TREF=REFERENCE TIME=R/AREF= ,0001310 SEC

T/TREF= 2,54805

ISOBAR	PRESSURE/PREF
1	,386
2	,563
3	,740
4	,917
5	1,094
6	1,271
7	1,449
8	1,626
9	1,803
10	1,980
11	2,157
12	2,334
13	2,511
14	2,688
15	2,865
16	3,042
17	3,219
18	3,396
19	3,573
20	3,750

PANCAKE MOTOR-4

PRESSURE ISOBARS

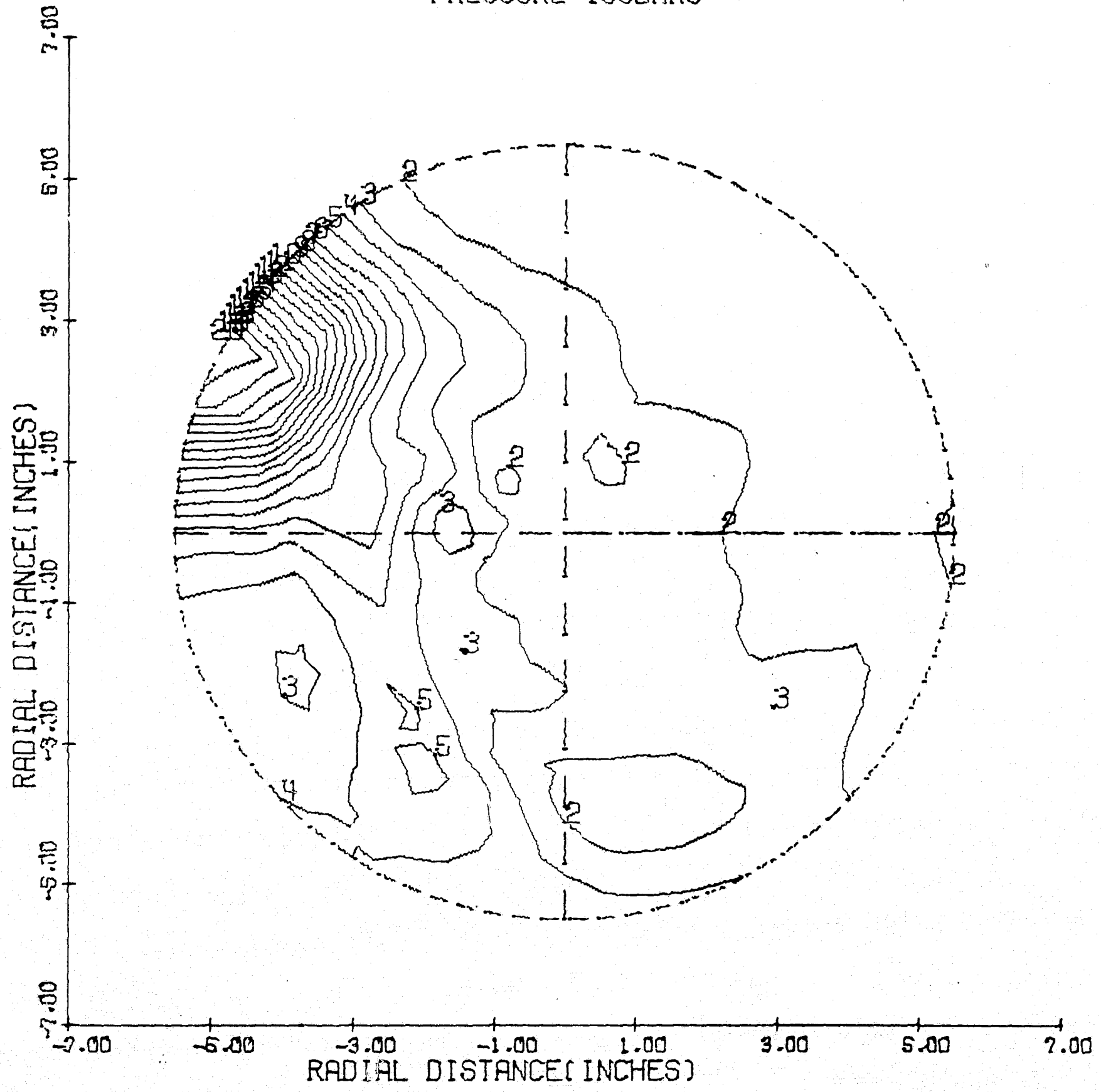

T= .423 MILLISECONDS

Figure 49

PANCAKE MOTOR-4

T= ,423 MILLISECONDS

ISOBAR	PRESSURE(PSI)
1	147,888
2	210,435
3	272,981
4	335,527
5	398,073
6	460,619
7	523,166
8	585,712
9	648,258
10	710,804
11	773,350
12	835,896
13	898,443
14	960,989
15	1023,535
16	1086,081
17	1148,627
18	1211,174
19	1273,720
20	1336,266

PANCAKE MOTOR-4

PREF=REFERENCE PRESSURE = 300,00 PSI
AREF=REFERENCE SOUND SPEED= 3498,5 FT/SEC
R =CHAMBER RADIUS = ,45830 FEET
TREF=REFERENCE TIME=R/AREF=,0001310 SEC

T/TREF= 3,22728

ISOBAR	PRESSURE/PREF
1	,493
2	,701
3	,910
4	1,118
5	1,327
6	1,535
7	1,744
8	1,952
9	2,161
10	2,369
11	2,578
12	2,786
13	2,995
14	3,203
15	3,412
16	3,620
17	3,829
18	4,037
19	4,246
20	4,454

PANCAKE MOTOR-4

PRESSURE ISOBARS

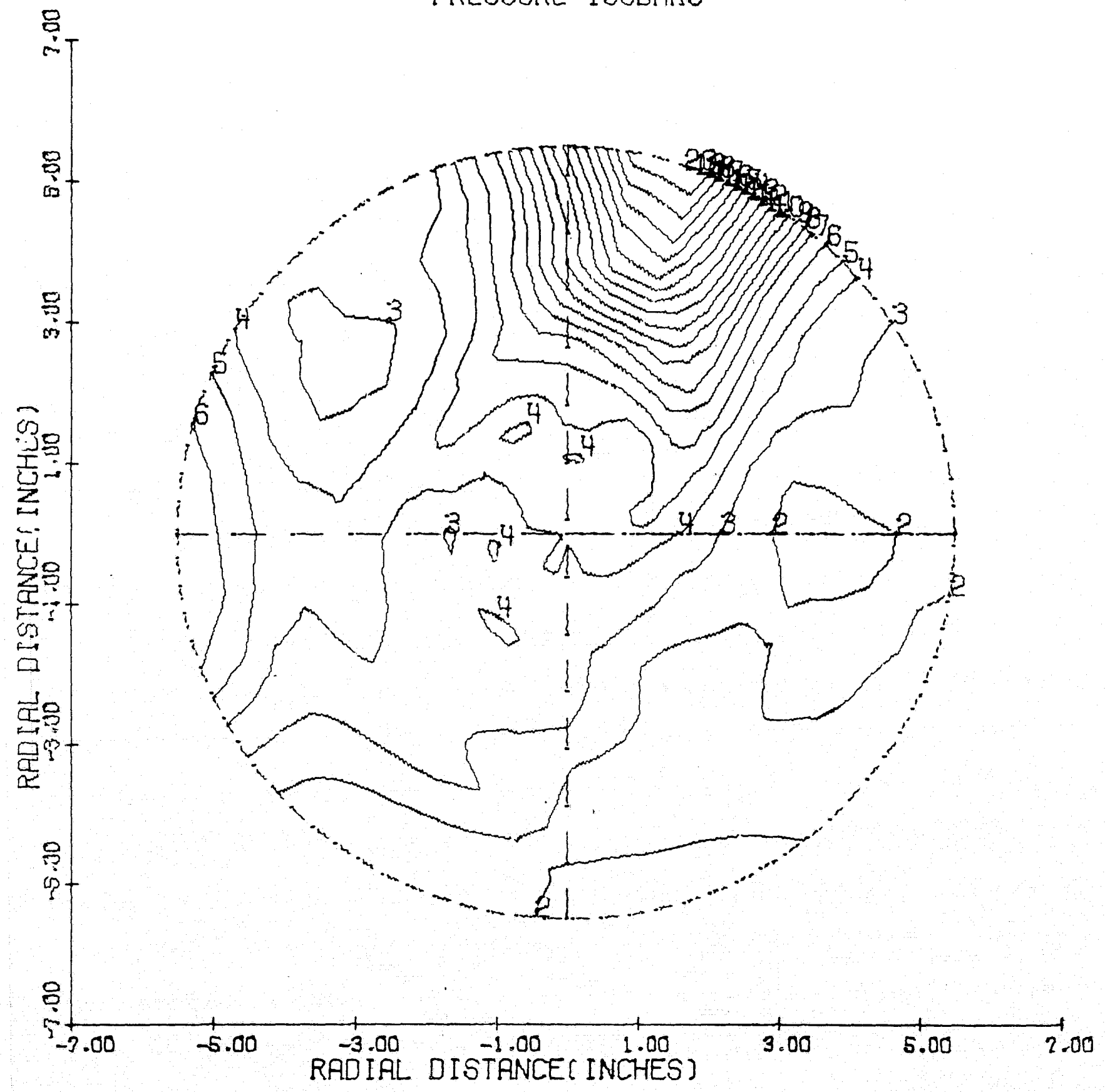

T= .517 MILLISECONDS

Figure 50

PANCAKE MOTOR-4

T= ,517 MILLISECONDS

ISOBAR	PRESSURE(PSI)
1	123,450
2	177,535
3	231,620
4	285,705
5	339,790
6	393,875
7	447,960
8	502,045
9	556,130
10	610,215
11	664,301
12	718,386
13	772,471
14	826,556
15	880,641
16	934,726
17	988,811
18	1042,896
19	1096,981
20	1151,066

PANCAKE MOTOR-4

PREF=REFERENCE PRESSURE = 300,00 PSI
AREF=REFERENCE SOUND SPEED= 3498,5 FT/SEC
R =CHAMBER RADIUS = ,45830 FEET
TREF=REFERENCE TIME=R/AREF=,0001310 SEC

T/TREF= 3,94745

ISOBAR	PRESSURE/PREF
1	,412
2	,592
3	,772
4	,952
5	1,133
6	1,313
7	1,493
8	1,673
9	1,854
10	2,034
11	2,214
12	2,395
13	2,575
14	2,755
15	2,935
16	3,116
17	3,296
18	3,476
19	3,657
20	3,837

PANCAKE MOTOR-4

PRESSURE ISOBARS

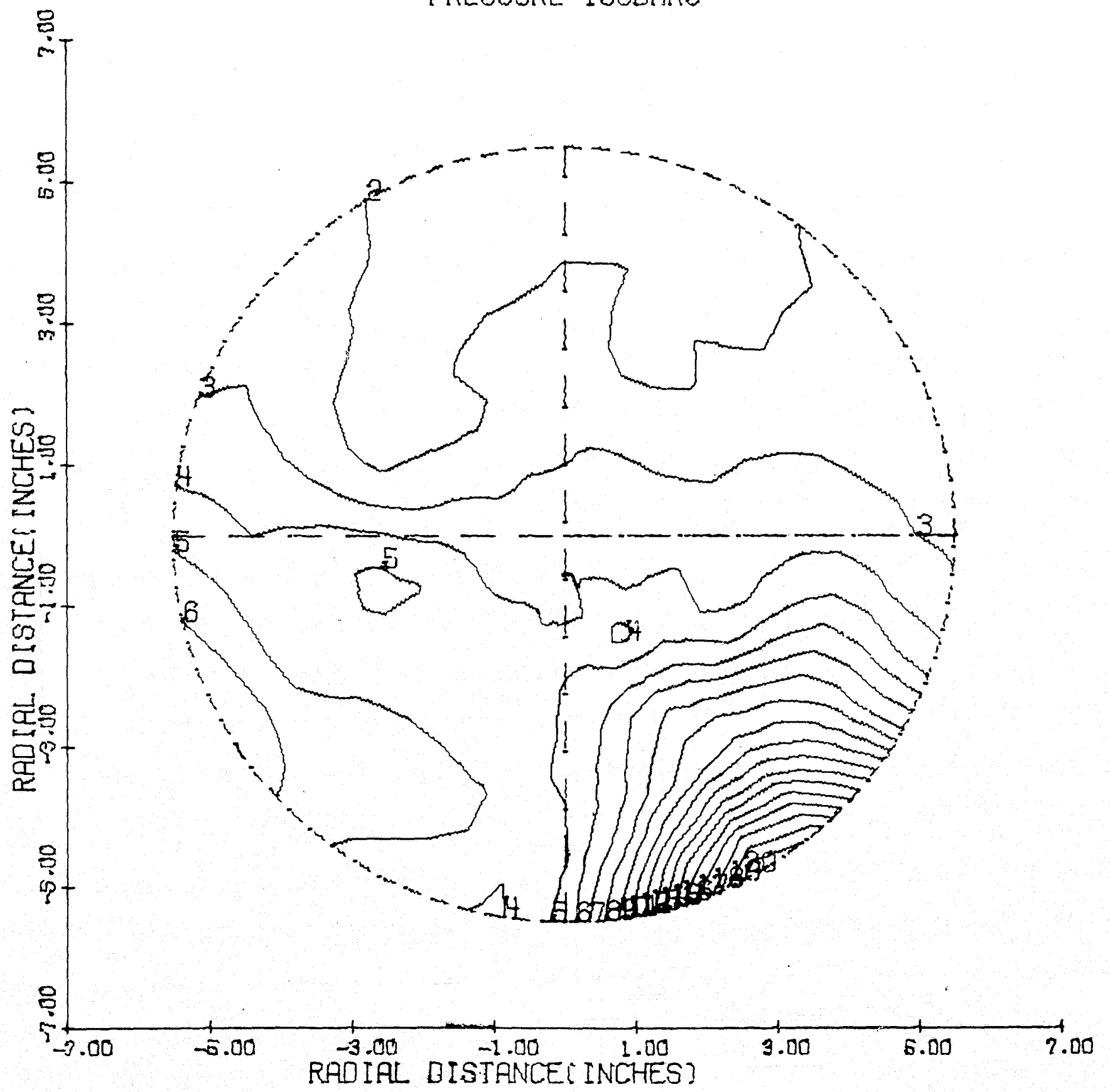

T= 1.087 MILLISECONDS

Figure 51

PANCAKE MOTOR-4

T= 1,087 MILLISECONDS

ISOBAR	PRESSURE(PSI)
1	115,495
2	172,677
3	229,860
4	287,042
5	344,224
6	401,407
7	458,589
8	515,771
9	572,954
10	630,136
11	687,318
12	744,501
13	801,683
14	858,865
15	916,048
16	973,230
17	1030,412
18	1087,595
19	1144,777
20	1201,959

PANCAKE MOTOR-4

PREF=REFERENCE PRESSURE = 300,00 PSI
AREF=REFERENCE SOUND SPEED= 3498,5 FT/SEC
R =CHAMBER RADIUS = ,45830 FEET
TREF=REFERENCE TIME=R/AREF=,0001310 SEC

T/TREF= 8,29882

ISOBAR	PRESSURE/PREF
1	,385
2	,576
3	,766
4	,957
5	1,147
6	1,338
7	1,529
8	1,719
9	1,910
10	2,100
11	2,291
12	2,482
13	2,672
14	2,863
15	3,053
16	3,244
17	3,435
18	3,625
19	3,816
20	4,007

PANCAKE MOTOR-4

PRESSURE ISOBARS

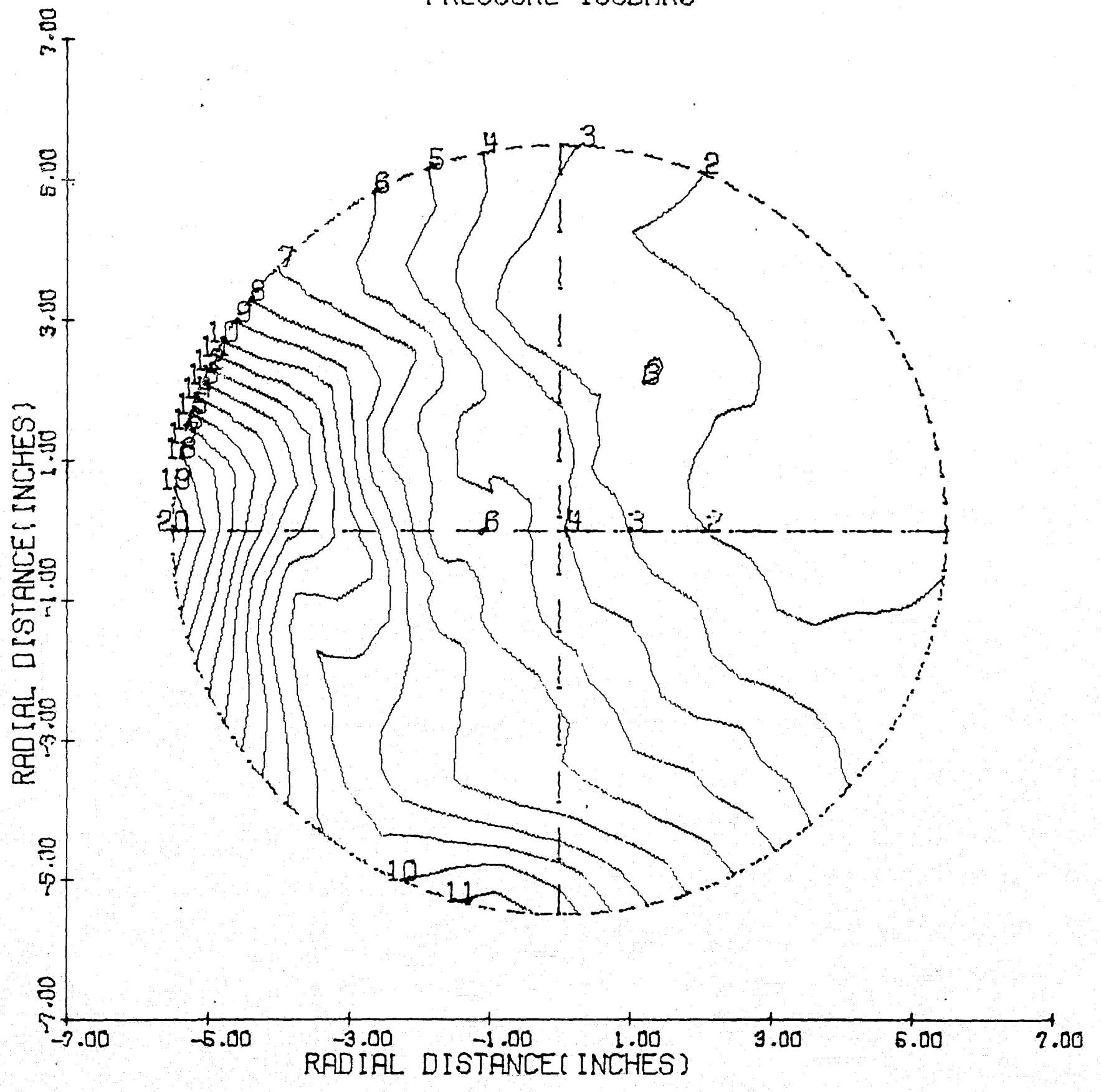

T= 1.611 MILLISECONDS

Figure 52

PANCAKE MOTOR-4

T= 1,611 MILLISECONDS

ISOBAR	PRESSURE(PSI)
1	115,467
2	155,925
3	196,382
4	236,840
5	277,298
6	317,755
7	358,213
8	398,671
9	439,128
10	479,586
11	520,044
12	560,501
13	600,959
14	641,417
15	681,874
16	722,332
17	762,790
18	803,247
19	843,705
20	884,163

PANCAKE MOTOR-4

PREF=REFERENCE PRESSURE = 300,00 PSI
AREF=REFERENCE SOUND SPEED= 3498,5 FT/SEC
R =CHAMBER RADIUS = ,45830 FEET
TREF=REFERENCE TIME=R/AREF=,0001310 SEC

T/TREF= 12,29963

ISOBAR	PRESSURE/PREF
1	,385
2	,520
3	,655
4	,789
5	,924
6	1,059
7	1,194
8	1,329
9	1,464
10	1,599
11	1,733
12	1,868
13	2,003
14	2,138
15	2,273
16	2,408
17	2,543
18	2,677
19	2,812
20	2,947

PANCAKE MOTOR-4

PRESSURE ISOBARS

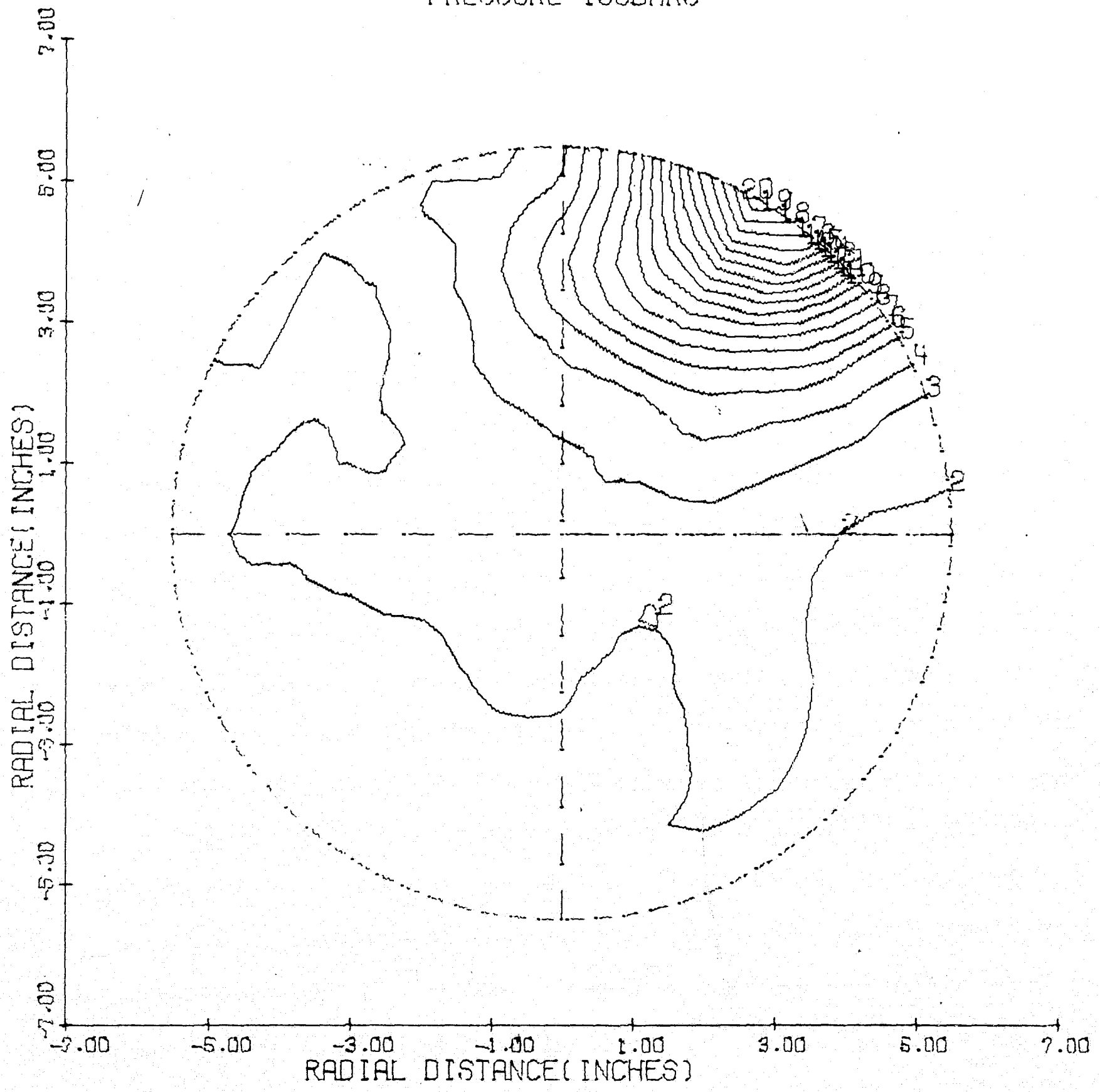

T= 2.168 MILLISECONDS

Figure 53

PANCAKE MOTOR-4

T= 2,168 MILLISECONDS

ISOBAR	PRESSURE(PSI)
1	179,265
2	238,772
3	298,278
4	357,784
5	417,291
6	476,797
7	536,303
8	595,809
9	655,316
10	714,822
11	774,328
12	833,835
13	893,341
14	952,847
15	1012,353
16	1071,860
17	1131,366
18	1190,872
19	1250,379
20	1309,885

PANCAKE MOTOR-4

PREF=REFERENCE PRESSURE = 300,00 PSI
AREF=REFERENCE SOUND SPEED= 3498,5 FT/SEC
R =CHAMBER RADIUS = ,45830 FEET
TREF=REFERENCE TIME=R/AREF=,0001310 SEC

T/TREF= 16,55067

ISOBAR	PRESSURE/PREF
1	,598
2	,796
3	,994
4	1,193
5	1,391
6	1,589
7	1,788
8	1,986
9	2,184
10	2,383
11	2,581
12	2,779
13	2,978
14	3,176
15	3,375
16	3,573
17	3,771
18	3,970
19	4,168
20	4,366

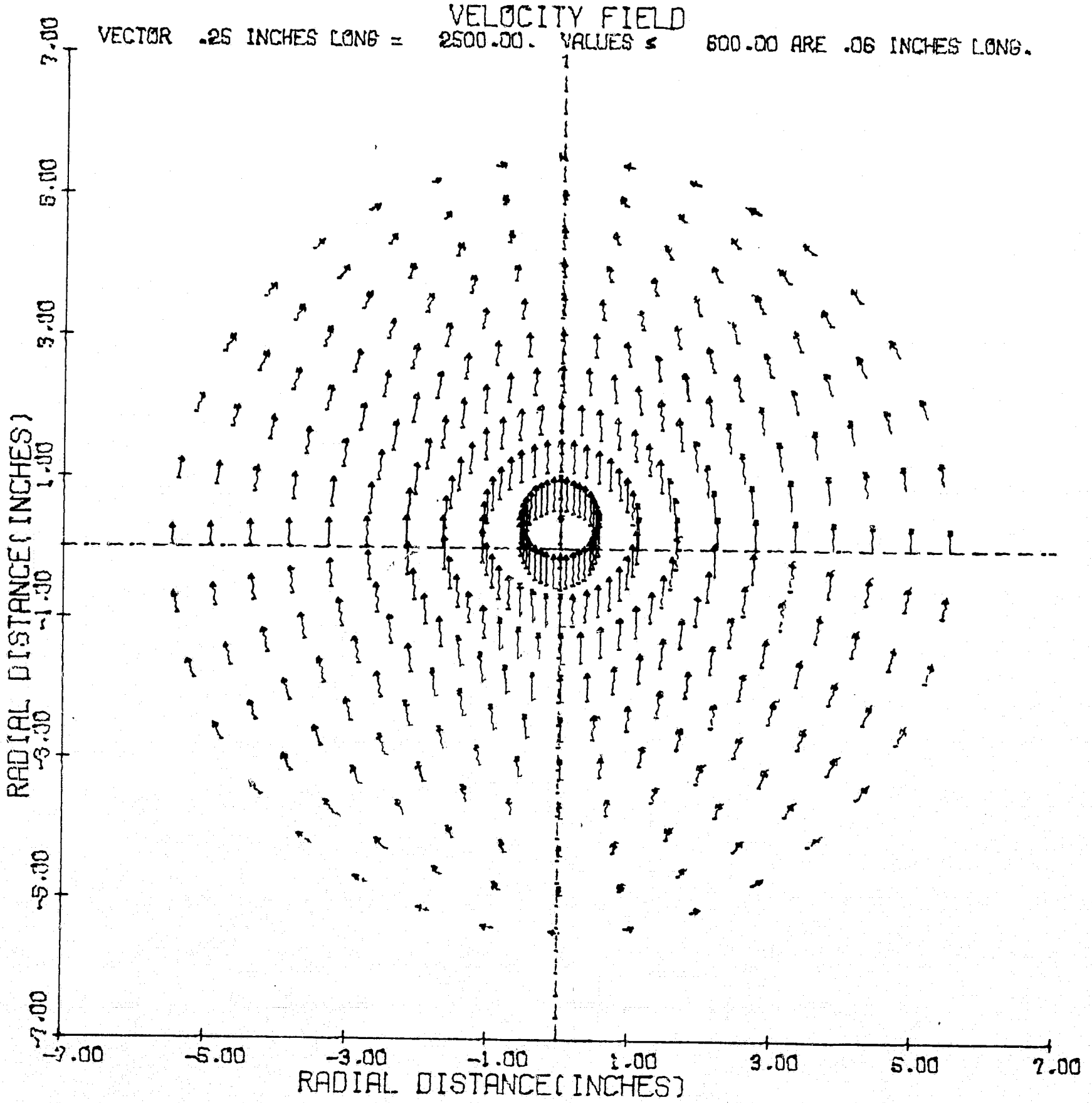
PANCAKE MOTOR-4
VELOCITY FIELD
VECTOR .25 INCHES LONG = 2500.00. VALUES ≤ 600.00 ARE .06 INCHES LONG.
RADIAL DISTANCE(INCHES)
7.00
5.00
3.00
1.00
-1.00
-3.00
-5.00
-7.00
-7.00
-5.00
-3.00
-1.00
1.00
3.00
5.00
7.00
RADIAL DISTANCE(INCHES)
T= 0.000 MILLISECONDS

Figure 54

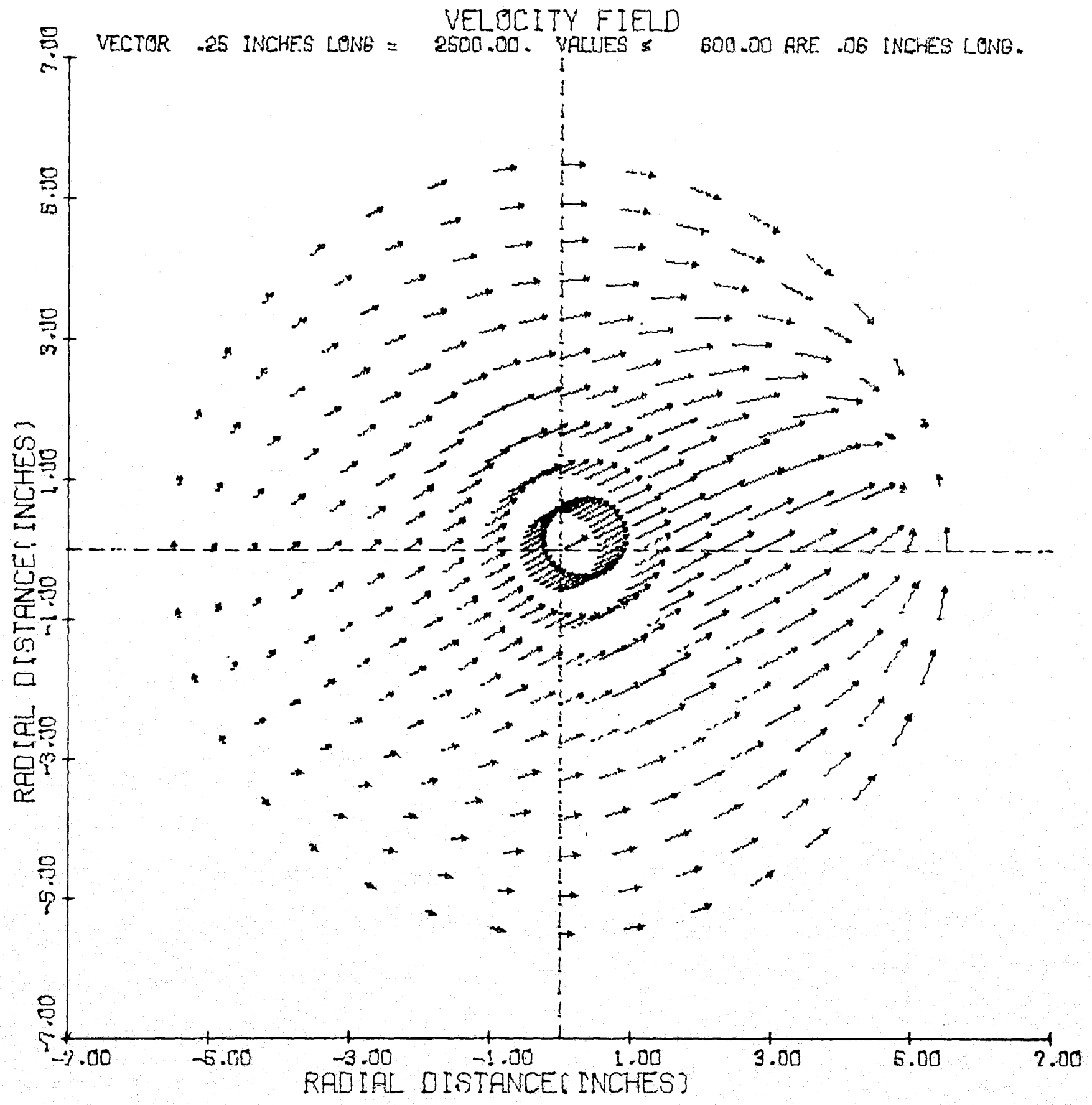
PANCAKE MOTOR-4
VELOCITY FIELD
VECTOR .25 INCHES LONG = 2500.00. VALUES ≤ 600.00 ARE .06 INCHES LONG.
RADIAL DISTANCE(INCHES)
7.00
5.00
3.00
1.00
-1.00
-3.00
-5.00
-7.00
-7.00
-5.00
-3.00
-1.00
1.00
3.00
5.00
7.00
RADIAL DISTANCE(INCHES)
T= .082 MILLISECONDS

Figure 55

PANCAKE MOTOR-4

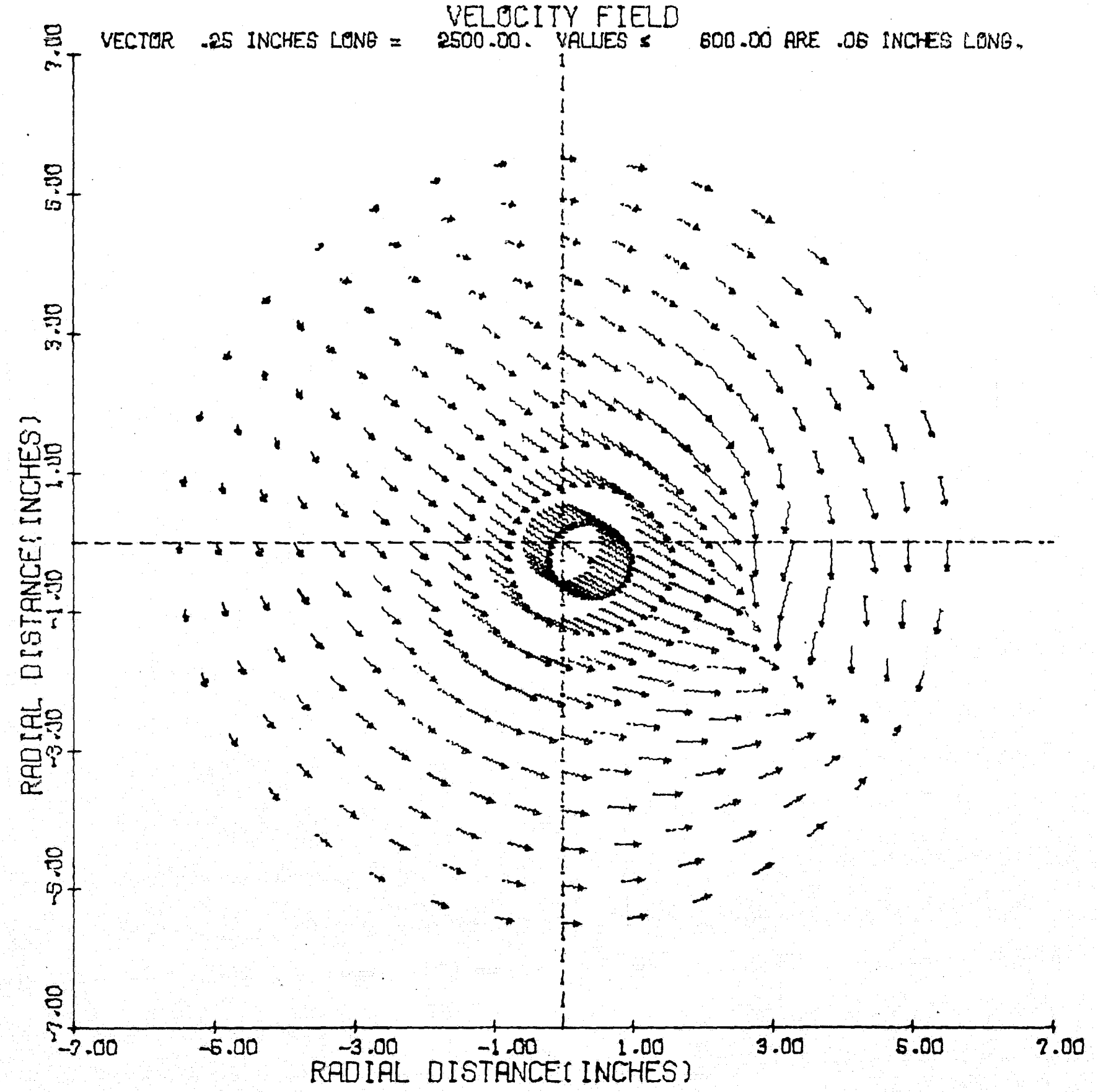

T= .163 MILLISECONDS

Figure 56

PANCAKE MOTOR-4

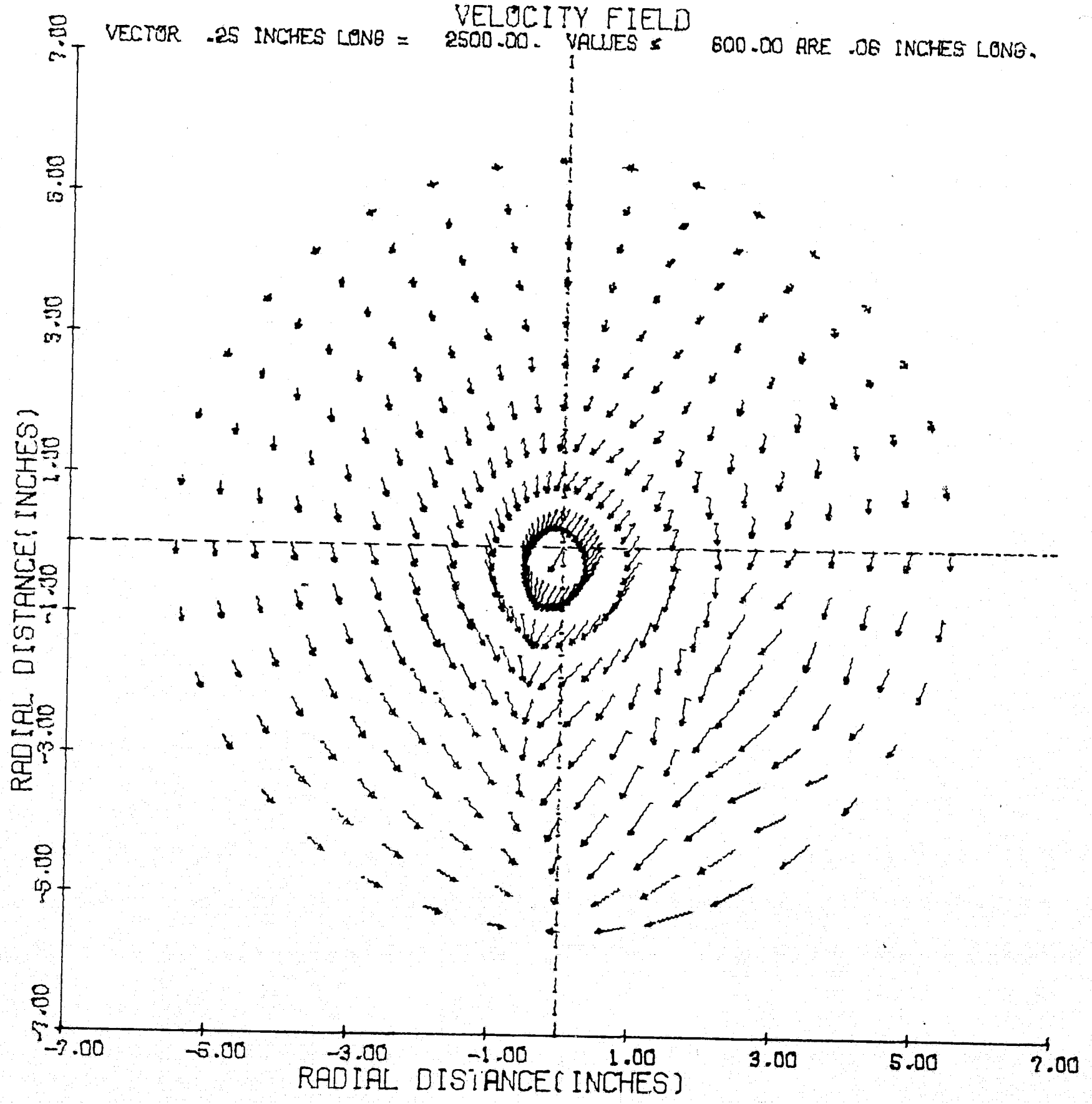

T= .245 MILLISECONDS

Figure 57

PANCAKE MOTOR-4

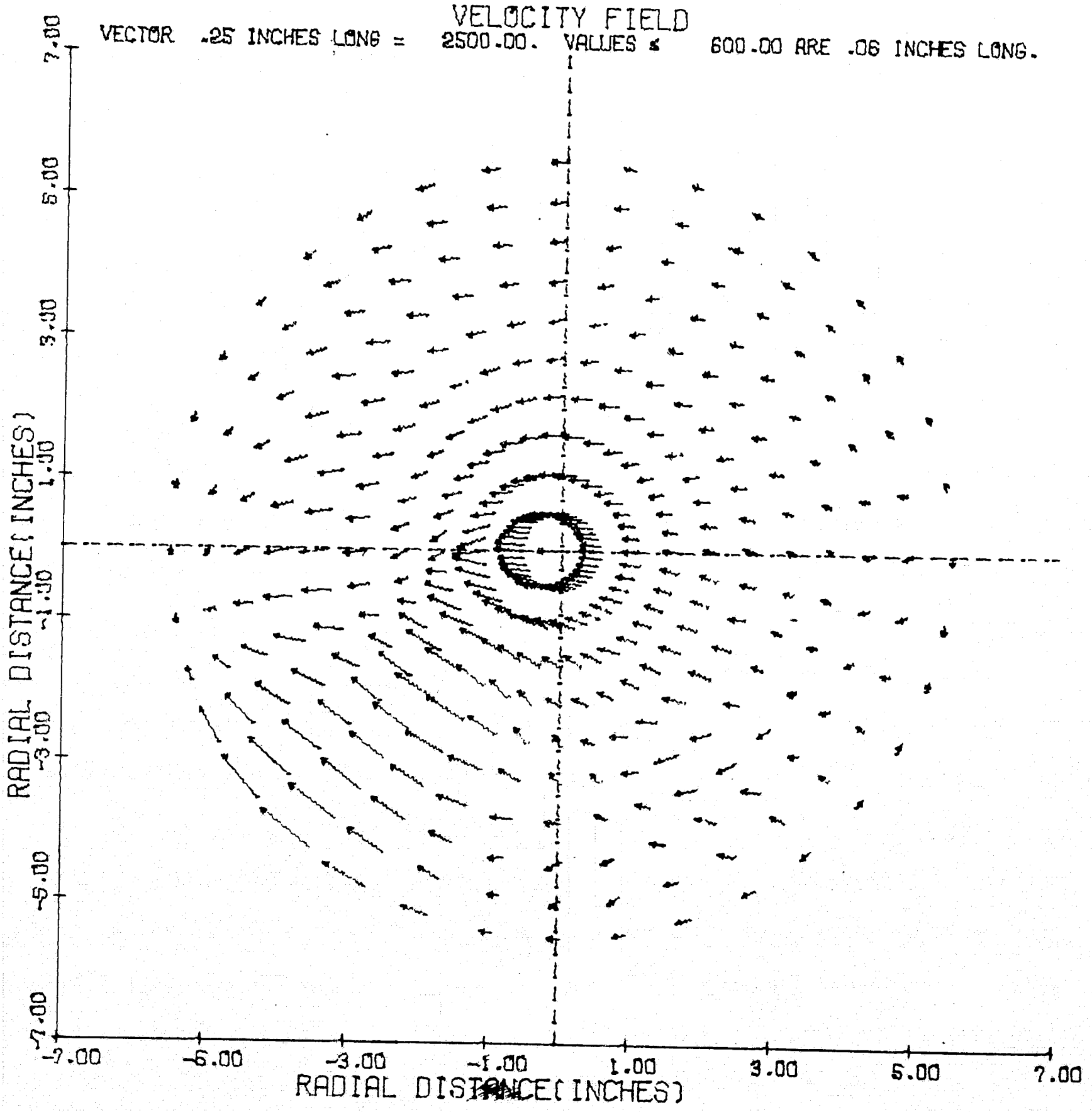

T= .334 MILLISECONDS

Figure 58

PANCAKE MOTOR-4

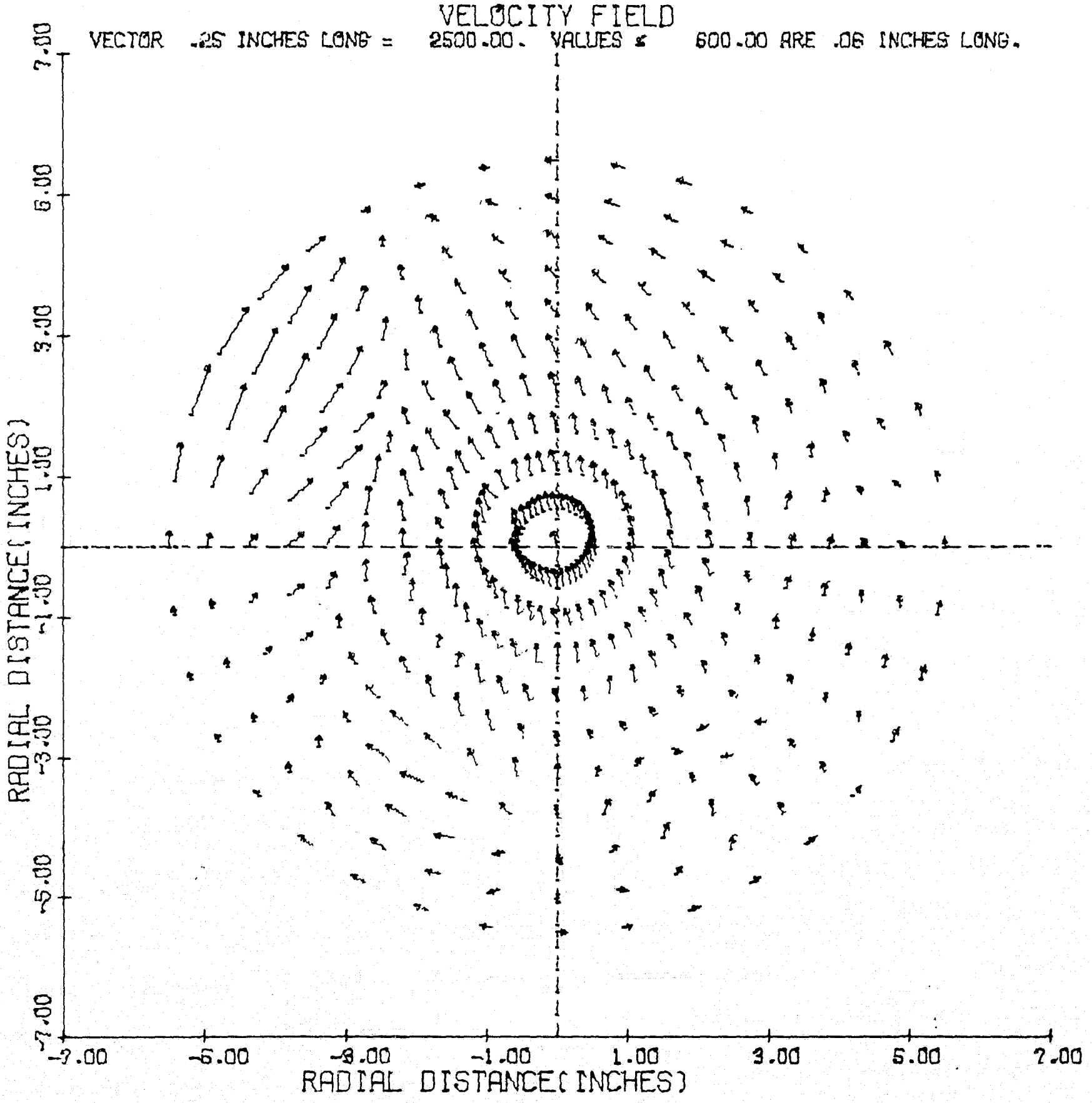

T= .423 MILLISECONDS

Figure 59

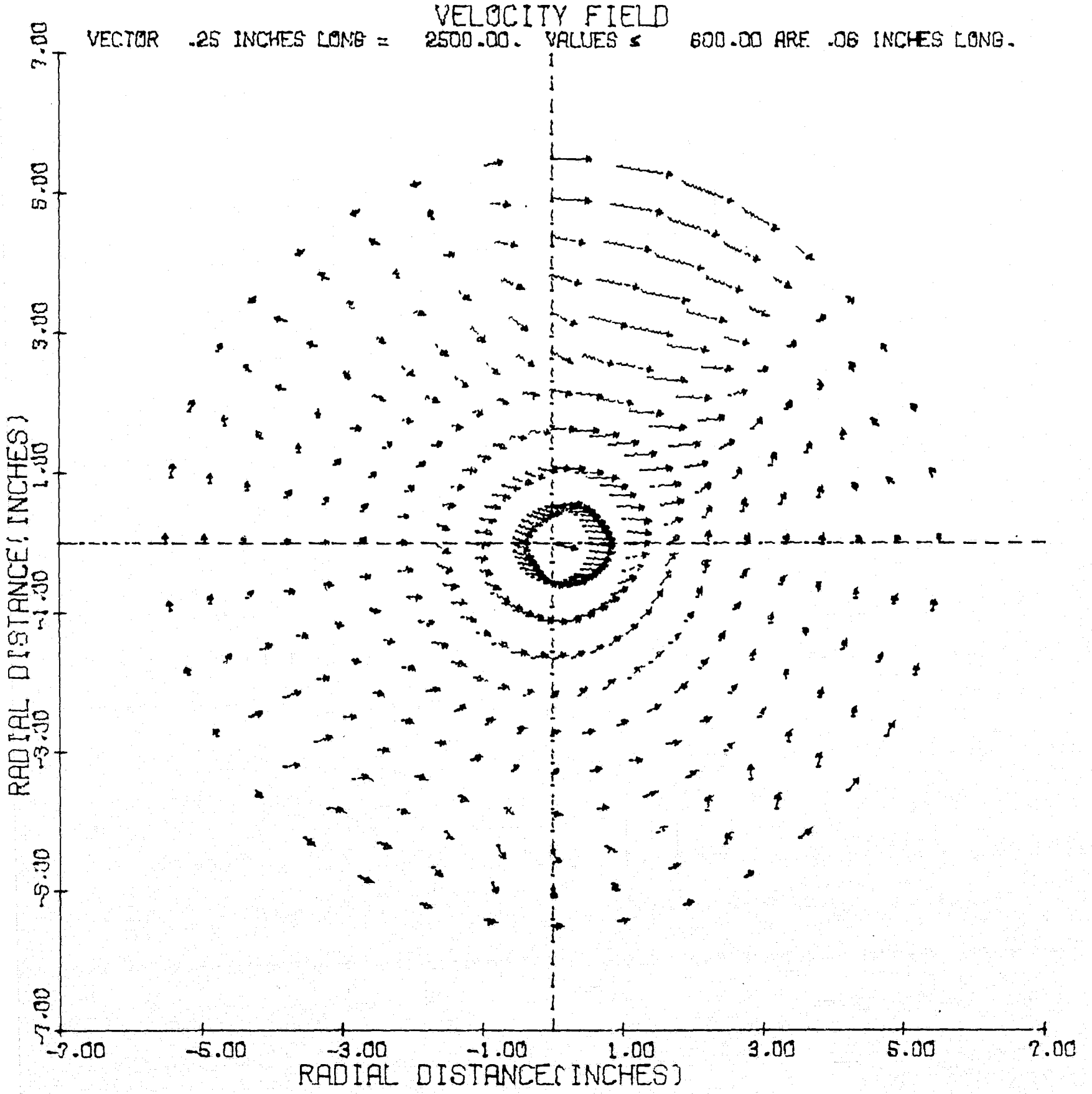
PANCAKE MOTOR-4
VELOCITY FIELD
VECTOR .25 INCHES LONG = 2500.00. VALUES ≤ 600.00 ARE .06 INCHES LONG.
RADIAL DISTANCE(INCHES)
7.00
5.00
3.00
1.00
-1.00
-3.00
-5.00
-7.00
-7.00
-5.00
-3.00
-1.00
1.00
3.00
5.00
7.00
RADIAL DISTANCE(INCHES)
T= .517 MILLISECONDS

Figure 60

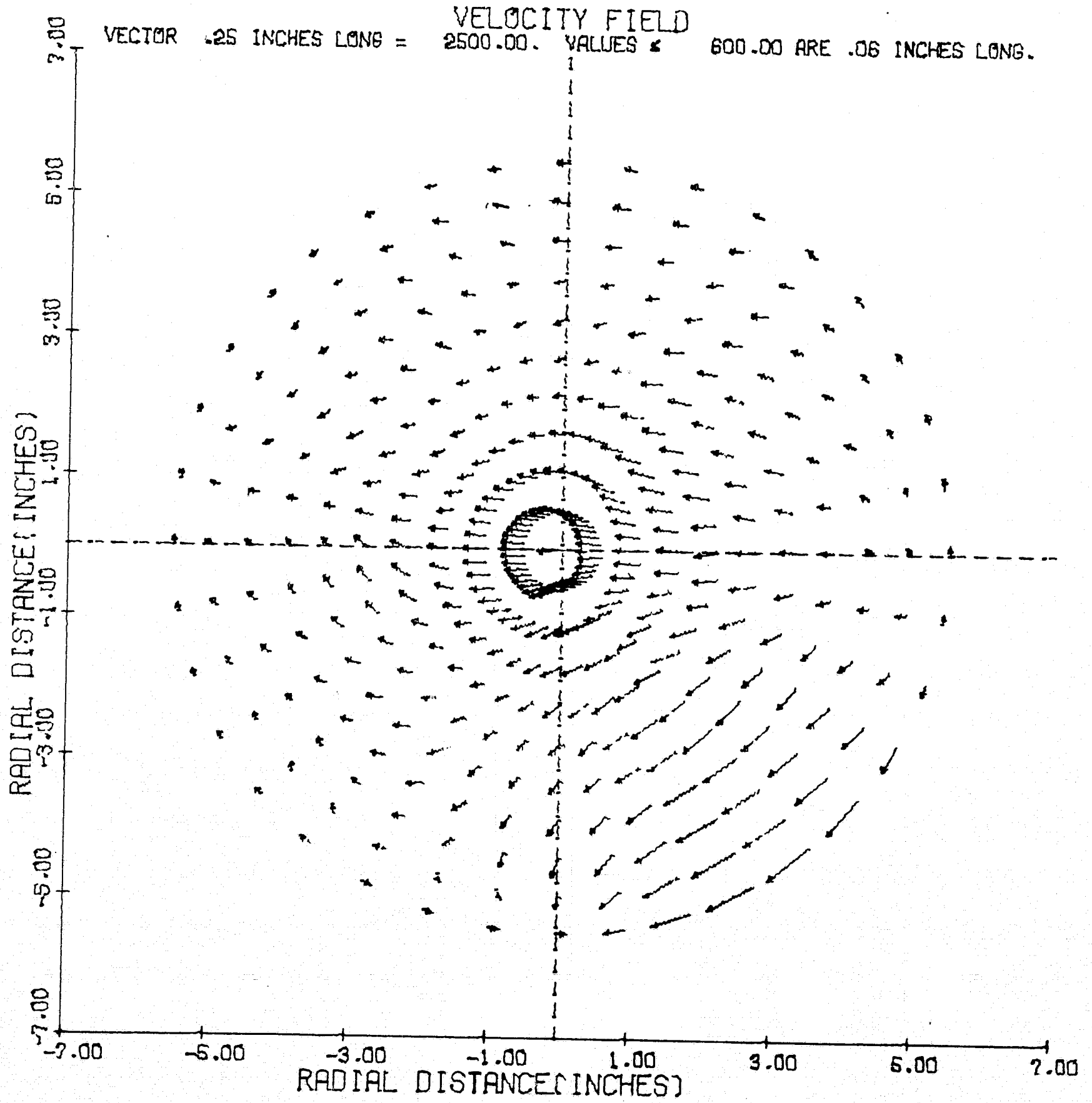
PANCAKE MOTOR-4
VELOCITY FIELD
VECTOR .25 INCHES LONG = 2500.00. VALUES ≤ 600.00 ARE .06 INCHES LONG.
RADIAL DISTANCE(INCHES)
3.00
1.00
-1.00
-3.00
-5.00
-7.00
RADIAL DISTANCE(INCHES)
-7.00
-5.00
-3.00
-1.00
1.00
3.00
5.00
7.00
T= 1.087 MILLISECONDS

Figure 61

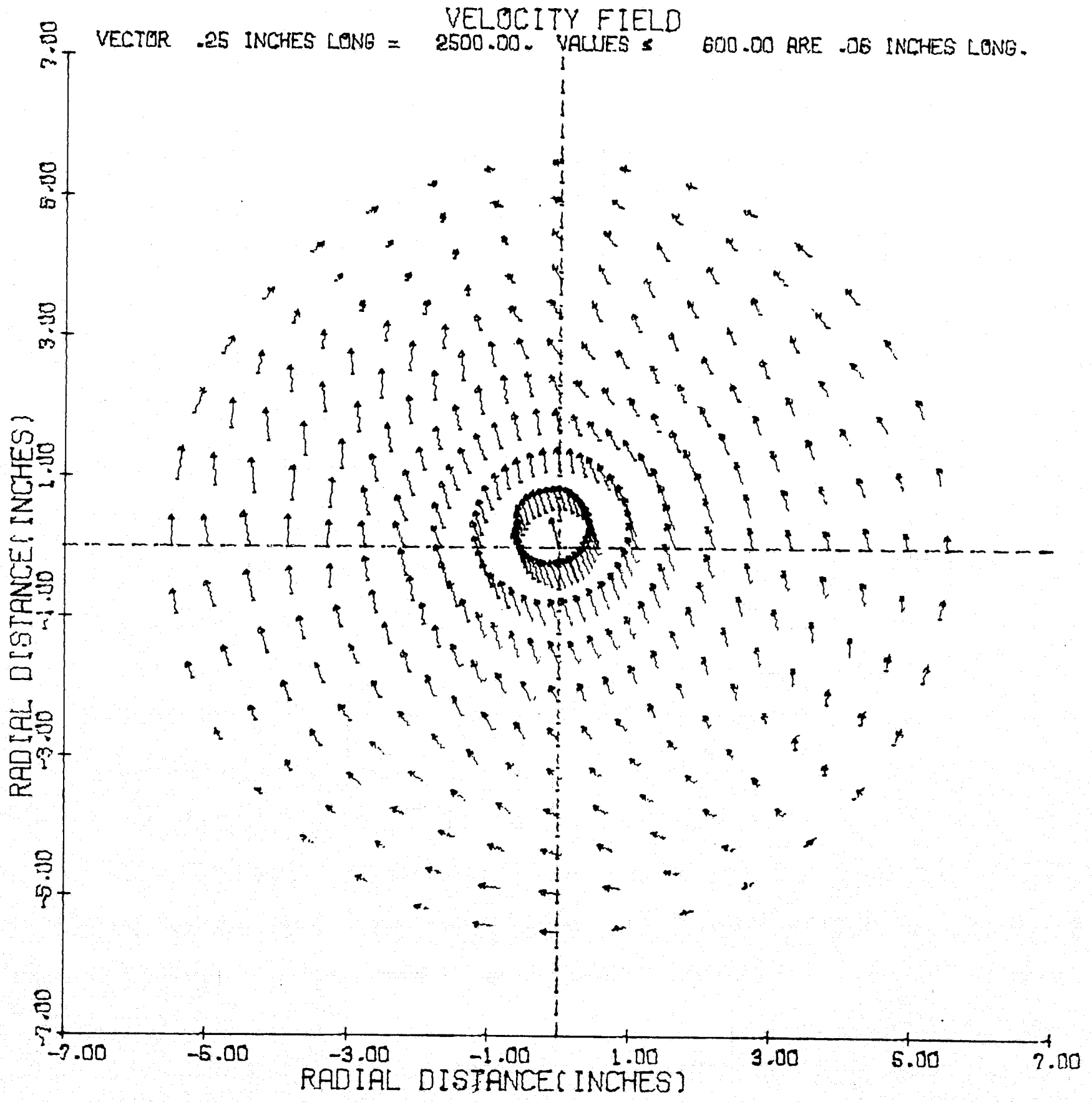
PANCAKE MOTOR-4
VELOCITY FIELD
VECTOR .25 INCHES LONG = 2500.00. VALUES ≤ 600.00 ARE .06 INCHES LONG.
RADIAL DISTANCE(INCHES)
7.00
5.00
3.00
1.00
-1.00
-3.00
-5.00
-7.00
-7.00
-5.00
-3.00
-1.00
1.00
3.00
5.00
7.00
RADIAL DISTANCE(INCHES)
T= 1.611 MILLISECONDS

Figure 62

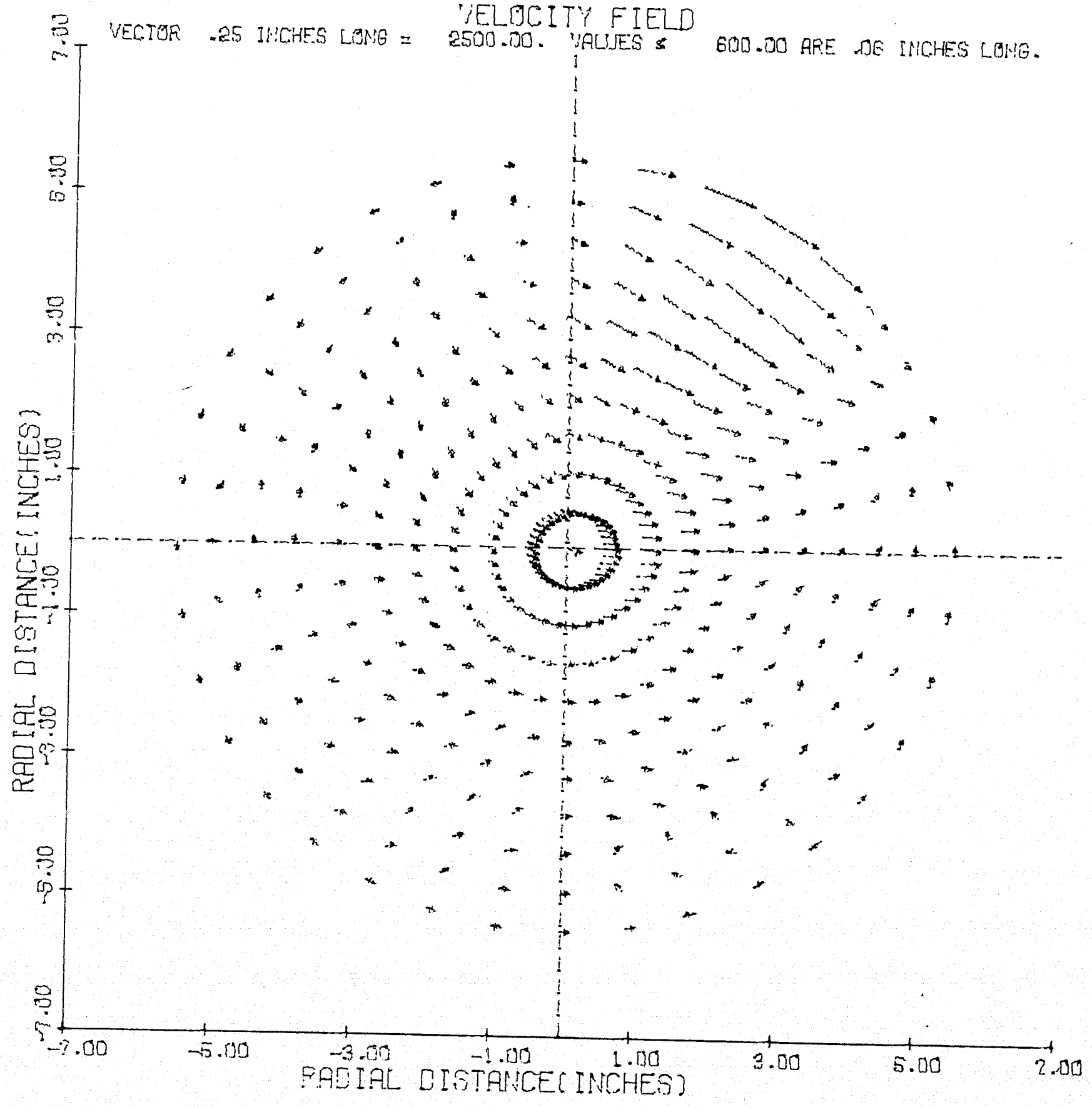
PANCAKE MOTOR-4
VELOCITY FIELD
VECTOR .25 INCHES LONG = 2500.00. VALUES ≤ 600.00 ARE .06 INCHES LONG.
RADIAL DISTANCE(INCHES)
7.00
5.00
3.00
1.00
-1.00
-3.00
-5.00
-7.00
-7.00
-5.00
-3.00
-1.00
1.00
3.00
5.00
7.00
RADIAL DISTANCE(INCHES)
T= 2.168 MILLISECONDS

Figure 63

PANCAKE MOTOR-4

PRESSURE AT RADIAL DISTANCE OF 5.50 INCHES

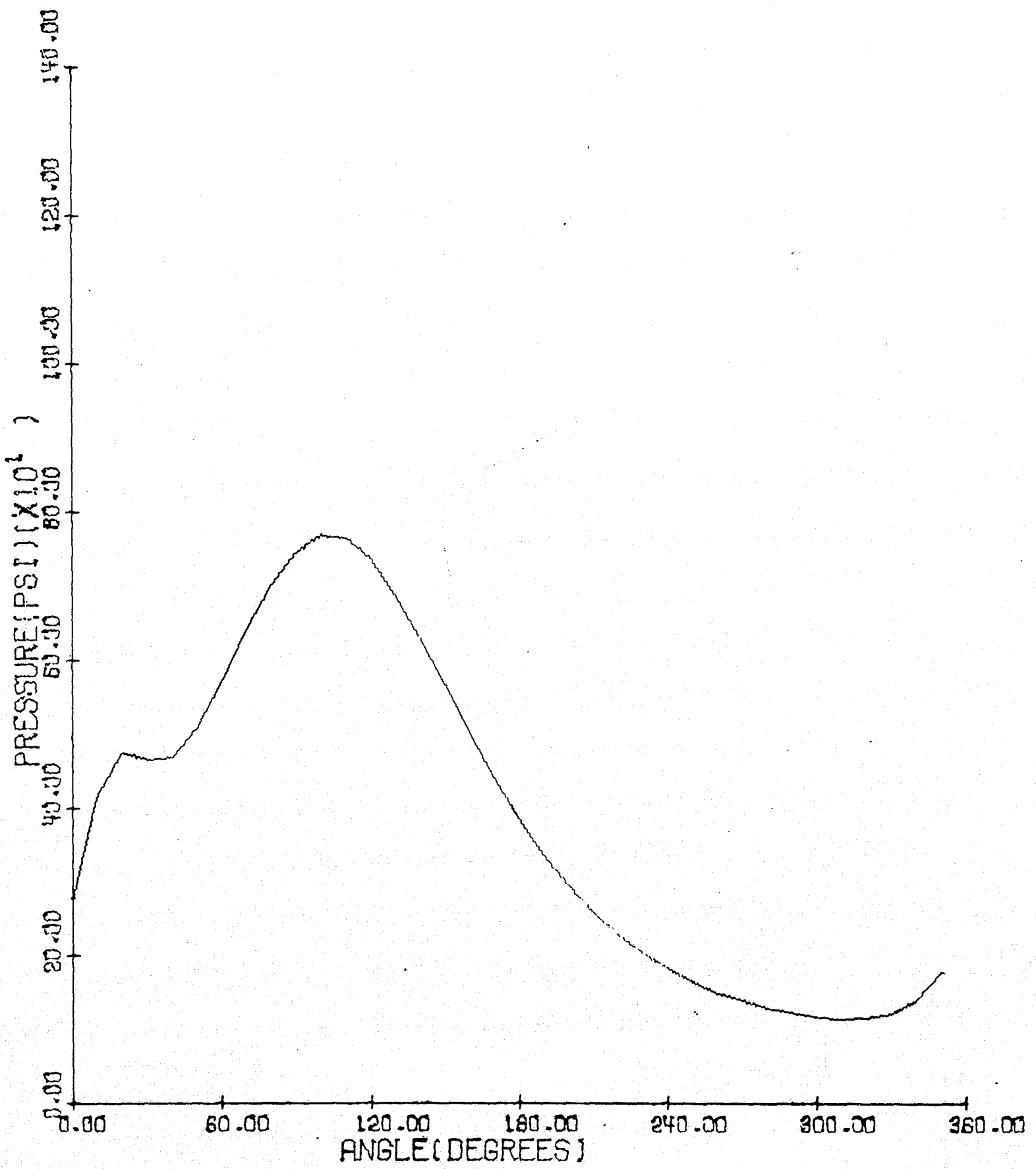

T= .082 MILLISECONDS

Figure 64

PANCAKE MOTOR-4

PRESSURE AT RADIAL DISTANCE OF 5.50 INCHES

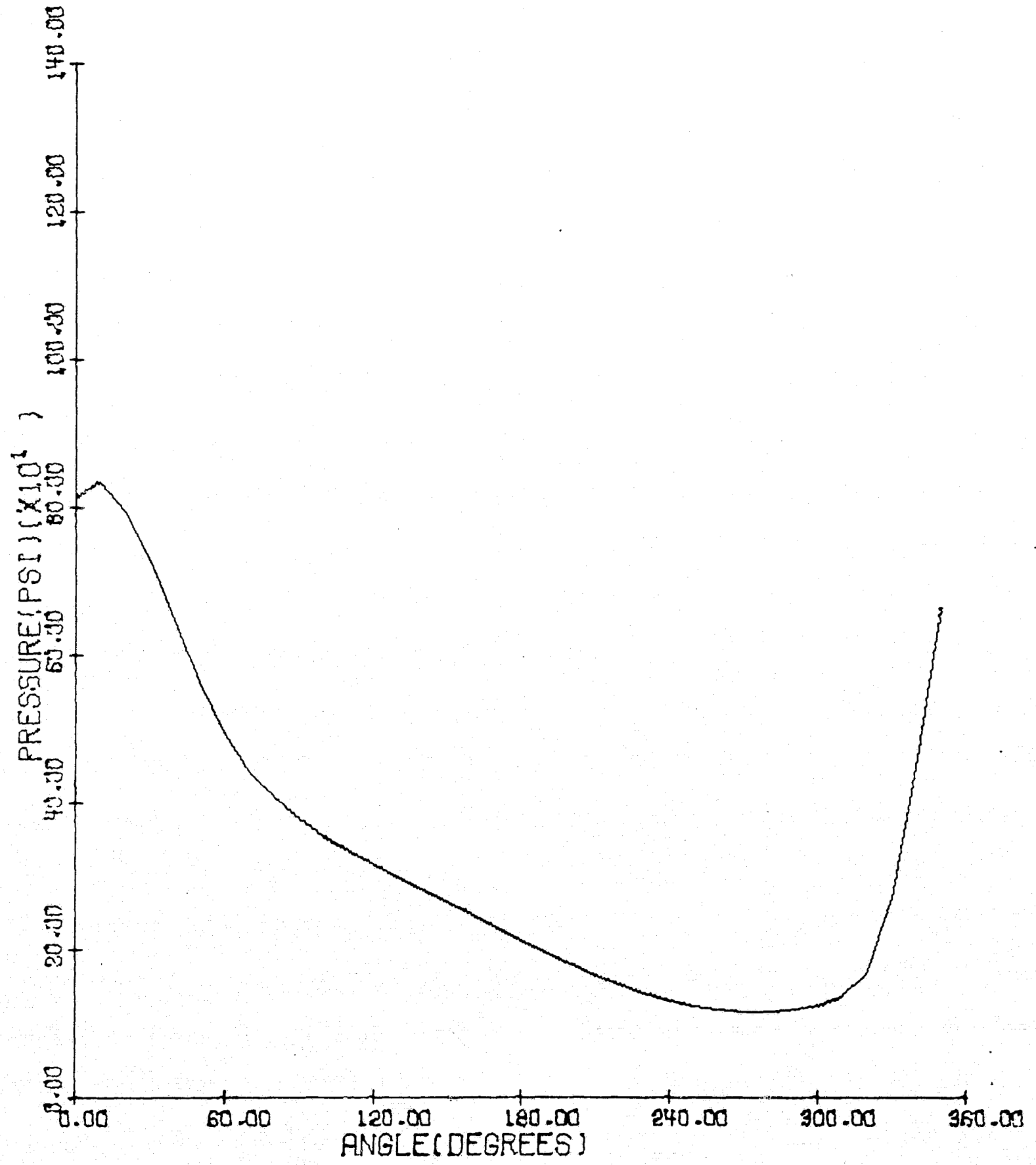

T= .163 MILLISECONDS

Figure 65

PANCAKE MOTOR-4

PRESSURE AT RADIAL DISTANCE OF 5.50 INCHES

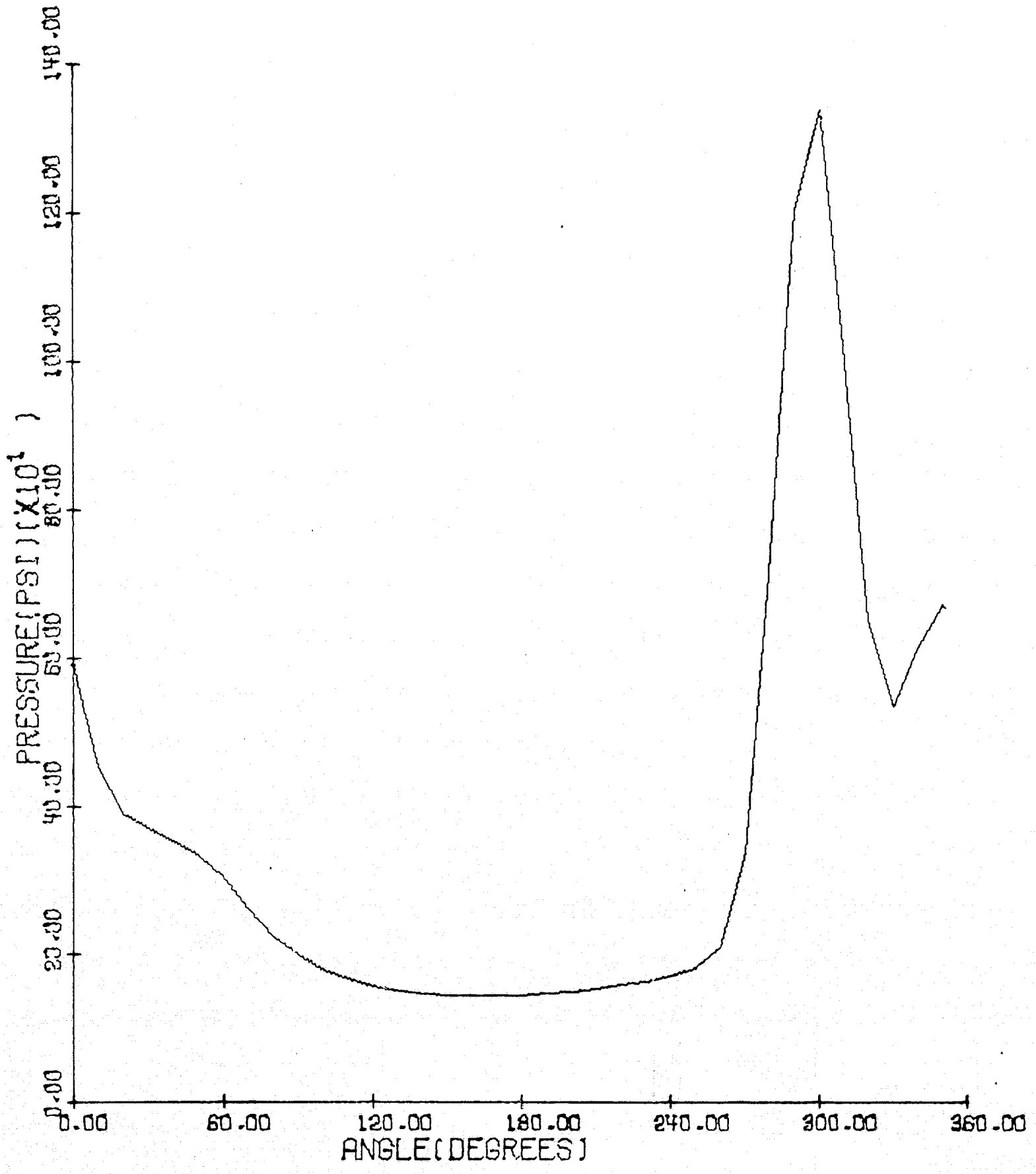

T= .245 MILLISECONDS

Figure 66

PANCAKE MOTOR-4

PRESSURE AT RADIAL DISTANCE OF 5.50 INCHES

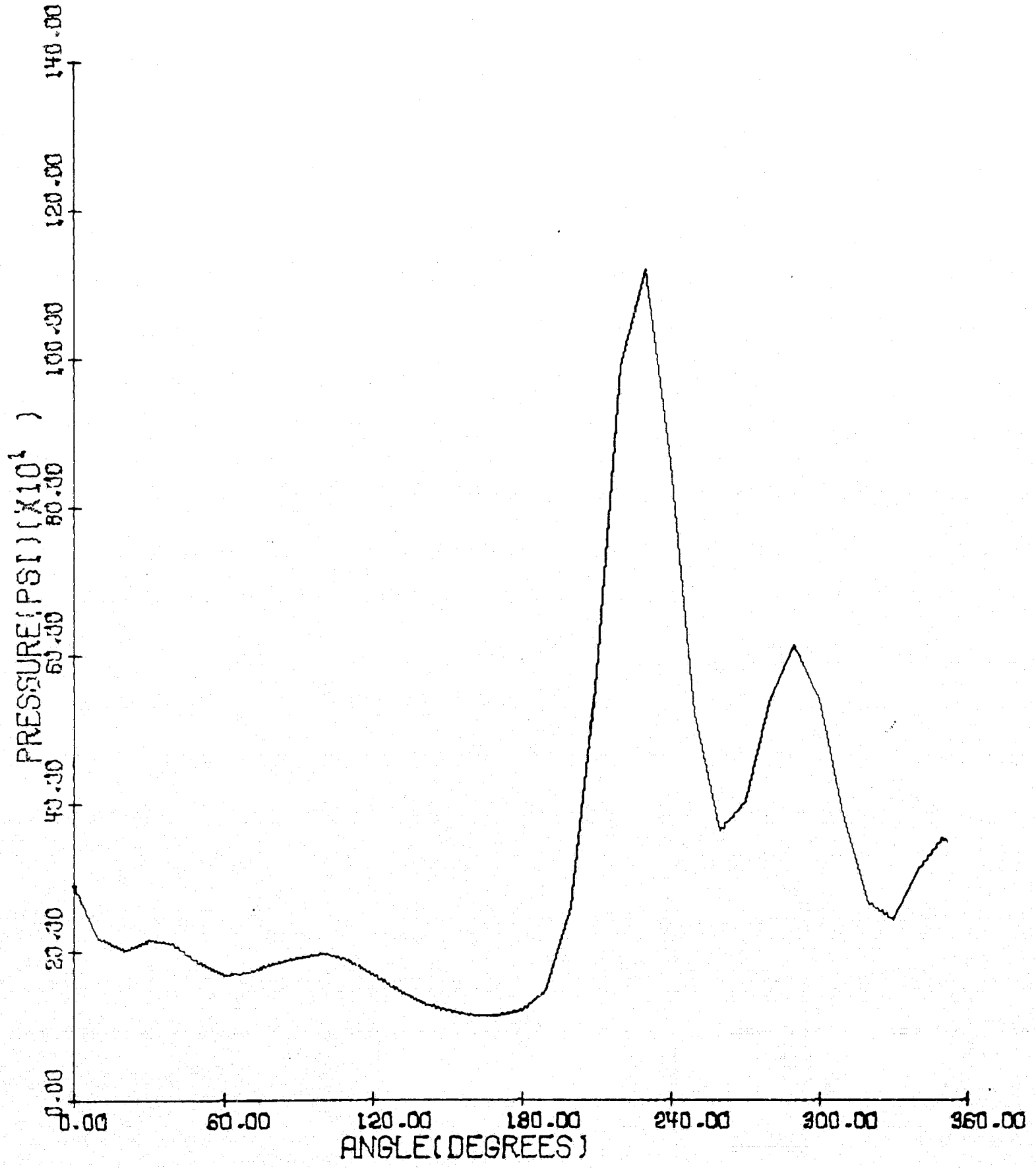

T= .334 MILLISECONDS

Figure 67

PANCAKE MOTOR-4

PRESSURE AT RADIAL DISTANCE OF 5.50 INCHES

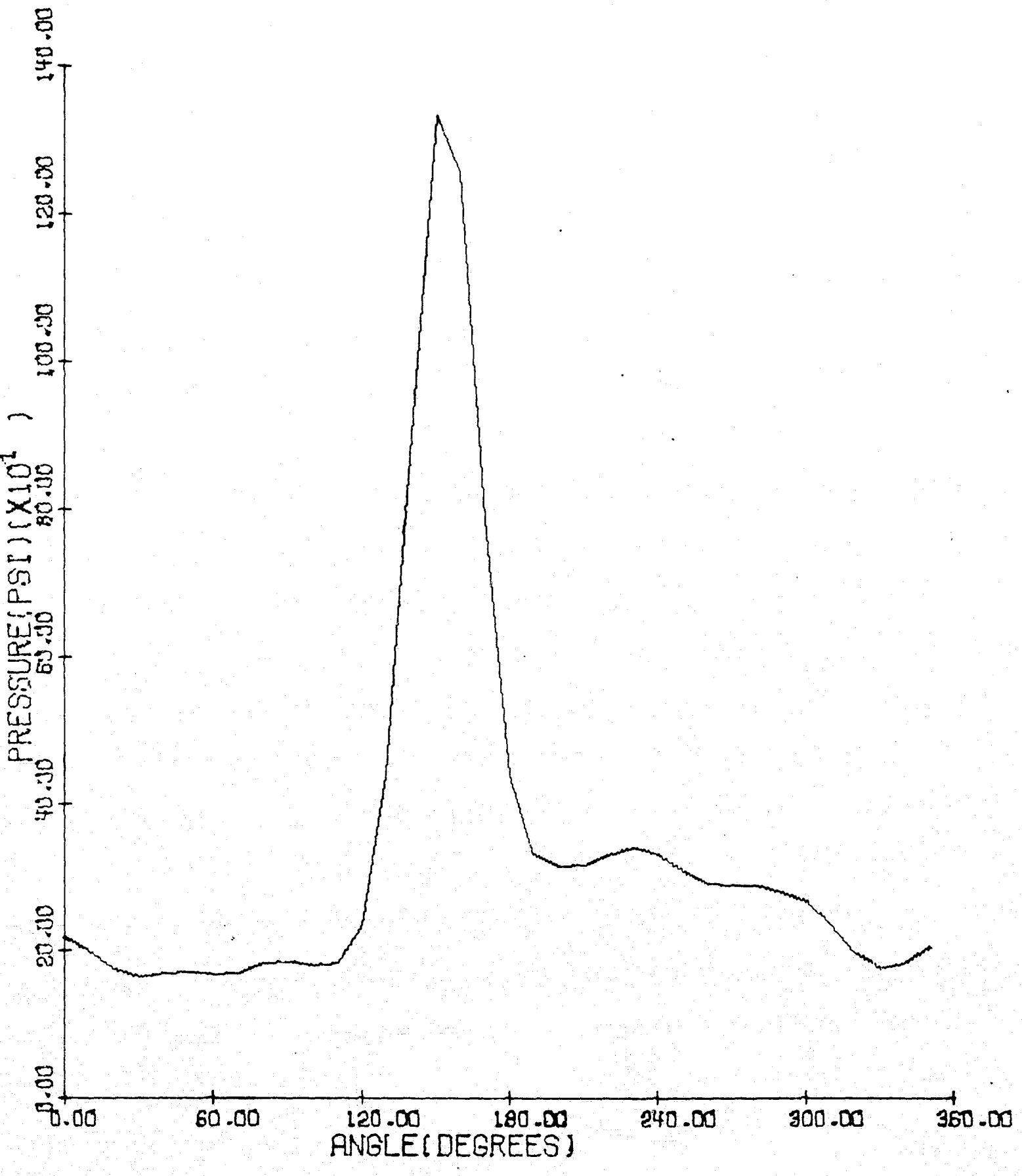

T= .423 MILLISECONDS

Figure 68

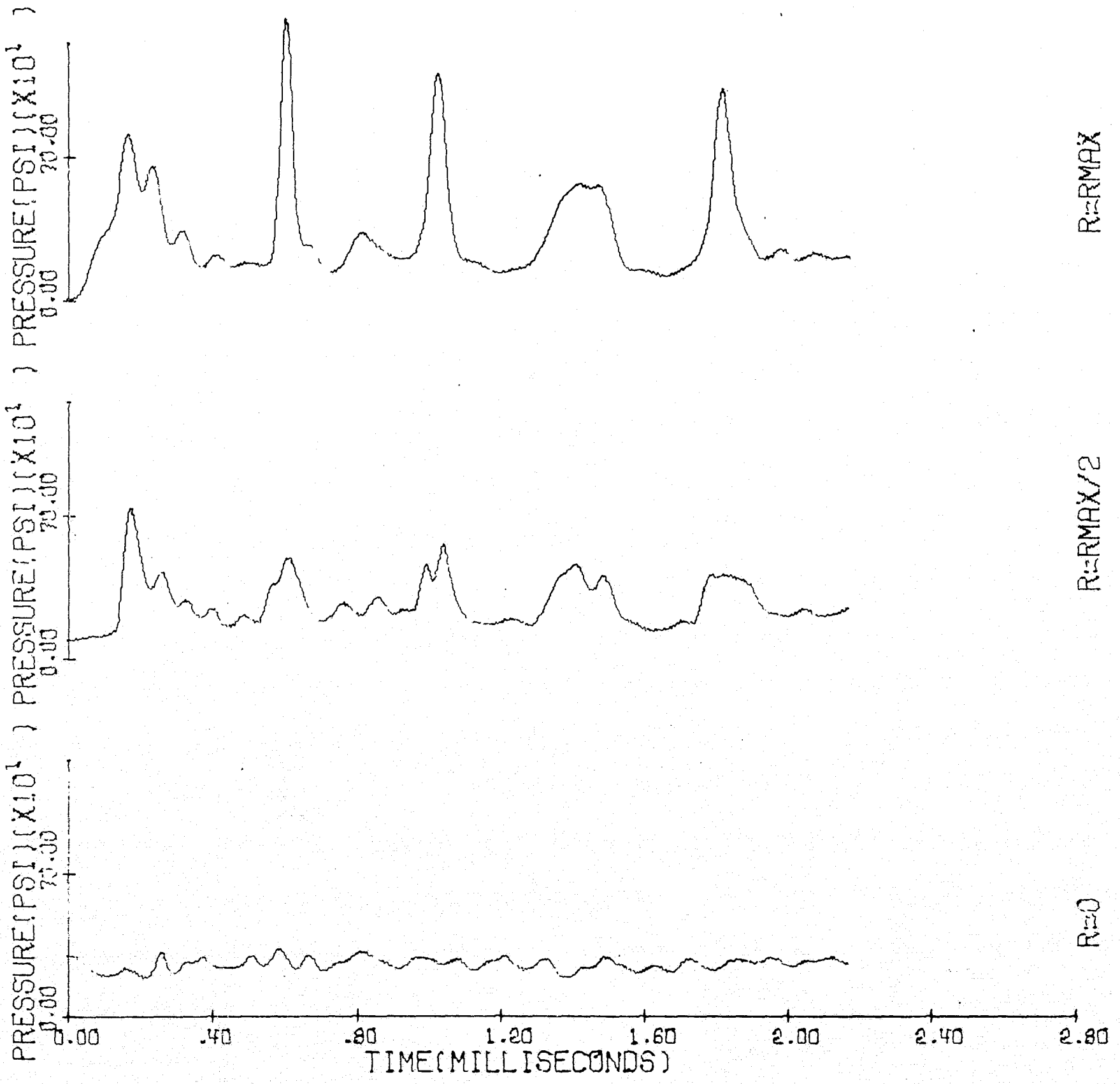
PANCAKE MOTOR-4
PRESSURE(PSI)(X10¹)
0.00
20.00
R=RMAX
PRESSURE(PSI)(X10¹)
0.00
20.00
R=RMAX/2
PRESSURE(PSI)(X10¹)
0.00
20.00
R=0
0.00
.40
.80
1.20
1.60
2.00
2.40
2.80
TIME(MILLISECONDS)

Figure 69

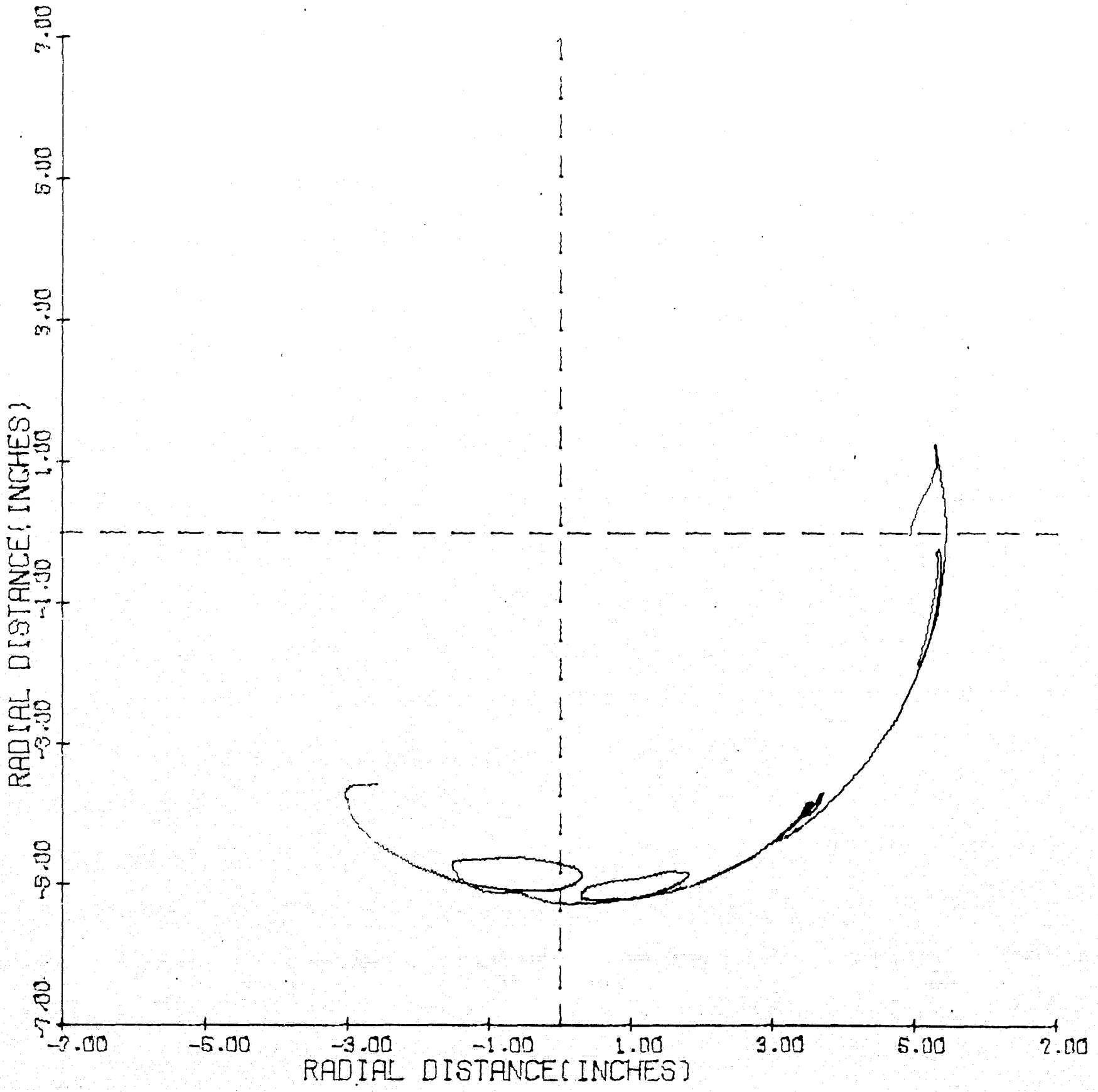
PANCAKE MOTOR-4
STREAKLINE
RADIAL DISTANCE(INCHES)
7.00
5.00
3.00
1.00
-1.00
-3.00
-5.00
-7.00
-7.00
-5.00
-3.00
-1.00
1.00
3.00
5.00
7.00
RADIAL DISTANCE(INCHES)
T= 2.168 MILLISECONDS

Figure 70

PANCAKE MOTOR-5

PRESSURE ISOBARS

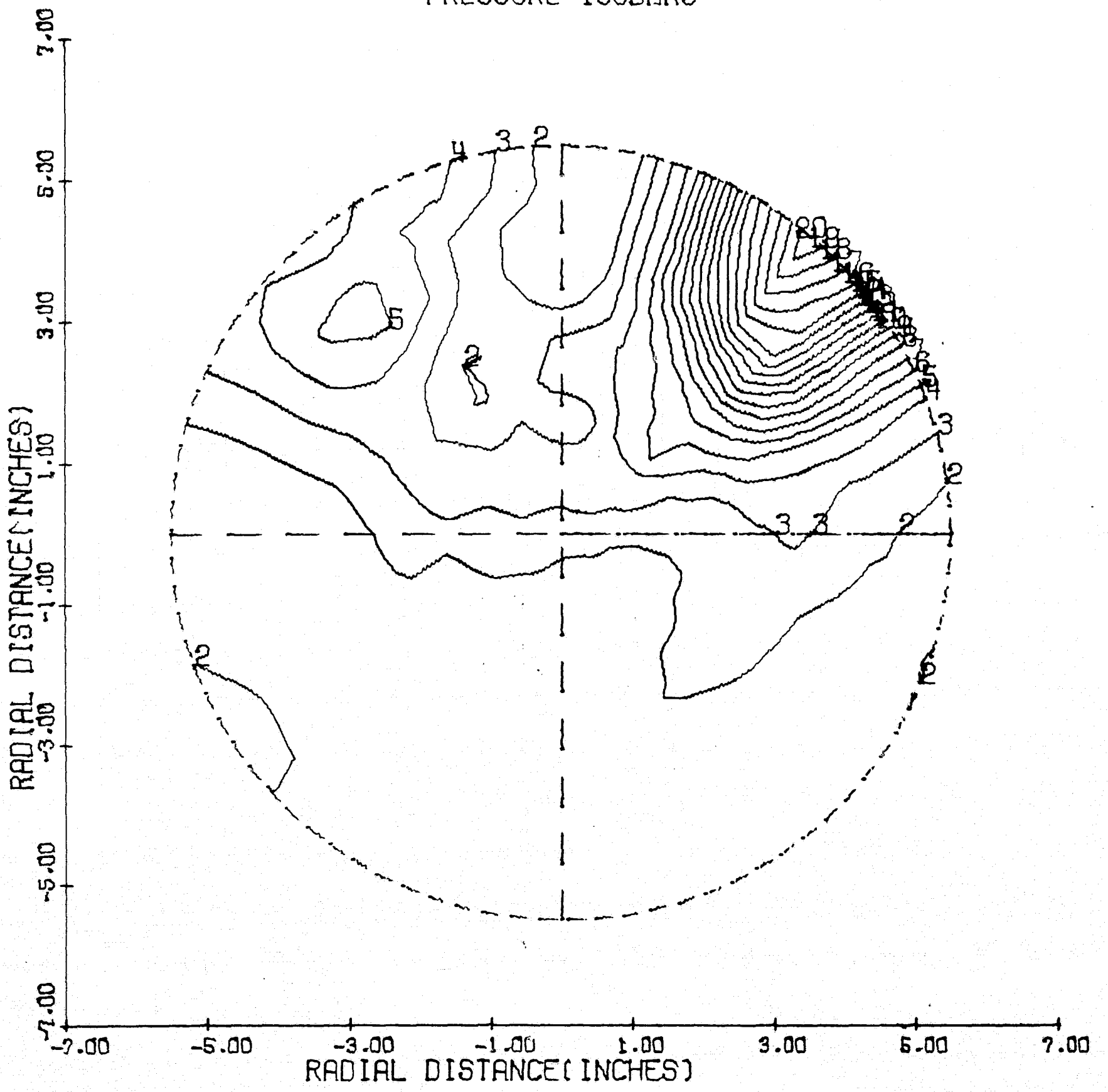

T= .447 MILLISECONDS

Figure 71

PANCAKE MOTOR-5

T= .447 MILLISECONDS

ISOBAR	PRESSURE(PSI)
1	677.406
2	867.490
3	1057.574
4	1247.658
5	1437.743
6	1627.827
7	1817.911
8	2007.995
9	2198.079
10	2388.163
11	2578.247
12	2768.331
13	2958.415
14	3148.500
15	3338.584
16	3528.668
17	3718.752
18	3908.836
19	4098.920
20	4289.004

PANCAKE MOTOR-5

PREF=REFERENCE PRESSURE = 300.00 PSI
AREF=REFERENCE SOUND SPEED= 3498.5 FT/SEC
R =CHAMBER RADIUS = .45830 FEET
TREF=REFERENCE TIME=R/AREF=.0001310 SEC

T/TREF= 3.40925

ISOBAR	PRESSURE/PREF
1	2.258
2	2.892
3	3.525
4	4.159
5	4.792
6	5.426
7	6.060
8	6.693
9	7.327
10	7.961
11	8.594
12	9.228
13	9.861
14	10.495
15	11.129
16	11.762
17	12.396
18	13.029
19	13.663
20	14.297

PANCAKE MOTOR-5

PRESSURE ISOBARS

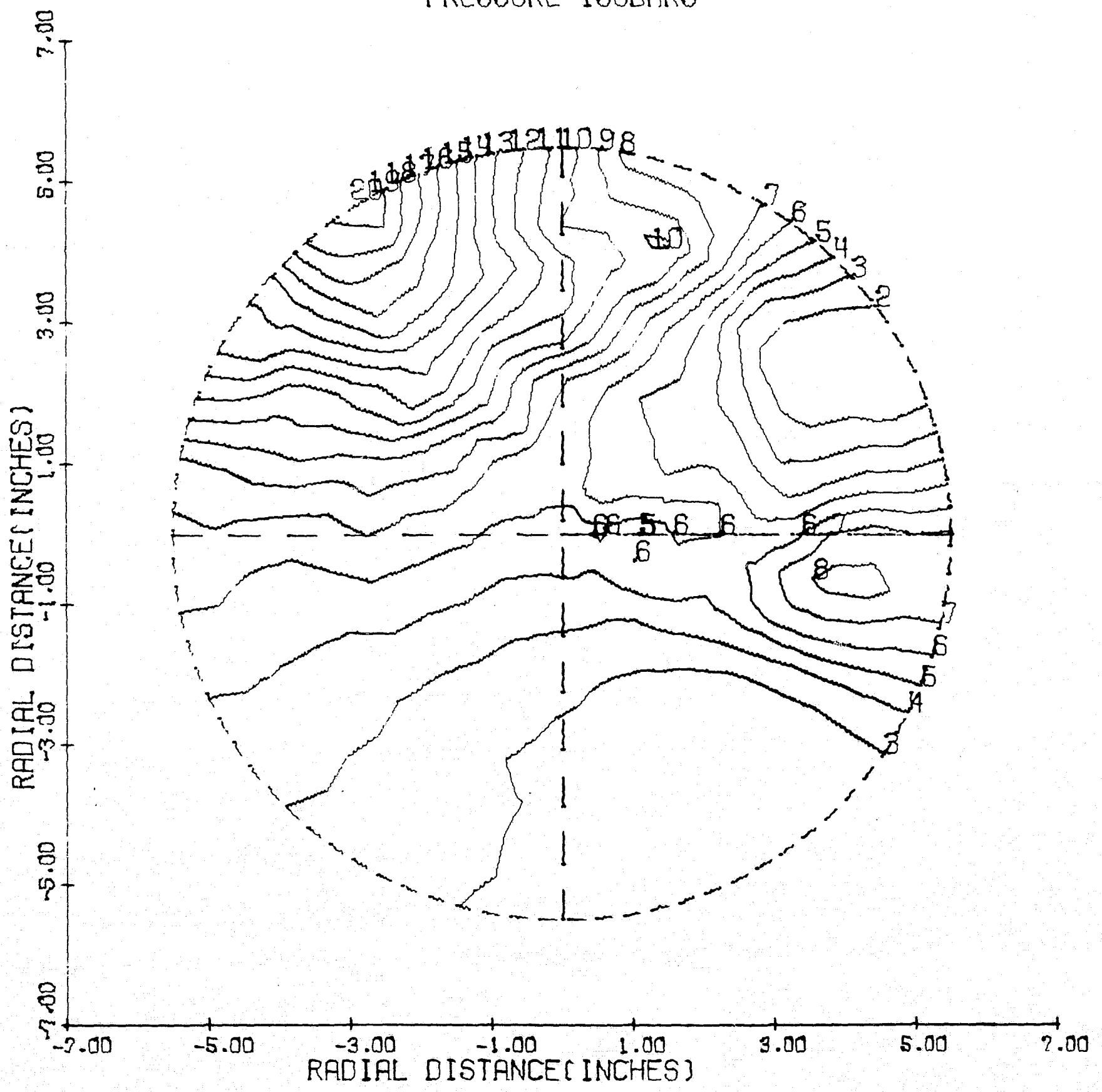

T= .583 MILLISECONDS

Figure 72

PANCAKE MOTOR-5

T= .583 MILLISECONDS

ISOBAR	PRESSURE(PSI)
1	1468.762
2	1808.382
3	2148.001
4	2487.620
5	2827.239
6	3166.858
7	3506.477
8	3846.096
9	4185.715
10	4525.334
11	4864.953
12	5204.573
13	5544.192
14	5883.811
15	6223.430
16	6563.049
17	6902.668
18	7242.287
19	7581.906
20	7921.525

PANCAKE MOTOR-5

PREF=REFERENCE PRESSURE = 300.00 PSI
AREF=REFERENCE SOUND SPEED= 3498.5 FT/SEC
R =CHAMBER RADIUS = .45830 FEET
TREF=REFERENCE TIME=R/AREF=.0001310 SEC

T/TREF= 4.44888

ISOBAR	PRESSURE/PREF
1	4.896
2	6.028
3	7.160
4	8.292
5	9.424
6	10.556
7	11.688
8	12.820
9	13.952
10	15.084
11	16.217
12	17.349
13	18.481
14	19.613
15	20.745
16	21.877
17	23.009
18	24.141
19	25.273
20	26.405

PANCAKE MOTOR-5

PRESSURE ISOBARS

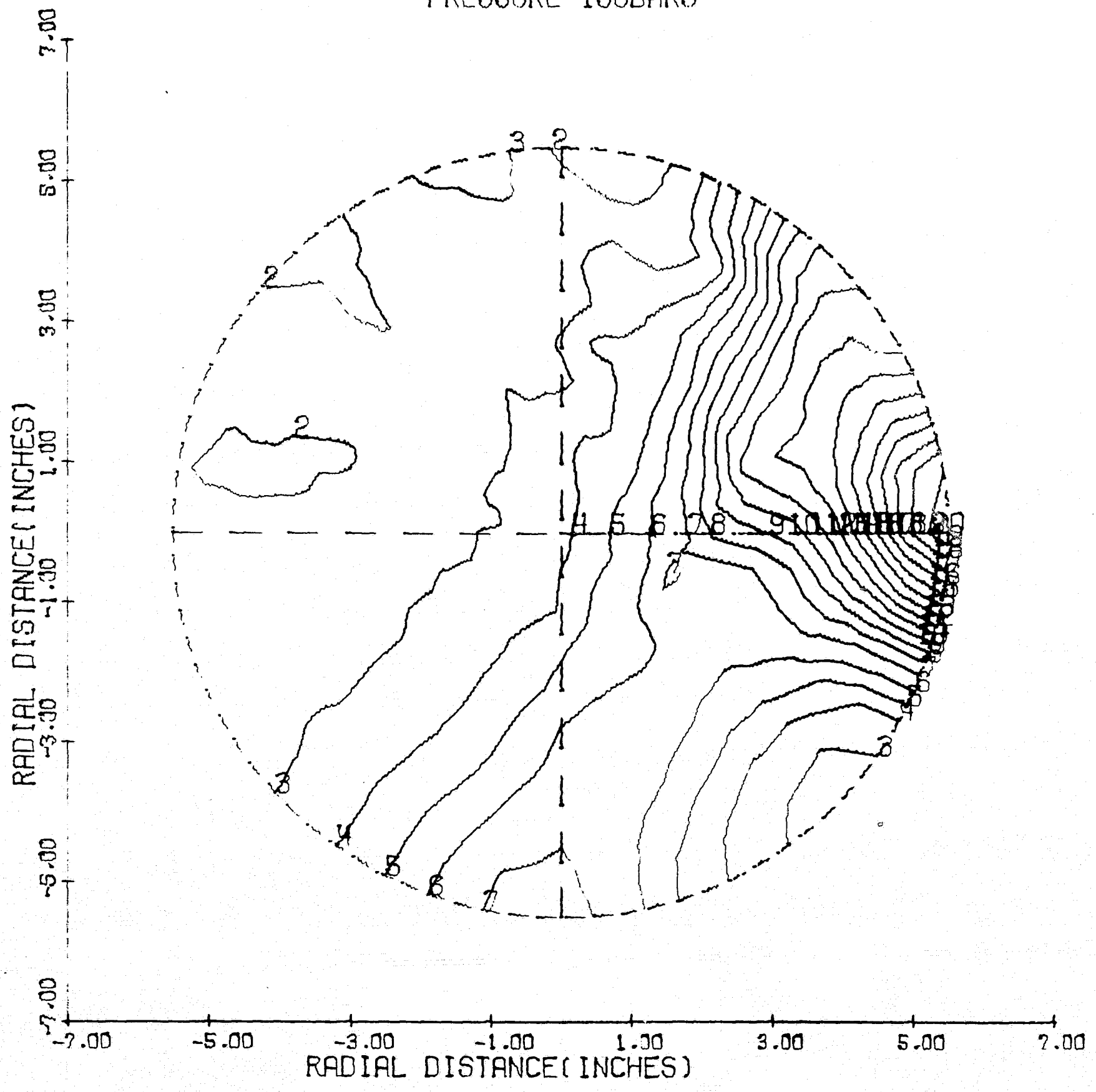

T= .625 MILLISECONDS

Figure 73

PANCAKE MOTOR-5

T= .625 MILLISECONDS

ISOBAR	PRESSURE(PSI)
1	2626.082
2	3165.320
3	3704.558
4	4243.796
5	4783.034
6	5322.272
7	5861.510
8	6400.748
9	6939.986
10	7479.224
11	8018.462
12	8557.700
13	9096.938
14	9636.176
15	10175.414
16	10714.652
17	11253.890
18	11793.128
19	12332.366
20	12871.604

PANCAKE MOTOR-5

PREF=REFERENCE PRESSURE = 300.00 PSI
AREF=REFERENCE SOUND SPEED= 3498.5 FT/SEC
R =CHAMBER RADIUS = .45830 FEET
TREF=REFERENCE TIME=R/AREF=.0001310 SEC

T/TREF= 4.77236

ISOBAR	PRESSURE/PREF
1	8.754
2	10.551
3	12.349
4	14.146
5	15.943
6	17.741
7	19.538
8	21.336
9	23.133
10	24.931
11	26.728
12	28.526
13	30.323
14	32.121
15	33.918
16	35.716
17	37.513
18	39.310
19	41.108
20	42.905

PANCAKE MOTOR-5

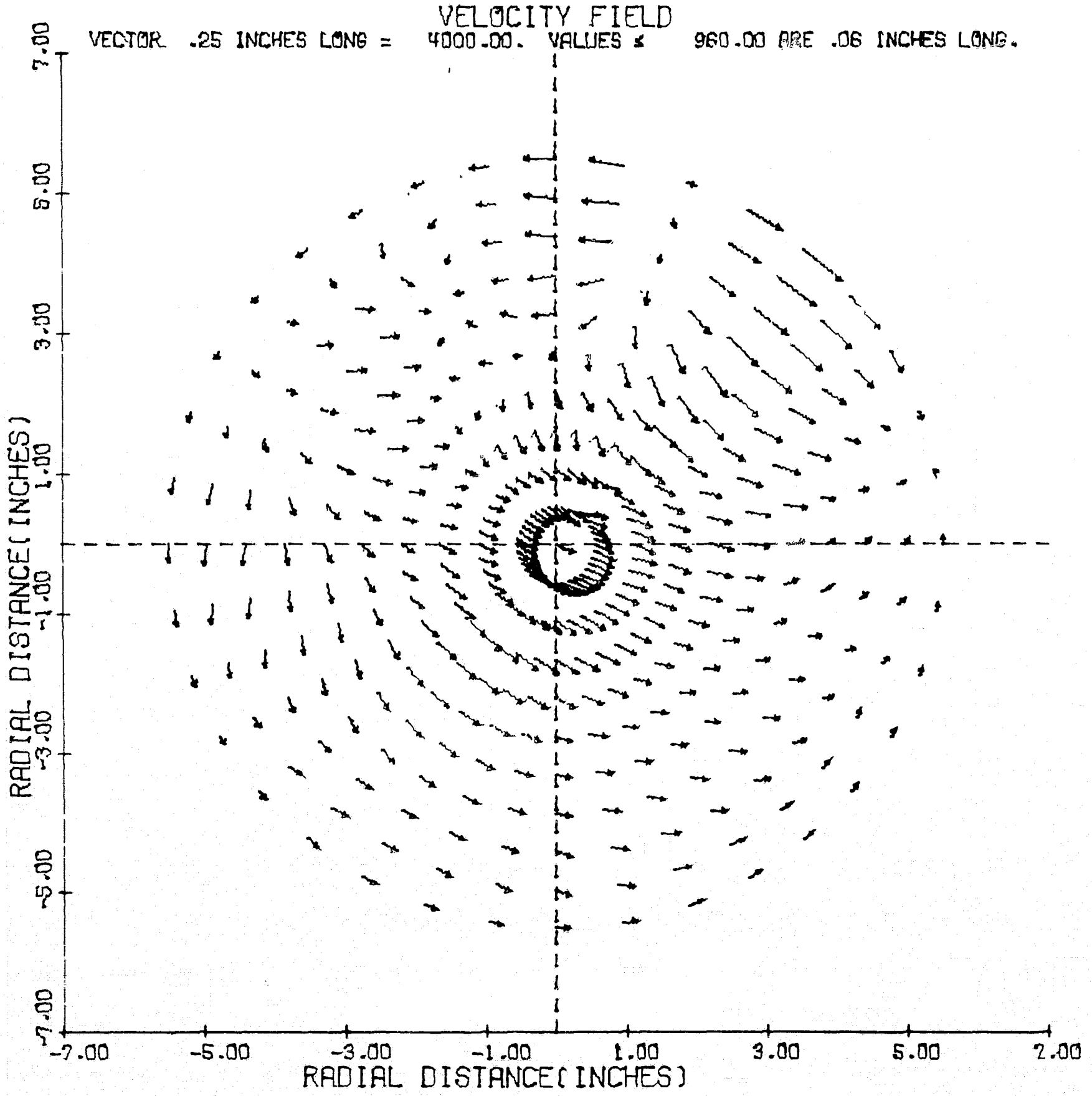

T= .447 MILLISECONDS

Figure 74

PANCAKE MOTOR-5

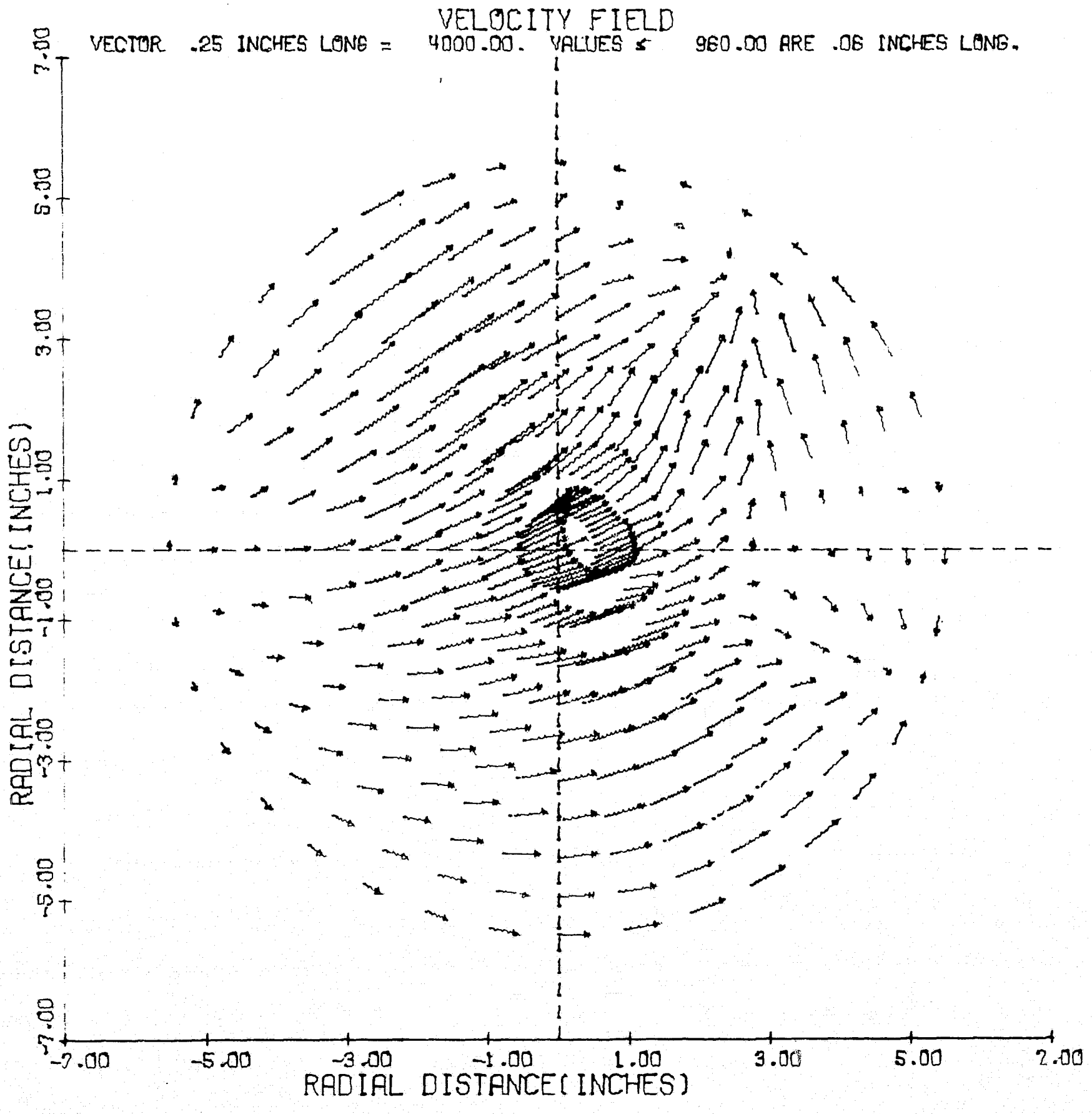

T= .583 MILLISECONDS

Figure 75

PANCAKE MOTOR-5

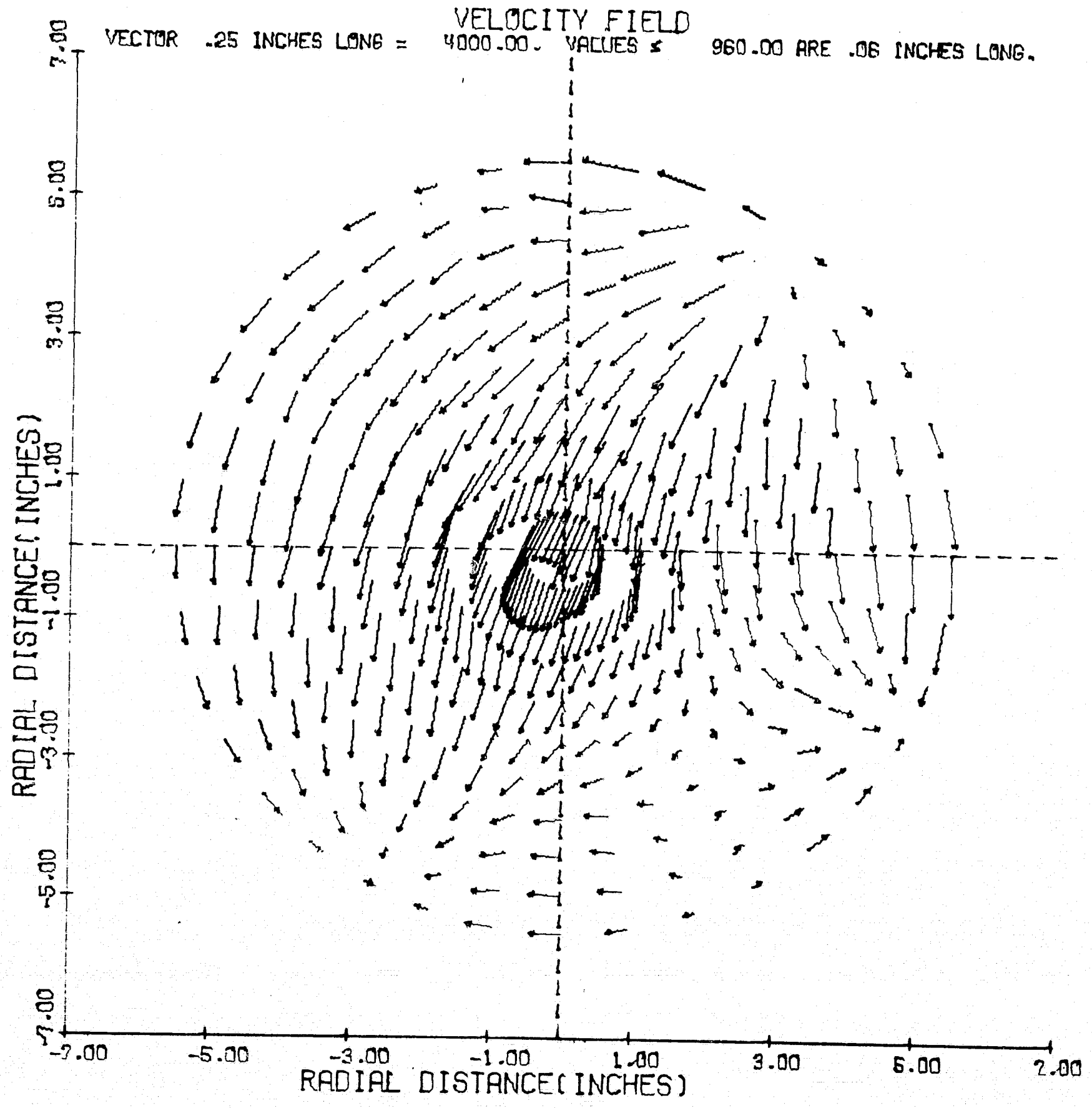

T= .625 MILLISECONDS

Figure 76

PANCAKE MOTOR-5

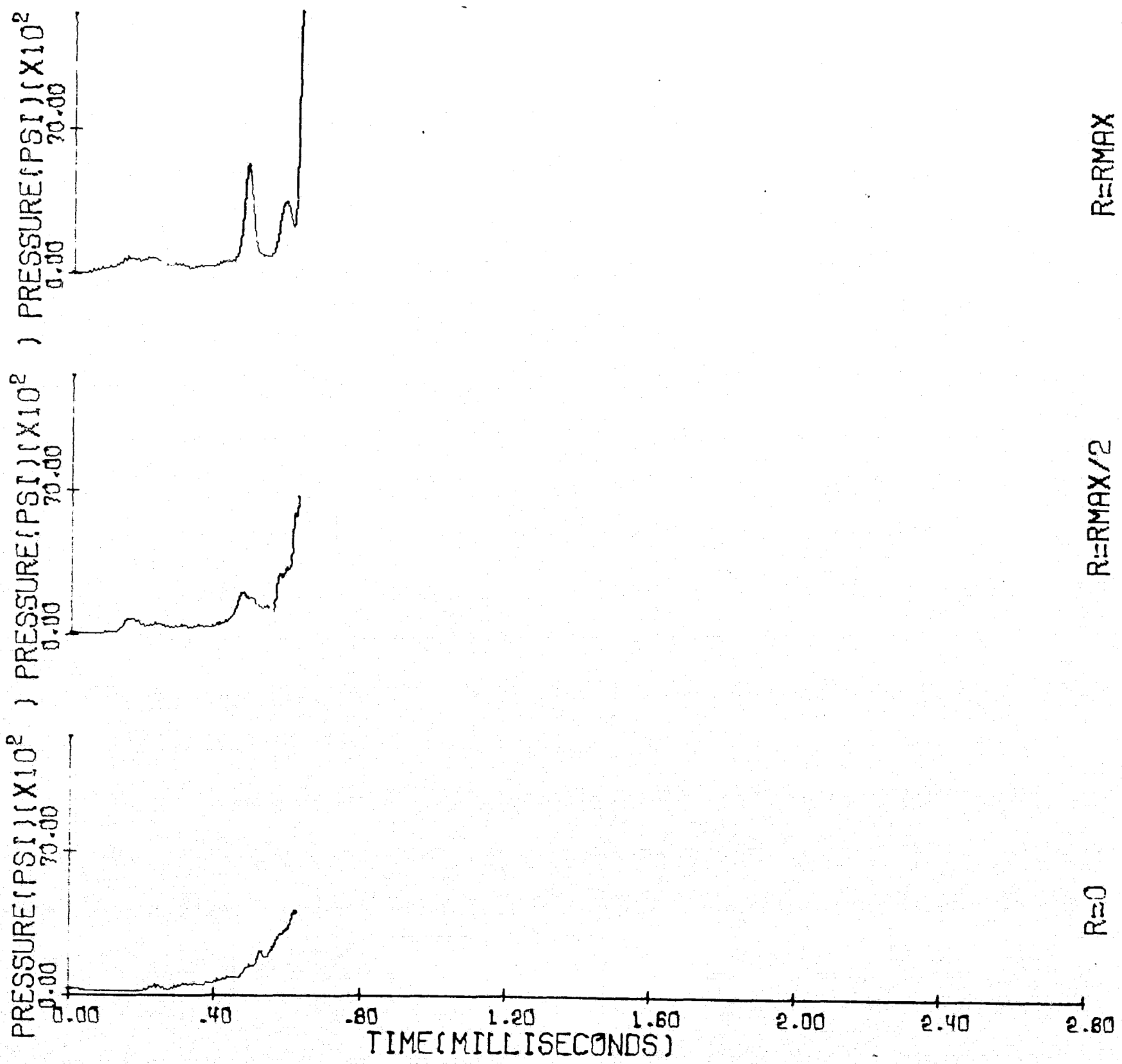

Figure 77

PANCAKE MOTOR-3

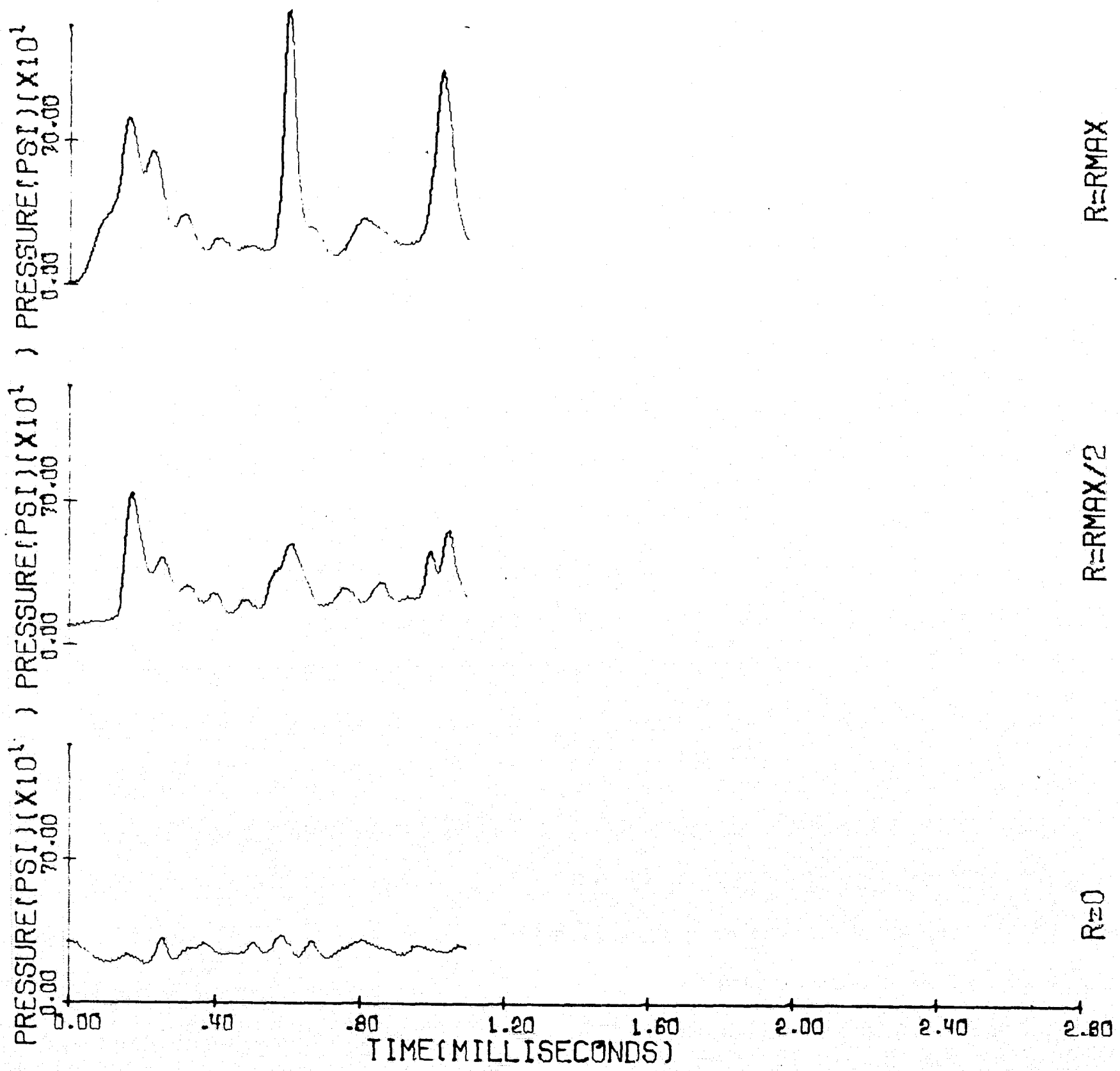

Figure 78

PANCAKE MOTOR-6

PRESSURE ISOBARS

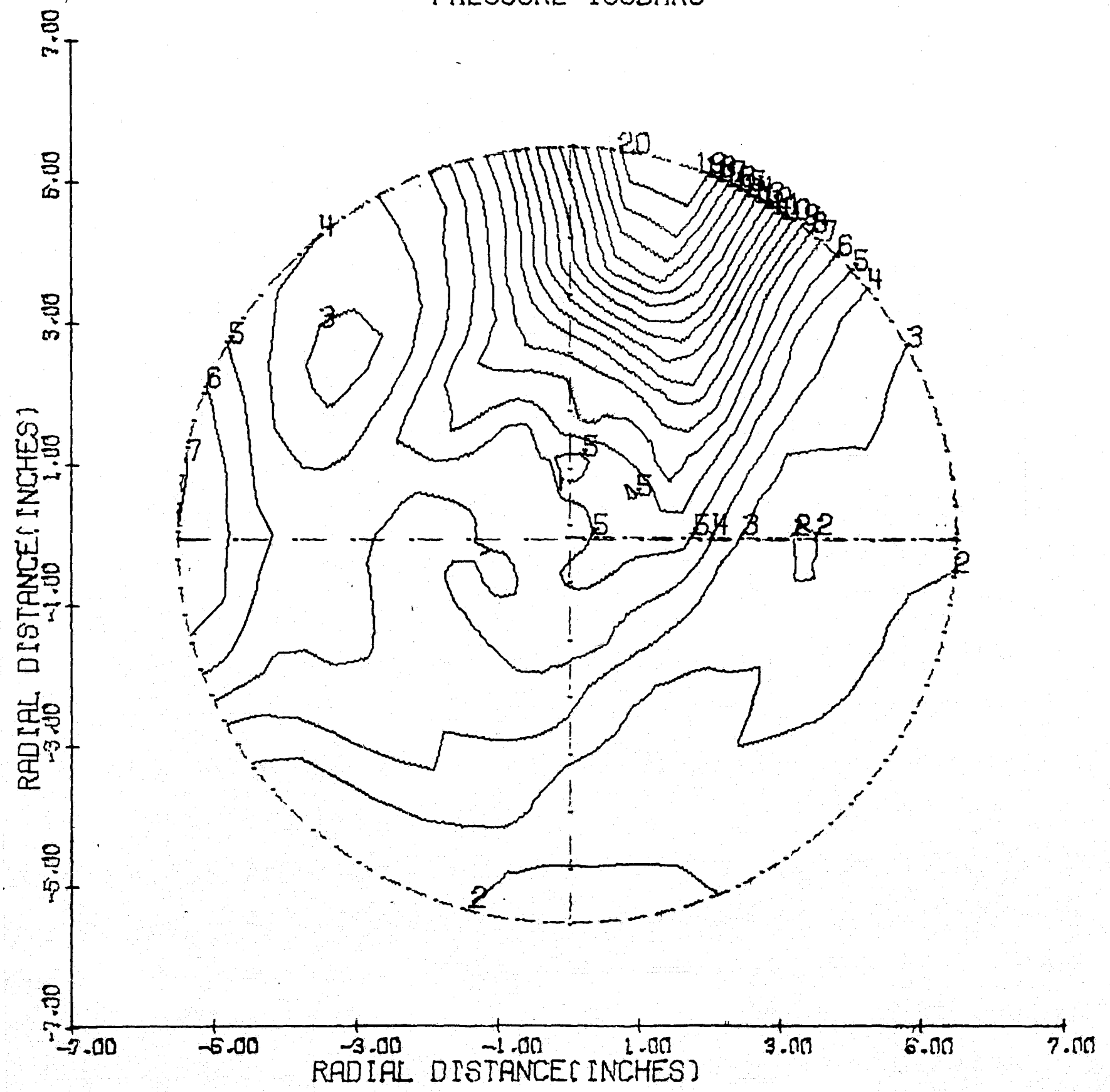

T= .525 MILLISECONDS

Figure 79

PANCAKE MOTOR-6

T= ,525 MILLISECONDS

ISOBAR	PRESSURE(PSI)
1	291,949
2	348,403
3	404,857
4	461,311
5	517,765
6	574,219
7	630,673
8	687,127
9	743,581
10	800,035
11	856,489
12	912,943
13	969,397
14	1025,852
15	1082,306
16	1138,760
17	1195,214
18	1251,668
19	1308,122
20	1364,576

PANCAKE MOTOR-6

PREF=REFERENCE PRESSURE = 300,00 PSI
AREF=REFERENCE SOUND SPEED= 3498,5 FT/SEC
R =CHAMBER RADIUS = ,45830 FEET
TREF=REFERENCE TIME=R/AREF=,0001310 SEC

T/TREF= 4,00677

ISOBAR	PRESSURE/PREF
1	,973
2	1,161
3	1,350
4	1,538
5	1,726
6	1,914
7	2,102
8	2,290
9	2,479
10	2,667
11	2,855
12	3,043
13	3,231
14	3,420
15	3,608
16	3,796
17	3,984
18	4,172
19	4,360
20	4,549

PANCAKE MOTOR-6

PRESSURE ISOBARS

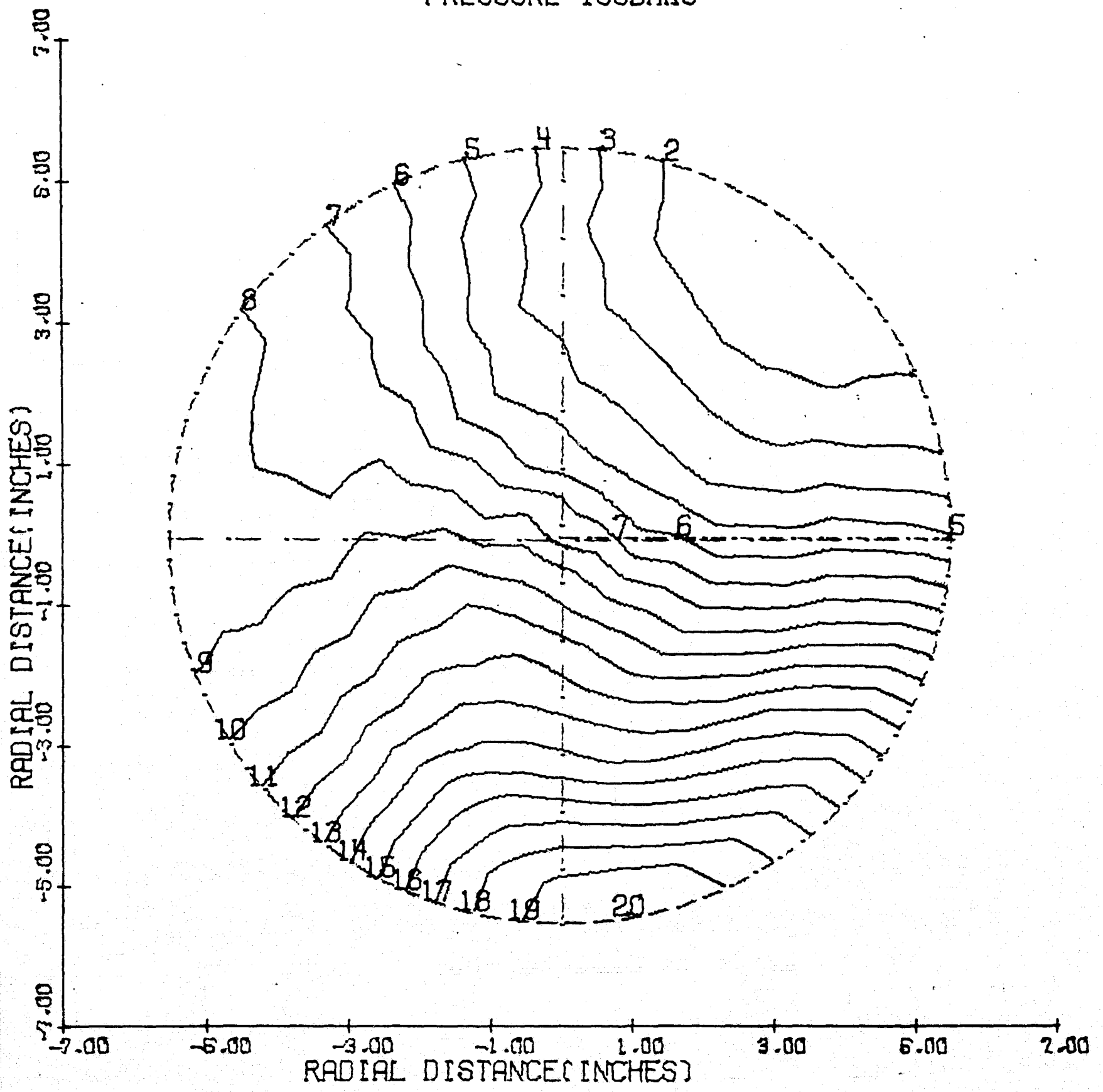

T= 1.228 MILLISECONDS

Figure 80

PANCAKE MOTOR-6

T= 1,228 MILLISECONDS

ISOBAR	PRESSURE(PSI)
1	1924,651
2	1994,453
3	2064,254
4	2134,056
5	2203,857
6	2273,659
7	2343,461
8	2413,262
9	2483,064
10	2552,865
11	2622,667
12	2692,469
13	2762,270
14	2832,072
15	2901,873
16	2971,675
17	3041,477
18	3111,278
19	3181,080
20	3250,881

PANCAKE MOTOR-6

PREF=REFERENCE PRESSURE = 300,00 PSI
AREF=REFERENCE SOUND SPEED= 3498,5 FT/SEC
R =CHAMBER RADIUS = ,45830 FEET
TREF=REFERENCE TIME=R/AREF=,0001310 SEC

T/TREF= 9,37127

ISOBAR	PRESSURE/PREF
1	6,416
2	6,648
3	6,881
4	7,114
5	7,346
6	7,579
7	7,812
8	8,044
9	8,277
10	8,510
11	8,742
12	8,975
13	9,208
14	9,440
15	9,673
16	9,906
17	10,138
18	10,371
19	10,604
20	10,836

PANCAKE MOTOR-6

PRESSURE ISOBARS

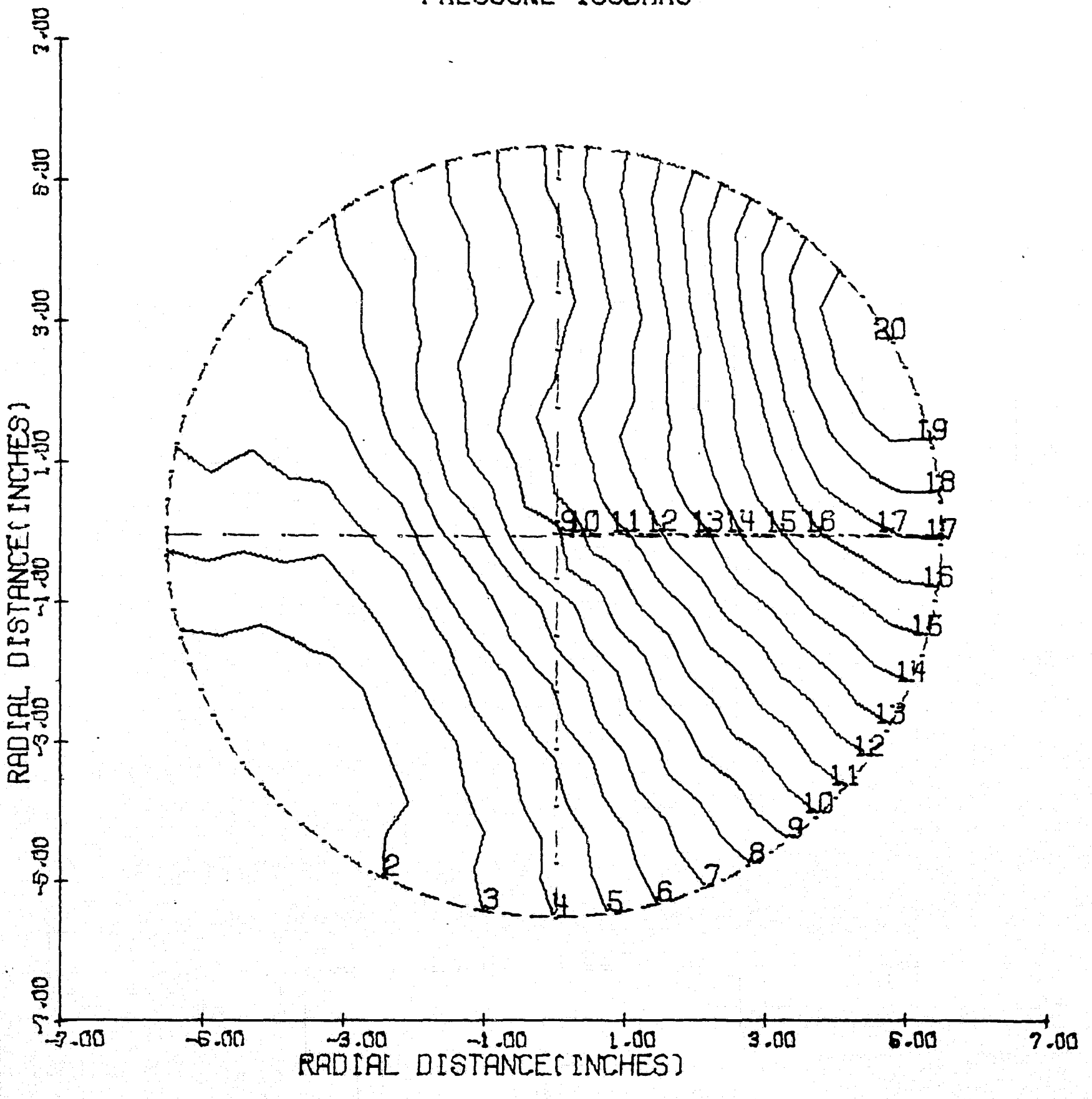

T= 1.984 MILLISECONDS

Figure 81

PANCAKE MOTOR-6

T= 1,984 MILLISECONDS

ISOBAR	PRESSURE(PSI)
1	4286,109
2	4359,135
3	4432,160
4	4505,186
5	4578,211
6	4651,237
7	4724,263
8	4797,288
9	4870,314
10	4943,340
11	5016,365
12	5089,391
13	5162,417
14	5235,442
15	5308,468
16	5381,493
17	5454,519
18	5527,545
19	5600,570
20	5673,596

PANCAKE MOTOR-6

PREF=REFERENCE PRESSURE = 300,00 PSI
AREF=REFERENCE SOUND SPEED= 3498,5 FT/SEC
R =CHAMBER RADIUS = ,45830 FEET
TREF=REFERENCE TIME=R/AREF=,0001310 SEC

T/TREF= 15,14166

ISOBAR	PPESSURE/PREF
1	14,287
2	14,530
3	14,774
4	15,017
5	15,261
6	15,504
7	15,748
8	15,991
9	16,234
10	16,478
11	16,721
12	16,965
13	17,208
14	17,451
15	17,695
16	17,938
17	18,182
18	18,425
19	18,669
20	18,912

PANCAKE MOTOR-6

PRESSURE ISOBARS

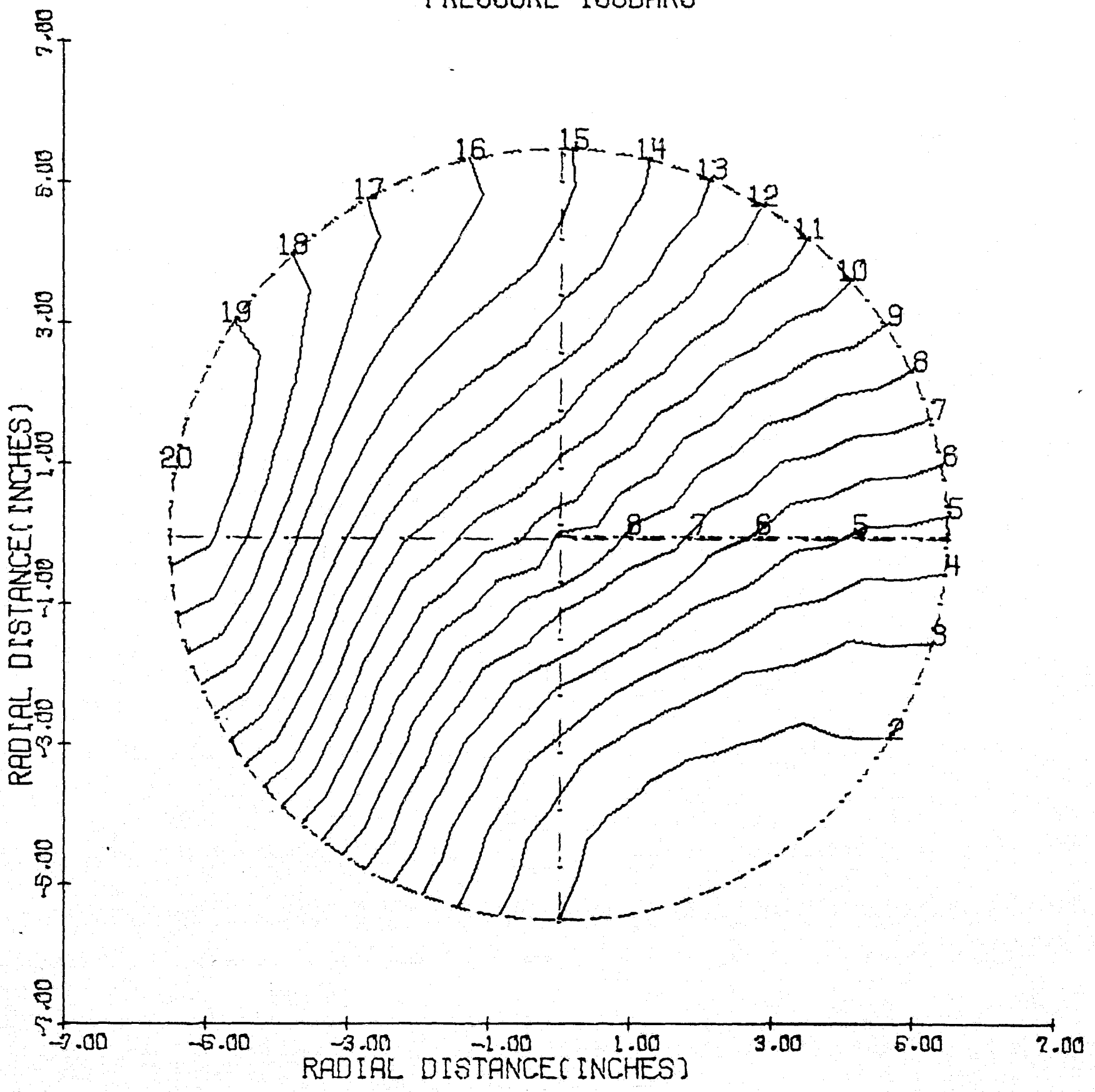

T= 2.761 MILLISECONDS

Figure 82

PANCAKE MOTOR-6

T= 2,761 MILLISECONDS

ISOBAR	PRESSURE(PSI)
1	6738,050
2	6837,767
3	6937,483
4	7037,200
5	7136,916
6	7236,632
7	7336,349
8	7436,065
9	7535,781
10	7635,498
11	7735,214
12	7834,930
13	7934,647
14	8034,363
15	8134,079
16	8233,796
17	8333,512
18	8433,228
19	8532,945
20	8632,661

PANCAKE MOTOR-6

PREF=REFERENCE PRESSURE = 300,00 PSI
AREF=REFERENCE SOUND SPEED= 3498,5 FT/SEC
R =CHAMBER RADIUS = ,45830 FEET
TREF=REFERENCE TIME=R/AREF=,0001310 SEC

T/TREF= 21,07631

ISOBAR	PRESSURE/PREF
1	22,460
2	22,793
3	23,125
4	23,457
5	23,790
6	24,122
7	24,454
8	24,787
9	25,119
10	25,452
11	25,784
12	26,116
13	26,449
14	26,781
15	27,114
16	27,446
17	27,778
18	28,111
19	28,443
20	28,776

PANCAKE MOTOR-6

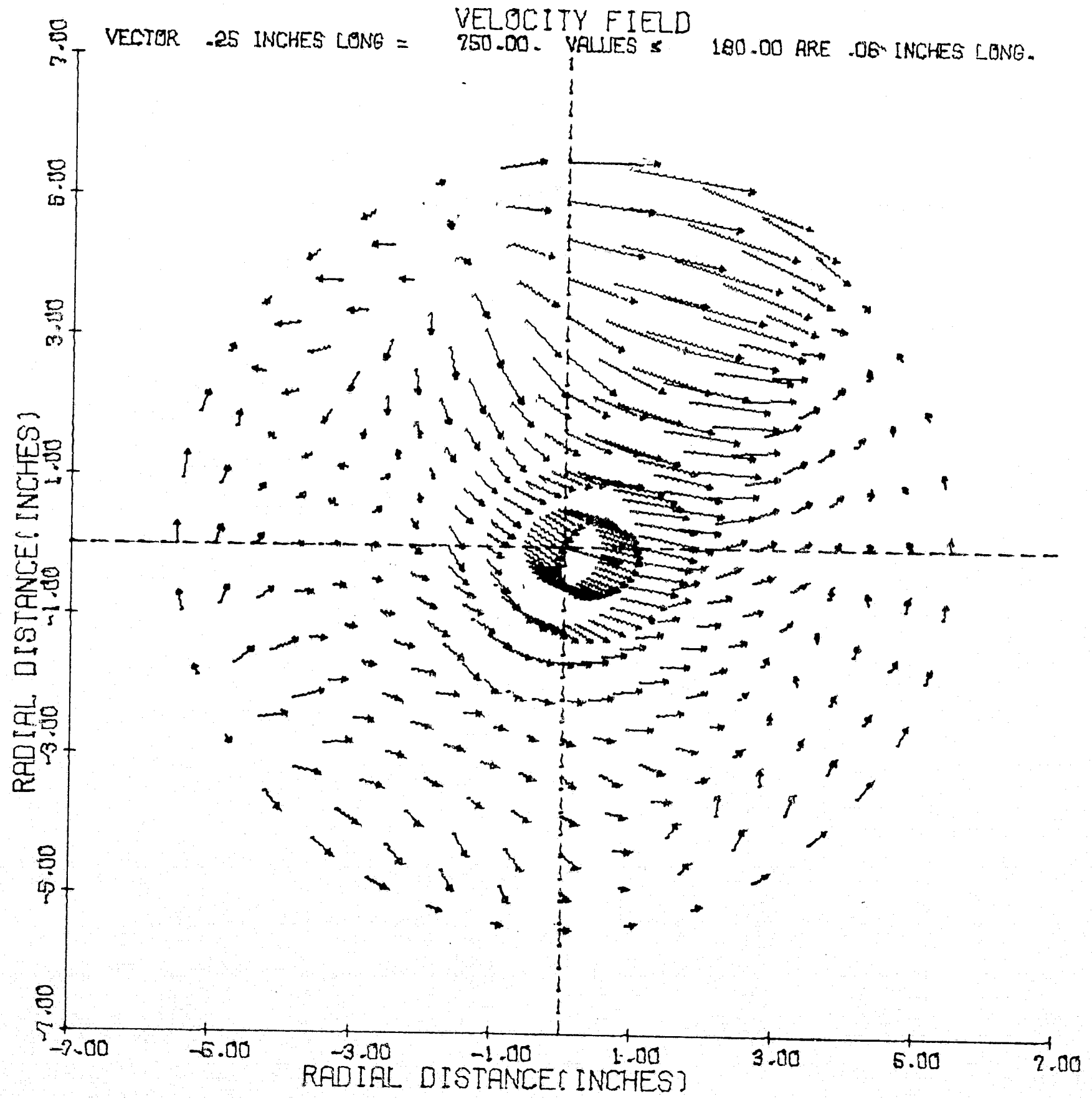

T= .525 MILLISECONDS

Figure 83

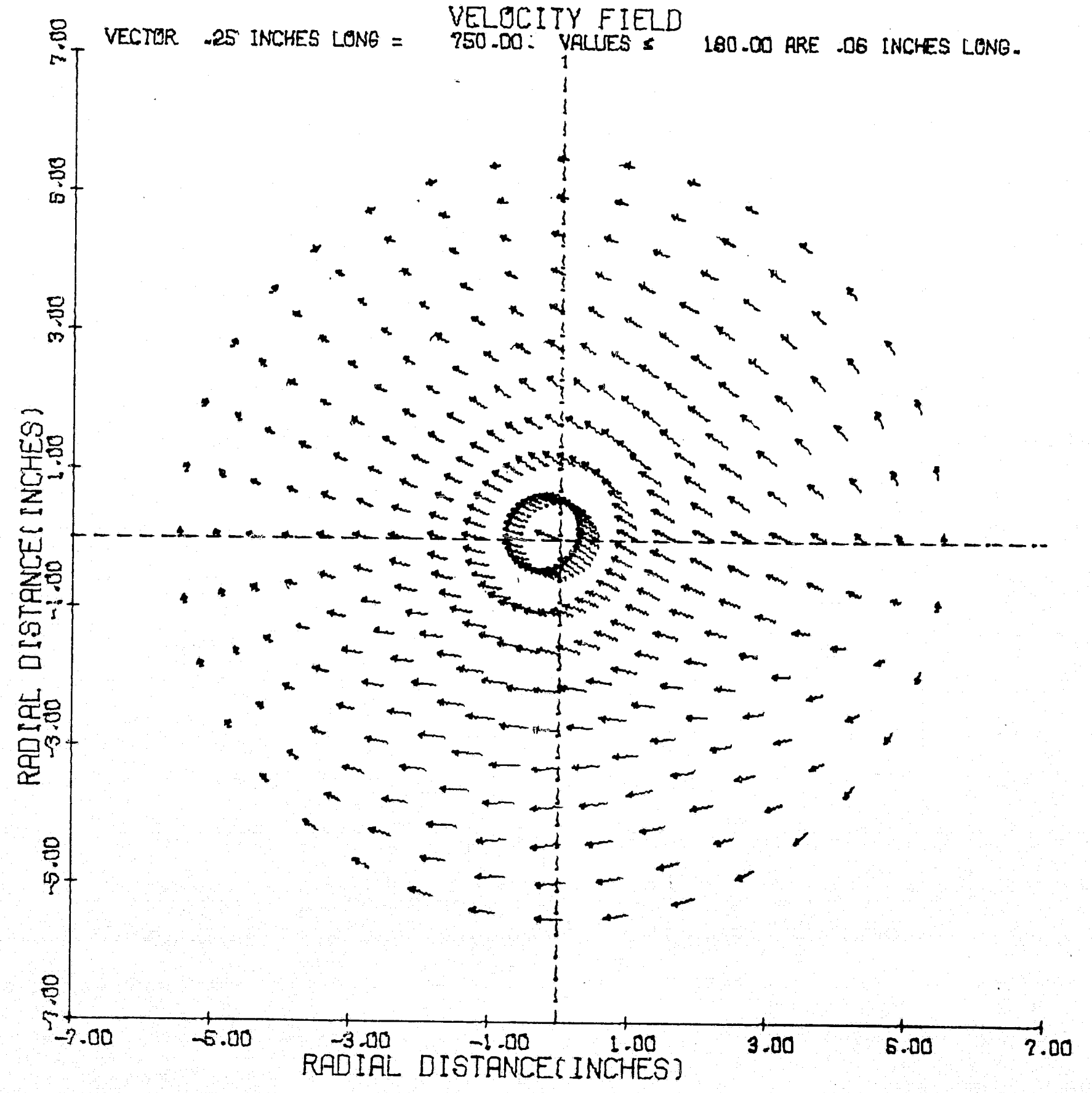
PANCAKE MOTOR-6
VELOCITY FIELD
VECTOR .25 INCHES LONG = 750.00. VALUES ≤ 180.00 ARE .06 INCHES LONG.
RADIAL DISTANCE(INCHES)
7.00
5.00
3.00
1.00
-1.00
-3.00
-5.00
-7.00
-7.00
-5.00
-3.00
-1.00
1.00
3.00
5.00
7.00
RADIAL DISTANCE(INCHES)
T= 1.228 MILLISECONDS

Figure 84

PANCAKE MOTOR-6

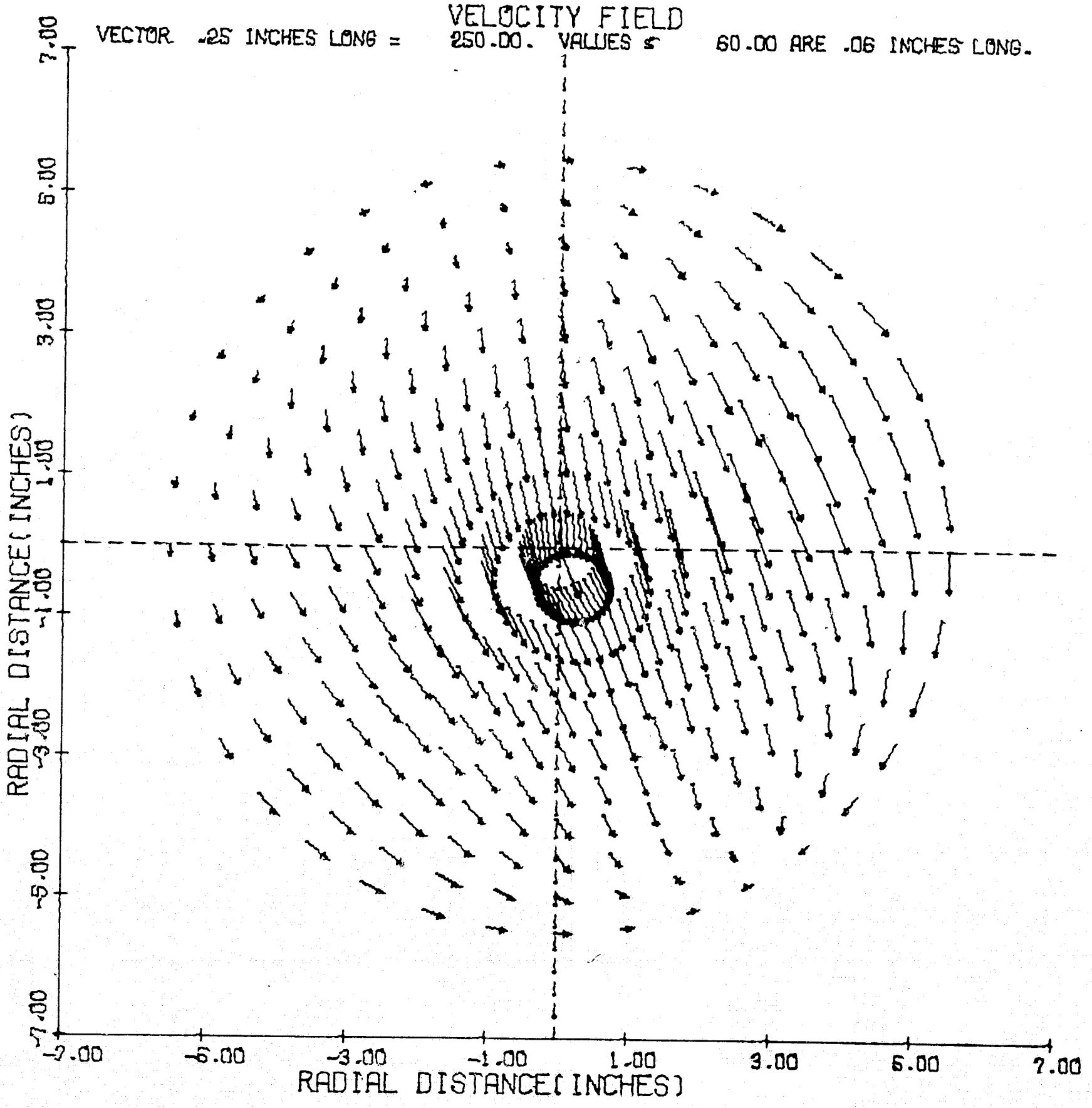

T= 1.984 MILLISECONDS

Figure 85

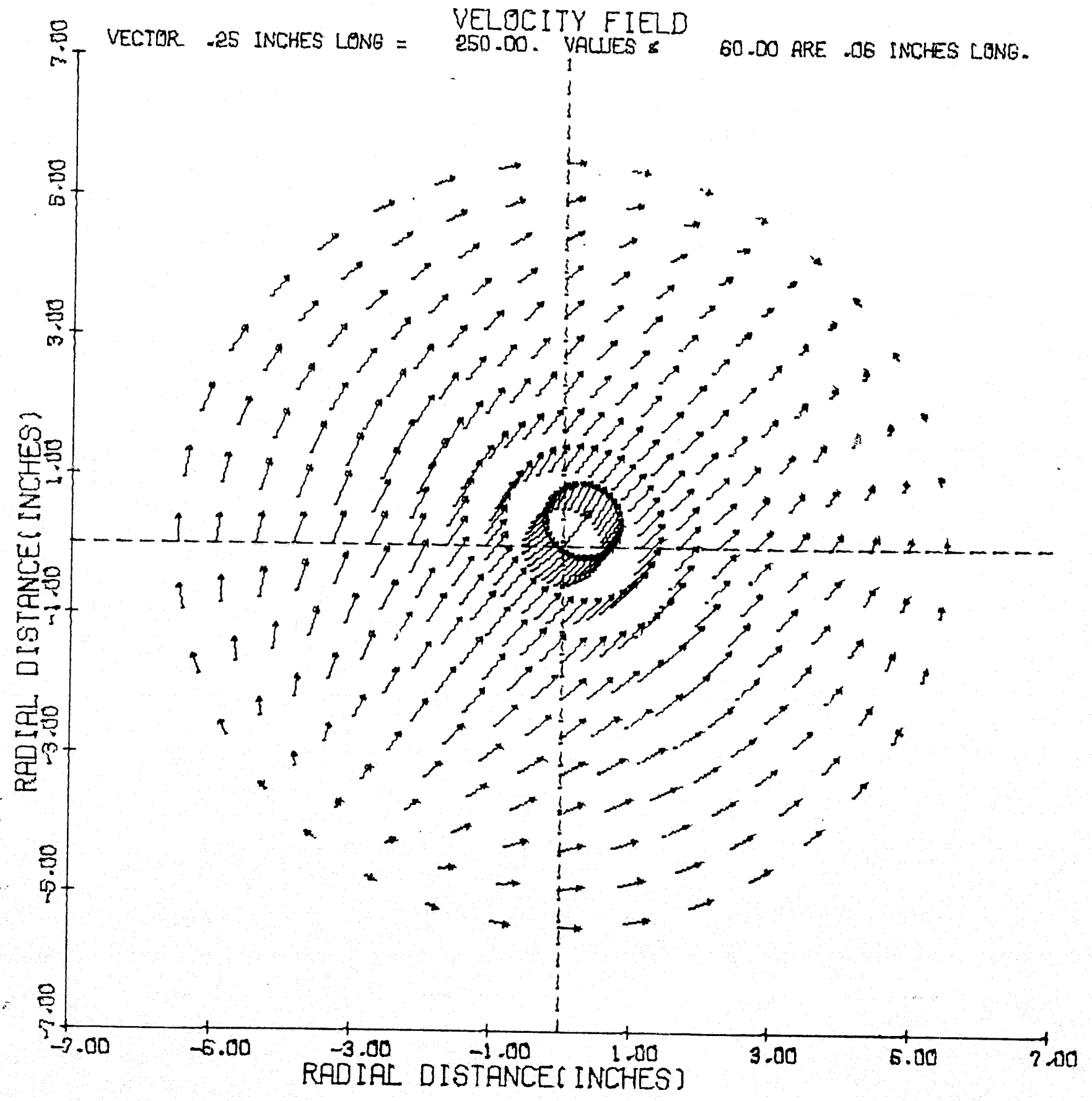
PANCAKE MOTOR-6
VELOCITY FIELD
VECTOR .25 INCHES LONG = 250.00. VALUES ≤ 60.00 ARE .06 INCHES LONG.
RADIAL DISTANCE(INCHES)
7.00
5.00
3.00
1.00
-1.00
-3.00
-5.00
-7.00
-7.00
-5.00
-3.00
-1.00
1.00
3.00
5.00
7.00
RADIAL DISTANCE(INCHES)
T= 2.761 MILLISECONDS

Figure 86

PANCAKE MOTOR-6

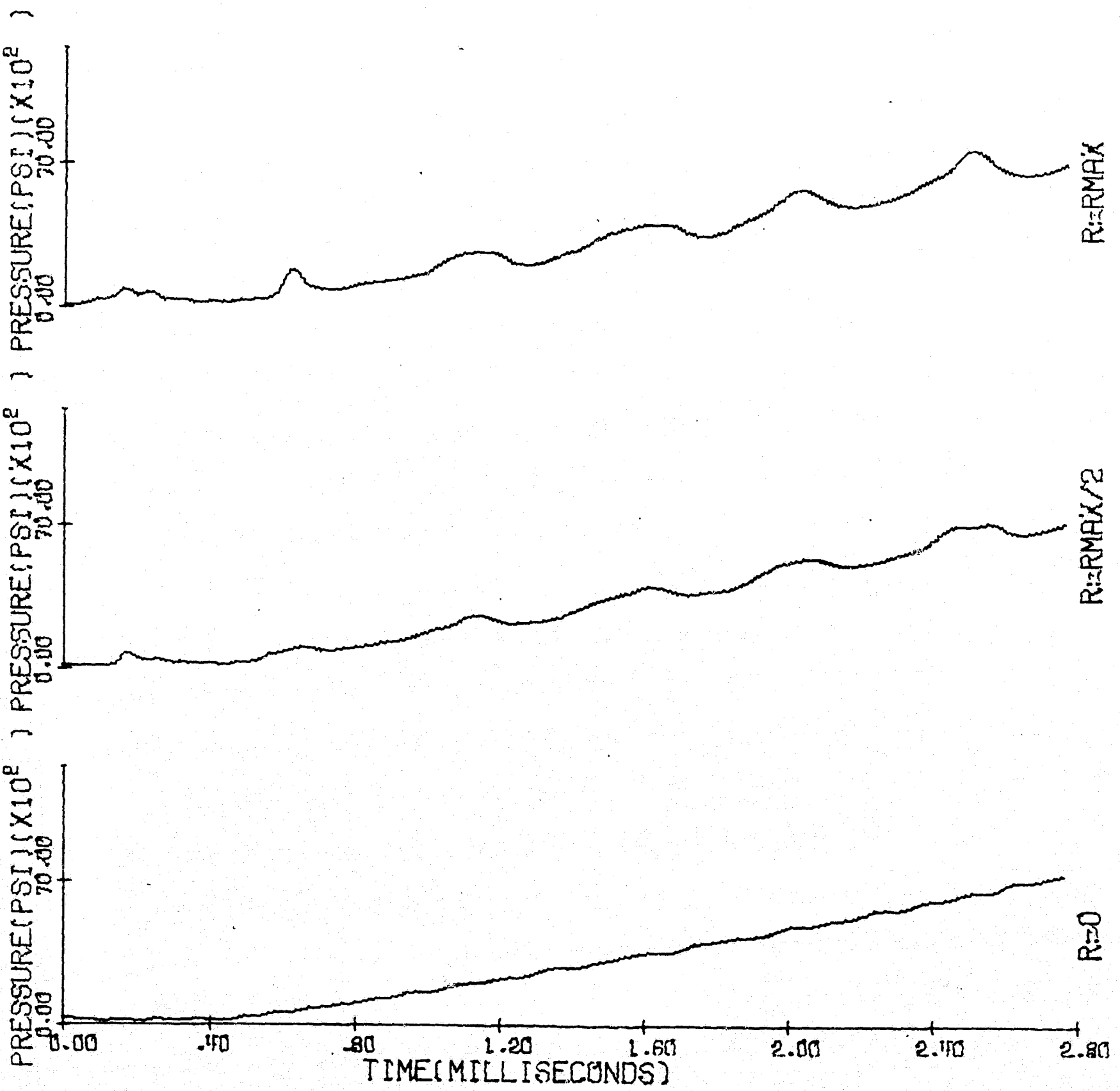

Figure 87

FIG. 88. TEMPERATURE - TIME HISTORIES FOR THE N_2H_4/N_2O_4 REACTION AT 1, 10, 20 ATM.

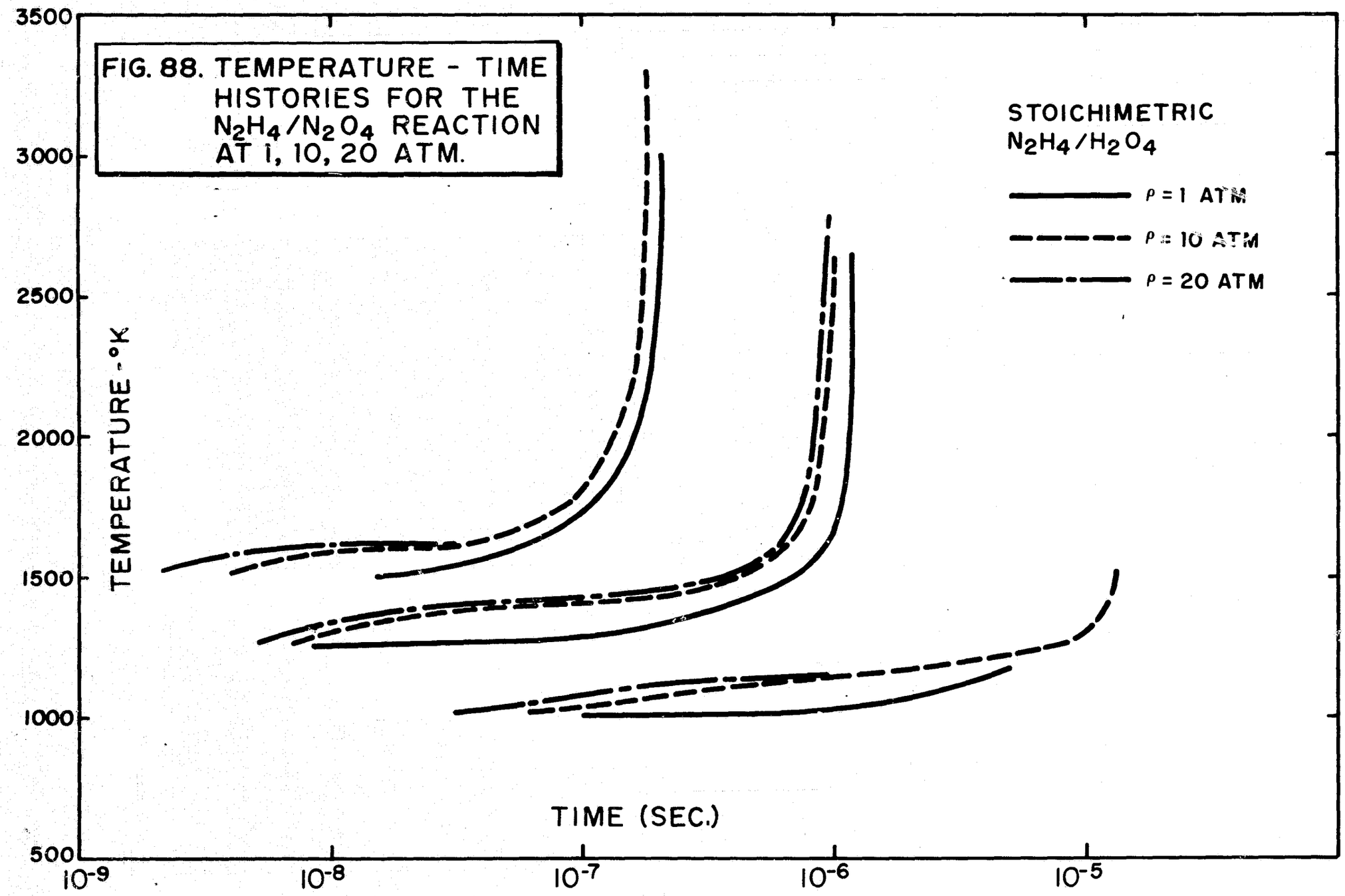

FIG. 89. IGNITION DELAY TIME vs. RECIPROCAL (INITIAL) TEMPERATURE FOR N_2H_4-N_2O_4 REACTIONS

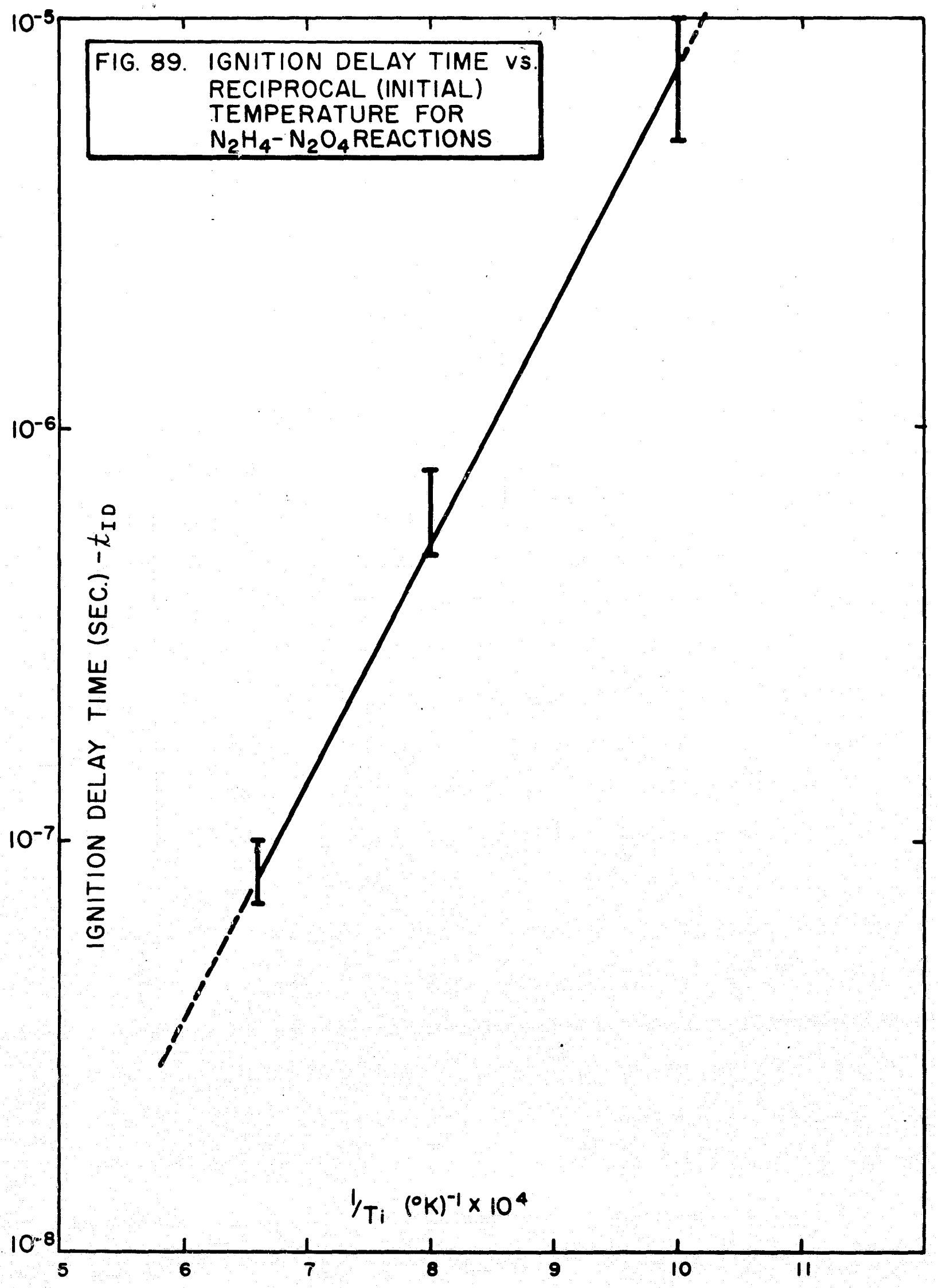

FIG. 90. COMPARISON BETWEEN EXACT AND GLOBAL MODELS FOR THE DISAPPEARANCE OF HYDRAZINE

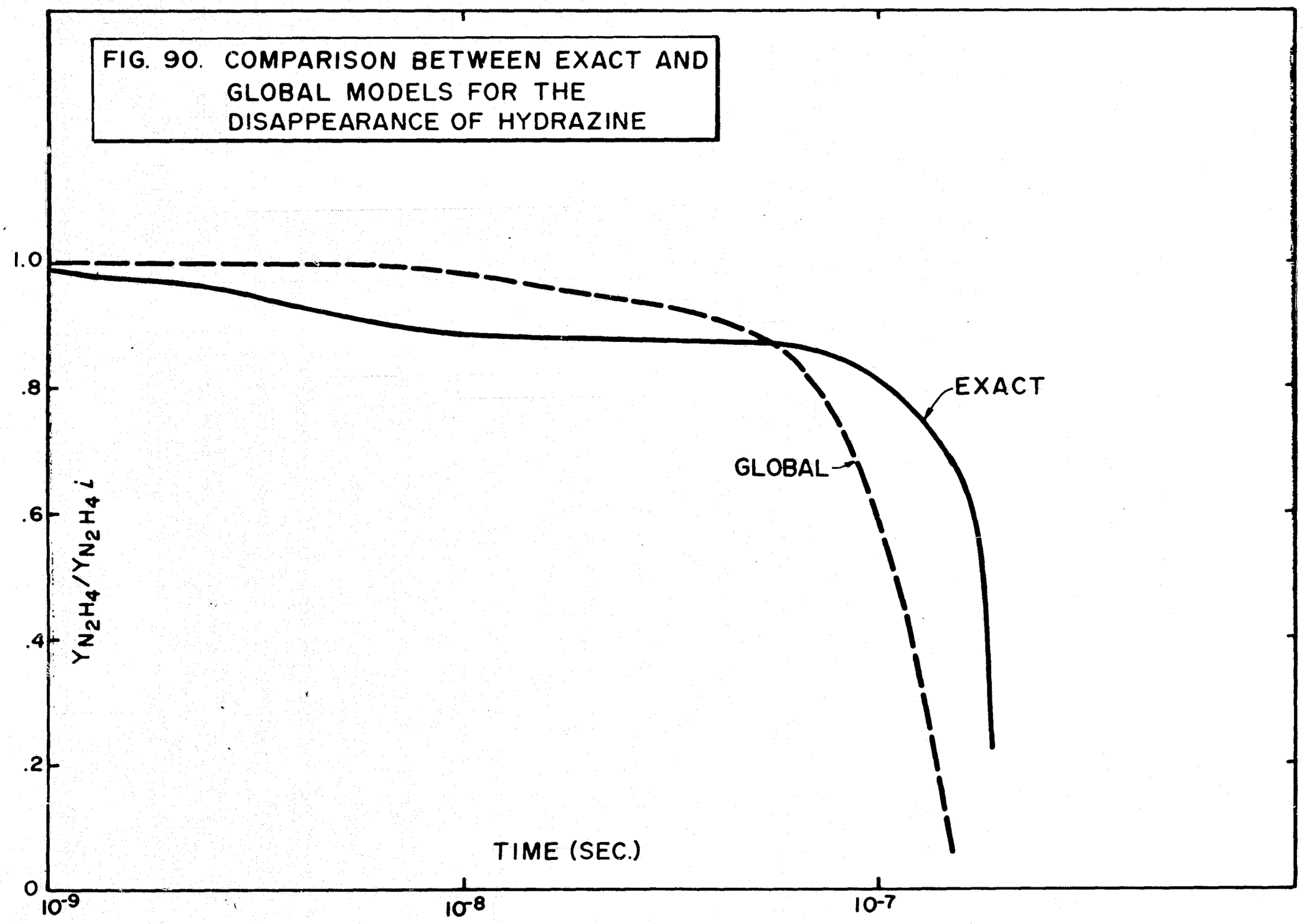

FIG. 91. DEPENDENCE OF BURNING RATE ON DROPLET DIAMETER AND AMBIENT PRESSURE

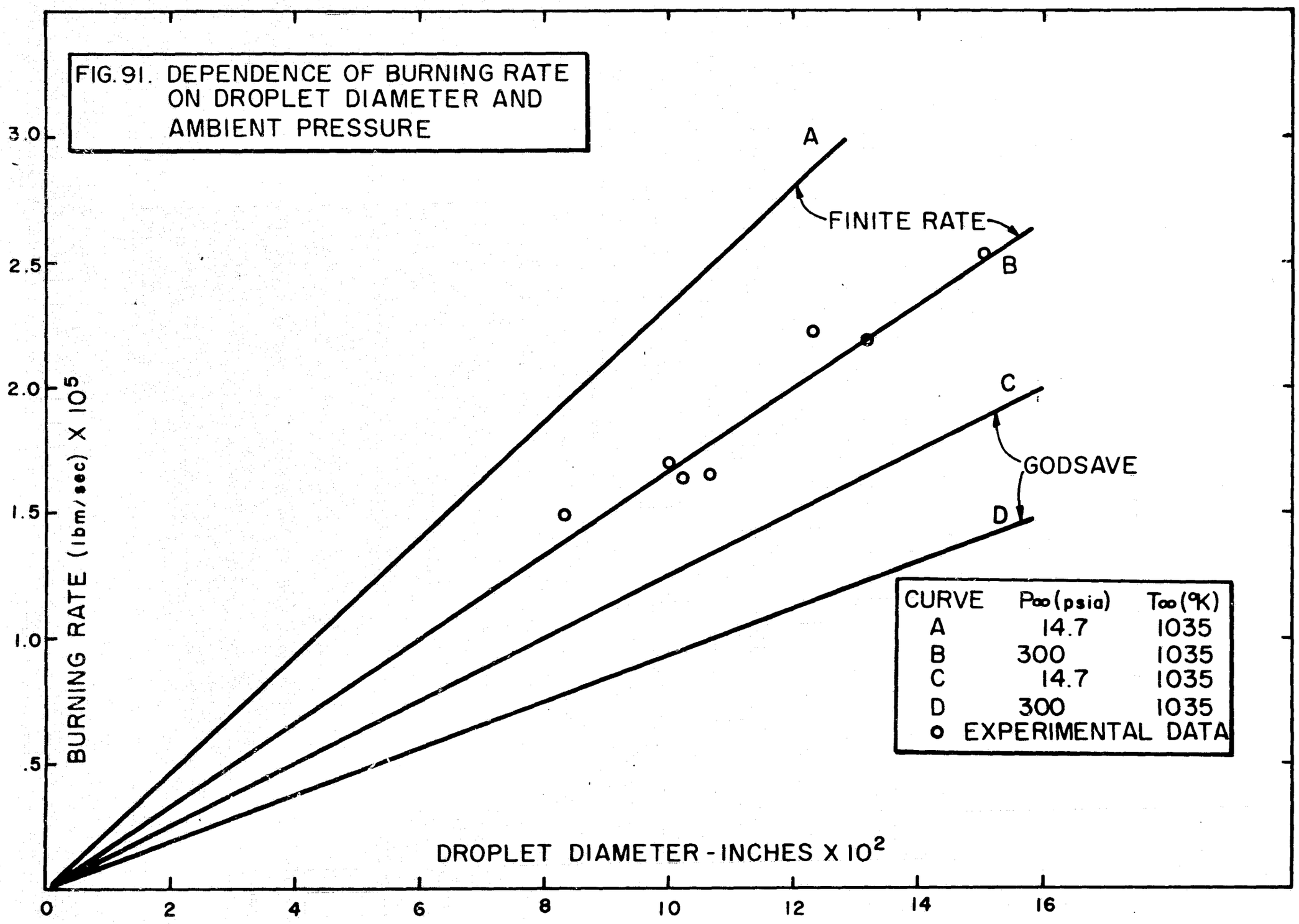

FIG. 92. EFFECT OF AMBIENT TEMPERATURE ON BURNING RATE.

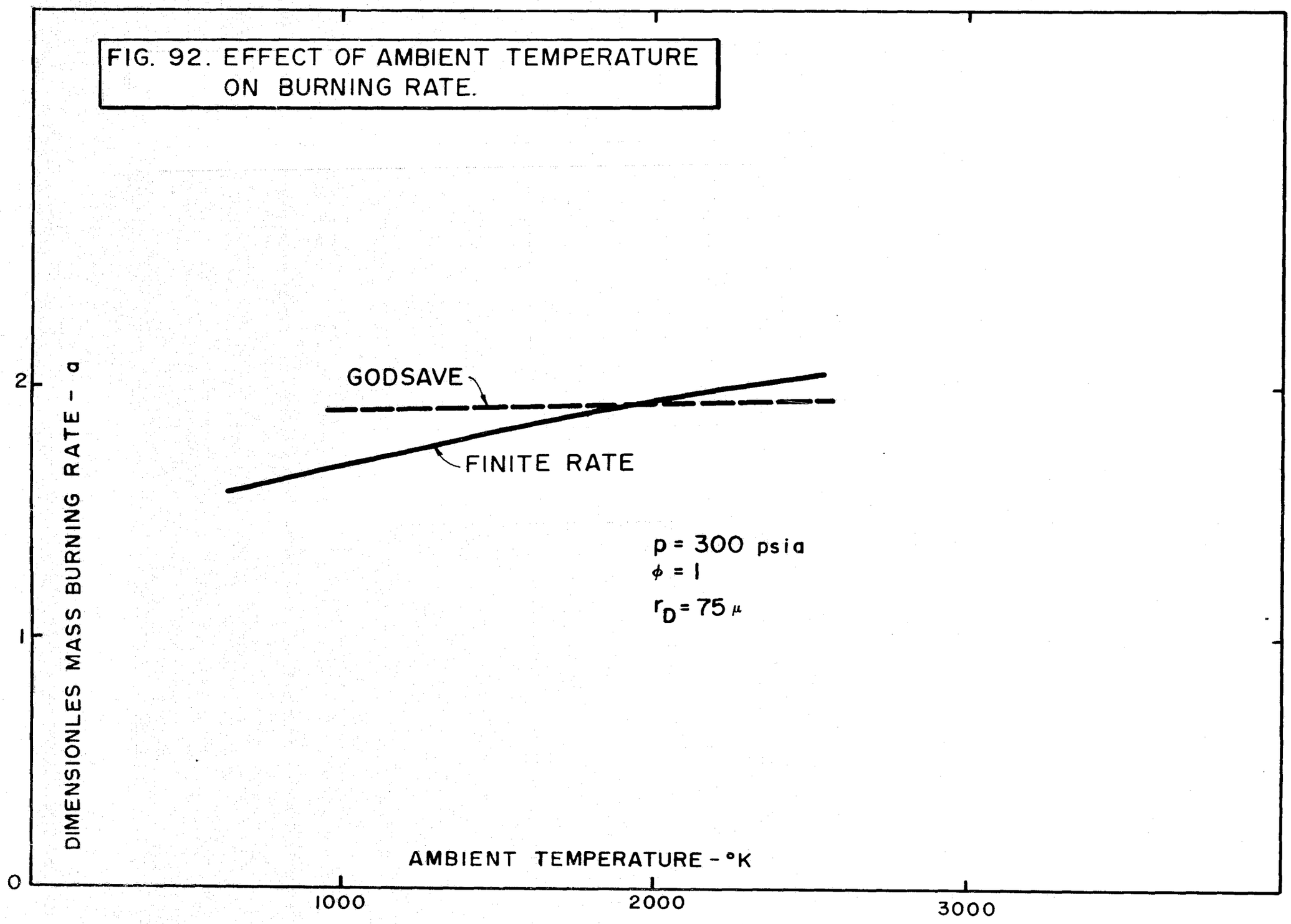

FIG. 93. EFFECT OF AMBIENT TEMPERATURE ON Y_{FS}, η^* AND T^*

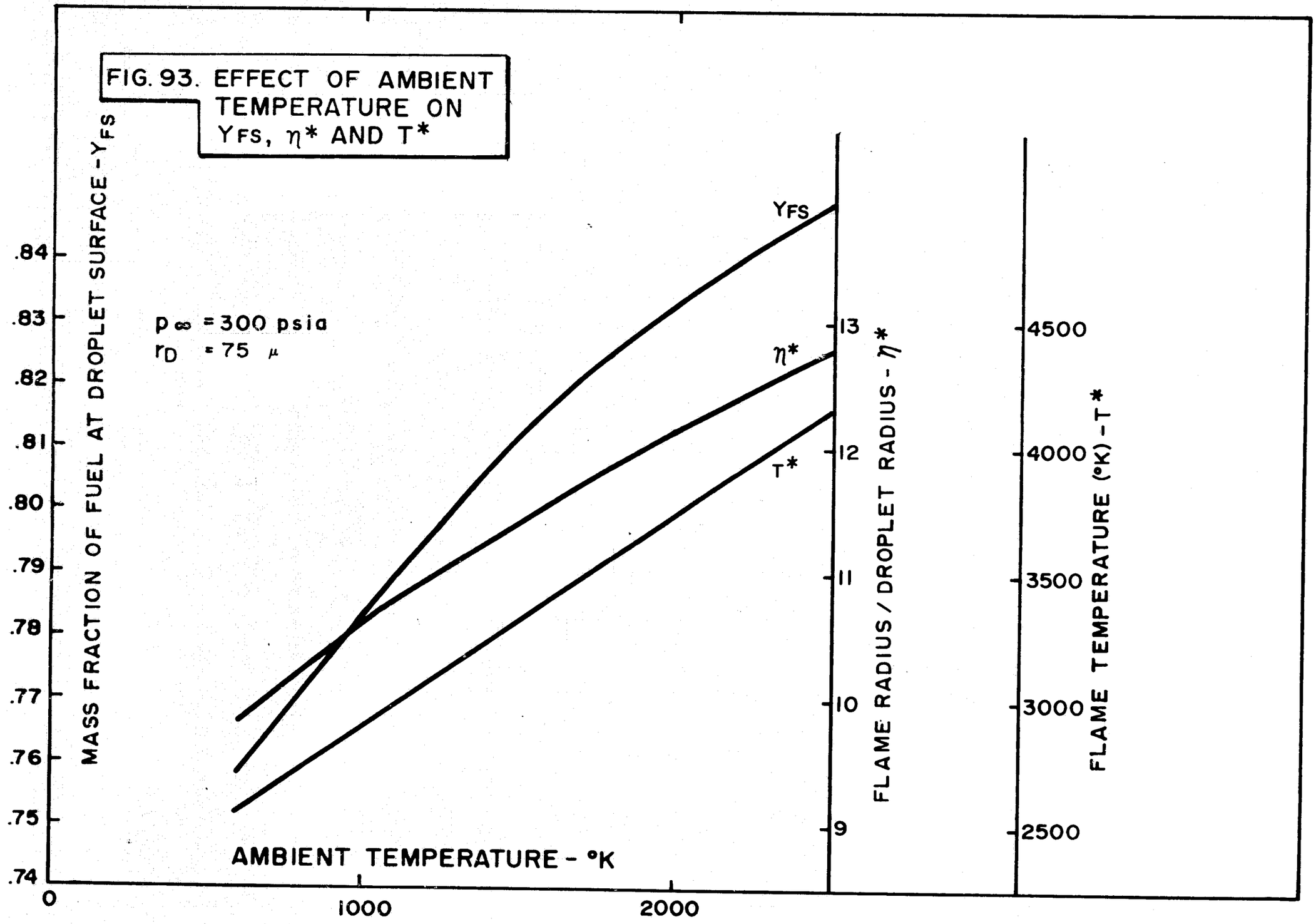

APPENDIX

A. DESCRIPTION OF THE COMPUTER PROGRAM COMB

COMB is the main program. It partially controls the storage and shifting of data for the computed values of fluid properties. It also calls other routines for the setting up of data at boundary points, the center point calculation, numerical display of fluid properties along selected rays, testing for completion of the run, outputting of data onto tape, etc.

After COMB has read in some of the data, the remaining data is read in by subroutine INITAL. INITAL then non-dimensionalizes the variables and computes certain values which remain constant throughout the run. The initial values of the variables are then either read in from a tape, which may have been created by a previous run, or subroutine BESFCT is called. BESFCT computes the initial values in terms of Bessel and trigonometric functions which are solution of a linearized form of the equations.

If the initial values were not read from tape, COMB calls subroutine CHARGE which adds the reflection points at the boundary to the mesh. Subroutine CONVRG is then called to determine the proper stepsize. Information necessary for future generation of pressure and velocity plots is then written onto tape 2. Subroutine PRTOUT then prints the initial data along selected rays.

Values of the data at the next time step are now calculated. First, subroutine MVPNT is called to find the new position of a

'particle' moving in the (r-θ) plane. The new values on the first row are then calculated by FRSTRO. The vectors F and G are computed by subroutines VECTFR and VECTRG, while VECTRS computes S-$\dot{\psi}$. The values on the other rows for the first step of the two step integration process are computed by QUAD 1. The vectors F, G, and S-$\dot{\psi}$ for these values are then computed by TEMPFW, TEMPGW and TEMPSW, respectively, while the final values are calculated by subroutine GENPT. Subroutine CENTER is then called to obtain the new center point and the reflection points at the boundary are obtained by calling CHARGE.

The values at the new time step are then tested for instabilities and CONVRG is called to obtain the new stepsize. The values of pressure at r=0, R/2 and R are then computed. When the input number of cycles have elapsed, the values necessary for plotting the moving 'particle' and the pressure as a function of time are written onto tape 2. A test is made to see if the problem is over. If so, plotting information is written onto tape 2, PRTOUT prints the flow field along selected rays, and restart information is written onto tape 3. If the problem is not over, tests are made to see if a printout or any of the plots are wanted at this time step or if restart information is to be written onto tape 3 and then the entire process is repeated for the next time step.

B. INPUT PREPARATION

There are basically two types of input data, integer and decimal. An integer is a number without a decimal point which must be right adjusted in its field. A decimal is a number with a decimal point which may be followed by an exponent of the form $E^{\pm}n$. The $\pm n$ represents the power of 10 by which the number is to be multiplied and n may consist of up to three digits. The + may be omitted if n is positive and the E need not appear if either + or - is present. A description of the necessary input cards for both programs follows:

Card	Columns	Type	Description
1	1-5	Integer	<0 end of input deck. =0 find starting conditions on tape 1. >0 generate starting conditions.
	6-10	Integer	=0 do not save conditions on tape 3. =n>0 save every nth cycle on tape 3.
2	1-40		Any alphanumeric information to be printed on plots.
3	1-5	Integer	Total number of mesh points on each ray including center point and reflection point at boundary.
	6-10	Integer	Total number of rays.

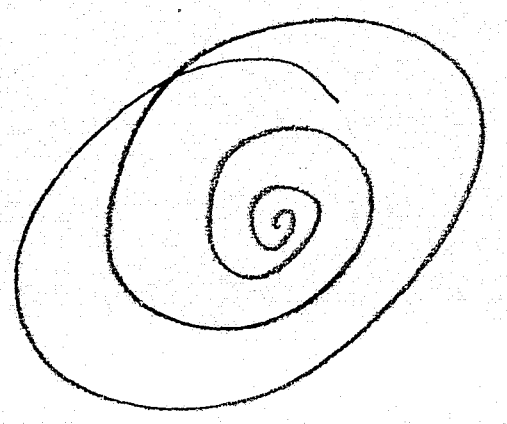

Card	Columns	Type	Description
4	1-5	Integer	Total number of cycles for case.
	6-10	Integer	Number of cycles between edited printouts.
	11-15	Integer	Number of cycles between writing of plotting information on tape 2.
	16-20	Integer	=0 no printout of W. ≠0 printout of entire W vector whenever edited printout appears.
	21-25	Integer	=0 no plot of linearized solution. ≠0 plot of solution of linearized equations whenever plots of nonlinear equation obtained.
	26-30	Integer	=n>0 plot tangential pressure distribution every n cycles. =0 no plot.
	31-35	Integer	Value of radius at which tangential pressure plot to be made. This is given by mesh point number from 2 for first row to 1 less than the number on card 3 columns 1-5 for the boundary.
	36-40	Integer	Number of cycles between streakline plots of 'particle' moving in r-θ plane and pressure vs. time plots.

Card	Columns	Type	Description
4	41-45	Integer	Number of cycles between points retained for streakline plot and pressure vs. time plots.
5	1-10	Decimal	Safety factor for time stepsize.
	11-20		Not used
	21-30	Decimal	>0- factor to control magnitude of simple forcing function. =0 use droplet evaporation forcing function. <0 set forcing function to zero.
	31-40	Decimal	r coordinate of 'particle' to be tracked.
	41-50	Decimal	θ coordinate of 'particle' to be tracked.
	51-60	Decimal	Droplet density used in evaporation model.
6	1-14	Decimal	Specific heat ratio cp/cv=γ.
	15-28	Decimal	Pressure in chamber in psia.
	29-42	Decimal	Maximum amplitude of a pressure disturbance in psia.
	43-56		Not used.
	57-66	Decimal	Chamber radius in feet.

Card	Columns	Type	Description
7	1-14	Decimal	Molecular weight of fluid in chamber.
	15-28	Decimal	Stagnation temperature.
	29-42	Decimal	Root of derivative of first order Bessel function to be used in generating initial data.

The entire sequence of cards may be repeated in order to run several different cases. However, no more than one case should use an input tape or an output tape.

C. DESCRIPTION OF OUTPUT FROM COMB

The printed output consists first of various input and calculated values that remain constant throughout the program. Properties of the flow field are printed along the rays $\theta=0$, π, $\pi/2$ and $3\pi/2$. These are the density, radial velocity, tangential velocity, internal energy, pressure and Mach number. If printout of the entire W vector is requested these values are printed in the order of row of constant radius.

D. DESCRIPTION OF PLOT PROGRAM COMPLT

The plot program produces plots of the information on tape 4 using a CALCOMP type digital incremental plotter. It uses a standard subroutine package to generate the actual plots (or a tape to be used with the plotter). A set of subroutines for producing contour and vector plots is also used. These subroutines, in turn, use the standard plot package.

Five basic types of plots are produced. The first is a plot of pressure isobars which is produced by using subroutine CONTOUR. The pressure levels may be equally spaced values between the minimum and maximum pressure, or they may be input values. The isobars are plotted as radial distance in inches against tangential angle in degrees. Each isobar is marked with a number which increases with increasing pressure. The program produces a printed page which shows the pressure corresponding to each isobar number. Both dimensional and non-dimensional values are given.

The second type of plot is of the velocity vector field. The foot of the vector is located at the point of given radial distance in inches and tangential angle in degrees. The length of the vector is proportional to the speed at that point. The scale of vector length in inches to speed in ft/sec is printed at the top of the plot.

The third type of plot is of the pressure in psia at a given radial distance as a function of tangential angle in degrees.

The fourth type of plot is of pressure in psia against time in milleseconds. Several graphs appear on each plot. These graphs are of the pressure at the radial distances r=0, R/2 and R.

The fifth type of plot shows the path of a 'particle' moving in the r-θ plane.

All of the plots have the title associated with each run printed across the top. The time of occurrence in milleseconds is printed at the bottom of the contour, vector and pressure vs. angle plots.

E. INPUT PREPARATION FOR PROGRAM COMPLT

Card	Columns	Type	Description
1	1-5	Integer	<0 end of input deck. =0 produce pressure vs. angle plots. >0 do not produce pressure vs. angle plots.
	6-10	Integer	=0 produce pressure vs. time plots. >0 do not produce pressure vs. time plots.
	11-15	Integer	=0 produce plot of moving 'particle'. >0 do not produce plot of moving 'particle'.
	16-20	Integer	Number of cycle numbers at which some plot is desired.
	21-25	Integer	First cycle number at which a plot is desired.

Card	Columns	Type	Description
1	26-30	Integer	Second cycle number, repeated each five columns for the number specified in columns 16-20.
2	1-5	Integer	Number of pressure isobars to be plotted.
	6-10	Integer	=0 plot number of isobars specified in columns 1-5 at equally spaced values between the minimum and maximum pressure. =n>0 plot isobars of n input values of pressure in addition to the minimum and maximum pressure.
	11-20	Decimal	Radial distance in inches corresponding to seven inches of plot.
	21-30	Decimal	Speed in ft/sec corresponding to 0.25 inches of plot for vector plots.
	31-40	Decimal	Value of pressure in psia at origin of pressure vs. angle plot.
	41-50	Decimal	Value of pressure in psia corresponding to seven inches for pressure vs. angle plot.

Card	Columns	Type	Description
2	51-60	Decimal	Value of pressure in psia at origin for pressure vs. time plots.
	61-70	Decimal	Value of pressure in psia corresponding to two inches for pressure vs. time plots.
	71-80	Decimal	Time in milleseconds corresponding to seven inches of plot.
3	1-10	Decimal	Pressure level of first isobar.
	11-20	Decimal	Pressure level of second isobar.

Repeated for all isobars, eight to a card. Card 3 should not appear if equally spaced values are calculated by the program.

The entire set of input cards may be repeated for each file on tape 4.

F. PROGRAM LISTING AND CARD DECKS

Organizations desiring a program listing or a duplicate card deck may request same from:

Jet Propulsion Laboratory
4800 Oak Grove Drive
Pasadena, California 91103

Att: TIDD, Jack G. Jackson, Jr.

All such requests should reference JPL Contract No. 951946.

MAGI

FORTRAN CODING FORM

PROGRAM NAME | PROJECT & TASK

AUTHOR | DATE | PAGE OF

COMMENT	STATEMENT NO.	CONT.	FORTRAN STATEMENT	IDENTIFICATION
			0 = ZERO 1 = ONE 2 = TWO Ø = ALPHA O I = ALPHA I Z = ALPHA Z SPECIAL INSTRUCTIONS card code = 026 029	
			SAMPLE INPUT FOR PROGRAM COMB	
	1		200	
PANCAKE MOTOR-2				
	12		36	
	2400		100 100 0 0 100 11 2400 5	
0	.85		1.0 -1.0 0.9 0.0 5.0 E8	
1	.2		300.0 450.0 0.4583	
2	3.0		4720.0 1.84118378	
-1				
			SAMPLE INPUT FOR PROGRAM COMPLT	
	0		0 0 11 0 100 200 300 400 500 600 1200 1800 2400 2400	
	20		07.0 2500.0 0.0 1400.0 0.0 1400.0 2.8	
-1				

TOTAL TIME= 7,73584E-01 NUMBER OF CYCLES= 100 NUMBER OF REVS= ,22 TIME STEP= 7,73329E-03 REAL TIME= 78,918

SOLUTION ALONG THE RAY THETA = 0

RHO	U	V	INT ENERGY	PRESSURE	MACH NO.
8,89897E-01	3,47413E-01	6,83279E-02	4,06944E+00	7,24276E-01	3,58273E-01
8,69102E-01	3,62783E-01	7,17893E-02	4,05102E+00	7,04149E-01	3,75059E-01
8,52661E-01	3,73178E-01	7,58741E-02	4,03600E+00	6,88268E-01	3,86929E-01
8,43368E-01	3,71790E-01	7,91097E-02	4,02709E+00	6,79264E-01	3,86644E-01
8,43618E-01	3,56014E-01	7,95150E-02	4,02719E+00	6,79481E-01	3,71050E-01
8,56688E-01	3,20766E-01	7,87296E-02	4,03989E+00	6,92185E-01	3,35429E-01
8,84563E-01	2,66729E-01	7,51175E-02	4,06682E+00	7,19472E-01	2,80486E-01
9,16992E-01	1,97047E-01	7,19057E-02	4,09748E+00	7,51471E-01	2,11520E-01
9,48715E-01	1,29678E-01	6,75157E-02	4,12616E+00	7,82909E-01	1,46917E-01
9,63389E-01	6,17693E-02	6,41169E-02	4,13677E+00	7,97063E-01	8,93516E-02
9,42272E-01	-1,78821E-11	6,79070E-02	4,26744E+00	8,04218E-01	6,71004E-02
7,08228E-01	-6,17693E-02	7,83651E-02	5,06163E+00	7,97943E-01	9,05322E-02

SOLUTION ALONG THE RAY THETA = PI

RHO	U	V	INT ENERGY	PRESSURE	MACH NO.
8,89897E-01	-3,47413E-01	-6,83279E-02	4,06944E+00	7,24276E-01	3,58273E-01
9,14542E-01	-3,24404E-01	-6,30998E-02	4,09127E+00	7,48327E-01	3,33515E-01
9,39406E-01	-2,98402E-01	-5,71847E-02	4,11349E+00	7,72849E-01	3,05790E-01
9,65326E-01	-2,69675E-01	-5,19431E-02	4,13672E+00	7,98656E-01	2,75625E-01
9,89899E-01	-2,39509E-01	-4,63433E-02	4,15781E+00	8,23162E-01	2,44213E-01
1,01364E+00	-2,05762E-01	-4,10483E-02	4,17793E+00	8,46984E-01	2,09533E-01
1,03247E+00	-1,69889E-01	-3,57583E-02	4,19349E+00	8,65930E-01	1,73056E-01
1,04590E+00	-1,29807E-01	-3,13965E-02	4,20470E+00	8,79538E-01	1,32944E-01
1,05403E+00	-8,63381E-02	-2,71079E-02	4,21116E+00	8,87742E-01	9,00144E-02
1,05884E+00	-4,11345E-02	-2,40800E-02	4,21366E+00	8,92319E-01	4,73978E-02
1,07848E+00	-2,70521E-11	-1,78666E-02	4,13467E+00	8,91833E-01	1,79356E-02
8,66324E-01	4,11345E-02	-2,94311E-02	5,15082E+00	8,92456E-01	4,54911E-02

SOLUTION ALONG THE RAY THETA = PI/2

RHO	U	V	INT ENERGY	PRESSURE	MACH NO.
8,89897E-01	6,83279E-02	-3,47413E-01	4,06944E+00	7,24276E-01	3,58273E-01
9,47907E-01	6,05745E-02	-3,47750E-01	4,12147E+00	7,81353E-01	3,54916E-01
1,01320E+00	4,85853E-02	-3,47803E-01	4,17737E+00	8,46504E-01	3,50730E-01
1,08457E+00	3,37960E-02	-3,44857E-01	4,23523E+00	9,18683E-01	3,43693E-01
1,16138E+00	1,96398E-02	-3,37374E-01	4,29385E+00	9,97362E-01	3,32902E-01
1,23776E+00	5,71519E-03	-3,26715E-01	4,34862E+00	1,07651E+00	3,19856E-01
1,31391E+00	-2,80968E-03	-3,12587E-01	4,40062E+00	1,15641E+00	3,04176E-01
1,37942E+00	-8,37495E-03	-2,96265E-01	4,44305E+00	1,22577E+00	2,87017E-01
1,43459E+00	-7,88746E-03	-2,77115E-01	4,47766E+00	1,28472E+00	2,67427E-01
1,47232E+00	-5,03026E-03	-2,56671E-01	4,49859E+00	1,32467E+00	2,47068E-01
1,45784E+00	2,86567E-10	-2,42240E-01	4,61136E+00	1,34452E+00	2,30264E-01
1,20462E+00	5,03026E-03	-3,13709E-01	5,58774E+00	1,34622E+00	2,70931E-01

SOLUTION ALONG THE RAY THETA = 3*PI/2

RHO	U	V	INT ENERGY	PRESSURE	MACH NO.
8,89897E-01	-6,83279E-02	3,47413E-01	4,06944E+00	7,24276E-01	3,58273E-01
8,40334E-01	-7,29089E-02	3,39973E-01	4,02363E+00	6,76238E-01	3,53829E-01
7,98015E-01	-7,41660E-02	3,30306E-01	3,98313E+00	6,35719E-01	3,46242E-01
7,62857E-01	-7,22222E-02	3,19264E-01	3,94684E+00	6,02175E-01	3,36323E-01
7,33254E-01	-6,73541E-02	3,06314E-01	3,91547E+00	5,74207E-01	3,23536E-01
7,10585E-01	-5,88750E-02	2,91539E-01	3,89055E+00	5,52913E-01	3,07798E-01
6,92406E-01	-4,98483E-02	2,75249E-01	3,87020E+00	5,35950E-01	2,90243E-01
6,80989E-01	-3,76235E-02	2,57271E-01	3,85710E+00	5,25329E-01	2,70241E-01
6,73383E-01	-2,59388E-02	2,38440E-01	3,84810E+00	5,18249E-01	2,49578E-01
6,70713E-01	-1,30808E-02	2,18433E-01	3,84359E+00	5,15589E-01	2,27836E-01
6,89708E-01	-5,39250E-10	1,89818E-01	3,74117E+00	5,16063E-01	2,00322E-01
5,48765E-01	1,30808E-02	2,66974E-01	4,76252E+00	5,22701E-01	2,50015E-01

TOTAL TIME= 1,5354286E+00 NUMBER OF CYCLES= 200

SAMPLE OUTPUT FOR PROGRAM ● COMB

PANCAKE MOTOR-2

TOTAL NUMBER OF CYCLES FOR THIS CASE=2400 NUMBER OF CYCLES BETWEEN PICTURES= 100

GAMMA	CHAMBER PRESSURE PSI	PULSE PRESSURE PSI	PULSE DURATION SEC	CHAMBER RADIUS FT
1,2000000E+00	3,0000000E+02	4,5000000E+02	7,0000000E-01	,4583

MOL WEIGHT	CHAMBER TEMPERATURE
2,3000000E+01	4,7200000E+03

REDUCED PRESSURE	REF SOUND SPEED	REF DENSITY	DELTA R	DELTA THETA	PRESSURE AND INTERNAL ENERGY RATIO OF PULSE	
8,3333333E-01	3,4985451E+03	1,3625144E-01	1,0000000E-01	1,7453293E-01	1,5000000E+00	7,5000000E+00

REF TIME SCALE= .131[illegible]
MILLISEC

********** END OF INITILIZATION PHASE **********

TOTAL TIME= 0. NUMBER OF CYCLES= 0 NUMBER OF REVS= 0.00 TIME STEP= 7.69711E-03 REAL TIME= 1.053

SOLUTION ALONG THE RAY THETA = 0

RHO	U	V	INT ENERGY	PRESSURE	MACH NO.
1.00000E+00	-1.14757E-09	3.58044E-01	4.16667E+00	8.33333E-01	3.58044E-01
9.33912E-01	0.	3.56529E-01	4.11008E+00	7.67690E-01	3.58975E-01
8.68586E-01	0.	3.52009E-01	4.05090E+00	7.03711E-01	3.57004E-01
8.05689E-01	0.	3.44562E-01	3.99045E+00	6.43013E-01	3.52087E-01
7.46892E-01	0.	3.34311E-01	3.93043E+00	5.87122E-01	3.44211E-01
6.93826E-01	0.	3.21430E-01	3.87292E+00	5.37427E-01	3.33397E-01
6.48030E-01	0.	3.06133E-01	3.82039E+00	4.95145E-01	3.19706E-01
6.10883E-01	0.	2.88672E-01	3.77555E+00	4.61284E-01	3.03256E-01
5.83537E-01	0.	2.69335E-01	3.74113E+00	4.36617E-01	2.84241E-01
5.66832E-01	0.	2.48434E-01	3.71946E+00	4.21661E-01	2.62946E-01
5.61231E-01	0.	2.26304E-01	3.71208E+00	4.16667E-01	2.39760E-01
4.63772E-01	0.	3.03642E-01	4.62982E+00	4.29436E-01	2.88054E-01

SOLUTION ALONG THE RAY THETA = PI

RHO	U	V	INT ENERGY	PRESSURE	MACH NO.
1.00000E+00	2.43288E-09	-3.58044E-01	4.16667E+00	8.33333E-01	3.58044E-01
1.06523E+00	1.26901E-09	-3.56529E-01	4.21966E+00	8.98977E-01	3.54283E-01
1.12804E+00	1.22056E-09	-3.52009E-01	4.26828E+00	9.62956E-01	3.47794E-01
1.18699E+00	1.14134E-09	-3.44562E-01	4.31199E+00	1.02365E+00	3.38706E-01
1.24075E+00	1.03357E-09	-3.34311E-01	4.35037E+00	1.07954E+00	3.27177E-01
1.28817E+00	9.00279E-10	-3.21430E-01	4.38312E+00	1.12924E+00	3.13393E-01
1.32824E+00	7.45204E-10	-3.06133E-01	4.41005E+00	1.17152E+00	2.97565E-01
1.36016E+00	5.72680E-10	-2.88672E-01	4.43105E+00	1.20538E+00	2.79928E-01
1.38331E+00	3.87516E-10	-2.69335E-01	4.44603E+00	1.23005E+00	2.60736E-01
1.39731E+00	1.94851E-10	-2.48434E-01	4.45500E+00	1.24501E+00	2.40260E-01
1.40198E+00	1.41377E-18	-2.26304E-01	4.45797E+00	1.25000E+00	2.18785E-01
1.14326E+00	-1.94851E-10	-3.03642E-01	5.52881E+00	1.26417E+00	2.63597E-01

SOLUTION ALONG THE RAY THETA = PI/2

RHO	U	V	INT ENERGY	PRESSURE	MACH NO.
1.00000E+00	3.58044E-01	1.79022E-09	4.16667E+00	8.33333E-01	3.58044E-01
1.00000E+00	3.53503E-01	6.39934E-10	4.16667E+00	8.33333E-01	3.53503E-01
1.00000E+00	3.40008E-01	6.31822E-10	4.16667E+00	8.33333E-01	3.40008E-01
1.00000E+00	3.17940E-01	6.18454E-10	4.16667E+00	8.33333E-01	3.17940E-01
1.00000E+00	2.87919E-01	6.00056E-10	4.16667E+00	8.33333E-01	2.87919E-01
1.00000E+00	2.50788E-01	5.76935E-10	4.16667E+00	8.33333E-01	2.50788E-01
1.00000E+00	2.07589E-01	5.49478E-10	4.16667E+00	8.33333E-01	2.07589E-01
1.00000E+00	1.59530E-01	5.18138E-10	4.16667E+00	8.33333E-01	1.59530E-01
1.00000E+00	1.07949E-01	4.83430E-10	4.16667E+00	8.33333E-01	1.07949E-01
1.00000E+00	5.42789E-02	4.45915E-10	4.16667E+00	8.33333E-01	5.42789E-02
1.00000E+00	3.93829E-10	4.06193E-10	4.16667E+00	8.33333E-01	5.65768E-10
8.18182E-01	-5.42789E-02	5.45007E-10	5.09259E+00	8.33333E-01	4.90972E-02

SOLUTION ALONG THE RAY THETA = 3*PI/2

RHO	U	V	INT ENERGY	PRESSURE	MACH NO.
1.00000E+00	-3.58044E-01	-3.07553E-09	4.16667E+00	8.33333E-01	3.58044E-01
1.00000E+00	-3.53503E-01	-1.91980E-09	4.16667E+00	8.33333E-01	3.53503E-01
1.00000E+00	-3.40008E-01	-1.89547E-09	4.16667E+00	8.33333E-01	3.40008E-01
1.00000E+00	-3.17940E-01	-1.85536E-09	4.16667E+00	8.33333E-01	3.17940E-01
1.00000E+00	-2.87919E-01	-1.80017E-09	4.16667E+00	8.33333E-01	2.87919E-01
1.00000E+00	-2.50788E-01	-1.73081E-09	4.16667E+00	8.33333E-01	2.50788E-01
1.00000E+00	-2.07589E-01	-1.64844E-09	4.16667E+00	8.33333E-01	2.07589E-01
1.00000E+00	-1.59530E-01	-1.55442E-09	4.16667E+00	8.33333E-01	1.59530E-01
1.00000E+00	-1.07949E-01	-1.45029E-09	4.16667E+00	8.33333E-01	1.07949E-01
1.00000E+00	-5.42789E-02	-1.33775E-09	4.16667E+00	8.33333E-01	5.42789E-02
1.00000E+00	-3.93829E-10	-1.21858E-09	4.16667E+00	8.33333E-01	1.28064E-09
8.18182E-01	5.42789E-02	-1.63502E-09	5.09259E+00	8.33333E-01	4.90972E-02

TOTAL TIME= 7.7358351E-01 NUMBER OF CYCLES= 100